Istituto Universitario di Studi Superiori di Pavia

Beyond Simple Scalar Ground Motion Intensity Measures for Seismic Risk Assessment

A Thesis Submitted in Partial Fulfilment of the Requirements
for the Degree of Doctor of Philosophy in

EARTHQUAKE ENGINEERING AND ENGINEERING SEISMOLOGY/ RISK AND EMERGENCY MANAGAMENT / WEATHER RELATED RISK

Obtained in the framework of the Doctoral Programme in
Understanding and Managing Extremes

by

Mohsen Kohrangi

Istituto Universitario di Studi Superiori di Pavia

Beyond Simple Scalar Ground Motion Intensity Measures for seismic risk assessment

A Thesis Submitted in Partial Fulfilment of the Requirements
for the Degree of Doctor of Philosophy in

EARTHQUAKE ENGINEERING AND ENGINEERING SEISMOLOGY/ RISK AND EMERGENCY MANAGAMENT / WEATHER RELATED RISK

Obtained in the framework of the Doctoral Programme in
Understanding and Managing Extremes

by

Mohsen Kohrangi
Supervisor: Paolo Bazzurro

ABSTRACT

A realistic assessment of building economic losses and collapse induced by earthquakes requires monitoring several response measures both story-specific and global. Typically a conditioning Intensity Measure (IM), assumed commonly as the spectral acceleration at the first mode of vibration of the building, is applied to connect the seismic hazard of the site to the response of the structure named as Engineering Demand Parameters (EDPs). In this procedure the structural response is commonly predicted using nonlinear dynamic analysis of 2D structural models. The analyst, therefore, should make two important choices in IM selection and ground motion record selection both of which can have significant effects on the structural response and loss estimates. This study attempts to bring an insight to both of these topics for building-specific and portfolio loss estimation for 2D and 3D building models. The first topic is tackled by building response estimation and risk assessment using a pool of scalar and vector IMs. The EDP prediction benefits from using multiple ground motion IMs that are, in general, correlated. To allow the inclusion of multiple IMs in the risk assessment process it is necessary to have a practical tool that computes the vector-valued hazard of all such IMs at the building site. In part of this study, vector-valued Probabilistic Seismic Hazard Analysis (VPSHA) is implemented as a post processor to scalar PSHA results. A group of candidate scalar and vector IMs based on spectral acceleration values, ratios of spectral acceleration values, and spectral accelerations averaged over a period range (*AvgSA*) are defined and their hazard evaluated. These IMs are used as structural response predictors of 3D models of reinforced concrete buildings. The advantages and disadvantages of using scalar and vector ground motion IMs are discussed for local, story-level seismic response assessment of 3D buildings. The response hazard curves were computed for three buildings with reinforced concrete infilled frames using the different IMs as predictors. Among the scalar IMs, *AvgSA* tends to be the best predictor of both floor accelerations and inter story drift ratios at practically any floor. However, there is an improvement in response estimation efficiency when employing vector IMs, specifically for 3D buildings subjected to both horizontal components of ground motion. This improvement is shown to be most significant for a tall plan-asymmetric building. The results of building response estimates using scalar and vector IMs are then extended to the building loss estimation. Despite all IMs being legitimate, and our use of conditional spectrum (CS)-based record selection, we find large differences in the estimated loss hazard. This points to the large uncertainty still lingering when connecting hazard to loss. Among the IMs considered here, the vector IMs and at least a scalar average of spectral accelerations showed a remarkable stability in their predictions for the 3D buildings, pointing to a potential for reliable applications. The second topic is investigated by introducing a new CS-based record selection scheme conditioned on an average of

spectral accelerations in a period range. Ground motion selection is a key step in seismic risk assessment of structures. The structural response estimates are reliable only if the sets of ground motion records used as input to response analyses are "hazard consistent", namely representative of those that the structure can experience at the site with given rates of occurrence. CS-based ground motion record selection is a robust method to obtain ensembles of accelerograms that link the seismic hazard at the site of interest with structural demands. However, the traditional CS-based approach hinges on spectral accelerations at specific oscillator periods as the link with hazard. Any single ground motion IM, such as spectral acceleration at the first modal period of structure or at any other period has been shown to be a poor predictor of all the different EDPs (e.g., peak interstory drift or peak floor acceleration) required for probabilistic seismic demand analysis (PSDA). In the recent years, average spectral acceleration in a period range, *AvgSA*, is shown to be an efficient IM for building response prediction as a replacement for typical spectral acceleration at a single period. *AvgSA* can also be easily predicted in hazard studies using current ground motion prediction equations. In this study, we take the advantage of combining *AvgSA* with record selection using a variant of the CS that is based on *AvgSA* in a period range as the conditioning IM. This procedure ensures not only seismic hazard consistency but also, efficiency in estimating the multiple EDPs needed in PSDA by means of a single IM. This record selection scheme is then extended to be used in a portfolio loss estimation. When performing loss assessment of a geographically dispersed building portfolio, the response or loss (fragility or vulnerability) function of any given archetype building is typically considered to be a consistent property of the building itself. On the other hand, recent advances in record selection have shown that the seismic response of a structure may not be independent of the nature of the hazard at the site of interest. This apparent contradiction begs the question: Are building fragility and vulnerability functions independent of site, and if not, what can be done to avoid having to reassess them for each site of interest? In part of this thesis, we show that there is a non-negligible influence of the site, the degree of which depends on the IM adopted for assessment. Employing a single-period (e.g., first-mode) spectral acceleration would require careful record selection at each site and result to significant site-to-site variability. On the other hand, an intensity measure comprising the geometric mean of multiple spectral accelerations would considerably reduce such variability, while in tandem with a conditional spectrum approach that accounts for multiple sites, it can offer a viable approach for incorporating the effect of site-dependence into fragility and vulnerability estimates.

ACKNOWLEDGEMENTS

I would like to thank my supervisor Professor Paolo Bazzurro for his new ideas, enthusiasm, patience and motivations in walking me through this thesis. Just to give a taste of how great it is to talk to a great supervisor like him, a fifteen minutes meeting in his car while waiting for her daughter formed chapter two and three of this thesis, almost one year ahead of me before the results came out! I am also grateful to Professor Dimitrios Vamvatsikos for his brilliant contributions in formation of the main ideas presented in this study and also his unforgettable hospitality at National Technical University of Athens during my stay in Athens. I was fortunate to work with such expert supervisors and to have long discussions to learn how to keep perseverance to find solutions for the most complicated problems. I thank them for their trust on me and all their endless encouragements. I would say, during this period, have not seen Stanford, I felt like Stanford came to Pavia! Lucky me.

I acknowledge Professor Rui Pinho, Dr. Romain Sousa, Professor Fabrizio Mollaioli and Dr. Andrea Lucchini for providing me with the building data used in Chapter 2, 3 and 4 of this thesis.

I would like to thank Dr. Marco Pagani, for helping me in the PSHA computations performed in this study. Despite his infinite responsibilities and commitments, he was always kindly available and collaborative to answer my never ending requests and questions.

Special thanks to my colleague and much more than that, my great friend Andrea Spillatura for all his company, helps, discussions and motivations in the last three years, particularly on completion of this thesis. I wish you success for the coming two years towards your PhD completion. Special thanks to Andrea for accepting to print and submit this document in the last minutes.

I would like to thank all my course instructors at UME School programme during my PhD programme, Professor Katrin Beyer, Professor Joel Conte, Professor Guido Magenes, Professor Edward Kavazanjian and Professor Steve Winterstein for their generous share of wisdom. I would like to specifically thank Professor Winterstein for his extraordinary teaching skills in explaining the most complicated subjects of "*probability*", in a simple way which made me more enthusiastic on following this subject towards this thesis.

I would like to thank the financial supports offered by ROSE programme at the UME School, IUSS Pavia. I also thank all the colleagues and staff at foundation of EUCENTRE and CAR College that made my stay in Pavia more pleasant and comfortable during these years.

I would like to show my deepest gratitude to my best mentor Mr. Aliasghar Taheri Behbahani who with all his motivations inspired me to start my journey to abroad. With all his constant supports, he kept me motivated to continue my efforts and keep being curious and interested in learning.

I would like to thank all my family: my sister, my brother and my magnificent parents, for their unconditional love for me. Without their encouragements, supports and patience during these years I would have never been able to continue my studies.

Finally, the last few words go to the love of my life. Your presence in the last few months of this thesis, made the pressure more tolerable. My dear Behnaz, it is not a long time that I have got to know you, but even in this short time you have brought me a world full of happiness, so I dedicate all the joy and happiness of this work to you. You have my full support in our journey to the future. I wish you best of luck in your upcoming exam!

TABLE OF CONTENTS

LIST OF FIGURES

LIST OF TABLES

LIST OF FIGURES IN APPENDIX

LIST OF TABLES IN APPENDIX

1. INTRODUCTION

1.1 MOTIVATION

Performance-Based Earthquake Engineering (PBEE) has been developed by Pacific Earthquake Engineering (PEER) research center over the past decade for design of new and assessment of existing structures [Cornell and Krawinkler, 2000]. The main objective of this procedure is quantifying the seismic performance and risk of engineered facilities using performance measures that are understandable for both engineers, on one hand, and stake holders and investors, on the other hand. It is based on the concept that the performance can be evaluated with quantifiable confidence to provide decision makers with the necessary tools to make informed and intelligent decisions for life-cycle considerations. With this objective, many numerical and experimental studies were carried out to date and the outcome of such studies led to generation of building design codes and guidelines such as [FEMA P-58, 2012]. The methodology developed by PEER integrates the following four steps in a unified probabilistic framework: (i) seismic hazard analysis, (ii) seismic demand analysis, (iii) fragility analysis, and (iv) loss analysis. This framework uses as interface variables, the ground motion Intensity Measure (IM), the Engineering Demand Parameter (EDP) and the Damage Measure (DM) to estimate the occurrence rate of a Decision Variable (DV). Figure 1.1 illustrates the PBEE model and the interface variables IM, EDP, DM and DV. This methodology is applied in this thesis for building specific loss estimation as the main framework, and all four steps of PBEE will be somehow addressed in different parts of this document as is explained in the following section.

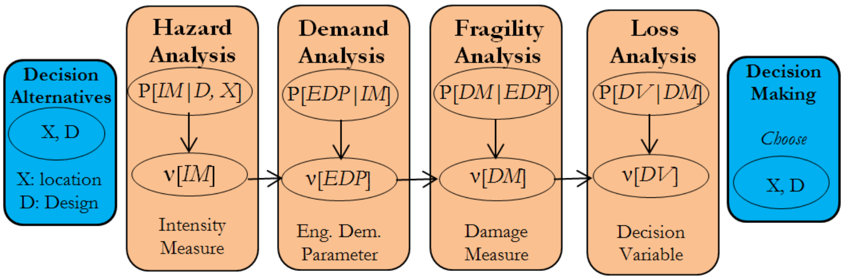

Figure 1.1. Schematic illustration of the Performance-Based Earthquake Engineering (PBEE) and the interface variables of IM, EDP, DM and DV.

Despite the vast amount of studies present in literature for generation and optimization of PBEE framework, there are still many aspects that could be further investigated. Specifically in the first two steps of Probabilistic Seismic Hazard Analysis (PSHA) and

Probabilistic Seismic Demand Analysis (PSDA), a couple of improvements in PSHA, record selection and structural modelling need further attentions as follows:

First, one of the most important steps in the procedure is a good choice of the IM. Commonly, PSHA is performed for this IM and is used in the ground motion selection in order to perform nonlinear dynamic analysis. This IM is a conditioning ground motion characteristic since it is then used for estimation of the response of the building. The choice of such IM is essentially critical because: (i) it should be a property of the ground motion that well represents the seismic severity of the site, on one hand, in addition; (ii) it should be a good predictor of the buildings response, on the other hand. In other words, the response of the building is somehow filtered through the conditioning IM. These two characteristics are referred to as *sufficiency* and *efficiency*. Sufficiency requires that the response of the building is only dependent in variability of IM and when used for prediction of the response of the building; the variability in other ground motion metrics does not alter the predicted response. High efficiency; on other hand, improves the accuracy of the response estimates even by use of few number of nonlinear dynamic analysis.

This IM is commonly chosen to be the 5% damped linear spectral acceleration at a given period which is most often taken as the fundamental period of the structure, $Sa(T1)$. Even though, $Sa(T1)$ was shown to be an efficient and sufficient IM, in many cases, some studies showed that it has a poor performance in other cases such as near-fault sites, response estimation of 3-D models or even with respect to collapse assessment or response estimation of different EDPs within 2-D models when higher mode effects are important or structural period elongation due to nonlinearity [Shome, 1999; Baker and Cornell, 2005; Luco and Cornell, 2007b; Lucchini *et al.*, 2011; Faggella *et al.*, 2013]. However, a realistic assessment of building economic losses and collapse, induced by earthquakes requires monitoring several response measures both story-specific and global. To address this shortcoming some alternatives have been proposed. One approach is using more complex IMs that can be a better predictor of the response. One such IM is the Inelastic spectral displacement (*Sdi*) [Tothong and Cornell, 2007] which was shown to be a good predictor of the nonlinear response of 2-D models. Another solution would be to benefit from using multiple ground motion intensity measures in scalar or vector format that are, in general, correlated. Spectral acceleration averaged in a period range [Cordova, *et al.* 2000 followed by Vamvatsikos, and Cornell 2005, Mehanny, 2009, Bianchini, *et al.* 2010, among others] is a scalar IM that can serve this requirement. Another approach is the application of a vector of IMs rather than a scalar so that the response will be well predicted and consequently more information of the ground the ground motion will be considered in the procedure [Bazzurro, 1998; Shome *et al.,* 1998; Bazzurro and Cornell, 2001; Bazzurro *et al.,* 2009, 2010]. Although these IMs have been tested in building response estimations, due to their complexity in PSHA, they have not been widely (if any) used in practice.

Second, another important step of the PBEE for building specific loss estimation when nonlinear dynamic analysis is used is the selection of an appropriate ground motion record set. Record selection is a tool that links the building response and seismic hazard of the site. Considerable attempts have been devoted in finding robust methodologies for selection of records that are consistent with the hazard of the site such as Conditional Mean Spectrum (CMS) [Baker and Cornell, 2006; Baker, 2011], Conditional Spectrum (CS) [Jayaram *et al.* 2011] and Generalised Conditional Intensity Measure (GCIM) approach [Bradley, 2010a] among others. The main scope of these methodologies has been focused on addressing the sufficiency with respect to spectral shape. These methodologies, however, have been mainly based on the simple conditioning IMs (e.g. spectral acceleration at single period) and other innovative IMs mentioned above have been rarely used in record selection, although they have been used in response prediction.

Third; most of the studies performed in the generation of the PBEE are based on the two-dimensional structural models whereas the three-dimensional buildings cannot always be reduced into two-dimensional models. For instance, for torsionally un-restrained buildings or for the buildings with very different behaviours in two main orthogonal directions, it is necessary to gauge the building response through a reasonably refined model. This objective is rarely achievable via simple 2-D models. In addition, there are structural and non-structural components in a building that are sensitive to the building excitation from multiple directions. For instance, masonry infill walls located within reinforced concrete frames are prone to in-plane and out-of-plane damages which are excited from excitations from both orthogonal directions. Moreover, given the interaction of the in plane and out-of-plane response, 2-D models fail in appropriate simulation of their behaviour.

1.2 **RESEARCH OBJECTIVES AND CONTRIBUTIONS**

Issues explained in the previous subsection motivated this study to give a fresh look into the full procedure of PBEE trying to challenge the most common approaches and discuss possible improvements based on creative methodologies. The main scope has been the evaluation of different approaches, all accepted in practice and legitimate to be used in building response estimation and loss calculations in order to compare their effectiveness in terms of simplicity of use and their improvement in accuracy. The objectives of this study could therefore be summarised as:

1. Implementation of Vector Probabilistic Seismic Hazard (VPSHA) software based on a simple 'indirect' approach that uses the results of the available Scalar PSHA software.
2. Implementation of PSHA for the averaged spectral acceleration in a period range under OpenQuake.
3. Comparison of the effectiveness of different scalar and vector IMs in structural response estimation, collapse prediction and loss estimation in building specific risk assessment of 3-D infilled reinforced concrete models.
4. Development of software for Conditional Spectra based record selection methodology based on alternative conditioning IMs other than simple spectral

accelerations as well as its application in risk based assessment of 2-D reinforced concrete structural model.

5. Development of a record selection methodology to be used in portfolio loss estimation incorporating the seismicity of multiple-sites.

1.3 OUTLINE OF THESIS

This dissertation consists of six chapters. The content of each chapter is outlined in the following paragraphs. It should be noted that, all chapters of this thesis could be read independently and each one addresses a subject that could be followed without aid of the other chapters. Anywhere in the text, if necessary, the reader is referred to other chapters for more information. In addition, in order to keep the length of each chapter reasonably short, the main methodologies, results and findings are presented in the body of the thesis and the additional, supplementary results and discussions are provided in Appendices for interested readers.

Chapter 1 explains the motivations, importance and the need for application of alternative Intensity Measures in the Performance Based Earthquake Engineering procedure in response estimation and record selection. In *Chapter* 2, the methodology used for computation of the Vector Probabilistic Seismic Hazard Analysis based on the conventional *direct* approach and the most recent *indirect* approach are explained. VPSHA is implemented in software as a post processor to scalar PSHA results based on the indirect approach. A group of candidate scalar and vector IMs based on spectral acceleration values, ratios of spectral acceleration values, and spectral accelerations averaged over a period range are defined. These IMs are used as structural response predictors of 3-D models of reinforced concrete buildings described in *Chapter* 3.

In *Chapter* 3, the advantages and disadvantages of using scalar and vector ground motion IMs are discussed for localized seismic response assessment of 3-D buildings. Candidate IMs are spectral accelerations, at a single period (*Sa*) or averaged over a period range (*AvgSA*). Consistent scalar and vector PSHA results were used to compute the response hazard of the tested 3-D building models. The response hazard curves were computed for three buildings with reinforced concrete infilled frames using the different IMs as predictors and the results were discussed on defining criteria for the choice of appropriate IMs based on different objectives and different EDP types of interest. In *Chapter* 4, the full framework of PBEE in loss computations using different scalar and vector IMs examined in previous chapters for 3-D structural models is further investigated. A methodology for consideration of fragilities for building components, sensitive to multiple EDPs, is proposed. The repair cost annual rate of exceedance based on different approaches is compared and the effectiveness of each with respect to others is compared.

In *Chapter* 5, a new approach for hazard consistent record selection based on Conditional Spectrum (CS) is proposed. The methodology uses alternative conditioning IMs of spectral accelerations averaged in a period range (*AvgSA or* I_{NP}) as a development in both addressing the sufficiency by keeping hazard consistent spectral shape and improving the efficiency in structural response estimation. The methodology is then applied for nonlinear dynamic analysis of 2-D reinforced concrete structures with different heights (4-, 7-, 12- and 20-stories). Discussions on different features of application of *AvgSA* in record selection and response estimation is provided in order to upgrade the PBEE in loss estimation and collapse risk assessment.

In *Chapter* 6, a methodology for record selection scheme to be used in building portfolio loss estimation is proposed. When performing loss assessment of a geographically dispersed building portfolio, the response or loss (fragility or vulnerability) function of any given archetype building is typically considered to be a consistent property of the building itself. On the other hand, recent advances in record selection have shown that the seismic response of a structure may not be independent of the nature of the hazard at the site of interest. This apparent contradiction begs the question: Are building fragility and vulnerability functions independent of site, and if not, what can be done to avoid having to reassess them for each site of interest? In *chapter* 6, we show that there is a non-negligible influence of the site, the degree of which depends on the intensity measure adopted for assessment. Employing a single-period (e.g., first-mode) spectral acceleration would require careful record selection at each site and result to significant site-to-site variability. On the other hand, an intensity measure comprising the geometric mean of multiple spectral accelerations would considerably reduce such variability, while in tandem with a conditional spectrum approach that accounts for multiple sites, it can offer a viable approach for incorporating the effect of site-dependence into fragility and vulnerability estimates. Finally, *Chapter* 7 summarises the outcomes of this research as well as providing recommendations for future pertinent studies.

2. VECTOR AND SCALAR IMS IN STRUCTURAL RESPONSE ESTIMATION: HAZARD ANALYSIS

2.1 INTRODUCTION

Performance-based earthquake engineering (PBEE) [Cornell and Krawinkler, 2000] has become commonplace in the industry for assessing response of buildings and other structures subjected to seismic loading. Studies based on PBEE are now routinely used by a variety of stakeholders such as building owners, developers, insurers, lending institution and earthquake engineers. For instance, owners of important buildings use it to make critical decisions about buying an appropriate level of earthquake insurance or identifying a retrofitting solution. Engineers use it for designing structural components to withstand forces and control displacements induced by target design ground motions with a margin of safety consistent with well performing, code-compliant structures. Regardless of the specific PBEE application, it is critical that estimates of the likelihood that a structure's response exceeds a given level of severity, ranging from onset of damage to incipient collapse, be as accurate as reasonably possible.

To increase the accuracy of estimating the structure's response, engineers have taken advantage of the computational capabilities of modern computers by developing more realistic two-dimensional (2-D) and three-dimensional (3-D) numerical models. These computer models are subjected to many different ground motions of different intensities to assess the structure's performance. Statistical techniques are typically used to provide functional relationships between the IMs of the ground motion and response measures that are associated with required levels of performance (e.g., operational, life safety or collapse).

The response of such complex models, however, is better estimated by monitoring multiple response measures, which are often referred to as Engineering Demand Parameters (EDPs). In turn, estimates of the maximum values of these measures are better predicted by a pool of IMs of the ground motion in both horizontal (and sometimes vertical) directions rather than by a single IM. For example, a good predictor of Maximum Inter Story Drift Ratio in the X- direction of a building (MIDRX) may be the spectral acceleration at the first period of vibration, T_{1x}, of the structure in its X-direction, $Sa_x(T_{1x})$; and similarly, $Sa_y(T_{1y})$ is a good predictor for MIDRY, where T_{1y} is the first period of vibration of the structure in its Y-direction. The collapse of a building, however, is more likely to happen when both MIDRX and MIDRY and, therefore, $Sa_x(T_{1x})$ and $Sa_y(T_{1y})$, are large rather than when either one is large. In addition, damage to structural, non-structural components and equipment of a building are better estimated by different EDP types (e.g.

peak floor spectral ordinate and maximum inter story drifts), whose estimation is better served by utilizing different appropriate IMs.

If EDPs are estimated via multiple IMs, the long-term risk computations require the convolution of IMs versus EDPs relationships [FEMA-P-58, 2012] and, therefore, the knowledge of the joint hazard probability distributions of the (generally correlated) IMs at the building site. The methodology for computing the joint hazard was first introduced in 1998 and was called vector-PSHA [Bazzurro, 1998; Bazzurro and Cornell, 2001 and 2002] or VPSHA for short. A few software programs were developed since for such a purpose [Bazzurro, 1998; Thio, 2010; 2003; 2010] but were limited to a vector of two IMs and were not capable of providing the disaggregation of the joint hazard. To avoid the complexity of the joint hazard computation for a vector of IMs, researchers over the years introduced several complex scalar IMs that are combination of multiple IMs [e.g., Fajfar *et al.,* 1990, Cordova *et al.,* 2002, followed by Vamvatsikos and Cornell, 2005, Luco *et al.,* 2005a; Luco and Cornell, 2007, Mehanny, 2009, Bianchini *et al.,* 2010, Bojórquez and Iervolino, 2011]. These complex IMs are often more effective in the prediction of EDPs than each single IM that compose them but arguably less effective than considering a vector of those IMs in the response prediction.

To help promoting the use of VPSHA, a methodology was developed and implemented [Bazzurro *et al.,* 2009 and 2010] that allows the computation of the joint hazard using results from any standard scalar PSHA software. This “indirect” approach to VPSHA is more computationally efficient than the original VPSHA “direct” integration method. It also has a major advantage over the direct integration method: it can accommodate a higher number of Random Variables (RVs) without significant loss of joint hazard accuracy.

In this Chapter, we review the direct and indirect VPSHA methodologies and elaborate on the pros and cons of each. The “indirect” method is then used to compute the VPSHA for a set of IMs in terms of spectral acceleration and average spectral acceleration for a site close to Istanbul based on the scalar PSHA results computed using the software OpenQuake. In *Chapter 3*, these PSHA and VPSHA results are used to perform a risk-based assessment of three 3-D models of reinforced concrete infilled frame buildings of 3-, 5- and 8-stories typical of the European Mediterranean countries.

2.2 **VECTOR-VALUED PROBABILISTIC SEISMIC HAZARD ANALYSIS (VPSHA)**

As mentioned earlier, the original methodology for computing the joint hazard of multiple ground motion IMs (e.g., Peak Ground Acceleration, PGA, and $S_a(1.0s)$), which are dependent RVs [Bazzurro, 1998; Bazzurro and Cornell, 2001 and 2002], is based on direct integration of the joint probability density function (pdf) of the same IMs at a site caused by each earthquake considered in the analysis. The joint distribution of correlated IMs at a site, which can be modeled as a multivariate Gaussian distribution if the IMs are represented by their natural logarithms [Jayaram and Baker, 2008b], is computed separately for each earthquake scenario. The total hazard is obtained by summing the contributions from all scenarios weighted by their occurrence rates. This method contains no approximation besides the implicit numerical accuracy of the integration solver. This so-called "direct method" is considered in this study only to obtain a set of joint hazard results for the many ground motion IMs considered. These results are used as a benchmark to validate the results from the indirect method.

The joint Gaussian pdf conditional on the parameters of the earthquake (i.e., magnitude M, source-to-site distance R, number of standard deviations from the mean GMPE prediction, ε, the rupture mechanism, and the soil conditions) can be computed when ground motion prediction Equations (GMPEs) are available for the IMs involved and with the knowledge of their variance-covariance matrix. Inoue [1990] and, more recently, Baker and Jayaram [2008], Goda and Hong [2008] and Akkar *et al.* [2014], have empirically derived the correlation structure for spectral accelerations with different periods and different record component orientations. Figure 2.1(a) shows one example of such empirical correlation structure. In addition, Bradley [2011a, 2011b, 2012a, 2012b] obtained empirical correlations between a few alternative IMs, such as Peak Ground Velocity (PGV), cumulative intensity measures, and ground motion duration. For example, Figure 2.1(b) shows the contours of the joint pdf for S_a(1.0s) and S_a(0.3s) for a site with Vs_{30}=760 m/s located 7km from a M_w=7.3 event with a strike-slip mechanism as predicted by the GMPE by Boore and Atkinson [2008]. According to Baker and Jayaram [2008], the correlation coefficient for S_a(1.0s) and S_a(0.3s) is 0.5735 for this particular case. Although conceptually straightforward, direct integration is numerically challenging, especially when (a) high precision in the tails of the distribution is sought; (b) the number of earthquake scenarios is large, which is usually the case in realistic applications; and (c) the number of IMs exceeds three or four. In fact, to our best knowledge of direct-VPSHA codes in existence, the only software capable of carrying out the computations for more than two RVs is documented in Bazzurro *et al.* [2010] and all the previous studies are limited to only two RVs [Bazzurro, 1998; Thio, 2003; Gülerce and Abrahamson, 2010]. As a consequence, the so-called *direct approach*, due to its complexity and heavy numerical computations, has not been used much so far in the scientific and engineering communities. In the computational efforts in the direct method, one approach would be application of the Monte Carlo simulation. For instance, Bazzurro *et al.* [2010] used an integration algorithm based on a quasi-Monte Carlo simulation developed by Genz and Bertz, [1999, 2002]. Although, these integration techniques seem appealing, still it might not, in any way, alleviate the computational burden of the direct method. To overcome this hurdle, Bazzurro *et al.* [2009] proposed an alternative approach for the calculation of VPSHA based on processing only the results of available scalar PSHA codes. This is what we called here the *indirect method,* which is discussed in the next section.

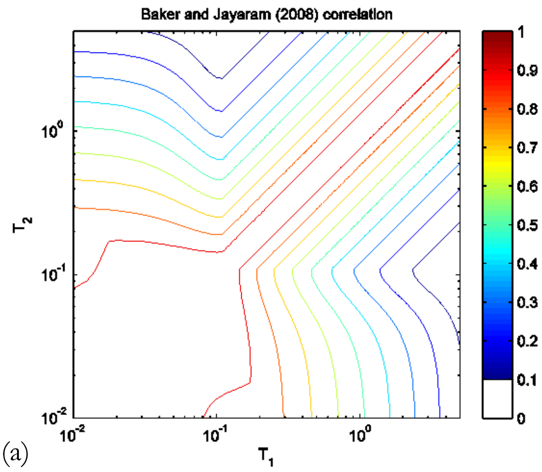

(a)

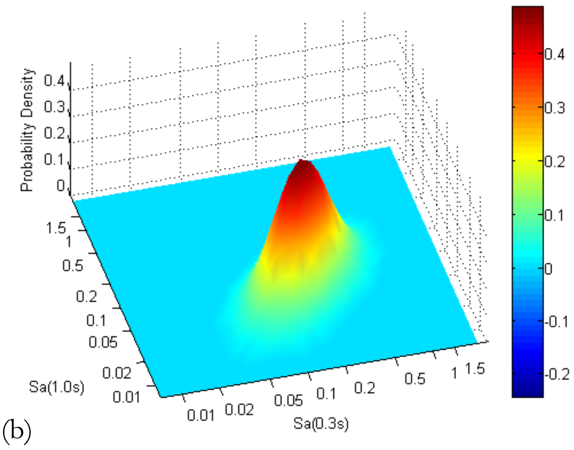

(b)

Figure 2.1. (a) The variance-covariance structure of log spectral accelerations at different periods in a random horizontal component of a ground motion record [Baker and Jayaram, 2008]; (b) the joint pdf for Sa(1.0s) and Sa(0.3s) for a given scenario earthquake (adopted from Bazzurro *et al.*, [2010]).

2.2.1 INDIRECT APPROACH TO VPSHA

Under the rational of joint normality of log IMs [Jayaram and Baker, 2008], the joint Mean Rate Density, MRD (for definition and details, see Bazzurro and Cornell, [2002]) or, similarly, the Mean Annual Rate (MAR) of occurrence of any combination of values of a pool of ground motion IMs could be computed only with the knowledge of the following items [Bazzurro *et al.,* 2009]:

1. ***Site-specific seismic hazard curves of the ground motion IMs considered in the vector*** — The vector of ground motion IMs is denoted herein as $\boldsymbol{S}$. This vector could include, for example, three parameters: the spectral acceleration at two different periods in one of the horizontal directions, and at one period in the orthogonal horizontal direction. These periods could correspond, for example, to the first and second mode of vibrations of a building in the longitudinal directions and the first mode in the transverse direction. The three hazard curves corresponding to these periods can be obtained with any standard PSHA code.
2. ***The variance-covariance matrix of all the ground motion IMs***— Empirical estimates of this variance-covariance matrix are available in the literature as discussed in previous section (see the reference list for some such studies).
3. ***The disaggregation results from scalar PSHA*** — The joint distributions of all the basic variables, **X**, including M, R, ε, the style of faulting, the distance to the top of the co-seismic rupture, and all other variables required by the GMPE of choice that contribute to the joint occurrence of specific values of IMs at the site. This is a straightforward extension of the disaggregation results routinely available from standard scalar PSHA codes.

For brevity, following Bazzurro *et al.* [2009] the details of the methodology are presented below only for the case of three IMs that, in this specific case, are spectral accelerations. However, this approach, which requires some straightforward matrix algebra, is scalable to a larger number of (RVs) and can include any other ground motion parameters (e.g., ground motion duration, near-source forward-directivity pulse period, Arias intensity and cumulative absolute velocity) if the proper correlation structure and prediction equations are available. For simplicity, in the derivations below the RVs are treated as discrete rather than continuous quantities.

Let $\boldsymbol{S}=[Sa_1;Sa_2;Sa_3]$ denote the vector of RVs for which we seek to obtain the joint hazard expressed by the mean annual rate of occurrence of the three spectral acceleration quantities Sa_1, Sa_2 and Sa_3 in the neighborhood of any combination of three spectral acceleration values a_1, a_2 and a_3, respectively. Mathematically, this is $\mathrm{MAR}[Sa_1; Sa_2; Sa_3] = \mathrm{MAR}_{Sa1; Sa2; Sa3}[a_1; a_2; a_3]$. Note that Sa_1, Sa_2 and Sa_3 represent here the natural logarithm of the spectral accelerations but the logarithm operator has been dropped to avoid lengthy notations. The quantity $\mathrm{MAR}[Sa_1; Sa_2; Sa_3]$ could, for example, denote the Mean Annual Rate (MAR) of observing at a building site values in the neighborhood of (the natural logarithm of) 1.0g, 1.5g, and 0.8g for the spectral acceleration quantities at the periods of the first and second modes of vibration in the building longitudinal direction and the spectral acceleration at the period of the first mode in the building transverse direction. These spectral acceleration values may be related to the onset of an important structural limit-state determined from a statistical analysis of the response of a structure subjected to many ground motion records. Then, using the theorem of total probability, one can express the following:

$$\mathrm{MAR}[Sa_1;Sa_2;Sa_3] = \mathrm{P}[Sa_1 \mid Sa_2;Sa_3]\cdot \mathrm{P}[Sa_2 \mid Sa_3]\cdot \mathrm{MAR}[Sa_3], \tag{2.1}$$

where:

$$\mathrm{P}[Sa_1 \mid Sa_2;Sa_3] = \sum_{\mathbf{X}} \mathrm{P}[Sa_1 \mid Sa_2;Sa_3;\mathbf{X}]\cdot \mathrm{P}[\mathbf{X} \mid Sa_2;Sa_3], \tag{2.2}$$

Equation (2.2) represents the conditional distribution of Sa_1, Sa_2 and Sa_3. This term can be numerically computed by conditioning it to the pool of variables **X** in a standard PSHA that appear in the selected GMPE and integrating over all possible values of **X**, as shown on the right hand side of Equation (2.2). Exploiting the joint log normality of $\boldsymbol{S}$, for every possible value of **X**, the quantity P[Sa_1; Sa_2; Sa_3] can be computed simply with the knowledge of the variance-covariance matrix of Sa_1, Sa_2 and Sa_3 and the GMPE of choice. Further details on the mathematics are provided below. P[**X** | Sa_2; Sa_3] can be obtained via disaggregation and Bayes theorem as follows:

$$\begin{aligned}\mathrm{P}[\mathbf{X} \mid Sa_2;Sa_3] &= \frac{\mathrm{P}[\mathbf{X},Sa_2 \mid Sa_3]}{\sum_{X} \mathrm{P}[Sa_2 \mid Sa_3;\mathbf{X}]\cdot \mathrm{P}[\mathbf{X} \mid Sa_3]}\\ &= \frac{\mathrm{P}[Sa_2 \mid Sa_3;\mathbf{X}]\cdot \mathrm{P}[\mathbf{X} \mid Sa_3]}{\mathrm{P}[Sa_2 \mid Sa_3]}\end{aligned} \tag{2.3}$$

Where P[**X** | Sa_3] can be derived using conventional scalar PSHA disaggregation. P[Sa_2 | Sa_3; **X**], as for the P[Sa_1 | Sa_2; Sa_3; **X**] term above, can be computed with the knowledge of the variance-covariance matrix of Sa_2 and Sa_3 and the adopted GMPE. $\sum_{\mathbf{X}} \mathrm{P}[Sa_2 \mid Sa_3;\mathbf{X}]\cdot \mathrm{P}[\mathbf{X} \mid Sa_3]$ can be evaluated as explained above. MAR[Sa_3] is the absolute value of the discretized differential of the conventional seismic hazard curve for the scalar quantity Sa_3 at the site. After some simplifications, Equation (2.1) can be rewritten as follows:

$$\begin{aligned}&\mathrm{MAR}[Sa_1;Sa_2;Sa_3] = \mathrm{MAR}[Sa_3]\cdot\\ &\sum_{\mathbf{X}} \mathrm{P}[Sa_1 \mid Sa_2;Sa_3;\mathbf{X}].\mathrm{P}[Sa_2 \mid Sa_3;\mathbf{X}]\cdot \mathrm{P}[\mathbf{X} \mid Sa_3]\end{aligned} \tag{2.4}$$

The two first conditional terms in Equation (2.4) (i.e., P[Sa_1 | Sa_2; Sa_3; **X**] and P[Sa_2 | Sa_3; **X**] can be evaluated using the multivariate normal distribution theorem. In general, if $\boldsymbol{S} = [Sa_1, Sa_2, \ldots, Sa_n]^T$ is the vector of the natural logarithm of the random variables for which the joint hazard is sought, then $\boldsymbol{S}$ is joint normally distributed with mean, μ, and variance-covariance matrix, $\boldsymbol{\Sigma}$, i.e., in mathematical terms $\boldsymbol{S} =\sim \mathrm{N}(\boldsymbol{\mu}, \Sigma)$. If $\boldsymbol{S}$ is partitioned into two vectors, $\boldsymbol{S_1} = [Sa_1 ; Sa_2; \ldots, Sa_k]^T$ and $\boldsymbol{S_1} = [Sa_{k+1} ; Sa_{k+2}; \ldots, Sa_n]^T$, where $\boldsymbol{S_2}$ comprises the conditioning variables (in the example above $\boldsymbol{S_1} = [Sa_1]^T$ and $\boldsymbol{S_2} = [Sa_2, Sa_3]^T$), one can write the following:

$$S = \left[\frac{S_1}{S_2}\right] \sim \mathrm{N}\left(\left[\frac{\boldsymbol{\mu}_1}{\boldsymbol{\mu}_2}\right], \begin{bmatrix} \boldsymbol{\Sigma}_{11} & \boldsymbol{\Sigma}_{12} \\ \boldsymbol{\Sigma}_{21} & \boldsymbol{\Sigma}_{22} \end{bmatrix}\right) \tag{2.5}$$

For jointly normal distribution, the conditional mean and variance can be determined as:

$$S_1 \mid S_2 \sim \mathrm{N}(\boldsymbol{\mu}_{1|2}, \boldsymbol{\Sigma}_{1|2}), \tag{2.6}$$

$$\boldsymbol{\mu}_{1|2} = \boldsymbol{\mu}_1 + \boldsymbol{\Sigma}_{12}\boldsymbol{\Sigma}_{22}^{-1} \cdot (\mathbf{S}_2 - \boldsymbol{\mu}_2); \boldsymbol{\Sigma}_{1|2} = \boldsymbol{\Sigma}_{11} - \boldsymbol{\Sigma}_{12}\boldsymbol{\Sigma}_{22}^{-1}\boldsymbol{\Sigma}_{21} \tag{2.7}$$

Equation (2.1) can be generalized to n variables as follows:

$$\begin{aligned} &\mathrm{MAR}[Sa_1;Sa_2;Sa_3;...;Sa_{n\text{-}1};Sa_n] = \\ &\sum_X \mathrm{P}[Sa_1 \mid Sa_2;Sa_3;...;Sa_{n\text{-}1};Sa_n;\mathbf{X}] \cdot \mathrm{P}[Sa_2 \mid Sa_3;...;Sa_{n\text{-}1};Sa_n;\mathbf{X}] \\ &\cdot \mathrm{P}[Sa_3 \mid Sa_4;...;Sa_{n\text{-}1};Sa_n;\mathbf{X}] \cdot \mathrm{P}[Sa_{n\text{-}1} \mid Sa_n;\mathbf{X}] \cdot \mathrm{MAR}[Sa_n] \end{aligned} \tag{2.8}$$

2.3 DIRECT VERSUS INDIRECT APPROACHES

Bazzurro *et al.* [2010] performed a series of comparison tests between the results obtained by both "direct" and "indirect" VPSHA. That study shows that, while both methods have their respective strengths and weaknesses, the indirect method has several qualities that, arguably, make it superior to the direct integration method. The advantages of the indirect method are:

1) its implementation does not require much modification of already existing scalar PSHA codes;
2) It can compute the joint hazard for a higher number of IMs than the direct method;

3) it is computationally faster than the direct method for two reasons. First, integrating multivariate standard normal distributions with three or more dimensions with very high accuracy is typically an extremely time consuming task. It should be noted that the indirect method has also mathematical challenges, such as matrix inversions, which, however, require considerably lower computation time. Second, in the direct method multi-dimension integration needs to be repeated for every earthquake considered in the PSHA. In the indirect method, the number of events affects only the total run time of the scalar hazard analyses, which is negligible when compared to the total run time of a comparable joint hazard study.

4) It is easily scalable to higher dimensions of variables;

5) given its recursive nature, when adding the *n*-th dimension, the indirect method can re-use results previously computed for the first *n*-1 dimensions. Conversely, adding an additional dimension in the direct method requires restarting the hazard analysis.

In fairness, the "indirect" method has also some weaknesses such as:

1) it requires larger computer memory space than the direct method;

2) It yields results that are approximate when the number of bins used to discretize the domains of the RVs is limited, a restriction which becomes a necessity in applications with four or more IMs. However, a judicious selection of bins guided by disaggregation results can limit the error in the estimates of the joint and marginal MARs to values typically lower than 3% for the entire range of IMs of engineering significance (Bazzurro *et al.*, [2010]).

In light of the considerations above, the "Indirect VPSHA" methodology is applied herein to evaluate the joint hazard of vectors of IMs that contain average spectral accelerations over a period range and ratios of spectral accelerations at different periods. The definition of such IMs and the technicalities needed for their inclusion in the VPSHA framework are presented in the sections below.

2.4 AVERAGE SPECTRAL ACCELERATION

The average spectral acceleration, Sa_{avg}, is a complex scalar IM that is defined as the geometric mean of the log spectral accelerations at a set of periods of interest [Cordova *et al.*, 2000; Bianchini *et al.*, 2010]. These periods, for example, could be equally spaced in the range from $0.2 \cdot T_1$ to $2 \cdot T_1$, where T_1 is the first-mode elastic period of the structure. This array of periods might cover higher mode response and also the structural period elongation caused by the nonlinear behavior due to the accumulation of damage. Alternatively, perhaps more effectively, Sa_{avg} could be defined as the geometric mean of log spectral accelerations at relevant vibration periods of the structure, such as T_{1x}, T_{1y}, T_{2x}, T_{2y}, $1.5 \cdot T_{1x}$, and $1.5 \cdot T_{1y}$, where x and y refer to the two main orthogonal axes of the buildings and the indices 1 and 2 refer to the first and second vibration modes of the structure in those directions. Mathematically, Sa_{avg} can be defined in the following two equivalent ways:

$$Sa_{avg} = \left[\prod_{i=1}^{n} Sa(T_i) \right]^{1/n}, \tag{2.9}$$

$$\ln(Sa_{avg}) = \left(\frac{1}{n} \right) \cdot \sum_{i=1}^{n} \ln(Sa(T_i)) \tag{2.10}$$

Therefore, from Equation (2.10) it is clear that the mean and variance of $\ln(Sa_{avg})$are:

$$\mu_{\ln(Sa_{avg})} = \left(\frac{1}{n} \right) \cdot \sum_{i=1}^{n} \mu_{\ln(Sa(T_i))}, \tag{2.11}$$

$$\mathrm{var}(\ln Sa_{avg}) = \left(\frac{1}{n} \right)^2 \cdot \sum_{i=1}^{n} \sum_{j=1}^{n} \rho_{\ln Sa(T_i),\ln Sa(T_j)} \cdot \sigma_{\ln Sa(T_i)} \cdot \sigma_{\ln Sa(T_j)} \tag{2.12}$$

where $\mu_{\ln Sa(Ti)}$ and $\sigma_{\ln Sa(Ti)}$ are the logarithmic mean and standard deviation of spectral accelerations at the i-th period obtained from a standard GMPE and $\rho_{\ln Sa(Ti),\ln Sa(Tj)}$ is the correlation coefficient between $\ln Sa(Ti)$ and $\ln Sa(Tj)$. The correlation coefficient of two average spectral acceleration at two orthogonal directions, $Sa_{avgX} = \left[\prod_{i=1}^{n} \left(Sa_x(T_i) \right) \right]^{1/n}$ and $Sa_{avgY} = \left[\prod_{j=1}^{m} \left(Sa_y(T_j) \right) \right]^{1/\mathrm{m}}$, could be computed as follows:

$$\rho_{\ln Sa_{avgX},\ln Sa_{avgY}} = \frac{\sum_{i=1}^{n}\sum_{j=1}^{m} \rho_{\ln Sa_x(T_{ix}),\ln Sa_y(T_{jy})} \cdot \sigma_{\ln Sa_x(T_{ix})} \cdot \sigma_{\ln Say(T_{iy})}}{m \cdot n \cdot \sigma_{\ln Sa_{avgX}} \cdot \sigma_{\ln Sa_{avgY}}} \tag{2.13}$$

2.5 **SPECTRAL ACCELERATION RATIO: GMPE AND CORRELATION COEFFICIENTS**

The vectors of *IM*s considered here include both spectral accelerations and also ratios of spectral accelerations at different ordinates of the spectrum. Ratios are considered to avoid any negative collinearity effects [e.g., Kutner *et al.*, 2004] due to the presence of high correlation between spectral accelerations at different but closely spaced periods. This operation, however, requires the evaluation of correlation coefficients of ratios of spectral accelerations and spectral accelerations at different periods. Equations (14) and (15), which show such correlation coefficients, were derived based on the hypothesis of joint normality of the distribution of the logarithm of spectral accelerations.

$$\rho_{\ln[Sa(T_1)],\ln\left[\frac{Sa(T_3)}{Sa(T_2)}\right]} = \frac{\rho_{1,3} \cdot \sigma_1 \cdot \sigma_3 - \rho_{1,2} \cdot \sigma_1 \cdot \sigma_2}{\sigma_{3/2}}, \tag{2.14}$$

$$\rho_{\ln\left[\frac{Sa(T_2)}{Sa(T_1)}\right],\ln\left[\frac{Sa(T_4)}{Sa(T_3)}\right]} = \frac{\rho_{1,3} \cdot \sigma_1 \cdot \sigma_3 + \rho_{2,4} \cdot \sigma_2 \cdot \sigma_4 - \rho_{1,4} \cdot \sigma_1 \cdot \sigma_4 - \rho_{2,3} \cdot \sigma_2 \cdot \sigma_3}{\sigma_{2/1} \cdot \sigma_{4/3}} \tag{2.15}$$

in which $\rho_{i,j}$ is the correlation coefficient between $Sa(\mathrm{T}_i)$ and $Sa(Ti)$, $\sigma_{i/j}$ is $\sigma_{\ln\left[Sa(T_i)/Sa(T_j)\right]}$, the dispersion of the spectral acceleration ratio. The mean and variance of this variable can be computed using the following equations based on a preferred GMPE and the corresponding correlation coefficients:

$$\mu_{\ln\left[\frac{Sa(T_i)}{Sa(T_j)}\right]} = \mu_{\ln Sa(T_i)} - \mu_{\ln Sa(T_j)}, \tag{2.16}$$

$$\sigma^2_{\ln\left[\frac{Sa(T_i)}{Sa(T_j)}\right]} = \sigma^2_{\ln Sa(T_i)} + \sigma^2_{\ln Sa(T_j)} - 2 \cdot \rho_{\ln Sa(T_i),\ln Sa(T_j)} \cdot \sigma_{\ln Sa(T_i)} \cdot \sigma_{\ln Sa(T_j)} \tag{2.17}$$

where $\mu_{\ln Sa(Ti)}$ and $\mu_{\ln Sa(Tj)}$ are the mean logarithm (or, equivalently, the logarithm of the median) of values of $Sa(T_i)$ and $Sa(T_j)$ obtained from the GMPE.

2.6 SITE SPECIFIC SEISMIC HAZARD ANALYSIS

The OpenQuake [Monelli *et al.*, 2012] open-source software for seismic hazard and risk assessment, developed by the Global Earthquake Model (GEM) foundation, was used to perform the seismic hazard computations. These computations are based on the area source model and the Fault Source and Background (FSBG) model (black and red lines in Figure 2.2(a), respectively) developed during the SHARE Project [Giardini *et al.*, 2013]. The former model assumes a homogeneous distribution of earthquakes in time and space. Area sources are polygons, each one comprising a region of homogeneous seismic activity. The latter model uses fault specific information, most importantly the fault slip rate, to estimate earthquake activity rates. This is different from the area source model, which uses solely the earthquake catalog to estimate the rates of occurrence of earthquakes occurring in a zone. These SHARE models were constructed via an iterative process of collecting, reviewing and updating national and regional models [Giardini *et al.*, 2013]. We adopted the GMPE proposed by Boore and Atkinson [2008].

2.7 INTENSITY MEASURES TESTED IN THIS STUDY

The group of considered scalar and vector IMs is listed in Table 2.1. The effectiveness of these IMs in the estimation of building EDPs is compared in *Chapter 3* while herein we only address the details of the hazard analysis methodology carried out for each IM. The IMs selected here are different combinations of the predictors most commonly available to engineers, namely the elastic pseudo spectral accelerations at different periods used singularly or jointly for assessing the response of 3-D buildings (as opposed to 2-D models, as often done). Therefore, other more complicated nonlinear IMs, such as inelastic spectral displacement [Tothong and Cornell, 2007] are not considered here. Still, it is important to note that IMs of practically any complexity can be incorporated in the assessment without needing to rerun the structural analyses. As observed by Vamvatsikos and Cornell [2005], changing the IM is simply an exercise in post processing. On the other hand, the estimation of hazard will need to be repeated using appropriate GMPEs, which are available for all the IMs tested herein, but not necessarily for other less common ones (e.g., the so-called Fajfar Index, I_v defined in Fajfar *et al.*, [1990]).

Table 2.1. IMs considered in the response estimation

INTENSITY MEASURE (IM) **	**ABBREVIATION***
SCALAR IMs	
Natural logarithm of arbitrary spectral acceleration at the first modal period $\ln\left[Sa_x(T_{1x})\right]$ or $\ln\left[Sa_y(T_{1y})\right]$.	Sa_{S1}
Natural logarithm of the geometric mean of spectral acceleration at the average period, $\ln\left[Sa_{g.m.}\left(\bar{T}=\left(T_{1x}+T_{1y}\right)/2\right)\right]$.	Sa_{S2}
$\ln\left[Sa_x\left(\alpha_1\cdot T_{1x}\right)\cdot Sa_x\left(T_{1x}\right)\cdot Sa_x\left(\alpha_u\cdot T_{1x}\right)\cdot Sa_y\left(\alpha_1\cdot T_{1y}\right)\cdot Sa_y\left(T_{1y}\right)\cdot Sa_y\left(\alpha_u\cdot T_{1y}\right)\right]$	Sa_{S3}
$\ln\left(\left[\prod_{i=1}^{n}\left(Sa_x\left(T_{xi}\right)\right)\right]^{1/n}\right)\cdot\ln\left(\left[\prod_{j=1}^{m}\left(Sa_y\left(T_{yj}\right)\right)\right]^{1/m}\right)$, $\alpha_1\cdot T_1\le T_i\le\alpha_u\cdot T_1, m=n=10$ §	Sa_{S4}
Natural logarithm of the geometric mean of Peak Ground Acceleration, $ln[PGA_{g.m.}]$	PGA
VECTOR IMs	
$\ln\left\{Sa_x(T_{1x}),\frac{Sa_y(T_{1y})}{Sa_x(T_{1x})},\frac{Sa_x(1.5\cdot T_{1x})}{Sa_y(T_{1y})},\frac{Sa_y(1.5\cdot T_{1y})}{Sa_x(1.5\cdot T_{1x})}\right\}$	Sa_{V1}
$\ln\left\{Sa_{g.m.}(\bar{T}),\frac{Sa_{g.m.}(0.5\cdot\bar{T})}{Sa_{g.m.}(\bar{T})},\frac{Sa_{g.m.}(1.5\cdot\bar{T})}{Sa_{g.m.}(0.5\cdot\bar{T})}\right\}$	Sa_{V2}
$\ln\left\{\left[Sa_x\left(\alpha_1\cdot T_{1x}\right)\cdot Sa_x\left(T_{1x}\right)\cdot Sa_x\left(\alpha_u\cdot T_{1x}\right)\right]^{1/3},\left[Sa_y\left(\alpha_1\cdot T_{1y}\right)\cdot Sa_y\left(T_{1y}\right)\cdot Sa_y\left(\alpha_u\cdot T_{1y}\right)\right]^{1/3}\right\}$	Sa_{V3}
$\ln\left\{\left(\left[\prod_{i=1}^{n}\left(Sa_x\left(T_{xi}\right)\right)\right]^{1/n}\right),\left(\left[\prod_{j=1}^{m}\left(Sa_y\left(T_{yj}\right)\right)\right]^{1/m}\right)\right\}$,	Sa_{V4}

*All the *IMs* are based on natural logarithm transformation. The notation ln is removed from the abbreviations for brevity
** α_1 is equal to 0.8, 0.2 and 0.2 for the 3-, 5- and 8-story, respectively. α_u is equal to 1.5 in all cases.
§ The periods are equally spaced.

The spectral acceleration at the first modal period of the structure, $Sa(T_1)$, termed Sa_{S1} in Table 2.1, is the most commonly adopted scalar IM for seismic response assessment of 2-D structural models. However, the selection of the value of T_1 might not be obvious for 3-D structural models of buildings especially when the first modal periods in the two main horizontal directions are significantly different.

Alternatively, the engineer may decide to carry out the assessment for each direction separately, hence disregarding the interaction between the responses of the building in the two main horizontal axes. This latter approach is often adopted with the understanding that it produces conservative results. In this context, FEMA P-58 [2012] suggests using the spectral acceleration at the average of the period in the two main horizontal orthogonal axes of the building, $\overline{T} = (T_1 + T_2)/2$, termed Sa_{S2}. However, this approach might not be effective for structures with well-separated periods in the two horizontal axes.

In addition, as the structure becomes nonlinear, the structural response is more correlated with spectral acceleration at vibration periods longer than the linear elastic response at T_1. Vamvatsikos and Cornell [2005] and Baker and Cornell [2008a] showed also that for tall structures one needs to account for both longer and shorter periods rather than just T_1 to appropriately describe both the inelastic response and the spectral shape (related to higher modes) expressed in terms of Maximum IDR. On the other hand, a desirable IM should be an efficient and sufficient predictor of *multiple response quantities* (i.e. IDRs and peak floor accelerations, PFAs, along the structure's height) rather than performing very well for predicting one EDP type and very poorly for predicting others. An efficient IM provides low dispersion of the predicted response given IM and a sufficient IM offers statistical independence of the response given IM from ground motion characteristics, such as magnitude, distance, etc. Efficiency helps reduce the number of time history analysis for reliable assessment of response, while sufficiency is a *sine qua non* requirement for combining PSHA with structural analysis results. See Luco and Cornell [2007b] for more detailed definitions of efficiency and sufficiency. As discussed by Kazantzi and Vamvatsikos [2015b] and in *Chapter 3*, an IM that is effective for predicting both IDR and PFA responses at all story levels should combine spectral accelerations at a wide range of periods bracketing the first mode. To this end, the hazard calculations for several scalar and vector IMs are addressed here.

Sa_{V1} and Sa_{V2} are vectors of $Sa(T_1)$ and the ratio(s) of spectral accelerations at different spectral ordinates and orientations. In Sa_{V1} the focus has been on addressing the IDR response estimation and, therefore, we utilized the arbitrary spectral acceleration component (Sa_{arb}, referred to Sa_x or Sa_y in Table 2.1) since it can capture the 3-D response of both orthogonal directions separately. This IM, however, is expected to be less effective in PFA response estimation since it lacks information about spectral accelerations at periods consistent with higher modes of the structure. Sa_{V2}, on the other hand, is a three-component vector IM based on the geometric mean of spectral acceleration at $\overline{T_1}$ and two periods lower and higher than $\overline{T_1}$. This IM is expected to be appropriate for both IDR and PFA response prediction; however, it might fail in capturing the 3-D modeling effect, as explained earlier. Two scalar IMs in the form of average spectral acceleration (Sa_{S3} and Sa_{S4} in Table 2.1) were also defined using the geometric mean to combine the intensities in two orthogonal directions. Sa_{S3} is constructed with the spectral accelerations at three building-specific spectral ordinates in both directions for a total of six components, whereas Sa_{S4} is defined over ten periods for a total of 20 components. Either of these two IMs is expected to be promising for different applications. Again, since Sa_{S3} and Sa_{s4} combine the two orthogonal excitations with equal weights, they are expected to be less effective for 3-D asymmetric structural models whose vibrations may be very different in the two main orthogonal directions. Hence, Sa_{V3} and Sa_{V4} are introduced as the corresponding vector IMs by separating the contribution of each horizontal ground motion component into a two-element vector.

In the range of periods longer than T_1, the value of T=1.5·T_1 has been selected as an appropriate upper period limit for all IMs. This was decided based on a preliminary nonlinear response history analysis for the three buildings where $Sa(T=1.5 \cdot T_1)$consistently provides the lowest dispersion in response estimation for all directions. As stressed earlier, in the range of periods lower than T_1, one needs to provide a balance in the efficiency of the same IM in the estimation of both PFA and IDR. It is well known that values of PFA are considerably more influenced by higher modes compared to those of IDR. In other words, adding many short period ordinates to a vector IM, or averaged spectral acceleration scalar IM, may help in PFA prediction only but it may not be as effective for predicting IDR. Opposite considerations hold when adding many spectral ordinates with periods longer than the fundamental one in the predictive vector. Therefore, care should be exercised when selecting the relative weight placed on the short versus the long period ranges for each building. In this study, minimum periods of 0.8, 0.2 and 0.2 of T_1 for the considered 3-, 5- and 8-story buildings, respectively, were observed to provide such balance in the response prediction. The PGA is also considered as a candidate IM here because it is expected to be a valuable predictor for estimating PFA, especially for short and relatively rigid structures or at lower floors of taller buildings, as confirmed in *Chapter 3*. Finally, as mentioned earlier, to avoid problems caused by multi-collinearity of different predictors in the vector IMs of Sa_{V1} and Sa_{V2}, all spectral accelerations other than the first component of the vector (i.e., $Sa_x(T_{1x})$) are normalized to the previous component in the series.

2.8 **PSHA AND VPSHA ANALYSIS RESULTS**

A site in the south of the Sea of Marmara in Turkey was considered in this study and all earthquake sources within 200 km from it where included in the hazard calculations. Figure 2.2(a) shows the site map along with the considered faults. A reference “stiff or soft rock” soil class with average shear wave velocity over the top 30m (Vs_{30}) equal to 620 m/s was assumed to be present at the site. The minimum magnitude of engineering significance used in the hazard analysis was M_w =4.5. The hazard calculations are based on the GMPE proposed by Boore and Atkinson [2008] that provides GMRotI50 of spectral acceleration (i.e., a median value of the geometric mean over multiple incident angles) rather than the geometric mean of the spectral accelerations of two recorded horizontal components or the spectral acceleration of one arbitrarily chosen component. Baker and Cornell [2006] showed that even though the GMRotI50, the geometric mean ($Sa_{g.m.}$) and the arbitrary component (Sa_{arb}) have statistically similar median values for any given earthquake at any given location, their logarithmic standard deviations are different (the values for Sa_{arb} being

(a)

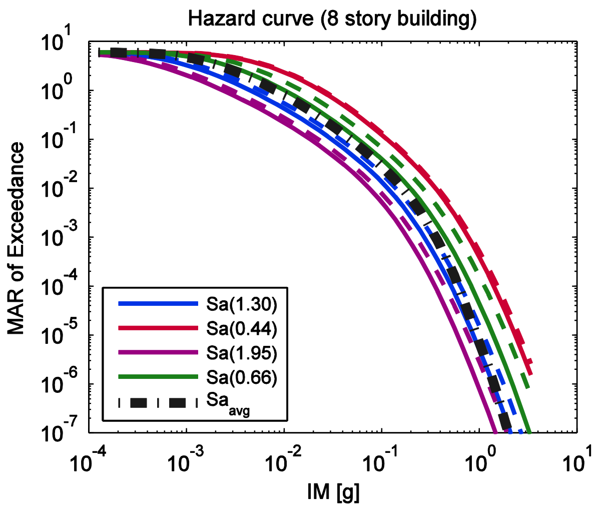

(b)

Figure 2.2. Hazard Analysis results: (a) Site map showing the location of fault sources (blue lines), background source model (red lines), the area source model (black lines), and the assumed location of the building (yellow pin), b) Mean Annual Rate (MAR) of exceedance of Sa at periods of relevance to the 8-story building (see *Chapter* 3) (solid line: $Sa_{g.m.}$, dashed line: Sa_{arb}) and Sa_{avg} made of the same spectral accelerations.

higher due to the component-to-component variability). Therefore, one should be careful in consistently applying the same definition of spectral acceleration both in hazard calculations and in the response assessment. In this study, consistent definitions of spectral acceleration variables (arbitrary component or geometric mean) were used by modifying the standard deviation of the applied GMPE, according to the definition of spectral acceleration considered.

Figure 2.2(b) shows the hazard curves related to the 8-story building described in the companion paper for spectral acceleration at four different periods (solid lines for the geometric mean and dashed lines for the arbitrary component) corresponding to T_{1x}=1.30s and T_{1y}=0.44s and periods 1.5 times the first vibration mode of each direction, along with the curve for their average, Sa_{avg}. As mentioned earlier, the VPSHA *indirect* approach was implemented using the PSHA output of OpenQuake. The disaggregation results for finely discretized bins of 0.5 magnitude unit and 2.5 km distance were considered. In the PSHA, the hazard curves for the spectral accelerations were computed for values ranging from 0.0001g to 3.5g with a logarithmic increment of ln(0.2) and the spectral acceleration ratios ranging from 0.01 to 50 with a constant logarithmic increment of ln(1.17). Such fine discretization of spectral acceleration hazard curves was employed as required to achieve sufficiently accurate estimates of the marginal MARs (see Bazzurro *et al.*, [2010]). Bazzurro *et al.*, [2010], performed a sensitivity analysis on the effect of bin size on the precision of the method and the interested reader is referred to that study.

The same GMPE [Boore and Atkinson, 2008] and site conditions were adopted for VPSHA for consistency reasons. In a real, complex case problem in which several GMPEs are considered in a logic tree format, the VPSHA indirect computations may also be complicated by the handling of multiple GMPEs and the corresponding proportions, which was avoided here. An additional simplification adopted is the assumption that all the earthquakes were generated by a strike-slip rupture mechanism. This eliminates the need for rupture mechanism bookkeeping when disaggregating the site hazard. The correlation coefficients proposed by Baker and Jayaram [2008] via Equations (2.13), (2.14) and (2.15) were used for the computation of the hazard of complex IMs. Note that, for simplicity, these correlation coefficients were applied to every scenario event, although a recent study [Azarbakht *et al.*, 2014] has shown some dependence of the correlation structure on magnitude and distance.

As an example, Figure 2.4(c) shows VPSHA results for a selected vector case with two components. Figure 2.4(d) displays the M and R disaggregation of the joint hazard at $Sa(T_1=0.57\text{s})=0.067\text{g}$ and $Sa(1.5 \cdot T_1)/Sa(T_1)=1.021$, which are IMs relevant for the 3-story building analyzed in *Chapter 3*. The code generated in this study is capable of computing the joint hazard for a vector up to 4 components. One simple, but not necessarily sufficient, validation for the vector PSHA is the comparison between the hazard curves obtained using scalar PSHA for each IM in the vector, with the marginal distributions of the joint IM distribution obtained from VPSHA for the same IMs. Such validation was performed for the entire vector computations tested here and good consistency was observed in all cases. Figure 2.4 (c) shows one such comparison for the VPSHA case of equaling pairs of $Sa(1.5 \cdot T_1)/Sa(T_1)$ and $Sa(T_1)$ values (see Figure 2.4(a)). In Figure 2.4(b), the MAR of exceeding for this example is shown.

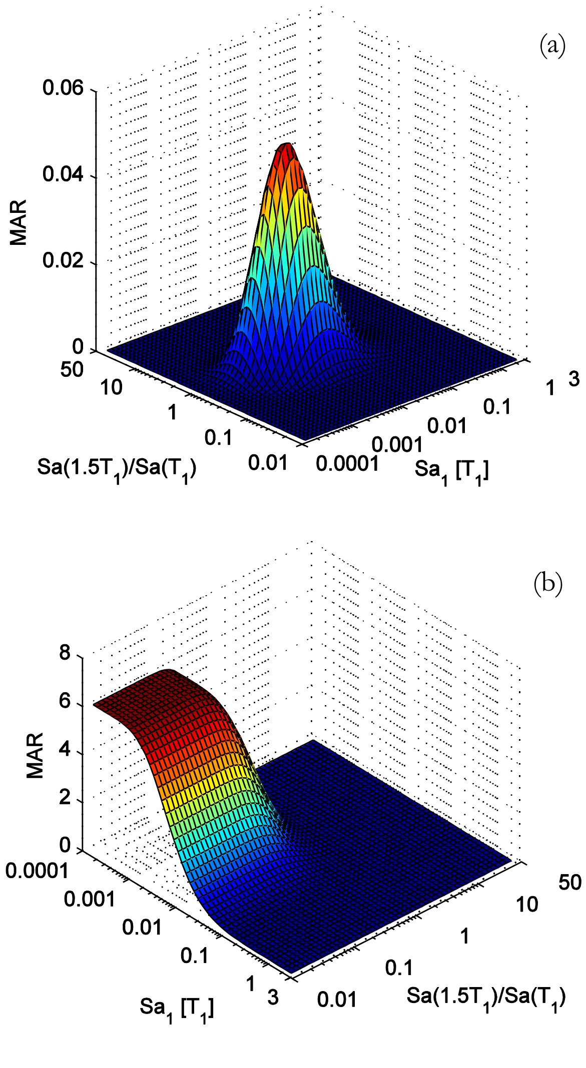

Figure 2.3. Hazard Analysis results: (a) MAR of equaling joint values of $Sa_x(T_{1x})$ and of $Sa_x(1.5 \cdot T_{1x})/Sa_x(T_{1x})$ at T_{1x}=0.57s, (b) MAR of exceeding joint values of $Sa_x(T_{1x})$ and of $Sa_x(1.5 \cdot T_{1x})/Sa_x(T_{1x})$ at T_{1x}=0.57s

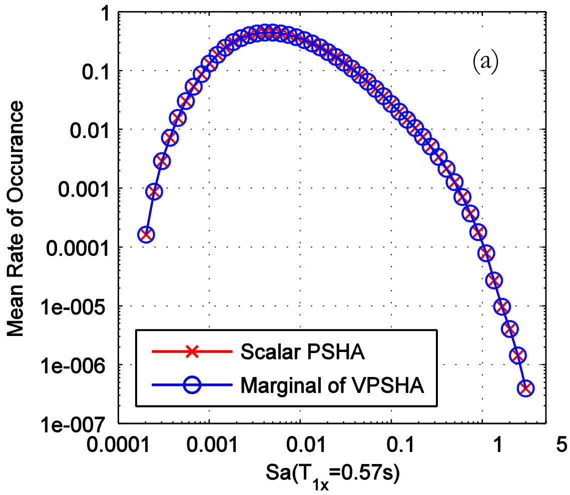

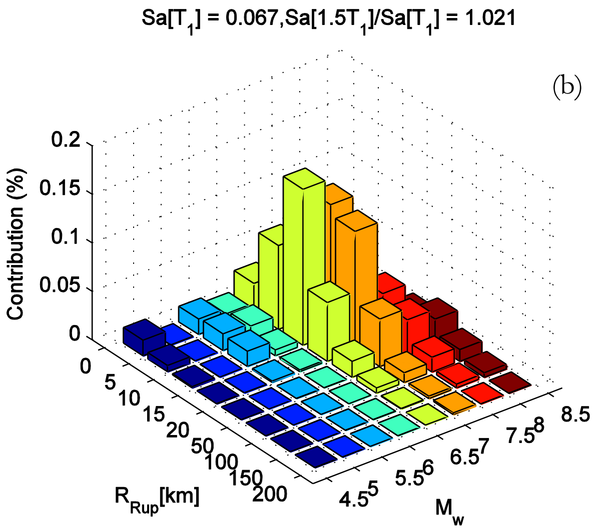

Figure 2.4. Hazard Analysis results: a) comparison of the MAR of equaling derived from the scalar PSHA and from the marginal of VPSHA; b) disaggregation results for a joint MAR of equaling at a given ground motion intensity level with $Sa_x(T_{1x})$ =0.067g and $Sa_x(1.5\cdot T_{1x})/Sa_x(T_{1x})$=1.021 at T_{1x}=0.57s.

It should be noted, again, that to achieve a good accuracy of the hazard estimates the domain of all the random variables considered in the VPSHA calculations must be well discretized especially around the region where the probability density function is more concentrated. For instance, the joint MAR of equaling for $Sa_x(T_{1x})$ and $Sa_x(1.5\cdot T_{1x})/Sa_x(T_{1x})$ ratio for T_{1x} =0.57s shown in Figure 2.4(a) needs a fine discretization especially in the 0.5

to 1.0 range for the $Sa_x(1.5{\cdot}T_{1x})/Sa_x(T_{1x})$ ratio and of 0.001g to 1.0g for $Sa_x(T_{1x})$. As explained earlier, in this study a constant and rather fine discretization was considered to cover all the ranges appropriately. However, the user can adopt different discretization schemes with respect to the importance of each adopted range, perhaps to reduce the analysis time and to reach the accuracy of interest.

An improvement of this software for carrying out VPSHA compared to previous ones is the ability to compute the contributions to the joint hazard in terms of the *M*, *R*, and, if needed, the rupture mechanism of the causative events. Although not implemented here, the joint hazard disaggregation could also be extended to identify the latitude and longitude of the events, so that the specific faults that control the hazard can be uniquely recognized [Bazzurro and Cornell, 1999]. Several refinements of the disaggregation exercise can be carried out to meet the requirements of the users. For example, in a 2-D joint hazard case, the disaggregation can be implemented to extract the contributions to the MAR of "equaling" a certain joint IM cell (e.g., $Sa(0.3\text{s})=0.2\text{g}$ and $Sa(1.0\text{s})=0.1\text{g}$), or to the MAR of equaling or exceeding it (e.g., $Sa(0.3\text{s}) \geq 0.2\text{g}$ and $Sa(1.0\text{s}) \geq 0.1\text{g}$). One example of such results is shown in Figure 2.4(d). The VPSHA software developed for this study in MatLab is available at Kohrangi, 2015c.

2.9 INCORPORATING MULTIPLE GMPES IN VPSHA

In a complex PSHA, where multiple GMPEs are used, one could proceed either by using a single GMPE, but accepting some level of inaccuracy; or by incorporating all the GMPEs in computing the median and standard deviation of the corresponding IM. In the latter option, the values of the median and the standard deviation needed in equations (2.18) and (2.19) could be approximately obtained using the following equations:

$$\mu_{\ln \mathrm{IM}_i|rup} \approx \sum_k p_k \mu_{\ln IM_{i,k}|rup} , \tag{2.18}$$

$$\sigma_{\ln \mathrm{IM}_i|\mathrm{rup}} \approx \sqrt{\sum_k p_k \left(\sigma^2_{\ln IM_{i,k}|\mathrm{rup}} + \left(\mu_{\ln IM_{i,k}|\mathrm{rup}} - \mu_{\ln IM_i|\mathrm{rup}} \right)^2 \right)} , \tag{2.19}$$

In which:

$\mu_{\ln \mathrm{IM}_i|rup}$, is the logarithmic mean obtained incorporating all the GMPEs of the *i*-th IM in the vector of IMs given a scenario (Magnitude, distance, etc.).

$\mu_{\ln IM_{i,k}|rup}$, is the logarithmic mean obtained from *k*-th GMPE in the logic tree of the *i*-th IM in the vector of IMs given a scenario (Magnitude, distance, etc.).

p_k is the PSHA weight assigned to the *k*-th GMPE in the logic tree.

$\sigma_{\ln \mathrm{IM}_i|\mathrm{rup}}$, is the logarithmic standard deviation obtained by incorporating all the GMPEs of the *i*-th IM in the vector of IMs given a scenario (Magnitude, distance, etc.).

$\sigma_{\ln \mathrm{IM}_{i,k}|\mathrm{rup}}$, is the logarithmic standard deviation obtained from *k*-th GMPE in the logic tree of the *i*-th IM in the vector of IMs given a scenario (Magnitude, distance, etc.).

2.10 **CONCLUSIONS**

Computing the seismic risk of realistic buildings for both loss estimation and collapse assessment requires monitoring building response measures that may include story-specific measures, such as peak inter story drifts and floor response spectra at all stories, and global measures, such as maximum peak inter story drift along the height of the building and residual, post-earthquake lateral displacement. A confident assessment of these response measures requires sophisticated structural and non-structural modelling that is better served by using 3-D computer models of the building. Predicting the response of such models in both the main horizontal axis and, in some cases, vertical direction (e.g., for assessing the damage to suspended ceilings) is facilitated by the use of more than one IM of the ground motion in one or more directions and at one or more oscillator periods.

Estimating response measures as a function of different IMs involves statistical and probabilistic techniques that have been already, in large part, developed and fine-tuned. However, which IMs are superior for a practical estimation of *both losses and collapse* of buildings modeled as 3-D structures and how to compute the joint hazard of these IMs at the building site is still a very fertile ground for research.

This chapter describes the use of more than one IM for assessing building response for both loss and collapse estimation. The present article focuses on defining the IMs that are jointly used as predictors of building response in the companion paper and outlines a method for performing vector-valued PSHA for these IMs. Performing vector-valued PSHA for complex IMs that are derived from common ones (e.g., spectral accelerations at different periods) is not trivial and requires modifying the existing ground motion prediction models and computing the variance-covariance matrix of such IMs.

All these aspects are covered here for the most common practical IMs appearing in the literature namely spectral accelerations, ratios of spectral accelerations and averages of spectral accelerations over different periods and orientations, which are used as predictors of building response both in scalar form and in vector form. More precisely, the scalar IMs considered here are spectral accelerations at first mode period of the structure in each orthogonal main directions of the building, or at the average of the first modal periods in the two orthogonal directions. Another scalar IM used is the averaged spectral acceleration at multiple periods of oscillation that are important for the structures considered. It is emphasized, however, that the methodology described for performing vector-valued

PSHA goes beyond the boundaries of these specific applications that use only spectral accelerations. Other less conventional IMs (e.g. *PGV, PGD*, Arias Intensity, duration, and Cumulative Absolute Velocity), can be used following the same approach provided that legitimate ground motion prediction models and correlation coefficients for those IMs are available.

For the applications at hand, the conventional scalar PSHA for scalar IMs and the vector-valued PSHA were performed using the software OpenQuake. The vector-valued PSHA were carried out using a methodology that was called the *"Indirect"* approach since it does not implement the numerical integration of the joint distribution of all the correlated IMs considered, as the "direct" approach does. The "indirect" approach uses the marginal hazard curve for each IM, the disaggregation results from those IMs, and the correlation coefficients for each pair of IMs to obtain the joint hazard. Hence, this method could be considered as a simple post processor of any available scalar PSHA code. This "indirect" method is arguably superior to the "direct" integration approach in many aspects as explained in the body of the paper. However, when applying the "indirect" approach to vector PSHA, care should be exercised in the selection of the bin sizes that discretize the mutli-dimensional domain of the IMs. The bin sizes should be rather small especially in the part of the domain where the highest concentration of probability is concentrated.

The software that post-process scalar PSHA results and that produced the joint hazard estimates used in this study is available at Kohrangi, [2015]. As will be discussed in *Chapter 3*, using vectors of IMs in seismic performance assessment of structures is a very promising avenue. It is hoped that the software for performing vector PSHA made available here will decrease the hurdle that has hindered its use in the past and will enable more complex and accurate seismic response assessment studies of realistic buildings.

3. VECTOR AND SCALAR IMs IN STRUCTURAL RESPONSE ESTIMATION: BUILDING DEMAND ASSESSMENT

3.1 INTRODUCTION

Performance Based Earthquake Engineering (PBEE) has been the focus of research on seismic assessment of buildings and bridges for more than a decade. The main scope of PBEE is to support decision-making regarding the seismic performance of structures within a probabilistic framework. This methodology consists of four steps that require a broad knowledge of: 1) Seismic Hazard Analysis; 2) Demand Analysis; 3) Damage Analysis and 4) Loss Estimation [Cornell and Krawinkler, 2000]. The first step uses an IM of the ground motion to predict the distribution of the structural response in terms of different Engineering Demand Parameters (EDPs), such as Inter Story Drift Ratio (IDR) and absolute Peak Floor Acceleration (PFA). EDP distributions are then used to measure the structural/nonstructural damages using discrete damage states for each building component [FEMA-P-58, 2012]. Finally, the likelihood of occurrence or exceedance of monetary losses, injuries and estimated downtime is computed using the consequence functions that link damage states and their repair strategies to repair costs, repair time, and physical consequences to inhabitants. This paper focuses on the second step of this procedure namely: Probabilistic Seismic Demand Analysis (PSDA). *Chapter* 2 addresses the first step that is Probabilistic Seismic Hazard Analysis (PSHA).

PSHA evaluates the Mean Annual Rate (MAR) of exceeding certain levels of IM at the building site. Some classical IMs are the ground motion peak values expressed in terms of the peak ground acceleration, velocity or displacement (PGA, PGV or PGD, respectively), and the Spectral acceleration at the first mode period of the structure, $Sa(T_1)$. Of interest are the efficiency and sufficiency of such IMs (See Luco and Cornell, 2007b]). An efficient IM provides low dispersion of the predicted response given IM and a sufficient IM offers statistical independence of the response given IM from ground motion characteristics, such as magnitude, distance, etc. Efficiency helps reduce the number of time history analysis for reliable assessment of response while sufficiency is a sine qua non requirement for combining PSHA with structural analysis results. For example, $Sa(T_1)$ is shown to be efficient and sufficient for assessing the response of some structures (e.g., first-mode dominated, low-rise buildings) and types of ground motion (e.g., ordinary far field motions) and not as effective in other cases, such as tall buildings [Shome and Cornell, 1999], and any building that are likely to be subject mainly to near source ground motions (Luco and Cornell, 2007b). In addition, due to the 3-D nature of structures and the multi-directionality of ground shaking excitations, a single scalar IM at a single ordinate of the spectrum does not seem to be a good predictor for the structural response [Faggella *et al.*, 2013; Lucchini *et al.*, 2011]. In general, the response of the structure is correlated to the spectral acceleration at higher modes and, when beyond the elastic range, also to the spectral acceleration at elongated periods. In addition, the response in one direction might be correlated to the excitation of the orthogonal direction, especially for torsionally unrestrained buildings and when some local failure modes are triggered (e.g., out-of-plane collapse of walls being facilitated by loss of in-plane strength).

Some more complex scalar IMs have been proposed by researchers to improve the predictive performance of traditional scalar IMs. For example, Tothong and Cornell, [2007] showed that the inelastic displacement of the building could be effectively estimated by the Inelastic Spectral Displacement, $S_{di}(T_1)$, of a nonlinear SDOF with vibration period consistent with the first modal period of the structure. Alternatively, for tall buildings, a combination of $S_{di}(T_1)$ with elastic spectral displacement at the second mode, $S_{de}(T_2)$, and the elastic participation factors was shown to be an effective predictor of building deformation response. Cordova *et al.*, [2000] followed by Vamvatsikos and Cornell, [2005] and Mehanny, [2009] introduced the power-law form, scalar-based seismic IM that was shown to reduce the dispersion in structural inelastic displacement response. Bianchini *et al.* [2010] proposed the similarly defined average spectral acceleration (Sa_{avg}), which is the geometric mean of the logarithmic spectral acceleration at multiple periods, in a relevant period range. At the other end, a number of record selection schemes have been introduced that rely on simpler IMs. First, Baker and Cornell, [2005] employed epsilon, i.e. a measure of the difference between ground motion's $Sa(T_1)$ and the median estimate of a ground motion prediction Equation (GMPE) for the given earthquake scenario, while Bradley, [2010a] proposed the Generalized Conditional Intensity Measure (GCIM) to select records using one or more simple IMs and record parameters to allow accounting for the conditional distribution of ground motion characteristics to remove issues of insufficiency.

There is no theoretical limitation forcing us to considering a scalar IM for response prediction. If advantageous, one could consider a vector of several relevant IMs for structural response estimations. The use of a set of different scalar IMs was introduced by Bazzurro, [1998] as a vector that included two spectral accelerations at different periods. Vamvatsikos and Cornell, [2005] studied the efficiency of a vector of $Sa(T_1)$ and a ratio of spectral accelerations at T_1 and a secondary period, while Baker and Cornell [2005, 2008a, 2008b] also investigated the further addition of epsilon. Although, it is intuitive to expect that the use of a vector IM would provide more efficiency and sufficiency in response estimation, it has not caught on in the scientific community due, in part, to the complexity of linking the response assessment with the joint hazard estimation at the site via Vector Probabilistic Seismic Hazard Analysis (VPSHA). In addition, some researchers, such as Rajeev *et al.* [2008] using a 2-D model, did not find the gain in response prediction accuracy worth the extra effort.

Chapter 2 and *Chapter 3*, intend to offer a fresh look into the issue of using scalar and vector IMs for probabilistic response estimation of 3-D buildings under two horizontal components of ground motion. Three building examples of common Mediterranean construction practice in reinforced concrete (RC) were examined. *Chapter 2* presents the approaches followed to carry out VPSHA. *Chapter 3* covers the record selection approach, the structural modeling and analysis, as well as the response estimation. Finally, the results obtained are discussed, with emphasis on the effectiveness of several scalar and vector IMs as response predictors to obtain the localized-response hazard curves for these buildings.

3.2 BUILDING EXAMPLES AND MODELING DESCRIPTIONS

This study considers three examples of 3-, 5- and 8-story buildings representative of typical Southern Europe old constructions designed without specific provisions for earthquake resistance (Figure 3.1). The 3-story RC frame building (SPEAR) is non-symmetric in X and Y directions with 3.0 m story height. The full-scale structure was built and tested within a European research project at JRC-ELSA [Fardis, 2002]. The 5- and 8-story buildings are models of real RC buildings in Turkey. The 5-story is regular in plan and height with 2.85 m story height, whereas the 8-story is irregular in plan (i.e., stiffer in Y than X direction) and height (i.e., first floor story height is 5.0m and other stories 2.7m). Detailed information about the 5- and 8- story structures is available in Bal *et al.* [2007]. The outer frames of all three buildings are filled with masonry walls except for the 8-story building in which no walls are present at the ground floor in the X direction.

3-D nonlinear models of the building structures were created in OpenSees [McKenna, 2000]. Beams and columns are modeled using force-based distributed plasticity elements and the actual properties of the floor diaphragms are considered by means of equivalent X-diagonal braces that represent the in-plan stiffness of the slab. The masonry infill panels were considered based on the model proposed by Kadysiewski and Mosalam [2009]. All material and structural properties are taken at their best deterministic (typically mean) estimates. The results of the modal analysis after application of gravity loads are listed in Table 3.1.

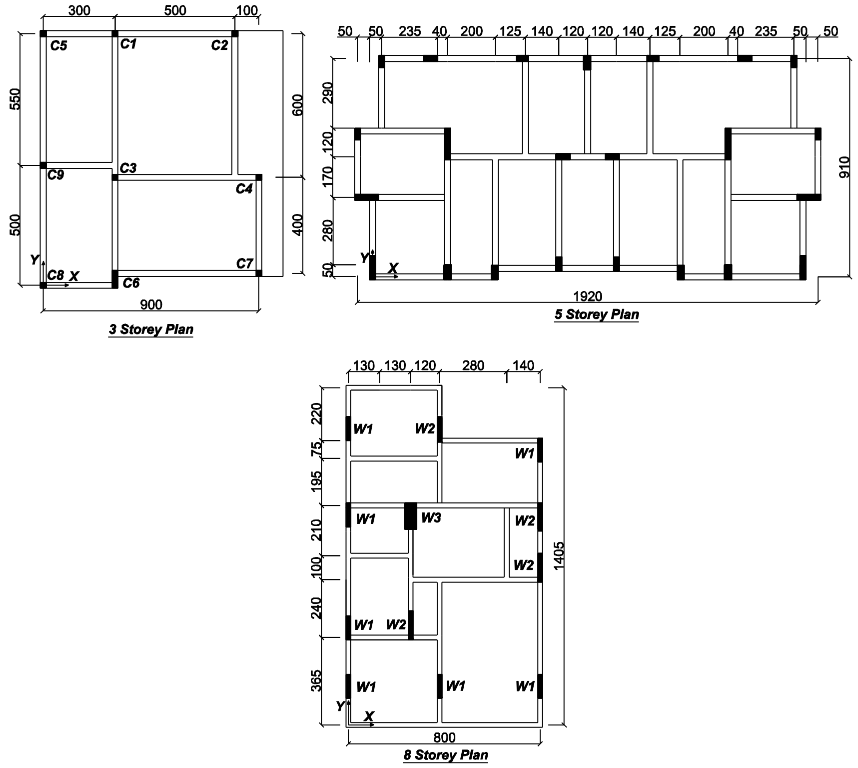

Figure 3.1. Plan view of the three considered structures (dimensions in cm)

The fundamental translational modes of the buildings have mass participation factors that are generally lower than 80%. The sole exception is the X-direction response of the 8-story building in which 99.04% of the modal participation is reached in the first mode due to the presence of a soft first story in this direction only. In addition, the translational response of all three buildings is coupled with torsion at least in one of the two horizontal directions, even for the 8-story structure: Due to the alignment of all walls with the Y axis, the 8-story building is flexible along X with a vibrational period of 1.30s and stiff along Y with a period of 0.44s. The pushover curves of all three buildings with and without masonry infill walls in the two orthogonal directions are shown in Figure 3.2. The difference between the stiffness and the base shear capacity in the two orthogonal directions of the 8-story building could be noticed in Figure 3.2(c). Note also that, because of the absence of infills at the ground floor, the values of the base shear capacity of the 8-story building in the X axis computed with and without infill walls are basically the same. More discussion about the building properties and modelling can be found in Kohrangi (Kohrangi, 2015a).

Table 3.1. Periods and participating mass ratios (PMR) of buildings' eigen modes for the translational (X, Y) and rotational (RZ) degrees of freedom after the application of gravity loads. The prefix Σ denotes the cumulative sum of the modes.

	Mode No.	Period (s)	PMRX (%)	PMRY (%)	PMRRZ (%)	ΣPMRX (%)	ΣPMRY (%)	ΣPMRRZ (%)
3-story	1	0.66	5.78	50.21	26.40	5.78	50.21	26.40
	2	0.57	77.16	8.28	0.03	82.94	58.49	26.43
	3	0.43	2.60	23.43	60.37	85.54	81.91	86.80
5-story	1	0.67	0.00	80.70	0.00	0.00	80.70	0.00
	2	0.46	71.28	0.00	10.45	71.28	80.70	10.45
	3	0.42	10.07	0.00	72.54	81.35	80.70	82.99
8-story	1	1.30	99.04	0.00	0.03	99.04	0.00	0.03
	2	0.46	0.02	18.48	73.00	99.07	18.48	73.03
	3	0.44	0.04	68.43	18.66	99.10	86.91	91.69

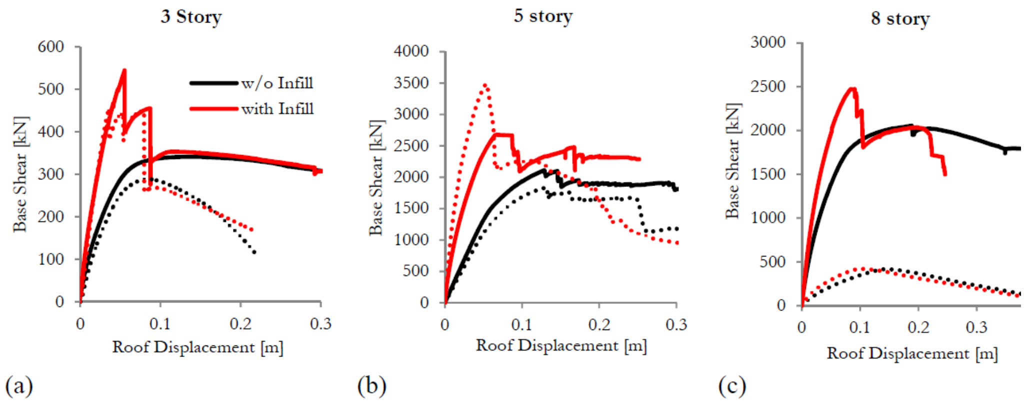

Figure 3.2. Pushover curves for three buildings with and without infill panels (Solid line: Y axis, Dotted line: X axis)

3.3 GROUND MOTION DATABASE

Nonlinear Dynamic Analysis is used to obtain the distribution of structural response, as expressed in terms of engineering demand parameters (e.g., MIDR and PFA), for different IM levels. Given the approximations included in the first of the four-step PEER approach, where the complexity of ground motions is represented most often by a single IM, the ground motion record selection may often play a key role in ensuring accuracy in the estimation of the responses. Loosely speaking, the ground motions selected should appropriately reflect the distribution of seismological characteristics not accounted for by an insufficient IM at the given site. Given the limitations in the existing databases of real accelerograms, any available method for record selection is imperfect. In this study we used the selection method [Jayaram, *et al.*, 2011; and Lin *et al.*, 2013a] based on the Conditional Spectrum, CS, to assemble three sets of input ground motion records. In this methodology, a suite of ground motions is selected and scaled such that each resulting suite collectively matches the entire conditional distribution of spectral accelerations given the IM value as represented by the CS. This way, both the mean and variance of the record set spectra are consistent with the seismic hazard at the site.

For this study, 10-12 intensity levels of spectral acceleration, $Sa(\bar{T})$, were used for the 3- and 8-story buildings and 12 levels for the 5-story building. Numerically they range from 0.037g to 2.46g and they were selected to cover the entire range of response from elastic to severely inelastic. Each stripe consists of both horizontal components of 20 accelerogram pairs in which the geometric mean of the spectra of the two components is used to match the corresponding anchoring point of the CS at the period $\bar{T}$. The GMPE of Boore & Atkinson [2008] and mean magnitude, distance and epsilon ($\bar{M}$, $\bar{R}$ and $\bar{\varepsilon}$) obtained from disaggregation results for each intensity level were used for computing the CS. The conditioning period ($\bar{T}$) in all cases is the average of the first mode building vibration periods in X and Y directions, $\bar{T} = \left(T_{1x} + T_{1y}\right)/2$, as proposed by FEMA P-58 for period-specific scalar IM*s* case to be used for assessing the response of 3-D buildings.

Table 3.2. Summary of the mean M, R and ε values obtained via disaggregation for the selected levels of $Sa(\bar{T})$ for the three considered buildings.

Intensity Level	$Sa(\bar{T})$ [g]	3- story ($\bar{T} = 0.62s$)			5- story ($\bar{T} = 0.57s$)			8- story ($\bar{T} = 0.87s$)		
		$\bar{R}$	$\bar{M}$	$\bar{\varepsilon}$	$\bar{R}$	$\bar{M}$	$\bar{\varepsilon}$	$\bar{R}$	$\bar{\bar{M}}$	$\bar{\varepsilon}$
IML1	0.04	68.7	5.7	0.7	69.3	5.6	0.7	66.3	5.9	0.8
IML2	0.07	57.0	5.9	0.9	57.5	5.9	0.9	54.0	6.2	0.9
IML3	0.12	43.4	6.2	0.9	44.0	6.2	0.9	39.7	6.5	1.0
IML4	0.22	31.0	6.5	1.1	31.5	6.4	1.1	28.6	6.7	1.2
IML5	0.33	25.4	6.6	1.3	25.7	6.6	1.3	23.7	6.7	1.6
IML6	0.50	21.2	6.7	1.7	21.5	6.7	1.6	19.8	6.8	1.9
IML7	0.61	19.4	6.7	1.8	19.6	6.7	1.7	17.7	6.8	2.2
IML8	0.74	17.5	6.7	2.1	17.7	6.7	2.0	15.6	6.8	2.2
IML9	0.90	15.3	6.7	2.2	15.7	6.7	2.2	12.2	6.7	2.2
IML10	1.35	6.3	6.5	2.1	7.7	6.5	2.1	2.6	6.4	2.4
IML11	2.01	-	-	-	2.6	6.4	2.4	-	-	-
IML12	2.46	-	-	-	2.5	6.7	2.5	-	-	-

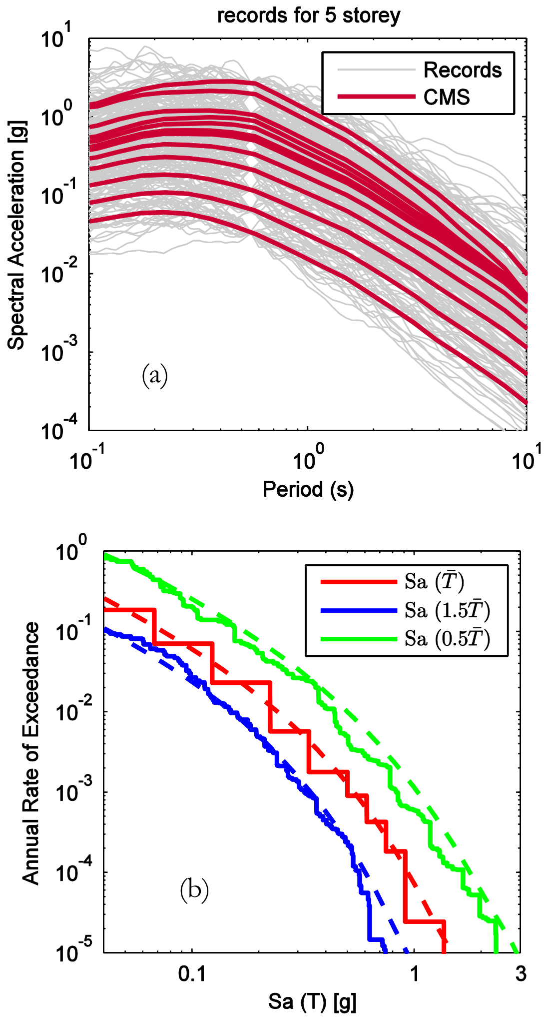

Figure 3.3. (a) The mean conditional spectra (CMS) at 12 intensity measure levels and the selected ground motion suites used as input to the nonlinear dynamic analysis of the 5-story building, (b) "Hazard consistency" verification of the selected ground motion records for the 8-story building based on the conditioning period $\bar{T} = 0.87s$ for CS matching (dashed line: Direct hazard curve from PSHA, solid line: Hazard curve from the selected records).

Since the same GMPE was applied both here and in the PSHA calculations, the results of the record selection could be considered accurate. However, some approximations might be introduced by neglecting the different causal earthquake scenarios that may not be adequately captured by the average M, R and ε values considered in the process (see Lin *et al.*, [2013a], for more details). The records in this database can be classified into two groups: ordinary far field records and pulse-like records. Based on the method proposed by Shahi

[2013], in this database 9 records for the 3-story building, 8 records for the 5-story building, and 22 records for the 8-story building are classified as pulse like.

As an example, Figure 3.3(a) shows the Mean of Conditional Spectra (CMS) at 12 intensity levels as well as the geometric mean of the spectra of the two components of all 240 (selected and scaled) individual records used as input to the nonlinear dynamic analysis of the 5-story building. The approach proposed by Lin *et al.* [2013b] was used to verify the hazard consistency of the selected records for the three buildings. Figure 3.3(b) compares the direct hazard curves of the site with the rate of exceedance of $Sa(\overline{T}_1)$, $Sa(0.5 \cdot \overline{T}_1)$ and $Sa(1.5 \cdot \overline{T}_1)$ in the record data set selected for the 8-story building. The consistency of the selected records with the hazard curves at different structural ordinates of the spectrum is acceptable. Although omitted here, this consistency was also verified for the record sets selected for the 3- and the 5-story buildings.

3.4 **NONLINEAR DYNAMIC ANALYSIS, INTENSITY MEASURES AND ENGINEERING DEMAND PARAMETERS**

Nonlinear Dynamic Analysis was performed for the risk-based assessment of the three buildings using the CS-based records. It is emphasized that the difference between what is done here and the well-known Incremental Dynamic Analysis (IDA) approach [Vamvatsikos and Cornell, 2002] is that this study uses different records for the lower, middle and higher stripes, whereas in IDA the same records are incrementally scaled up until collapse of the structure is reached. Thus, the present study does not depend as much on the quality of the IM to achieve reliable results.

Structural and non-structural deformation-sensitive damage is typically correlated to the peak (in time) inter story drift ratios (IDRX and IDRY) at each story. As a single indicator of global collapse, the respective maxima over height, MIDRX and MIDRY, may also be employed. For simplicity, the directionless square root of the sum of the squares (SRSS) of the corresponding X and Y EDPs in the two directions, termed IDR for individual stories or MIDR for the whole building, is sometimes used instead. In this study, as torsion may be an issue, such values are averaged over the four corners of the building's rectangular plan. To assess the acceleration-sensitive losses of nonstructural components and contents, the absolute peak floor acceleration is also employed. This is also taken as the peak (in time) of the SRSS of the floor accelerations in the two main orthogonal directions at the middle point of the floor slab. Note that the IDRs in X or Y direction are more suitable for monitoring the response of single components according to their orientation and, therefore, we chose to show the results of IDR for two orthogonal directions, separately. For PFA, however, for which the direction has less significance, we present the SRSS results instead. On the other hand, the use of directionless SRSS values may understate the magnitude of change observed in a specific direction, somewhat softening the perceived impact of 3-D ground motion excitation and the improvement brought on by some of the more specialized IMs tested.

The global response of the buildings in terms of (directionless) IDR and PFA is shown in is shown in Figure 3.4. The thin gray lines represent the maximum floor response of individual analyses while the thick blue lines identify their median at different IM levels. Two collapse criteria were considered. The first is the global side-sway collapse that we equated to non- convergence of the analysis after large lateral displacements were reached. In addition, we considered a local collapse criterion that can be associated to the loss of load bearing capacity of the non-ductile columns [Aslani and Miranda, 2005]. This was set at an *IDR* value of 0.04, on average.

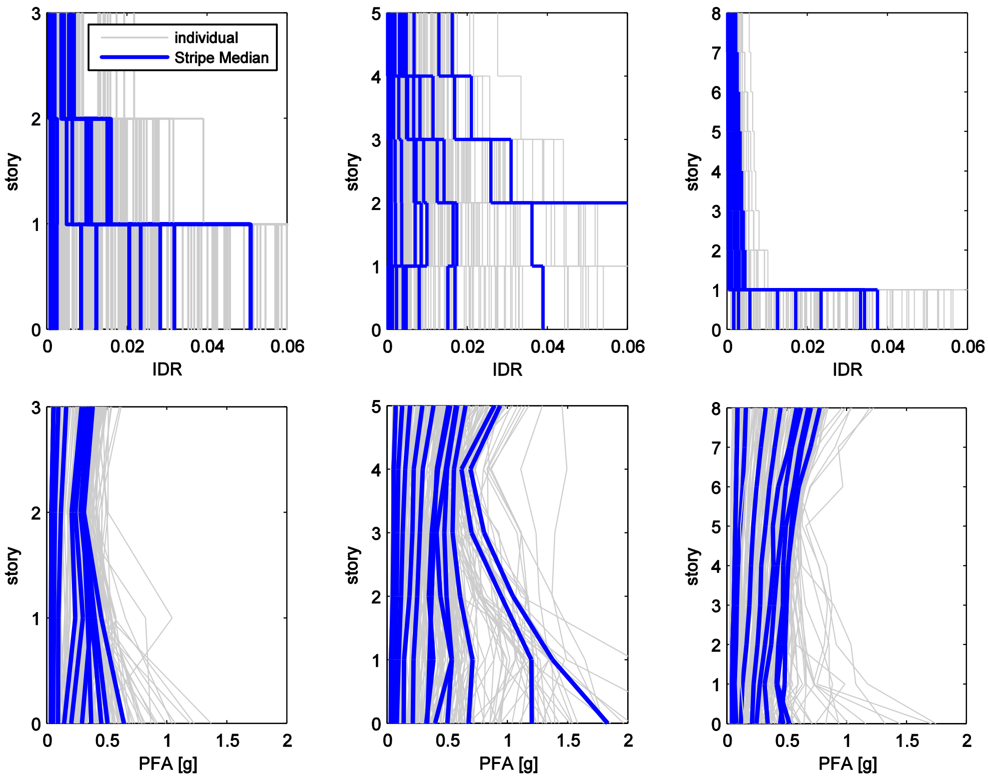

Figure 3.4. Structural response of for the 8-story building obtained from nonlinear dynamic analysis carried out for the CS-based selected records. Each thick blue line is the median of the responses for each stripe analysis.

The set of scalar and vector IM candidates considered are listed in Table 3.3. A detailed summary of the tested IMs and the criteria employed for selecting them are presented in *Chapter 2*.

Table 3.3. IMs considered in the response estimation

INTENSITY MEASURE (IM) *	**ABBR.**
SCALAR IMs	
Natural logarithm of arbitrary spectral acceleration at the first modal period $\ln\left[Sa_x\left(T_{1x}\right)\right]$ or $\ln\left[Sa_y\left(T_{1y}\right)\right]$	Sa_{S1}
Natural logarithm of the geometric mean of spectral acceleration at the average period, $\ln\left[Sa_{g.m.}\left(\bar{T}=\left(T_{1x}+T_{1y}\right)/2\right)\right]$.	Sa_{S2}
$\ln\left[Sa_x\left(\alpha_1\cdot T_{1x}\right)\cdot Sa_x\left(T_{1x}\right)\cdot Sa_x\left(\alpha_u\cdot T_{1x}\right)\cdot Sa_y\left(\alpha_1\cdot T_{1y}\right)\cdot Sa_y\left(T_{1y}\right)\cdot Sa_y\left(\alpha_u\cdot T_{1y}\right)\right]$	Sa_{S3}
$\ln\left(\left[\prod_{i=1}^{n}\left(Sa_x\left(T_{xi}\right)\right)\right]^{1/n}\right)\cdot\ln\left(\left[\prod_{j=1}^{m}\left(Sa_y\left(T_{yj}\right)\right)\right]^{1/m}\right)$, $\alpha_1\cdot T_1\leq T_i\leq\alpha_u\cdot T_1, m=n=10$ §	Sa_{S4}
Natural logarithm of the geometric mean of Peak Ground Acceleration, $ln[PGA_{g.m.}]$	PGA
VECTOR IMs	
$\ln\left\{Sa_x(T_{1x}),\frac{Sa_y(T_{1y})}{Sa_x(T_{1x})},\frac{Sa_x(1.5\cdot T_{1x})}{Sa_y(T_{1y})},\frac{Sa_y(1.5\cdot T_{1y})}{Sa_x(1.5\cdot T_{1x})}\right\}$	Sa_{V1}
$\ln\left\{Sa_{g.m.}(\bar{T}),\frac{Sa_{g.m.}(0.5\cdot\bar{T})}{Sa_{g.m.}(\bar{T})},\frac{Sa_{g.m.}(1.5\cdot\bar{T})}{Sa_{g.m.}(0.5\cdot\bar{T})}\right\}$	Sa_{V2}
$\ln\left\{\left[Sa_x\left(\alpha_1\cdot T_{1x}\right)\cdot Sa_x\left(T_{1x}\right)\cdot Sa_x\left(\alpha_u\cdot T_{1x}\right)\right]^{1/3},\left[Sa_y\left(\alpha_1\cdot T_{1y}\right)\cdot Sa_y\left(T_{1y}\right)\cdot Sa_y\left(\alpha_u\cdot T_{1y}\right)\right]^{1/3}\right\}$	Sa_{V3}
$\ln\left\{\left(\left[\prod_{i=1}^{n}\left(Sa_x\left(T_{xi}\right)\right)\right]^{1/n}\right),\left(\left[\prod_{j=1}^{m}\left(Sa_y\left(T_{yj}\right)\right)\right]^{1/m}\right)\right\}$	Sa_{V4}

*All the *IMs* are based on natural logarithm transformation. The notation ln is removed from the abbreviations for brevity

** α_1 is equal to 0.8, 0.2 and 0.2 for the 3-, 5- and 8-story, respectively. α_u is equal to 1.5 in all cases.

3.5 RESPONSE ESTIMATION AND IM EFFICIENCY ASSESSMENT

The selection of an appropriate IM is driven mainly by its efficiency and sufficiency [Luco and Cornell, 2007]. An efficient IM is one which, when used as predictor of an EDP, results in a relatively small variability in the EDP given the value of the IM. Sufficiency, on the other hand, reflects the independency of the distribution of EDP given IM from other ground motion characteristics, such as magnitude of the causative earthquake, distance of site from the source, epsilon of the record, etc. Higher efficiency results in the reduction in the necessary number of records needed to obtain a reliable estimate of the EDP|IM. Higher sufficiency results in decreased (or non-existent) bias. Due to the careful record selection approach adopted, we shall assume that sufficiency is achieved, at least with respect to spectral shape, and we will only concentrate on efficiency. As such, the efficiency of the examined IMs is gauged by the variance of the residuals of the linear regression analysis of the EDP as a function of the IM. For vector IMs, each element IM_i of the vector was employed separately as a predictor. The regression models adopted for response prediction and efficiency checking appear in Equation (1) and Equation (2), these having linear and complete quadratic IM terms, respectively. It should be noted that for scalar IMs the additional quadratic terms introduced in Equation (2) are not as useful, thus only Equation (1) is used.

$$\ln\left(EDP\right) = b_0 + \sum_{i=1}^{n}\left[b_i \cdot \ln\left(IM_i\right)\right] + \varepsilon_r \cdot \sigma_{\ln EDP|IM} \tag{3.1}$$

$$\begin{aligned} \ln\left(EDP\right) = b_0 + \sum_{i=1}^{n}\left[b_i \cdot \ln\left(IM_i\right)\right] + \frac{1}{2} \cdot \sum_{i=1}^{n}\sum_{j=1}^{n}\left[b_{ij} \cdot \ln\left(IM_i\right) \cdot \ln\left(IM_j\right)\right] \\ + \frac{1}{2} \cdot \sum_{i=1}^{n}\sum_{j=1}^{n}\left[b_{ii} \cdot \ln\left(IM_i\right)\right]^2 + \varepsilon_r \cdot \sigma_{\ln EDP|IM} \end{aligned} \tag{3.2}$$

In these equations the b_i values are the regression parameters; $\sigma_{\ln EDP|IM}$ is the standard error of estimation, and ε_r is the standardized error term. The advantage of the linear regression method is that it provides a well-developed theory regarding model selection and confidence intervals for regression coefficients, but there are a few disadvantages as well. Firstly, this approach assumes homoscedasticity, namely a single standard deviation of the error for the entire data range, whereas it is shown in earlier studies (e.g., Modica and Stafford, [2014], to name one of the most recent references) that structural response in terms of MIDR is indeed heteroscedastic, which in this case means that the response variance increases with increasing IM values. Secondly, the regression model extrapolates in the data range that is not covered well by the observed data points. For example, in the case of a vector of IMs, for certain values of T_1 it is rare to have real records with a low $Sa(T_1)$ value and a high $Sa(1.5 \cdot T_1)/Sa(T_1)$ value from a real ground motion. Luckily, this issue is not a very serious one because the mean rate of occurrence of such unlikely pairs of spectral acceleration values in the joint hazard is so small as to render irrelevant the perhaps inaccurate extrapolations of the model. Thirdly, the significance of each component of the vector of IMs might be different across the range of the data. For example, for low levels of $Sa(T_1)$ when the structure behaves mainly linearly, $Sa(1.5 \cdot T_1)$ is less effective in predicting the IDR response, whereas for high values of $Sa(T_1)$, when the structure is highly nonlinear, $Sa(1.5 \cdot T_1)$ has a significant predictive power on the nonlinear IDR response. This implies that IM interaction terms should be included in the multiple linear regression model (e.g., Baker, [2007]) when used for the vector IM cases. Modica and Stafford [2014], in fact, used a quadratic functional form consisting not only of interaction terms, $\ln(IM_i)\cdot\ln(IM_j)$, but also of quadratic ones, $\left[\ln(IM_i)\right]^2$, when assembling the prediction model for estimating EDP*s*.

An alternative method for response estimation is the non-parametric running median (or in general running quantile) approach. In this method, the median of a moving window of the data is computed and the standard deviation is obtained using 84th and the 16th percentiles of the residuals with the assumption of the normal or lognormal distribution of the data [Vamvatsikos and Cornell, 2005]. The primary advantages of this method are that it provides a standard deviation that varies across the data range, which is more faithful to the data, and that it does not need a parametric assumption for the error term. In addition, because it uses a quantile of the data (e.g., the 50% quantile for median), it can deal with collapse data points and non-collapse data points at the same time. Although appealing, this method may work well for scalar IMs but it becomes impractical as the number of components of the vector IM increases (e.g. more than 2) since the data points tend to be sparse in a multi-dimensional space. Hence, the need for fitting a model becomes unavoidable.

3.6 IM EFFICIENCY FOR INTER STORY DRIFT RATIOS

Figure 3.5 and Figure 3.6 compare the response dispersion profiles expressed in terms of IDRX, IDRY and PFA for the three buildings computed using different IMs. Note that, as explained earlier, the linear regression analysis of the response data points provides single dispersion at all IM levels. As such, in these figures the dispersion is not related to a specific IM level. The lowest dispersion of IDR|IM in the lower stories and in almost all cases and for both directions is provided by the vector Sa_{V1}. The decrease in dispersion of IDRX, IDRY given Sa_{V1} compared to the simplest scalars Sa_{S1} and Sa_{S2} is significant, whereas it is negligible when compared against vectors Sa_{V3} and Sa_{V4} for the 3-story building and moderate for the 5- and 8-story buildings. This could be explained by the fact that, the averaged spectral accelerations used as components of Sa_{V3} and Sa_{V4} indiscriminately combine *Sa* values at multiple periods, thus introducing a slight disadvantage for the taller structures.

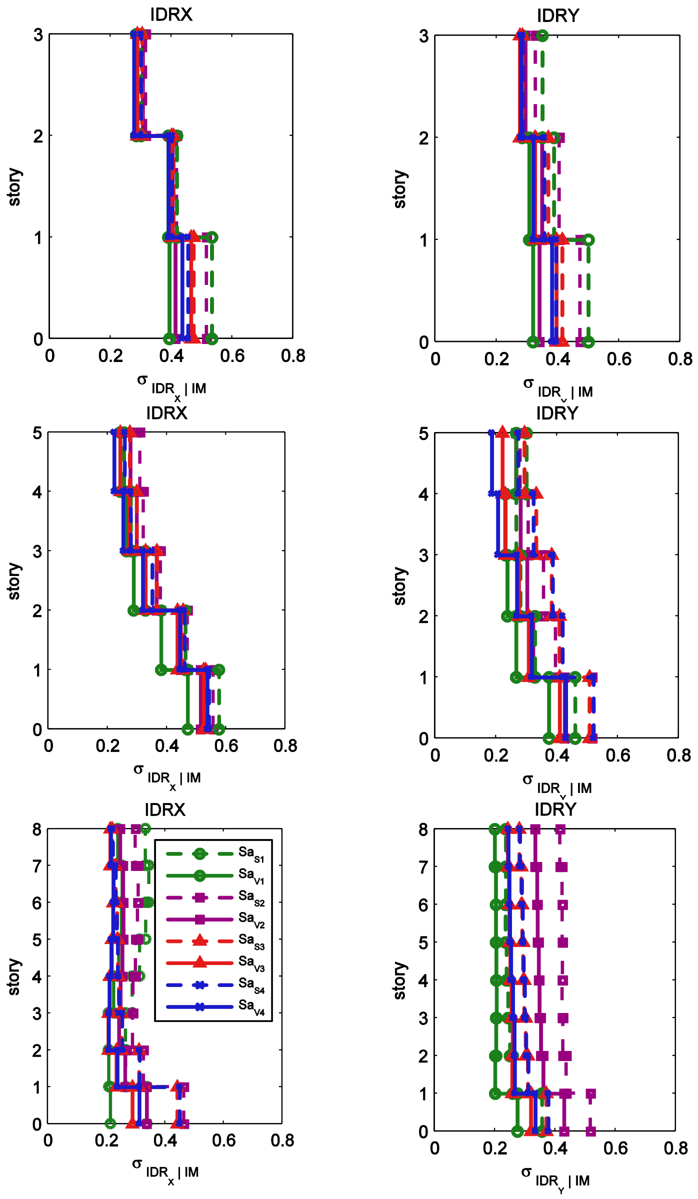

Figure 3.5. Comparison of the dispersion $\sigma_{\ln EDP|IM}$ profiles of IDRX, IDRY using different IMs for the 3-, 5- and 8-story buildings (note: Single dispersion is estimated for all IM levels)

For instance, in an average Sa, generally indicated as Sa_{avg} henceforth, incorporating only two spectral accelerations at T_1 and $1.5 \cdot T_1$, one record with $Sa(T_1)$=0.8g and $Sa(1.5 \cdot T_1)$=0.4g will provide the same value of Sa_{avg} of a record with the values switched (i.e. $Sa(T_1)$=0.4g and $Sa(1.5 \cdot T_1)$=0.8g), even though the response of the structure to these two records will be different. Therefore, a vector with separated spectral accelerations such as Sa_{V1} is expected to show a better performance in this case, as can be observed from the results here. The only saving grace of such indiscriminate averaging is the relative scarcity of one of the two equal- Sa_{avg} pairs (as discussed earlier). In addition, given the concentration of the nonlinearity in the lower floors for our case-studies, the IDR response of these floors is highly correlated with the spectral accelerations at elongated periods and less with the ones lower than T_1. That is why, even if Sa_{V1} does not reflect the spectral accelerations at the low range periods, it remains the best predictor of the response in the lower floors. In upper floors, on the other hand, where the higher mode effects become more important, Sa_{V1} slightly loses its effectiveness due to its lack of spectral accelerations at lower periods whereas Sa_{V3} and Sa_{V4} which contain such terms, become superior. Sa_{V2} being a vector IM, is similarly more effective compared to its corresponding scalar, Sa_{S2}. On the other hand, it is less efficient compared to other vector IMs used here, something that may be attributed to its use of the geometric mean Sa at each period rather than of the arbitrary component S_a.

Among the scalar IMs, Sa_{S3} and Sa_{S4} are superior to Sa_{S1} and Sa_{S2}. Sa_{S2} shows specifically a poor performance for the 8-story building with widely different periods in the two orthogonal directions (1.3s and 0.44s for X and Y directions, respectively). The difference in the dispersion estimated by Sa_{S3} and Sa_{S4} is very small which suggests the superiority of Sa_{S3} to Sa_{S4} because it is a simpler application of Sa_{avg} with only 6- components compared to 20 components of Sa_{S4}. It should be highlighted that there can be cases where the more complex Sa_{S4} becomes a better solution. For instance, for structures with multiple important higher modes, providing more weight to spectral accelerations at periods lower than T_1, essentially helps to improve the efficiency of this IM for such structures. The periods used in Sa_{S4} and Sa_{V4} are equally spaced between the minimum and maximum periods in this study, providing almost equal number of periods lower and higher than T_1, and consequently giving the same weight to the nonlinear elongated and linear higher mode response. On the other hand, using equally-spaced periods in a logarithmic scale will give more weight to periods lower than T_1. Such an IM could be more effective for structures with relatively significant importance of higher modes or for the estimation of PFA as discussed in the next section.

3.7 IM EFFICIENCY FOR PEAK FLOOR ACCELERATION

PGA is a superior predictor of PFA at the ground and maybe some additional lower floors than any other IM tested here, but it becomes progressively less effective with height. This could be simply explained by an example of a single-story single-degree-of-freedom (SDOF) system in which the PFA at the ground floor matches the PGA, while by definition it matches $Sa(T_1)$ at the level of the roof. This is why PGA will always be the best predictor for the ground floor. Recall that the PFA results shown here are the SRSS of the values for the two orthogonal directions of the building. This is the reason why a small dispersion of 10% is observed at the ground floor, since the PGA used as IM is based on the geometric mean (rather than the SRSS) of the two record components regardless of the times when the peaks occur. $Sa(T_1)$, on the other hand, is one of the worst IMs at the ground floor and its efficiency progressively improves with height. This might suggest the idea of using a vector IM including both PGA and $Sa(T_1)$, to cover the efficiency at the lower and upper floors for PFA prediction. However, since PGA is not a good predictor of IDRs for any but the shortest-period buildings, such a vector IM will not be globally effective, unless, for example the estimation of losses at the lowest floors is deemed to be the most significant contributor to losses.

Another interesting point is that PFA is more closely related to the seismic forces applied to the structure than deflections. When the structural ductility after yielding increases and the stiffness reduces, the seismic forces stabilize and do not increase appreciably, akin to an isolation effect. Therefore, the PFA values in most analyses are observed at a time or IM level where the structure is still in the linear elastic regime or close to it. This fact is even more emphasized for RC infill frames, such as those analyzed here, in which the stiffness of the structure is initially high due to the presence of the infill panels but decreases abruptly after they fail. This can explain the vector Sa_{V1} not providing considerable improvements compared to the corresponding scalar Sa_{S1}, since Sa_{V1} is more appropriate for nonlinear response prediction as was shown in the previous section. Scalars Sa_{S3}, Sa_{S4} and their corresponding vector IMs of Sa_{V3}, Sa_{V4} are fairly efficient IMs for PFA prediction and perform favorably well all along the height and for all the buildings tested here.

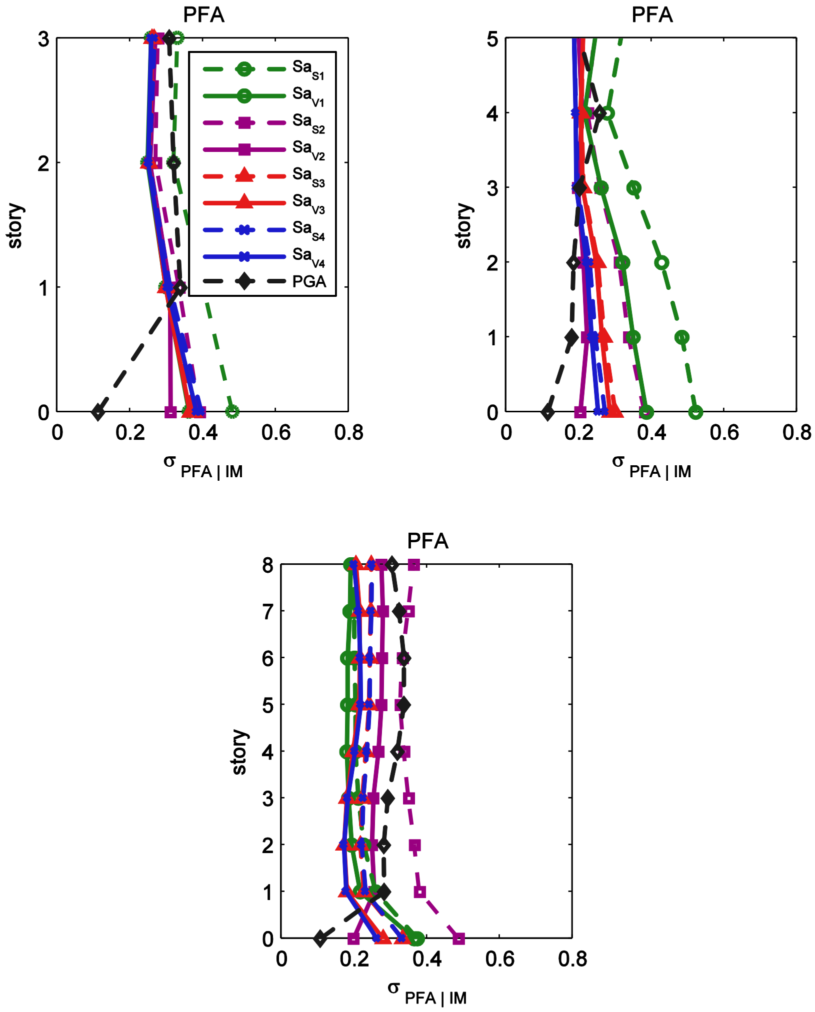

Figure 3.6. Comparison of the dispersion, $\sigma_{\ln EDP|IM}$, profiles of PFA using different IMs for the 3-, 5- and 8-story buildings (note: uniform dispersion is estimated for all IM levels)

As explained earlier, these IMs could become even more effective in PFA prediction by giving more weight to the spectral acceleration at periods lower than T_1. However, by doing so, they will lose some of their efficiency in IDR response estimation. This fact could be seen well expressed by the slight improvement of Sa_{S4} and Sa_{V4} compared to Sa_{S3} and Sa_{V3}, as they contain spectral acceleration at several more periods lower than T_1. Having said that, it should also be emphasized that for the vector IMs in case of Sa_{V3}, Sa_{V4} there is no traceable improvement compared to their counterpart scalar IMs of Sa_{S3}, Sa_{S4}. The reason is related to the fact that PFA here is an SRSS of the values at two main orthogonal directions of the structure, therefore, separating the excitation for X and Y directions apparently does not help to improve their efficiency. This fact can also explain the effectiveness of Sa_{V2} in the lower floors. This IM contains the geometric mean of spectral acceleration at $0.2 \cdot \overline{T}_1$, which is very close to the geometric mean of PGA, the top IM for PFA at the ground floor.

3.8 **RISK ASSESSMENT**

Following Shome and Cornell [1999] the rate of exceeding different values of an *EDP*, $\lambda\left(EDP > edp\right)$, can be computed using the conditional complementary cumulative distribution function of $EDP \mid IM$ for the non-collapsed data, $\mathrm{P}\left(EDP > edp \mid \mathrm{NC}, IM\right)$, and the probability of collapse given IM, $P_{col|IM}$, along with the rate of occurrence of the scalar or vector IM of interest, $\lambda(IM)$, formally:

$$\lambda(EDP > edp) = \int_{IM} \left[\mathrm{P}\left(EDP > edp \mid \mathrm{NC}, IM\right) \cdot \left(1 - P_{col|IM}\right) + P_{col|IM} \right] \cdot \left| d\lambda IM \right| \tag{3.3}$$

Logistic regression [Kutner *et al.*, 2004] was used to compute the probability of collapse for each IM level while linear regression (Equation (3.1)) was used to model $P\left(EDP > edp \mid \mathrm{NC}, IM\right)$. As an example of the results obtained, Figure 3.7 shows the response hazard curves for MIDRX and for maximum PFA all along the height for the 5-story building. The results for all other EDPs are similar. In this particular example, MIDRX values in the order of 3 to 4% are associated with collapse occurrence estimates of mean annual rates. The latter vary by an order of magnitude among the different IMs, that is from 2×10^{-5} (when Sa_{S4} was used as response predictor) to 2×10^{-4} (for Sa_{S1}). In theory, though, since even the lowly Sa_{S1} is riding on the back of careful CS-based record selection, there is no obvious argument that would lead us to prefer one estimate over another. Still, the remarkable consistency in the estimates provided by the vector IMs does lend some credence to the notion that they probably represent a more accurate estimate. Until further research provides a more concrete answer, we cannot assign bias to any of these bonafide estimates: We are bound to uniformly treat the entirety of the variance shown in Figure 7 as a product of epistemic uncertainty.

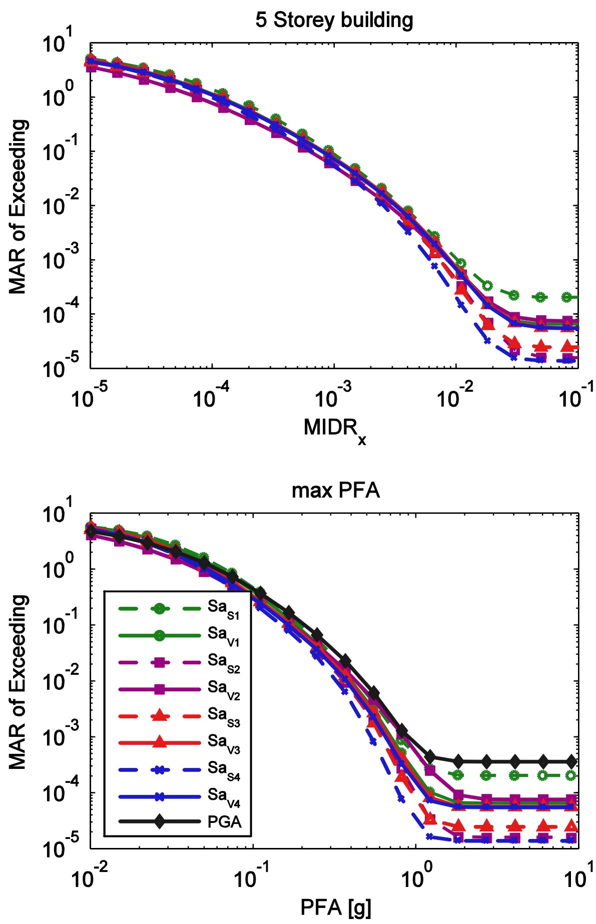

Figure 3.7. Comparison of response hazard curves obtained using different scalar IMs and a vector of IMs for the 5-story building: a) MIDRX, b) maximum PFA along the building height.

The fidelity of the linear regression analysis was checked for various IMs based on the confidence intervals of regression coefficients and their corresponding p-values. All the parameters used in the regression analysis were thus shown to be significant with few exceptions. For instance, for the 8-story building the elongated period in Y direction, $Sa_y(\alpha_u \cdot T_{1y}) / Sa_x(\alpha_u \cdot T_{1x})$, was shown to be insignificant in predicting MIDRX when Sa_{V1} is the IM. It should be noted that using spectral accelerations instead of the ratios of spectral accelerations in Sa_{V1} and Sa_{V2} would have led to wider confidence intervals for many of these coefficients making them less effective in response estimation. In addition, the results of the EDP hazard curves using regression with linear and quadratic terms showed some small differences in the low ranges of IDR, differences that are due to the effect of the interaction terms as explained previously.

3.9 **DISCUSSION**

Based on the data produced in this study and by looking at the results, only part of which is shown here, the following observations can be made:

- In general, one cannot claim with certainty which of the approaches applied provides the most accurate risk-based assessment and consequently is the most reliable method to be used for loss estimation; however, it is legitimate to expect that, given the lower dispersions suggested by some of the scalar or vector IMs used here, those IMs could be considered to be better options.
- We could say that among the applied scalar IMs, the ones based on Sa_{avg} are preferred. However, for asymmetric buildings or buildings with well-separated periods into the two orthogonal directions, like the 3- and 8-story buildings herein, other vector IMs, such as $\left\{Sa_{avgX}, Sa_{avgY}\right\}$, could provide a better solution. Such a vector IM consisting of two components is easier to compute and more practical to handle (e.g., in data fitting and programming) compared to three or four element vectors.
- A multi-element vector IM, such as Sa_{V1} can better discern the contribution of separate spectral ordinates, thus it should be a more effective IM compared to the simpler vectors or scalars based on the average of the same or similar ordinates, such as Sa_{S3}, Sa_{S4}, Sa_{V3} and Sa_{V4}. However, the addition of further spectral ordinates is easier to handle with scalar or two-component vector IMs using averaging, rather than adding too many elements in a vector. Computing a scalar hazard curve for spectral averages would not grow appreciably more complex with the number of spectral ordinates, while computing a joint hazard for a vector IM with more than 5 components, although theoretically doable, is practically cumbersome, computationally intensive, and prone to numerical inaccuracies. In addition, the “curse of dimensionality” will haunt model fitting in multiple dimensions via Equations (3.1) and (3.2), as the

inherent scarcity of data in multi-element vector spaces will eventually defeat any attempt to properly represent the IM-EDP relationship with the required detail.

- As a corollary, the higher efficiency of vector IMs, contrarily to what it implies for scalars [Luco and Cornell, 2007], should not necessarily mean that fewer records could be used in nonlinear dynamic analysis for achieving the same accuracy in the EDP estimates. The complexity of fitting a regression model using more than two predictors suggests always using a reasonably high number of analyses and records in order to provide reliable results. It can be stated here, however, that the smaller dispersion of EDPs given vector IMs is more likely to produce response estimates and, in turn, risk estimates that are not biased compared to those achieved using IMs that show a higher level of dispersion.
- Among the IMs tested, the response hazard curves based on different vector IMs are more consistent, showing only a small variation among them, whereas the scalar IMs produce less consistent results that more widely vary around their mean. While the best scalar candidates can get close to the performance of the vectors, some very bad scalar choices are obviously available that will lead the assessment to erroneous results. The MIDRX, MIDRY and maximum PFA (along the height) hazard curves of the individual (dotted lines) and the mean of all (solid line) are shown in Figure 3.8 in the left panels. In the right panels the Coefficient of Variation (C.o.V) of the MAR of response exceedance for all three buildings is presented. Clearly, the closer the building is to collapse, the more uncertain the result.

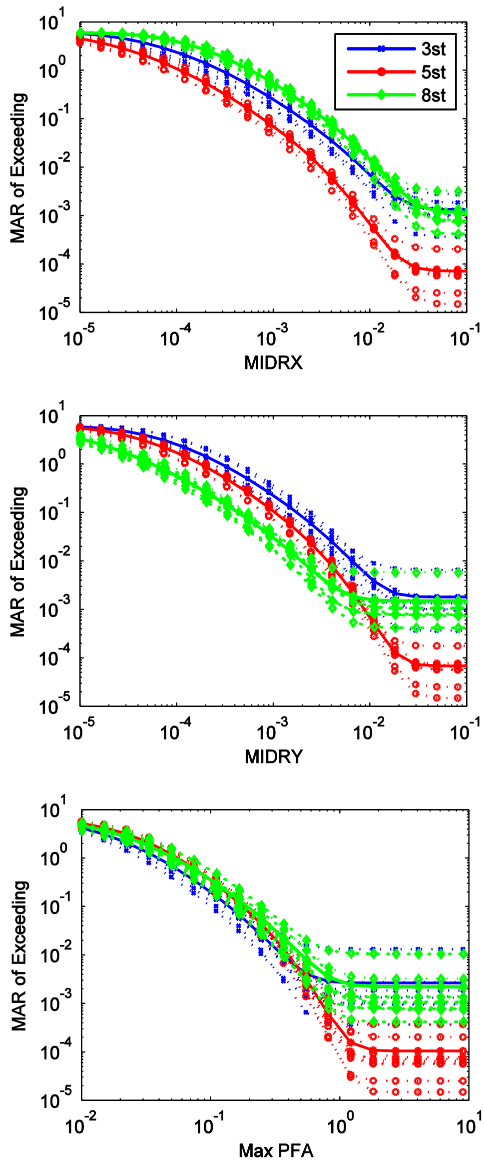

Figure 3.8. Left panels: Response hazard curves (Dotted lines: individual IM results; solid lines: mean) (blue = 3-story, red = 5-story, green = 8-story).

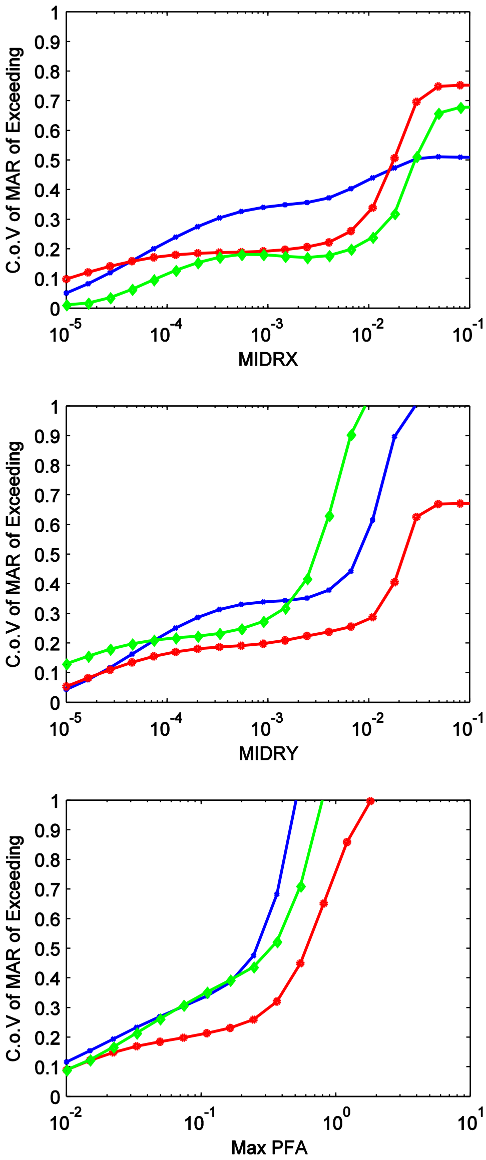

Figure 3.9: Coefficient of Variation (C.o.V) of the response exceeding rate for three building cases tested here (blue = 3-story, red = 5-story, green = 8-story).

3.10 **CONCLUSIONS**

An ideal IM for 3-D structures should be efficient in response prediction at any story within the building at both linear and nonlinear states of the structure. For a linear SDOF system or for a linear first mode dominated building, $Sa(T_1)$ is an appropriate IM. However, as the structure becomes nonlinear, the spectral acceleration at longer periods is needed. For MDOF systems, such as the ones tested herein, the effect of higher modes and spectral shape on the response becomes important. In addition, for a 3-D structural model, with coupled response in two orthogonal directions, this IM should contain separated information about the excitations in both directions. Moreover, such an ideal IM should have fairly balanced predictive potential for different structural response types such as IDR and PFA and work well all along the height of the building. As a scalar IM, average spectral acceleration is shown to be an appropriate IM for response prediction of both PFA and IDR. However, we observed here that its efficiency is relatively lower for 3-D asymmetric buildings or buildings with well separated periods in two main orthogonal directions. As such, a superior approach is offered that considers the average spectral acceleration of two orthogonal directions in a two-component vector IM. Such an IM, at least for the examples considered here, can enhance all of the advantages mentioned earlier for 3-D buildings in terms of PFA and IDR. The use of a vector IM, however, comes at a price since vector hazard estimation needs to be performed rather than the routine scalar PSHA for carrying out long-term response hazard or loss calculations. This vector IM route is more accessible if one uses the indirect method to vector hazard analysis, discussed in *Chapter 2*, rather than its original formulation.

4. MPLICATIONS OF IM SELECTION FOR SEISMIC LOSS ASSESSMENT OF 3D BUILDINGS

4.1 INTRODUCTION

In active seismic regions, earthquake might happen during the life cycle of the building causing life, monetary and downtime losses. In recent years methodologies have emerged to quantify these losses as the basis to make informed decisions about earthquake risk mitigation. In general, these methods could be divided into two main categories, namely regional and building-specific loss estimation approaches. This study is mainly concentrated on the latter, although the results of such building-specific studies are also useful to regional loss estimation.

The common approach to building-specific loss estimation is the integration of the hazard of the site with the building demands estimated via a nonlinear response history analysis of a 2D model of the building. The severity of the ground motion is often measured by $Sa(T1)$, which is the spectral acceleration at the first modal period of vibration of the structure. It is well known that to be a good intensity measure (IM) for this scope $Sa(T1)$, should be efficient, sufficient and practical. An efficient IM is a good predictor of the structural response, namely it provides low dispersion in the distribution of the engineering demand parameters (EDPs) selected to gauge the response given the IM. An IM is sufficient when the distribution of building EDPs conditioned on this IM is independent of other ground motion properties such as magnitude, distance, etc. Finally, practicality refers to the availability of such an IM for hazard computations, or in other words, to the existence of modern Ground Motion Prediction Equations (GMPEs) for that IM.

The accuracy of this common approach, however, is questionable. Firstly, during the recent years, several IMs have been shown to outperform $Sa(T1)$ for EDP prediction. Secondly, recent studies have shown that a reliable (efficient and sufficient) characterization of the EDP distribution given the IM is not a straightforward task especially, for example, for complex 3D structural models under multi-directional excitations [Faggella et al., 2013; Lucchini et al., 2011], for tall buildings [Shome and Cornell, 1999] or for buildings located at sites close to active faults where near-source type ground motions can be expected [Baker and Cornell, 2008b; Luco, 2002]. Thirdly, there are building components that are sensitive to more than one EDPs, such as infill masonry walls whose collapse damage state is sensitive to in-plane peak inter-story drift (IDR) and out-of-plane peak floor acceleration (PFA) jointly and simultaneously [Barrera, 2015]. An IM that is well correlated with the building response in the two main horizontal directions would decrease the uncertainty in the damage assessment of such components.

The complexities mentioned above suggest the necessity of exploring the availability of efficient, sufficient and practical IMs that reduce the uncertainty and bias in estimated losses, while maintaining the applicability and simplicity of the assessment procedure. In addition, most of the efforts in recent investigations on loss estimation were based on 2D structural models and scalar IMs [Aslani, 2005; Bradley *et al.*, 2009b; Goulet *et al.*, 2007; Jayaram et al., 2012; Mitrani-Reiser, 2007; Porter *et al.*, 2001; Porter *et al.*, 2002; Ramirez, 2009]. In the realm of more elaborate scalar IMs, Kazantzi and Vamvatsikos [2015a] showed that an average spectral acceleration (Sa_{avg}) is capable of capturing with an acceptable level of dispersion the response in terms of IDR and PFA all along the building height. Jayaram *et al.* [2012] went beyond scalar IMs and used a vector of spectral accelerations at multiple periods in response prediction for development of vulnerability functions for tall buildings. Along similar lines, Modica and Stafford [2014] developed vector fragility surfaces that use two correlated IMs for reinforced concrete (RC) frames in Europe. Beyond 2D models, Kohrangi *et al.* [2015f] observed that for buildings modeled as 3D structural entities separating a direction insensitive IM, such as the geometric mean of $Sa(T1)$, into two orthogonal components of the excitation (i.e. IM_X and IM_Y in a two-component vector) helps improving the accuracy of the response estimates. However, the advantages potentially brought by such advanced IMs (either scalar or vector) have not been carried forward to be tested in the assessment of loss.

Following the work of Chapter 2 and 3 that carried out hazard estimation for different spectral acceleration-based scalar and vector IMs, we investigate here the effect of the choice of the IM, which represents the severity of the ground motion and, therefore, the link to the hazard, on the loss estimates for three existing reinforced concrete buildings located at a seismically active site.

4.2 **SEISMIC LOSS ASSESSMENT FRAMEWORK**

Performance Based Earthquake Engineering (PBEE) has emerged to provide tools and develop methodologies for estimating the losses induced by probable future earthquakes. In the last decade, the Cornell-Krawinkler framing equation, adopted by the Pacific Earthquake Engineering Research Centre (PEER), has become the mainstream approach to PBEE. It comprises a four-step methodology that combines: i) Hazard Analysis, ii) Demand Analysis, iii) Damage Analysis, and, iv) Loss calculations, in a full probabilistic approach that takes into account different sources of uncertainty for the estimation of losses due to future seismic events. This procedure is summarized in Equation (4.1):

$$\lambda(DV) = \iiint G(\mathrm{DV} \mid \mathrm{DM}) \cdot \left|\mathrm{dG}(\mathrm{DM} \mid \mathrm{EDP})\right| \cdot \left|\mathrm{dG}(\mathrm{EDP} \mid \mathrm{IM})\right| \cdot \left|\mathrm{d}\,\lambda(IM)\right| \tag{4.1}$$

In this equation, IM is the Intensity Measure that gauges the level ground motion severity and that is also used for structural response estimation. Probabilistic Seismic Hazard Analysis (PSHA) provides the Mean Annual Rate (MAR) of exceeding any given level of seismic intensity, $\lambda(IM)$. Theoretically, this IM can be any ground motion property in scalar or vector format. Whatever it is, it should be an appropriate representation of the ground motion, on one hand, and a proper structural response predictor, on the other hand.

As mentioned earlier, EDPs can be the Peak Floor Acceleration (PFA), the peak Inter Story Drift ratio (IDR), as adopted by FEMA P-58 [2012], or whatever other structural response measure, perhaps indicative of local damage such as plastic rotations or curvature, that the engineer deems necessary.

Finally, DV is one or more Decision Variables (or performance measures) that are meant to support decision-making by stakeholders. These variables are commonly defined as monetary losses, downtime and casualties. $G(\cdot)$ is the complementary cumulative distribution function (CCDF), and $\lambda(\cdot)$ is the function of the mean annual rate of exceeding values of its argument, here the IM. These quantities are blended in Equation (4.1), which integrates elements of hazard analysis, structural response analysis, damage evaluation and loss assessment to assist in the decision-making process [Mitrani-Reiser, 2007]. The most practical approach for numerical computations of Equation (1) is performing the integration via Monte Carlo simulation, which is also the method used in this study.

The connection of IM and EDP requires careful structural modeling and nonlinear analysis for the estimation of $G(EDP|IM)$ distribution. This could be obtained by Incremental Dynamic Analysis (IDA) [Vamvatsikos and Cornell, 2002], or by means of cloud or multiple stripe analysis [Baker, 2007; Jalayer and Cornell, 2009]. In order to associate the derived EDP levels with structural damage, fragility functions (or curves) for specific Damage States (DS) of specific components (e.g., columns, partitions, etc.) are employed (see Kennedy and Ravindra, 1984 for one of the earliest studies and Porter *et al.* [2007] for one of the recent ones). For each component and damage state, a corresponding cost function is used for cost analysis of repair actions and losses. By integrating losses over each level of the IM, for all components in the building one can generate the so-called vulnerability (or, somewhat improperly, damage) functions that provide a complete probabilistic characterization of seismic loss of the entire building at each IM level. By integrating (in this case, numerically) the vulnerability function of the building with the seismic hazard curve, one can get the result of Equation (4.1).

FEMA P-58 [2012], as a result of the research efforts at US Federal Emergency Management Agency (FEMA), currently provides the most recent guidelines that form the state-of-the-art in the probabilistic estimation of the seismic loss for buildings. These guidelines along with the component-based fragility curve database and the cost functions and the companion software (called PACT) provide the necessary tools for carrying out the full procedure explained above. To this end, the user needs to group the structural and non-structural components and building contents into sub-groups that are expected to have the same behavior and damage, and that are sensitive to the same EDP. Such structural components are defined based on the same fragility curves that are functions of the same EDP. These component-based fragility functions are based mainly on either IDR or PFA at the story where the components are located. In each response analysis, besides monitoring damage/losses at the component level, maximum residual inter story drift ratio (MrIDR) of the global structure is also monitored to ascertain whether the building can be repaired or should be demolished (and replaced). Commonly, an empirical fragility curve is used to define the probability of non-reparability (i.e., demolition) given the MrIDR value [Ramirez and Miranda, 2009].

For each ground motion record, once the structural response in terms of different EDPs at each story and perhaps in the two main orthogonal directions is estimated, the damage state that each component ends up in is simulated and, through the connection of each damage state with a repair cost distribution, the corresponding repair costs of each damaged component is also simulated from the corresponding fragility curve (or surface). This exercise is done a number of times for each ground motion and repeated for all ground motions at each IM level. The fragility curves (or surfaces) are usually assumed to be log-normally distributed and the repair functions are assumed to be normally distributed. The loss estimates are the output of this large Monte Carlo simulation where the uncertainties in the different aspects of the problem are explicitly accounted for. It should be noted that, for any given ground motion and realization of the component-by-component repair cost, the overall integrity of the building is also simulated given the value of MrIDR. More precisely, a simulation is performed on whether the building has collapsed and, if not, whether it is repairable. If the simulation indicates that the building is collapsed or non-repairable, then the loss for that simulation is equal to the total building replacement cost plus, in the latter case, the cost of demolition.

Note that for all the records at each IM level, the software tool provides the disaggregation of the expected repair cost for each component type (structural, non-structural, contents or specific components) or due to collapse and non-reparability [Mitrani-Reiser, Aslani, 2005; 2007]. This detailed information is useful for understanding what parts of the structure are most vulnerable and potentially help guide appropriate retrofitting schemes.

4.3 **SCALAR AND VECTOR IMs CONSIDERED IN THIS STUDY**

In order to compare the uncertainty introduced to the losses estimated using Equation 1 from the response estimation based on different conditioning IMs, we considered the group of scalar and vector IMs listed in Table 4.1. The goal is to study the effectiveness in estimating the EDPs of the most natural predictors available to engineers, namely the elastic spectral accelerations at different periods used singularly or jointly. We carried out this analysis for 3D models of buildings, as opposed to 2D models, as usually done. In Table 4.1 the names of all the IMs that are composed of spectral accelerations start with *Sa*. The first index, either *S* or *V*, defines whether the IM is a scalar or a vector. The second index is meant simply to distinguish each Sa-based IM from another. Note that we also consider PGA as a predictor for the EDPs.

Table 4.1. IMs considered in the response estimation

INTENSITY MEASURE (IM) **	ABBREVIATION*
SCALAR IMs	
Natural logarithm of arbitrary spectral acceleration at the first modal period $\ln\left[Sa_x(T_{1x})\right]$ or $\ln\left[Sa_y(T_{1y})\right]$.	Sa_{S1}
Natural logarithm of the geometric mean of spectral acceleration at the average period, $\ln\left[Sa_{g.m.}\left(\bar{T}=\left(T_{1x}+T_{1y}\right)/2\right)\right]$.	Sa_{S2}
$\ln\left[Sa_x\left(\alpha_1\cdot T_{1x}\right)\cdot Sa_x\left(T_{1x}\right)\cdot Sa_x\left(\alpha_u\cdot T_{1x}\right)\cdot Sa_y\left(\alpha_1\cdot T_{1y}\right)\cdot Sa_y\left(T_{1y}\right)\cdot Sa_y\left(\alpha_u\cdot T_{1y}\right)\right]$	Sa_{S3}
$\ln\left(\left[\prod_{i=1}^{n}\left(Sa_x\left(T_{xi}\right)\right)\right]^{1/n}\right)\cdot\ln\left(\left[\prod_{j=1}^{m}\left(Sa_y\left(T_{yj}\right)\right)\right]^{1/m}\right)$, $\alpha_1\cdot T_1\le T_i\le\alpha_u\cdot T_1, m=n=10$ §	Sa_{S4}
Natural logarithm of the geometric mean of Peak Ground Acceleration, $ln[PGA_{g.m.}]$	PGA
VECTOR IMs	
$\ln\left\{Sa_x(T_{1x}),\frac{Sa_y(T_{1y})}{Sa_x(T_{1x})},\frac{Sa_x(1.5\cdot T_{1x})}{Sa_y(T_{1y})},\frac{Sa_y(1.5\cdot T_{1y})}{Sa_x(1.5\cdot T_{1x})}\right\}$	Sa_{V1}
$\ln\left\{Sa_{g.m.}(\bar{T}),\frac{Sa_{g.m.}(0.5\cdot\bar{T})}{Sa_{g.m.}(\bar{T})},\frac{Sa_{g.m.}(1.5\cdot\bar{T})}{Sa_{g.m.}(0.5\cdot\bar{T})}\right\}$	Sa_{V2}
$\ln\left\{\left[Sa_x\left(\alpha_1\cdot T_{1x}\right)\cdot Sa_x\left(T_{1x}\right)\cdot Sa_x\left(\alpha_u\cdot T_{1x}\right)\right]^{1/3},\left[Sa_y\left(\alpha_1\cdot T_{1y}\right)\cdot Sa_y\left(T_{1y}\right)\cdot Sa_y\left(\alpha_u\cdot T_{1y}\right)\right]^{1/3}\right\}$	Sa_{V3}
$\ln\left\{\left(\left[\prod_{i=1}^{n}\left(Sa_x\left(T_{xi}\right)\right)\right]^{1/n}\right),\left(\left[\prod_{j=1}^{m}\left(Sa_y\left(T_{yj}\right)\right)\right]^{1/m}\right)\right\}$,	Sa_{V4}

*All the *IMs* are based on natural logarithm transformation. The notation ln is removed from the abbreviations for brevity

** α_1 is equal to 0.8, 0.2 and 0.2 for the 3-, 5- and 8-story, respectively. α_u is equal to 1.5 in all cases.

§ The periods are equally spaced.

More precisely, Sa_{S1} corresponds to the simple spectral acceleration at the first mode period of the structure in X or Y directions of the building. Sa_{V1} corresponds to a four-component vector IM that includes the first modal periods of the building in X and Y directions and corresponding elongated periods. Sa_{S2} stands for the spectral acceleration at the averaged period, $\bar{T}=(T_x+T_y)/2$, of the structure in the two main building orthogonal directions, X and Y (as proposed for 3D structural models by FEMA P-58, 2012). The corresponding vector IM that average spectral accelerations is Sa_{V2}, which includes such averages centered at $0.5 \cdot \overline{T}$, $\overline{T}$ and $1.5 \cdot \overline{T}$. Note that, to avoid problems caused by multi-collinearity of different predictors in the regression analyses to come, in the vector IMs of Sa_{V1} and Sa_{V2}, all of the spectral accelerations, other than the first component of the vector, are normalized to the previous component. This artifact significantly reduces the correlation between each vector components.

In addition, Sa_{S3} and Sa_{S4} represent average spectral acceleration [Bianchini *et al.*, 2009; Cordova *et al.*, 2000] in two different formats. Sa_{S3} consists of spectral acceleration at six relevant periods, three for each one of the two main orthogonal horizontal directions of the building: the first mode period, a period longer than the first mode ($\alpha_u \cdot T_1$) and a period shorter than the first mode corresponding to higher modes ($\alpha_1 \cdot T_1$). α_1 and α_u are defined in Table 4.1 for each building. Sa_{S4} considers a range of periods (ten for each main orthogonal directions of the building for a total number of twenty) that brackets the first modal period. The corresponding vectors Sa_{V3} and Sa_{V4} have the same components that are averaged in Sa_{S3} and Sa_{S4}. The difference is in the spectral accelerations from X and Y components of the ground motions that are separated in two to form the vector IMs. Finally, PGA as one of the best-known and ubiquitous scalar IMs is also added for comparison purposes. It should be noted that, in all of these cases, except for Sa_{S2}, Sa_{V2} and PGA that use the geometric mean of the ground motion horizontal components, the values are based on the arbitrary ground motion component. It is stressed here that there is full consistency for all these IMs in the hazard calculation and response estimation. In particular the definition of the sigma in the GMPE considers whether the IM is extracted from an arbitrary component or is calculated using the geometric mean definition (Baker and Cornell, 2006). More information about the criteria that guided the definition of these IMs for response prediction could be found in Kohrangi *et al.* [2015f].

4.4 CASE STUDY BUILDINGS, SITE SPECIFIC PSHA AND RECORD SELECTION

Three examples of 3-, 5- and 8-story buildings representative of typical Southern Europe design and construction practices, designed without provisions for earthquake resistance, are selected for this study (Figure 4.1). More details about the properties of these building examples, their structural modeling, and their modal, static and dynamic response can be found in Kohrangi *et al.* [2015f].

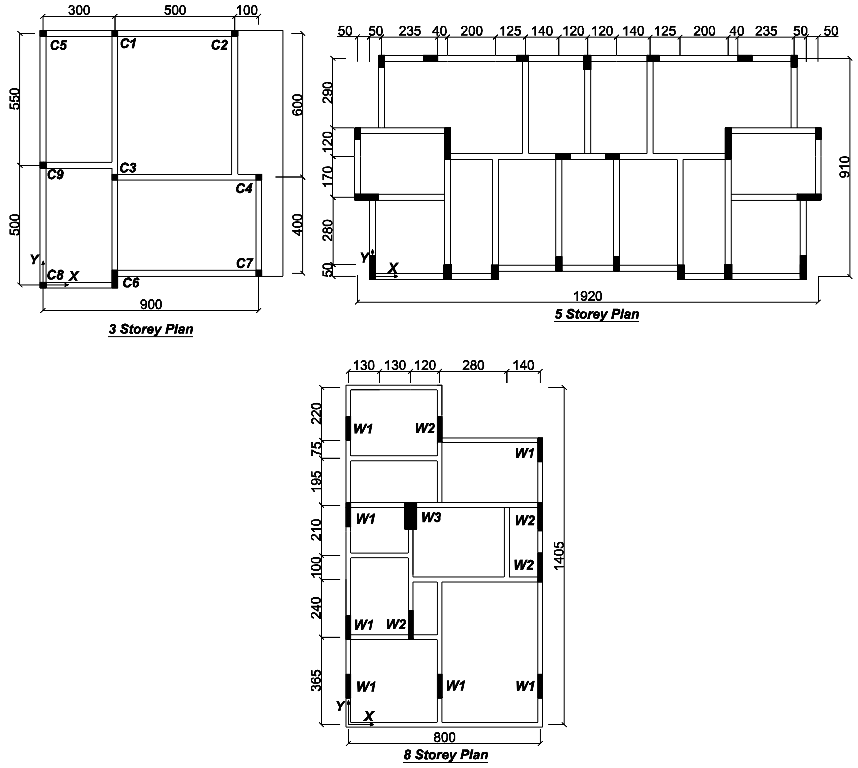

Figure 4.1. Plan view of the three considered structures (dimensions in cm)

A site in southern Marmara Sea in Turkey with latitude and longitude of 29.1 and 41.0, respectively, was selected for this study (4.2a). All sources within 200 km from the site have been considered in the calculations. OpenQuake [Monelli *et al.*, 2012] which is open-source software for seismic hazard and risk assessment developed by the Global Earthquake Model (GEM) organization, was used to perform the seismic hazard computations. These computations are based on the Area Source model and Fault Source and Background (FSBG) model developed during the Seismic Hazard Harmonization in Europe (SHARE) Project [Giardini *et al.*, 2013]. The scalar and vector PSHA (VPSHA) calculations for all IMs listed in Table 4.1 were computed via the "indirect" approach to VPSHA [Bazzurro et al., 2009]. This method does not uses specialized vector PSHA software but rather utilizes the scalar PSHA output results of OpenQuake, that is disaggregation and hazard curves (see: Kohrangi *et al.*, 2015e). Figure 4.2(b) shows as an example the Mean Annual Rate (MAR) of equaling different levels of acceleration for the two-component vector IM of Sa_{V4} evaluated for the period range pertinent to the 8-story building.

(a)

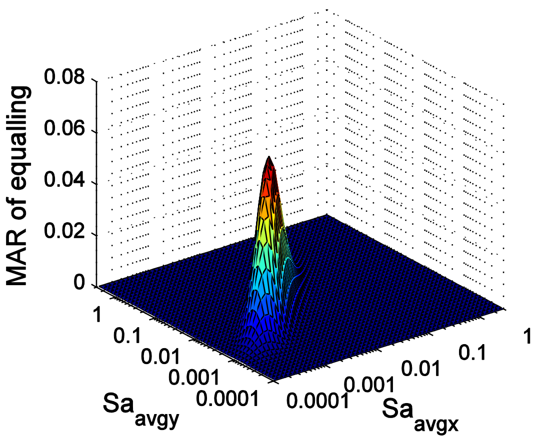

(b)

Figure 4.2. Hazard Analysis results: (a) Site map showing the location of fault sources (blue lines), background source model (red lines), the area source model (black lines), and the assumed location of the building (yellow pin), b) MAR of jointly equaling values of averaged spectral acceleration for X and Y components (Sa_{avgX} and Sa_{avgY}, respectively) of Sa_{Y4} for periods related to the 8-story building.

Three sets of records for 10, 12 and 10 IM levels based on the Conditional Spectrum (CS) method [Jayaram *et al.*, 2011] forY the periods relevant to the 3-, 5- and 8-story buildings, respectively, were selected. In this methodology, each level of the conditioning IM (which was selected to be Sa_{S2} in this study) uses a suite of 20 ground motion records selected and scaled to match the entire conditional distribution of spectral accelerations, represented by the CS. This way, both the mean and variance of the record set are consistent with the seismic hazard of the site. Kohrangi *et al.* [2015f] includes the details of record selection and hazard consistency.

4.5 RESPONSE AND COLLAPSE ESTIMATION

To gain a continuous representation of the distribution of EDP given IM, a linear regression is utilized of the form $\ln EDP = a + \sum_{i=1}^{n} b_i \cdot \ln IM_i$, where IM_i is the i-th element of the a vector IM with n elements, or the single scalar IM and a and b are the regression coefficients (see also Kohrangi *et al* 2015b).. The efficiency [Luco and Cornell, 2007b] of each IM presented in Table 4.1 was compared based on the corresponding conditional dispersion of $EDP|IM$ for each building example at each story level and in the two main directions [Kohrangi *et al.*, 2015f]. Certainly a suitable IM should be capable of response prediction in terms of structural deflections (e.g., IDR along the height of the building) in the linear and nonlinear ranges of the response since the safety of the building depends on limiting deflections. On the other hand, structural, non-structural and contents in a building are sensitive to different EDPs. Although most of the structural elements are IDR-sensitive, with the notable exception of partitions, non-structural components and contents are mainly PFA-sensitive. However, research has shown that IDR and PFA in different story levels are often best predicted by means of different scalar IMs, which is the opposite of what done in common practice where $Sa(T_1)$ is applied as the only predictor for all the EDPs everywhere in the building both in the linear elastic and in the severe post-elastic response regimes. As the integration with hazard is much simpler if performed using a single IM as predictor of EDPs, it is a challenge to select one that can improve upon $Sa(T_1)$, offer efficient and sufficient response estimation both in the linear elastic and post-elastic range of all required EDPs in the structure, and is itself predictable (namely has a GMPE developed for it).

Moreover, it is clear that the predicting the response of 3D structural models under multi-directional excitation estimated in the main directions of the building requires using separate information from each ground motion component, [Kohrangi *et al.*, 2015f]. This fact is particularly significant for asymmetric buildings or for buildings with well separated periods in two main orthogonal directions. This increased resolution of the response monitoring via multiple direction-specific EDPs is useful for improving damage estimation of building components that are less sensitive to maximum response in the two orthogonal directions or their Square Root Sum of Squares (SRSS) value. In general, it was observed that for an accurate response prediction in terms of IDR in the severe post-elastic range one is well served by considering, for example, the spectral acceleration at an elongated period of the structure (e.g., 1.5 or 2 times T_1, the fundamental period of the structure), that is more related to the nonlinear response of the building. In addition, for tall buildings, influenced by the higher mode effects, spectral accelerations at periods lower than the first modal period are needed within the IM predicting pool. These higher spectral ordinates are also significantly important for PFA prediction especially at the mid-height of the structure.

These observations, at least for the tested buildings, led to the conclusion that an average spectral acceleration in a suitable period range had the potential to provide good response estimation equally appropriate for the PFA and IDR everywhere in the building. An even higher efficiency can be achieved for the response estimation in the X and Y directions when the ground motion excitations were kept separated in a two-component vector (as in Sa_{V3} and Sa_{V4} in Table 1), representing separately the excitation of each direction. This applies especially to 3D asymmetric buildings or to those with well-separated periods in two main orthogonal directions.

As an example of the response analyses results, Figure 4.3(a) shows the IDR estimates at the first story of the 3-story building and Figure 4.3(b) displays the building collapse prediction based on logistic regression using the $IM=Sa_{V4}$. Two collapse criteria were considered: the global side-sway collapse, which we equated to the failure in convergence of the Nonlinear Dynamic Analysis at large displacements; and In addition, we considered a local collapse criterion corresponding to the exceedance of the median IDR that can be associated to the loss of load bearing capacity of the non-ductile columns [Aslani, 2005]. Following Shome and Cornell [1999], the rate of exceeding different values of an *EDP*, $\lambda(EDP > edp)$, can be computed using the conditional complementary cumulative distribution function of $EDP|IM$ for the non-collapsed data, $\mathrm{P}(EDP > edp \mid \mathrm{NC}, IM)$, and the probability of collapse given *IM*, $\mathrm{P}_{collapse|IM}$, along with the rate of occurrence of the scalar or vector IM of interest, $\lambda(IM)$.

Logistic regression [Kutner *et al.*, 2005] was used to compute the probability of collapse for each IM level while linear regression was used to model $\mathrm{P}(EDP > edp \mid \mathrm{NC}, IM)$. Figure 4.4(a) shows the response hazard curve of the MIDR in Y-direction for the 3-story building while. Figure 4.4(b) illustrates the response hazard curve for PFA at the first story of the 3-story building. The observed scatter in the response of MAR of exceeding low EDP values (i.e., those in the linear or quasi-linear state of the building response) using different IMs is small while it increases for larger EDP values, as expected. Note that since the 3-story building is subject to torsional behavior, the response in one direction is also correlated with the excitation in the orthogonal direction. Thus, IMs that contain information from the excitation in one direction only (such as Sa_{S1}) or the ones that indiscriminately combine the excitations from the two directions (such as Sa_{S2}, Sa_{S3} and Sa_{S4}), introduce more scatter in the response prediction. Therefore, the response hazard curves using such IMs can arguably be considered to be less reliable.

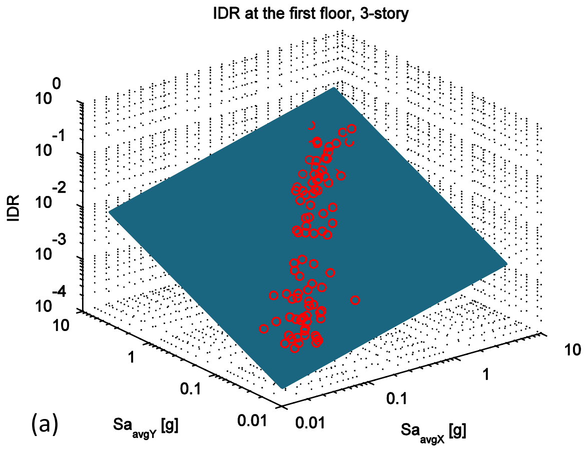

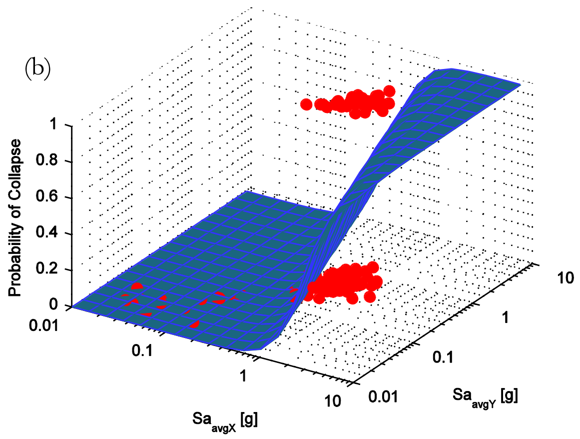

Figure 4.3. Examples of building response estimation using *IM = Sa*$_{V4}$ as predictor: (a) Response estimation of the SRSS of IDR at first story for the 3-story building, (b) Collapse fragility surface based on logistic regression (red dots show the binary data: Collapse=1, non-collapse=0).

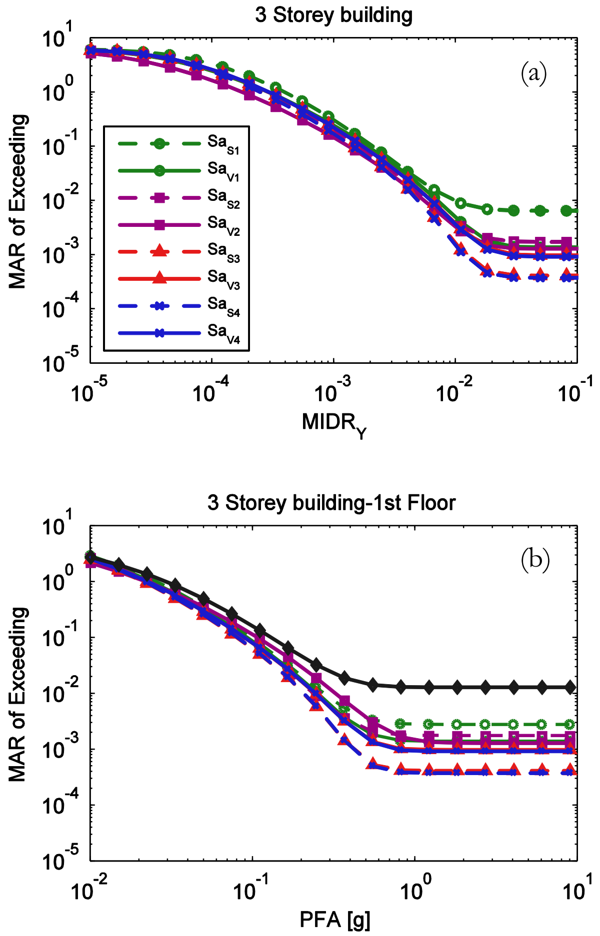

Figure 4.4. Comparison of response hazard curves obtained using different scalar and vector IM predictors for the 3-story building: (a) Maximum (along the height) Inter Story Drift Ratio in Y direction (MIDRY), (b) PFA at the 1-st floor.

To engineers the MAR of collapse is the most important estimate to extract from such curves [Zareian and Krawinkler, 2007]. To risk analysts the MAR of collapse, which corresponds to losses equal to the replacement cost of the building, are somewhat less crucial since, statistically speaking, these extreme events occur very rarely for engineered buildings. Mathematically, the MAR of collapse, which corresponds to the flat part of a response hazard curve, can be computed as follows:

$$\lambda(collapse) = \int_0^\infty P_{collapse|IM} \cdot |d\lambda IM| \tag{4.2}$$

presents a summary of the MAR of collapse for the three buildings as estimated using the different IM types considered here and Table 4.2 summarizes the coefficients of variation of MAR computed a) using the estimates from all the nine IMs (called C.o.V_{all}) in Table 1, b) using the estimates only from the six scalar IMs (called C.o.V_S), and c) using the estimates from the four vector IMs (called C.o.V_V). As anticipated, the variation in the estimates of MAR from the vector IM cases is much lower than that from the scalar IM cases.

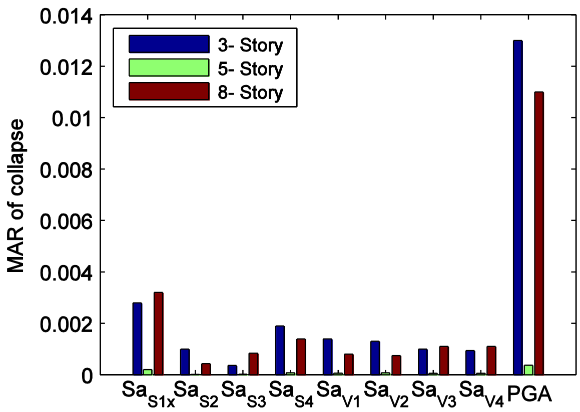

Figure 4.5. Comparison between MAR of collapse for 3-, 5- and 8-story building and for different scalar and vector IMs.

Table 4.2. Coefficient of variation of MAR of collapse as estimated using scalar and vector IMs

Building	C.o.V_{all}	C.o.V_S	C.o.V_v
3- story	1.50	1.37	0.19
5- story	1.08	1.10	0.15
8- story	1.47	1.30	0.20

4.6 LOSS ESTIMATION

The final target of the applied performance assessment is to estimate the losses for a given performance measure (or decision variable). This measure here is defined as the monetary losses, or direct cost of repairing the physical damage suffered by structural and non-structural components of a building. The effect of using different IMs for the EDP prediction is examined based on the building inventory component fragility functions and the corresponding estimated repair or replacement costs. In the following sections, the method used for response and collapse simulation and the building inventory components is explained and finally the results of the analysis for different building examples and different IM types are presented.

4.7 **RESPONSE SIMULATION METHODOLOGY**

The response distribution (parameterized in terms of median and dispersion of EDP|IM) for IDR, PFA, MIDR and MrIDR at each structural level and each direction of the building and the corresponding covariance matrix of all the EDPs were used to simulate the structural demands at each scalar or vector IM level. The response covariance matrix is obtained from the non-collapse data points and, in addition, it is assumed to be constant at all IM levels. The effect of global collapse was incorporated by sampling from the collapse IM distribution obtained from the logistic regression. This assumption of a constant covariance matrix is admittedly an approximation since the correlation between different demand parameters (e.g. IDR at different story levels) does change at different response levels. Note that Jayaram *et al.* [2012] found that such covariance matrices are relatively constant across different ground motion Intensity levels.

A more effective approach to resolve the complexity of accounting in terms of EDP correlation matrix would be using IDA or multiple stripe analysis in which the correlation between EDPs is automatically built in each single run. However, these approaches are less practical when we use vector IMs as predictors, as done in this study. Hence, we are forced here to work with a cloud of data for response estimation.

For this study, the response simulation algorithm proposed by Yang *et al.* [2006, 2009] for the ATC-58 Project was used. Note that we considered only on the record-to-record variability whereas sources of epistemic uncertainty, such as modelling uncertainty, were neglected. The reader interested on the effect of epistemic uncertainty on collapse and loss assessment results is referred to Liel *et al.* [2009] and Jayaram *et al.* [2012].

4.8 **BUILDING INVENTORY FRAGILITY AND CONSEQUENCE FUNCTIONS**

The damage state (DS) (i.e., minor damage) that a component of a given subsystem (e.g., columns, beams, walls) at any given story finds itself in when subject to a certain value of an EDP is simulated based on the fragility function derived here. A component fragility function for a given DS describes the probability of a component reaching or exceeding that DS when subject to various levels of and EDP. Note that the component-based fragility curves are probability valued function of the EDP unlike a building fragility function, which is a probability valued function of a ground motion IM. The fragility functions utilized to calculate the probability of component j (e.g., partitions) at the k-th story to be in a damage state ds_i or worse for a given EDP (denoted by EDP_{jk}) are assumed to be cumulative lognormal distribution functions as shown below [Jayaram *et al.*, 2012]:

$$P(DS \geq ds_i \mid \mathrm{EDP}_{jk}) = \Phi\left(\frac{\ln(\mathrm{EDP}_{jk} / \mu_{ijk})}{\beta_{ijk}}\right), \tag{4.3}$$

The quantities μ_{ijk} and β_{ijk} denote the corresponding median and dispersion and $\Phi(\cdot)$ is the cumulative distribution function for the standard normal distribution. In this study, for simplicity we considered a perfect correlation between the damage states of components of the same type located at the same floor. In reality, nominally "identical" components may sustain different levels of damage for the same story-specific EDP input as their capacity is uncertain and typically not identical in different components. Jalayer and Cornell [2004], Baker [2008a] and Bradley and Lee [2010b] proposed an approach that considers the dependence in the damage capacity of a component rather than in its damage state.

The damageable components considered, for example, for the 5-story building are listed in Table 4.3. The building inventory components considered for the other two buildings are similar and could be found in Kohrangi [2015a]-Appendix F. Table 4.3 shows the component (or subsystem) name, the number of components per floor and whether they are aligned in X or Y direction (in the case of infill walls), number of damage states, the controlling EDP type and the median and dispersion values of the corresponding distributions. Beam-column joints, stairs and infill walls are IDR-sensitive. For instance, it is assumed that the RC walls aligned with the X direction of the building are only sensitive to the IDRX response of the story where they are located. This assumption may not strictly apply to some structural components that may be sensitive to EDPs in both orthogonal directions in which case a fragility surface rather than a curve may be a more suitable choice. An alternative approach suggested by some researchers is the application of the SRSS of the response (in time) from both orthogonal horizontal directions. For instance, Mitrani-Reiser [2007] showed that this parameter is more useful than others (e.g., maximum IDRX or IDRY or the mean of these two maximum IDRs) for damage estimation of RC columns. As such, in this study IDRX and IDRY are used to predict losses for structural walls and their SRSS value (indicated as IDR) is used instead for beam-column joints and concrete stairs.

Most of non-structural elements and contents used here, on the other hand, are PFA-sensitive. It should be noted that the PFA values used herein for all DSs, except for the collapse limit state of the infill walls, are the maximum (in time) SRSS of the PFA values in X and Y directions, since the behavior of these components or contents is assumed to be independent of the direction in which the maximum demand occurs. In any case, we lack the detailed data on how these are oriented in the building at the time of the earthquake to have any chance of a better prediction. In this study, the component fragility function for masonry infill walls is obtained in part based on the experimental data and numerical computations explained in the next section. Finally note that the vertical ground motions were not considered here. The limitation of not having an IM related to the vertical motion at our disposal to use as predictor of EDPs and, in turn, for prediction of damage states may be relevant for some non-structural components, such as suspended ceilings or fire sprinkler piping systems that have been shown to be sensitive to vertical accelerations (see Soroushian *et al.* [2015] and Ryu *et al.* [2012], for example).

Table 4.3. Median and dispersion parameters of the fragility functions for the damage states of the different components of the 5-story building and mean and dispersion of the associated repair costs

Component	Quant per story	Damage state	Fragility Function Parameters: Median IDR*	Fragility Function Parameters: Median PFA* [g]	Fragility Function Parameters: dispersion	Repair Cost: Mean (€)	Repair Cost: dispersion	Reference
eam-column joints	9	DS1	0.0150		0.4	14750	0.28	FEMA P-58
		DS2	0.0175		0.4	23300	0.23	B1041.061a
		DS3	0.0200		0.4	28300	0.22	
Rectangular RC walls	8	DS1	0.0055		0.36	6220	0.18	FEMA P-58
	2:X	DS2	0.0109		0.30	14678	0.16	B1044.001
		DS3	0.0130		0.36	28498	0.15	
Concrete stairs	1	DS1	0.0175		0.4	450	0.57	FEMA P-58
		DS2	0.0225		0.4	2750	0.42	C2011.021a
		DS3	0.0322		0.4	18600	0.25	
Suspended Ceiling	6	DS1		0.9	0.4	250	0.39	FEMA P-58
		DS2		1.5	0.4	1950	0.37	C3032.001a
		DS3		2.2	0.4	4400	0.15	
Hydraulic Elevator*	1	DS1		0.5	0.3	700	0.82	FEMA P-58
						3180	0.32	D1014.021
						6060	0.44	
						1880	0.23	
Desktop electronics	5	DS1		0.4	0.4	700	0.3	FEMA P-58 E2022.023
Infill walls	8	DS1	0.002	0.3	0.2	80(€/m²)	0.30	Defined in this study
	4: X	DS2	0.008	0.4	0.3	200(€/m²)	0.20	
	4: Y	DS3	0.011	0.6		300(€/m²)	0.15	

* For cases denoted by X and Y, the EDP is directional while for all others the EDP value is computed via a SRSS operation.

** This component can assume four simultaneous DSs, in contrast to the mutually exclusive collective exhaustive DSs of all the other components (see FEMA 2012).

4.9 FRAGILITY FUNCTIONS FOR INFILL WALLS

As mentioned earlier, assuming that the damage of walls occurs mainly in-plane before collapse Sassun *et al.* [2016] we selected the value of IDR in the direction of the wall as the EDP, and we defined two Limit States (LS) corresponding to slight and moderate damage. For the collapse LS, however, the damage mechanism is more complex since collapse may happen either in-plane (IP) or out-of-plane (OOP) and the two failure modes are not independent [Kadysiewski and Mosalam, 2009a; Morandi *et al.*, 2015]. More specifically, Morandi *et al.* [2015] showed that the OOP strength of the wall reduces as the IP damage increases. Therefore, it is more realistic to consider a collapse fragility surface based on EDPs aligned with the wall direction and with the direction orthogonal to it.

Kadysiewski and Mosalam [2009a] derived a model for masonry infill walls together with the collapse criterion that is a function of the IP relative displacement of the infill wall (Δ_{IP}) and the OOP displacement of the wall at mid-height (Δ_{OOP}). This model was also used here in the analytical simulation (in OpenSees, McKenna *et al.*, 2000) of infills for response estimation when nonlinear dynamic analysis is performed. Although these two parameters are physically valid for collapse definition of the wall, alternatively, in a transient analysis, it is intuitive that what triggers the OOP displacement at mid-height of the wall is the floor acceleration (e.g., see Doherty *et al.* [2002], where the OOP wall model is based on the acceleration of its support). Hence, we defined a collapse fragility surface that is based on IDR in the IP direction and PFA in the OOP direction using the analytical model of Kadysiewski and Mosalam [2009a] with the typical properties of the infill walls in the tested buildings. Thus, in our response data obtained from Nonlinear Dynamic Analysis, an approximate equation that defines PFA_{OOP} as a function of Δ_{OOP} was obtained and substituted by Δ_{OOP} in the collapse criterion. Δ_{IP} , on the other hand, was simply normalized by the story height to become the in-plane IDR.

The final collapse criterion is shown in Figure 4.6(a) and the proposed fragility surface (depicted as discrete lines) is shown in Figure 4.6(b). Each line in this figure is defined based on the median in-plane IDR (which itself is a function of the PFA_{OOP} demand of every single realization) and the corresponding dispersion. The dispersion values were adopted based on the suggestions of the FEMA P-58 [2012] for analytically derived low-data fragility functions. This fragility surface is approximate and it certainly could be improved by more data and experimental results.

Morever, we assumed that at a given state of the infill wall during the dynamic analysis, the history of the response does not have any effect on the wall capacity. Instead, Barrera (2015), however, showed that, as far as the wall demand level exceeds a certain value, any subsequent damage that occurs to the wall either IP or OOP will accumulate. Therefore, a more accurate model would be the one which keeps the memory of damages within a time history analysis. Due to the complexity of such an approach, in this study the aforementioned simpler methodology is adopted. Despite its limitations, this damage model for infill walls is appropriate for illustrating the applicability of vector IMs as input to EDP and loss estimation, which is one of the purposes of the current study.

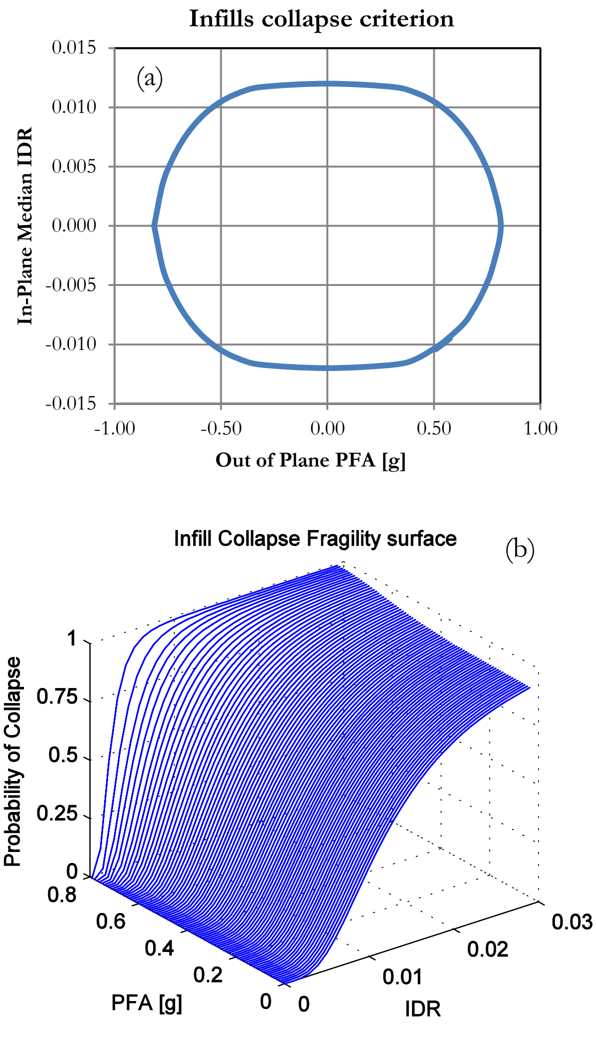

Figure 4.6. a) Infill walls collapse criterion surface; b) Infill walls collapse fragility surface

4.10 **LOSS RESULTS AND DISCUSSION**

We computed the monetary loss distributions for different IMs and building models Based on the aforementioned framework. The resulting estimates of the median and dispersion of the losses for the 5-story building predicted using the six scalar IMs in Table 1 are shown

Figure 4.7. Figure 4.7(a) shows the median loss for the entire building normalized by its replacement cost ratio as a function of the return period of the IM used as predictor of the EDP. These figures suggest that the median loss estimates computed by different ensembles of records conditioned on different IMs having the same return period at the site are not unique. The different estimates of the median loss depend on the predictability of the IM (i.e., the dispersion of the given ground motion rupture $\sigma_{IM|rup}$ from the GMPE), on the efficiency of the IM in predicting the EDP of choice (i.e., $\sigma_{EDP|IM}$), and the uncertainty in the component repair cost for a given damage state [Aslani, 2005; Bradley *et al.*, 2009b; Goulet *et al.*, 2007]. Since the uncertainty in the repair cost for a given damage state of the component is independent of the IM choice in the loss computations and the same set of records was used in the nonlinear response history analysis, the difference in the loss distributions can only be explained by the difference in predictability and efficiency of each IM. It was shown in Kohrangi *et al.* [2015f] that, in general, the average spectral acceleration (Sa_{S3} and Sa_{S4}) tends to decrease the dispersion in estimating both IDR and PFA along the height of the building compared with the more common cases of Sa_{S1} and Sa_{S2}. In addition, it was shown in Kohrangi *et al.* [2015d] that the averaged spectral acceleration has a significantly higher predictability (i.e. lower $\sigma_{IM|rup}$) than the spectral acceleration at any given period. Therefore, the higher efficiency and predictability of average spectral accelerations Sa_{S3} and Sa_{S4} may be the reason for the lower median loss estimates (Figure 4a) obtained when using Sa_{S3} and Sa_{S4}.

The logarithmic standard deviation of the loss given intensity (at equivalent return periods from seismic hazard) for the 5-story building is shown in Figure 4.7(b). While the median loss increases with the severity of the IM level, the dispersion of the loss estimates reduces as the loss distribution converges to the building replacement cost, as also observed by Krawinkler [2005] and Bradley *et al.* [2009a].

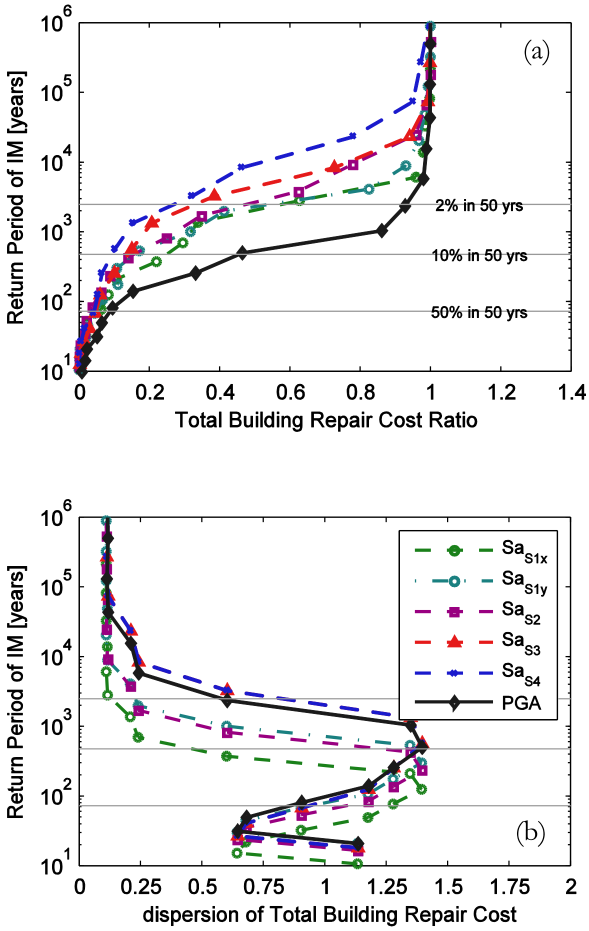

Figure 4.7. Parameters of distributions of losses normalized by the building replacement cost for the 5-story building computed using scalar IMs: (a) median, (b) dispersion.

Visual illustration of the median loss values for vector IM cases with more than two components is, of course, not possible. The median loss ratios based on the two-component vector of Sa_{v4} for the 3-story building is shown in Figure 4.8(a). Figure 4.8(b) depicts instead the variation of the probability of collapse of the 8-story building with the return period of the IM levels as computed for the six different scalar IMs in Table 1. Again the estimates of the collapse probabilities determined using the vectors Sa_{S3} and Sa_{S4} are significantly lower than those derived form the use of less efficient and predictable IMs.

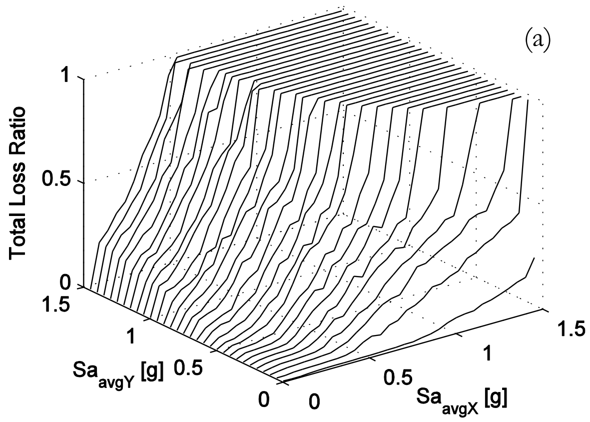

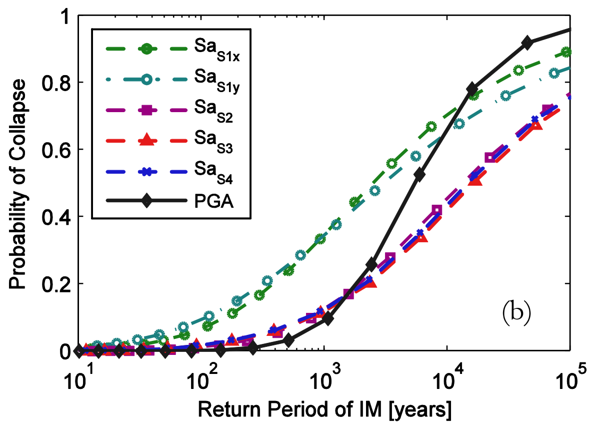

Figure 4.8. (a) Median loss values when using vector IM of Sa_{V4} for the 3-story building. (b) Probability of collapse for the 8-story building given different scalar IMs.

To gain additional insights about the differences in loss estimation caused by the choice of IM and on the components that contribute to losses at different levels of ground shaking, Figure 4.9 compares the breakdown of losses by component class for the 5-story building obtained using the ground motion records conditioned on the scalar IMs of Sa_{S1x} and Sa_{S4} corresponding to the 50% and 10% in 50 years events. The efficiency of the IM has a crucial role in predicting the distribution of the losses at any intensity level. By inspecting Figure 4.9 (a) and Figure 4.9 (c) it is clear that most of the loss contributions at 50% in 50 years event come from the infill walls and the acceleration-sensitive components. The analyses conditioned on Sa_{S4}, however, predict smaller loss percentage for beam column joints than those based on Sa_{S1x}. At higher intensity levels such as 10% in 50 years (Figure 9b and 9d), the contribution of displacement-sensitive components becomes more significant. The fraction of losses due to collapse and demolition are not significant loss factors for the 50% in 50 years probability of exceedance levels shown here. Of course, their contribution to the total losses generally grows with the intensity of the ground motions.

As can be seen in Figure 4.9 (b) and Figure 4.9 (d), the choice of IM leads to quite different damage predictions for the same intensity return period of 10% in 50 years. Sa_{S1x} predicts that the building is more vulnerable. In fact there is around 30% probability of replacing the building. Sa_{S4}, on the other hand, predicts a lower total cost with damages mostly confined to the nonstructural elements and negligible probability of collapse or demolition. Two engineers, therefore, performing the same analysis and using two different IMs will have quite different conclusions on the safety and losses of the building. We would claim that, perhaps the IM with higher sufficiency and efficiency may provide the better estimate.

Why records conditioned on different IMs having the same PE in 50 years at the site predict different losses and different loss breakdowns? It was pointed out in Kohrangi *et al.* [2015f] that the effectiveness of average spectral acceleration, such as Sa_{S4}, in predicting different EDP types is a function of the weights (i.e. the number) of the spectral ordinates at periods lower and higher than the fundamental period T_1 of the structure. Having more ordinates lower than $T1$ gives more weight to higher modes, improving PFA prediction. Having more ordinates higher than $T1$ improves the estimation capability for displacement-sensitive components and global collapse. In this case SaS_4 has a higher weight at the low period ranges, it is a better IM for prediction of PFAs while it tends to underpredict the EDP for the displacement-sensitive components, namely IDR here. In other words, different definitions of the average spectral acceleration represent different compromises in accuracy between PFA and IDR prediction. The vector IMs, by virtue of separation of ordinates, can be made less sensitive to this effect.

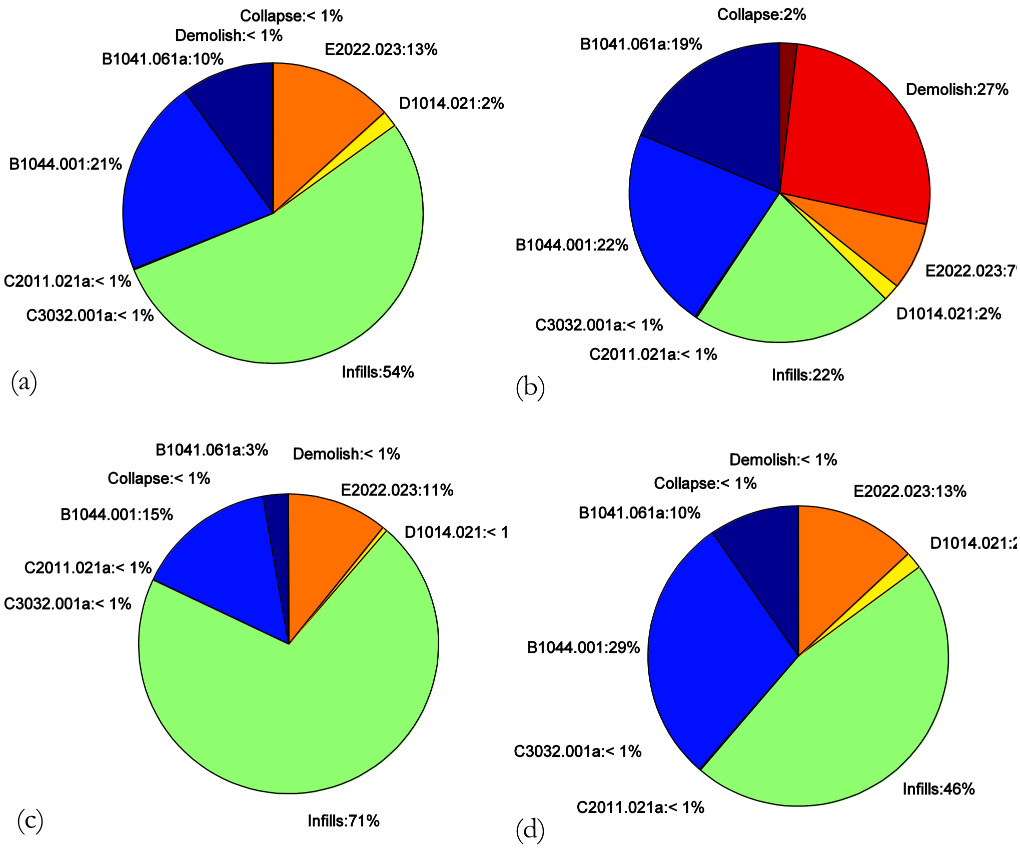

Figure 4.9. Disaggregation of Losses for of the 5-story building conditioned on (a) SaS1x at the 50% in 50 years probability of exceedance (PE), (b) SaS1x at the 10% in 50 years PE, (c) SaS4 at the 50% in 50 years PE, (d) SaS4 at the 10% in 50 years PE. Legend: B1041.061a: Beam-column joints; B1044.001: Rectangular RC walls C2011.021a: Concrete stairs; C3032.001a: suspended ceilings; D1014.021: Hydraulic Elevator; E2022.023: Desktop Electronics.

The values of the MAR of exceeding the building loss ratios as estimated using different IMs (scalar and vector) for the three building examples are shown in Figure 4.10. There is a common trend in all of the figures: PGA followed by Sa_{S1x} and Sa_{S1y} , namely the three scalar IMs, provide the highest exceeding rates and the Sa_{S3} and Sa_{S4}, namely two average spectral acceleration IMs, provide the lowest. It is interesting to note also that the vector IM cases have the lowest scatter and, therefore, we can argue that that by use of vector IMs the estimates of the loss MAR get closer to the "true" but unknown answer. We do not have solid evidence on what the "true" response is, as we do not have a "perfect" reference value to compare against. We are, however, sure that the MAR of losses that are estimated using the scalar IMs Sa_{S1x} and Sa_{S1y} are farther from the "true" answer and quite likely biased high. The consistency in the MAR values provided by the vector results points towards a higher fidelity, potentially indicating that they are closer (in the 3D examples tested) to providing an accurate answer.

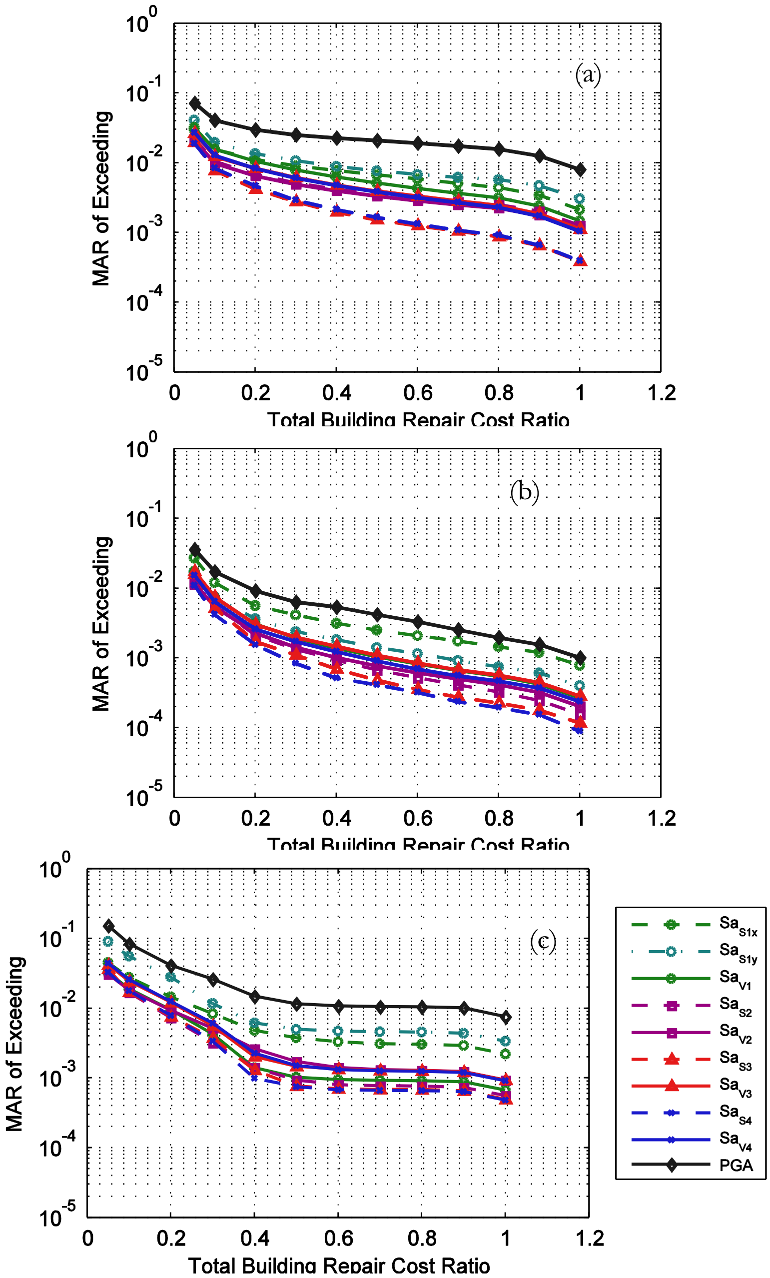

Figure 4.10. MAR of exceeding the total building loss ratio: a) 3-story, b) 5-story and c) 8-story buildings

Another useful metric in loss assessment is the Expected Annual Loss (EAL), which is the long-term average annual economic loss that the building is expected to experience due to earthquakes at that site. The EAL is useful to many stakeholders as the basis to make informed decisions about risk mitigation. An owner may use it for example to decide whether buying earthquake insurance and/or retrofit the building, while an insurance company uses it to set the technical premium that supports the computations of the insurance premiums offered to potential customers [Aslani, 2005]. An estimate of the EAL can be computed as:

$$EAL = \int_0^\infty c \cdot \left| d\lambda_c \right| \tag{4.4}$$

In which λ_c is the MAR of exceeding the cost value of *c*. If *c* is defined as a cost ratio instead, then the EAL ratio is provided by Equation (4.4).

The EAL ratios obtained conditioning on different IMs are compared in Figure 4.11. The differences in the AAL estimates from the vector cases and from the cases that use simple IMs, such as Sa_{S1x}, Sa_{S1y} and PGA are very significant. On the other hand, the differences between the MAR estimates from vector IM cases and scalar IM cases based on averaged spectral accelerations are somewhat less relevant. Note that this figure also shows the difference in the estimates of the EAL ratios that stems from the consideration for infill walls of the out-of-plane failure mode in addition to the in-plane one. The with and without interaction cases in the infill wall failure modes are only slightly different. This small difference, however, cannot be generalized, and may be due to the simplified failure model implemented here.

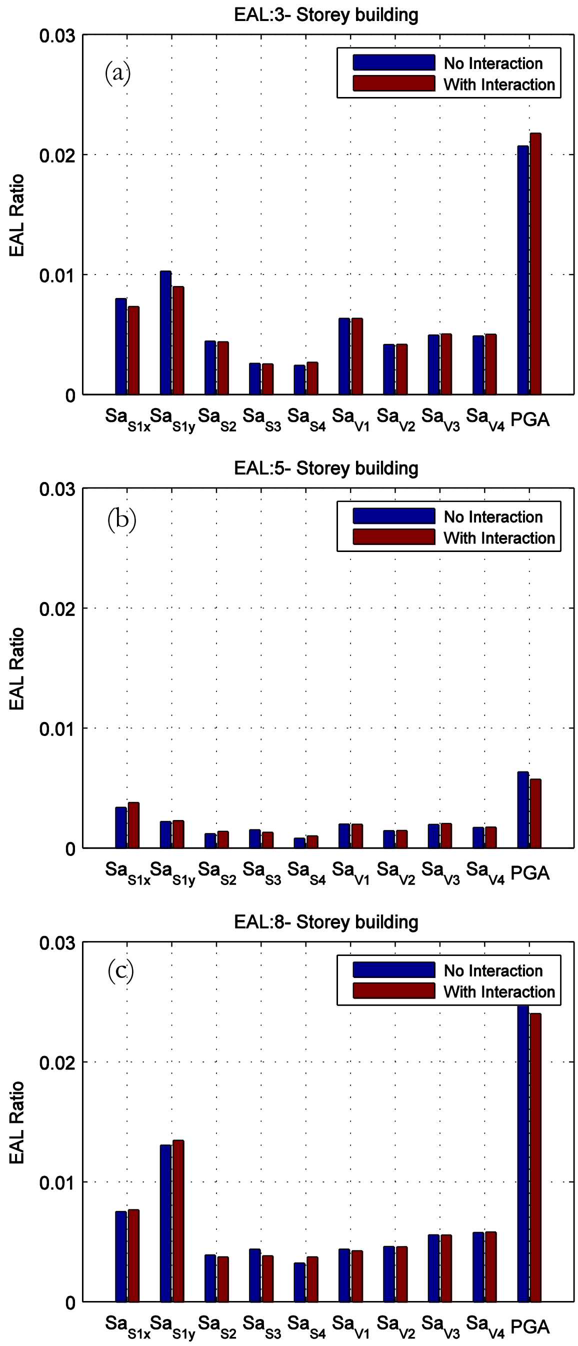

Figure 4.11. Expected Annual Loss ratio: comparison between different IM types using infill collapse fragility curves with/without interaction: a) 3-story; b) 5-story and c) 8-story.

4.11 Conclusions

The main focus of this study is to extend the current state-of-the-art PBEE procedure for building-specific loss estimation beyond the use of simple ground motion Intensity Measures (IMs) as predictor of Engineering Demand Parameters (EDPs) and, in turn, of damage states and loss of realistic 3D structural models. The investigated set of IMs still considers simple scalar spectral acceleration and PGA, as reference to common practice. However, it also includes average spectral acceleration in a period range relevant to the specific building under consideration and also various combinations of vector IMs that preserve the direction of action of the ground motion. The ground motion IM used as input to the response of these buildings is kept fully consistent with the hazard, which has been probabilistically computed for the same IM, be it simple or complex, scalar or vector, using appropriate Ground Motion Prediction Equations. Three 3D building examples of 3-, 5- and 8-story RC infilled frames, typical of old Mediterranean construction were considered as test cases for testing this methodology.

The PEER Center style loss estimation approach adopted allows detailed component-based loss analysis considering the vector of building EDPs locally at all stories rather than using only one global response parameter (e.g., the maximum inter story drift ratio). The use of vector IMs, because of the correlation of the different EDPs with multiple spectral ordinates, increases the response estimation power, therefore leading to less uncertain loss estimates. In addition, since the building response at each of the two orthogonal directions of the 3D building models is correlated to the ground motion excitation in the same direction, there is higher accuracy in the response prediction.

For the building components that are sensitive to more than one response type and/or direction of excitation, component fragility surfaces could be adopted and parameterized on more than one EDP. The results here showed that even in such cases using vector IMs, given the lower dispersion in the collapse and response prediction, lead to less dispersed loss estimates. A procedure for considering the effect of the infill walls in-plane and out-of-plane interaction based on a function of the infill demand was also implemented. However, for the building examples tested here and compared with the total building repair cost, insignificant changes were observed in the total loss values and the Expected Annual Loss. Based on the methodology introduced in this study, this approach could be adopted for other types of building components (e.g., suspended ceilings) that are sensitive to more than one EDP.

To conclude, it should be noted that all the IMs utilized in this study represent legitimate choices that are usable in practice. However, the results presented show that there is significant scatter in the estimates of the MAR of exceedance of losses. When vector IMs are used, at least of the kind utilized here, this scatter is considerably tightened.

The use of vector IMs both in hazard assessment and response estimation, as done here, might be considered cumbersome and less appealing in practice. However, using a vector IM, at the very least, can provide important insights on how far are MAR estimates obtained from simpler scalar choices from the 'true' but unknown response. Although only three buildings were studied and more research is still needed, it can be claimed that the loss assessment of 3D structures can benefit considerably from the explicit consideration of seismic intensity in the two orthogonal directions, preferably in a vector form or, at least, in a sophisticated scalar form, such as those based on spectral acceleration averaged over a building-specific period range used here. More specifically, based on the results of these analyses, the spectral acceleration at the first mode of vibration of the structure (Sa_{S1x} and Sa_{S1y}) and PGA, provide loss estimates that can arguably considered as conservative when compared to those of the other sophisticated scalar and vector IMs tested here. This large difference may pose a question mark about the effectiveness of such simple scalar IMs in capturing well the story-specific engineering demand parameters needed for assessing losses in 3D structural models.

5. CONDITIONAL SPECTRUM-BASED GROUND MOTION RECORD SELECTION USING AVERAGE SPECTRAL ACCELERATION

5.1 **INTRODUCTION**

Ground motion record selection is the link between seismic hazard and probabilistic seismic demand analysis (PSDA) of a structure. Record selection is commonly carried out based on the following procedure: first, Probabilistic Seismic Hazard Analysis (PSHA) [Cornell, 1968] is performed for one or more ground motion Intensity Measures (IMs) at the site; second, the characteristics of the events (e.g., magnitude, rupture-to-site distance, and fault type) most contributing to a given rate of exceeding or "equaling" any desired level of one of the selected IMs are obtained using disaggregation analysis [Bazzurro and Cornell, 1999]; third, based on these events' characteristics and using an appropriate Ground Motion Prediction Equation (GMPE) for their rupture mechanisms, an adequate target spectrum is defined for the scope at hand; and, fourth and last, a set of records to be used for structural response estimation is selected to "match" this spectrum.

The first and second steps of this procedure are fairly standard and will not be discussed here. The focus of this contribution is on steps three and four. The procedure to define the target spectrum and, once defined, to choose ground motion records that "match" it, is not unique. One such a procedure utilizes the Uniform Hazard Spectrum (UHS) for spectral accelerations as the target and then uses either real or synthetic records selected or generated in such a way that, *on average*, their spectra match the target within a given tolerance (say, ±5%). The matching is enforced either for every oscillator period of the UHS or, more commonly, for a period range of interest. The records are often, but not always, chosen without an explicit use of disaggregation analysis. This UHS-based approach provides sets of records that, when used as input to structural analysis, tend to produce probabilistically conservative estimates [Baker and Cornell, 2006] of the mean response of the structure for the selected ground motion hazard level unless the structure exhibits only elastic first-mode response. The going explanatory argument for this conservatisms states that real records do not usually have energy content as broad as that of the UHS and, therefore, records that match the UHS are "unnaturally" aggressive. This UHS-based approach has been used since the 1980s mostly for design of new structures or requalification of existing ones for hazard levels corresponding to the distinct limit states (e.g., serviceability or ultimate limit states) specified in design codes [ASCE, 2010; Eurocode8, 2004; ICC, 2003]. This approach was not intended to be used for risk estimation purposes.

A recent and more suitable approach for risk calculations is based on the Conditional Mean Spectrum (CMS) [Baker and Cornell, 2006] or, better, on the Conditional Spectrum (CS) [Jayaram *et al.*, 2011]. The former considers only the mean acceleration response spectrum for a given scenario event (e.g., magnitude, rupture-to-site distance, and fault mechanism) conditional on a spectral acceleration at a given period T^*, whereas the latter accounts for the variability around the CMS of the spectral accelerations at all oscillator periods except for T^* at which, by design, such a variability is zero. Along the same lines Bradley [2010a] proposed the Generalized Conditional Intensity Measure (GCIM) approach, which is a straightforward generalization of the CS method for cases where non-spectral ground motion IMs (e.g., record duration or Arias intensity) are important to the prediction of structural response. The focus of CS is on improving the *sufficiency* with respect to spectral shape while the focus of GCIM is the same but conceptually broader since the sufficiency improvement is sought with respect to all ground motion characteristics that affect the response. Sufficiency here simply means that two different sets of records that have the same spectral shape in the CS framework or, say, the same Arias Intensity in the GCIM framework, but different distributions of other characteristics (e.g., cumulative absolute velocity) generate statistically indistinguishable estimates of the Engineering Demand Parameter (EDP) chosen to gauge the response of the structure. Computational algorithms for selecting ground motions for both these methods are available [Jayaram *et al.*, 2011; Bradley, 2012c]. In this article we will not discuss the GCIM method further since it is conceptually similar to the CS method and its inclusion does not significantly contribute to the main argument presented in this paper.

In the CS approach, the pivotal ground motion IM is the elastic spectral acceleration at the conditioning period, SAT^*, where T^* is selected such that SAT^* is a good predictor of the EDP of choice. For a specific SAT^* level (e.g., SAT=0.5g, where T=1s), a suite of records is selected and scaled to "match" the target CS. Note that for hazard levels of engineering interest, the spectral acceleration values of the CMS at periods other than T^* are lower than the corresponding ordinates of the UHS.

Is the selection of a suitable value of T^* important for engineering analyses record selection? Lin *et al.* [2013b] showed that when using the CS method for *risk-based assessment* of a structure, the estimates of the annual rate, λ_{ij}, of exceeding any different level j of EDP i (e.g., 1% interstory drift ratio) are relatively insensitive to the choice of the anchoring period T^*. Lin *et al.* [2013c] pointed out, however, that the choice of T^* can have a substantial impact on the estimates of the rate, $\lambda_{ij,h}$, of exceeding any different level j of EDP i for a *given hazard level, h*. Namely records that match two different CS anchored at two different ordinates of the same UHS may, and usually do, generate vastly different estimates of λ_{ijh}. In the latter case, which is called *intensity-based assessment* and is used mainly to meet design specifications, the choice of a suitable conditioning period T^* is, therefore, crucial for obtaining robust estimates of the $\lambda_{ij,h}$ for the EDP of interest. Kwong *et al.* [2015] in fact, recommends that the engineer iteratively select an appropriate value of T^* during the design process when the dynamic characteristics of the structure are not yet finalized.

Although not as fundamental for risk based assessment as it is for intensity-based assessment, it is certainly fair to state that an unwise choice of T^* may lead to undesired consequences in probabilistic structural demand and risk computations, as we will see later in this paper. Lin et al. [2013b] points out that the choice of a suitable conditioning period T^* (or of a better conditioning IM altogether, in the GCIM method), can certainty help to achieve a more precise response prediction (this relates to the sufficiency issue discussed above). In addition, it should always be kept in mind that, besides the issue of sufficiency, a judicious choice of T^* leads to the selection of an *efficient* SAT^* (i.e., the response variability is limited for a given SAT^* value, an issue which is called *efficiency* in the literature) and, consequently, the following estimates of the $\lambda_{ij,h}$'s for the EDP i of choice obtained with a fixed, and in real applications usually limited, number of nonlinear dynamic analyses are less likely to be biased.

What should then an engineer interested in risk assessment do if he/she is unsure about an appropriate selection of T^* and is concerned about the potentially inaccurate risk estimates caused by a weak T^* choice? Selecting an appropriate value of T^* is everything but trivial and the selection depends on the objective of the analysis. If the interest is, for example, in assessing the collapse probability of a building perhaps a value of T^* that is 1.5 or 2 times the fundamental period, T_1, of the structure may be an appropriate choice. This is because SAT^* for $T^*=1.5 \cdot T_1$ or $2.0 \cdot T_1$ is a good predictor for the maximum (along the height) of the peak (in time) interstory drift ratio, MIDR, which is an EDP well correlated with collapse [Kohrangi *et al.*, 2015f].

However, usually the motivation for performing such a challenging exercise is broader than assessing the ultimate response of a building. The engineer may also want to assess *with the same set of analyses* whether the serviceability limit state of the building, namely when the structure behaves in the linear elastic regime or close to it, is met. In that case, T_1 may be a better choice for T^*. Or, again, using the same set of analyses, he/she may also want to estimate the risk of experiencing economic losses due to damage to structural (e.g., beams and columns) and non-structural (e.g., elevators, suspended ceilings, piping) components and to contents (e.g., bookcases, TV sets). Some of the non-structural components and contents are not sensitive to structural deformation but to story-specific peak floor acceleration (PFA), which is a completely different EDP than MIDR. Therefore, in complex but frequent PSDA cases, the choice of T^* based on simplistic considerations about the fundamental period of vibration of the structure is no longer adequate.

A conceptually straightforward but very impractical solution would be to repeat the same CS-based risk assessment calculations for multiple choices of T^* [Baker and Cornell, 2006] and adopt for each EDP the most conservative estimates obtained using the different values of T^*. This approach, which is consistent with the seismic hazard at the site, is, however, not only extremely time consuming but also conservative. For example, consider an ensemble of records that is consistent with a CS anchored at SAT^* with $T^*=1.5 \cdot T_1$ from a severe hazard level at the site (e.g., 10% in 50yrs probability of exceedance). This set of records tends to generate large peak interstory drift ratios (IDRs) but relatively low PFA values in a building. On the other hand, a second ensemble of CS-based records anchored at SAT^* with $T^*=0.2 \cdot T_1$ at the *same hazard level* as above tends to generate higher PFA values and lower interstory drift ratios. The first ensemble of records would estimate higher structural damage and lower non-structural damage than the second ensemble but both sets have the same occurrence rate at the site. Should the engineer perform both analyses and select the worse damage/loss estimate of the two? This example clearly shows that a conservative approach, which is often sought during design, would be undesirable for risk assessment.

An alternative, practical and arguably unbiased approach might involve the selection of an IM that is a good predictor for the ensemble of *all* the EDPs of interest but perhaps not the best for any single one. Following this insight, many researchers have considered using as the conditioning IM various versions of an average of spectral acceleration, *AvgSA*, in an appropriate range of periods [Cordova *et al.*, 2000; Baker and Cornell, 2006; Mehanny, 2009; Bianchni *et al.*, 2009; Bojórquez and Iervolino, 2011; Kazantzi and Vamvatsikos, 2015a; Eads et al., 2015; Kohrangi *et al.*, 2015e; Kohrangi *et al.*, 2015f] bracketing the structural fundamental period T_1. In this approach, it could be argued that the issue of *efficiency* would be addressed by an IM choice that is a "good" predictor for all the EDPs of interest and the issue of *sufficiency* would be addressed by performing a careful record selection based on that IM.

As in the previous literature cited above, we explore the use of different definitions of *AvgSA* as the pivotal IM of choice in Probabilistic Seismic Demand Analysis (PSDA) but here we go one step further. Although it is possible to perform the record selection based on one conditioning *IM* (e.g., SAT^*) and use a different IM (e.g., SAT' where $T' \neq T^*$) for response prediction [Vamvatsikos and Cornell, 2005 and Kohrangi *et al.*, 2015f], it is certainly preferable to be consistent by keeping the same conditioning IM in both aspects of the analysis. Hence, to ensure this consistency, we introduce here the CS-based record selection conditioned on *AvgSA*. We call CS(*AvgSA*) this variant of the conditional spectrum. The details of its definition and of its use are discussed below.

5.2 CONDITIONAL SPECTRUM BASED ON *AvgSA*

We consider the average spectral acceleration, *AvgSA*, defined as the geometric mean of the log spectral accelerations at a set of periods of interest for the estimation of multiple EDPs that are crucial for risk assessment and loss estimation of a structure of interest. These periods, for example, could be equally spaced in the $0.2 \cdot T_1$ to $1.5 \cdot T_1$ range, where T_1 is the first mode elastic period of vibration of the structure. This array of periods could cover higher mode response and also the structural period elongation caused by the nonlinear behavior due to the accumulation of damage. Alternatively, and perhaps more effectively, it could be defined as the geometric mean of log spectral accelerations at relevant elastic vibration periods of the structure, such as T_{1x}, T_{1y}, T_{2x}, T_{2y}, $1.5 \cdot T_{1x}$ and

$1.5 \cdot T_{1y}$, where x and y refer to the two main orthogonal directions of the buildings and the indices 1 and 2 refer to the first and second modes of vibration of the structure in those directions. Mathematically, $AvgSA$ is defined in Equation (5.1) and, more conveniently, by Equation (5.2) where the natural logarithm has been applied to both sides of Equation(5.1) :

$$AvgSA = \left[\prod_{i=1}^{n} SAT_i \right]^{1/n} \tag{5.1}$$

$$\ln AvgSA = \left(\frac{1}{n} \right) \cdot \sum_{i=1}^{n} \ln SAT_i \tag{5.2}$$

The quantity n refers here to the number of SAT's being averaged. Therefore, from Equation (5.2) the mean and variance of ln$AvgSA$ could be calculated using (5.3) equation (5.4) and, respectively.

$$\mu_{\ln AvgSA} = \left(\frac{1}{n} \right) \cdot \sum_{i=1}^{n} \mu_{\ln SAT_i} \tag{5.3}$$

$$\mathrm{var}(\ln AvgSA) = \left(\frac{1}{n} \right)^2 \cdot \sum_{i=1}^{n} \sum_{j=1}^{n} \rho_{\ln SAT_i, \ln SAT_j} \cdot \sigma_{\ln SAT_i} \cdot \sigma_{\ln SAT_j} \tag{5.4}$$

Where $\mu_{\ln SAT_i}$ and $\sigma_{\ln SAT_i}$ are the logarithmic mean and standard deviation of the spectral acceleration at the i-th period in the selected range as obtained from a standard GMPE. $\rho_{\ln SAT_i, \ln SAT_j}$ is the correlation coefficient between lnSAT_i and lnSAT_j. The CMS conditioned on ln$AvgSA$=x, i.e. without consideration of the variance in the spectrum, was first introduced by Baker and Cornell [2006]. The logarithmic mean and variance of CS($AvgSA$) at all periods of the spectrum can be computed as follows:

$$\mu_{\ln SAT|\ln AvgSA=x} = \mu_{\ln SAT} + \rho_{\ln SAT, \ln AvgSA} \cdot \sigma_{\ln SAT} \cdot \varepsilon_{\ln AvgSA} \tag{5.5}$$

$$\sigma_{\ln SAT|\ln AvgSA=x} = \sigma_{\ln SAT} \cdot \sqrt{1 - \rho^2_{\ln SAT, \ln AvgSA}} \tag{5.6}$$

In these equations: $\mu_{\ln SAT|\ln AvgSA=x}$ and $\sigma_{\ln SAT|\ln AvgSA=x}$ are the logarithmic mean and standard deviation of the spectral acceleration at the generic period T conditioned on ln$AvgSa$=x. The quantity $\varepsilon_{\ln AvgSA}$ is the number of standard deviations that the ln$AvgSA$ value of a record is away from the mean of ln$AvgSA$ predicted by a GMPE (see Equation

(5.3)) for the same rupture characteristics (e.g., magnitude, source-to-site distance and fault type). $\rho_{\ln SAT,\ln AvgSA}$ is the correlation coefficient between $\ln SAT$ and $\ln AvgSA$, which can be computed according to Equation (5.7) below:

$$\rho_{\ln SAT,\ln AvgSA} = \frac{\sum_{i=1}^{n} \rho_{\ln SAT,\ln SAT_i} \cdot \sigma_{\ln SAT_i}}{\sum_{i=1}^{n}\sum_{j=1}^{n} \rho_{\ln SAT_i,\ln SAT_j} \cdot \sigma_{\ln SAT_i} \cdot \sigma_{\ln SAT_j}} \tag{5.7}$$

Of course, this is not the only possible definition of spectral acceleration average that could be considered both as a conditioning IM of a CS and for record selection. In fact, we also investigated another version of *AvgSA*, called I_{NP} [Bojórquez and Iervolino, 2011], that is a normalized version of *AvgSA* to *SAT*1. The investigation of CS(I_{NP}) and related record selection, however, did not bring a significant advantage over CS(*AvgSA*) and, therefore, its treatment is omitted herein. The interested reader can find the derivation of CS(I_{NP}) and the results obtained using it in Kohrangi [2015a]-Appendix E.

5.3 UNIFORM HAZARD AND CONDITIONAL MEAN SPECTRA

As examples of the proposed record selection procedure that utilizes CS(*AvgSA*), we carry out both risk- and intensity-based assessments of four specific buildings located at a highly seismic hazard site close to Istanbul. The characteristic of such buildings will be presented in the next section. To compare and contrast advantages and disadvantages of this procedure we also perform the analysis using other more conventional IMs, such as *SAT*1. For illustration purposes only, Figure 1(b) shows the CMS for *AvgSA* and *SAT*1, called CMS(*AvgSA*) and CMS(*SAT*1), respectively, for three different hazard levels of 2%, 10% and 50% probability of exceedance in 50 years at the selected site along with the corresponding UHS. in UHS and CMS are computed using the GMPE of Boore and Atkinson [2008] and the three CMS are based on the mean scenario contributing to each hazard level obtained via seismic hazard disaggregation. Hazard levels and mean scenarios for the site are reported in Table 5.1. *SAT*1 in this example is the spectral acceleration at T_1=1.0s and the *AvgSA* is defined as the combination of *SAT*'s at the seven periods that go from $T_{min}=0.2\cdot T_1$ to $T_{max}=1.5\cdot T_1$ with an increment of 0.2s. We used the work of Baker and Jayaram [2008b] to estimate the correlation coefficient between spectral ordinates at any pair of periods T_i and T_j. Figure 5.1(a) compares the hazard curves at the selected site for *SAT*1, *AvgSA* and spectral acceleration at the seven periods in the range considered in *AvgSA*. Note that almost everywhere in the T_{min} to T_{max} period range, the CMS(*AvgSA*) lies between the corresponding UHS and CMS(*SAT*1) and, as expected, the differences between UHS and CMS(*AvgSA*) are larger for the rarer hazard level (e.g. 2% in 50yrs).

Table 5.1. Summary of mean disaggregation results for three different hazard levels

Event	*SAT*1				*AvgSA*			
	IM Level [g]	$\bar{\varepsilon}$	$\bar{M}$	$\bar{R}$	IM Level [g]	$\bar{\varepsilon}$	$\bar{M}$	$\bar{R}$
2% in 50 yrs	0.48	2.2	6.8	16.3	0.55	2.3	6.7	14.9
10% in 50 yrs	0.30	1.8	6.7	21.0	0.36	1.9	6.7	19.0
50% in 50 yrs	0.15	1.3	6.6	28.6	0.18	1.3	6.6	25.0

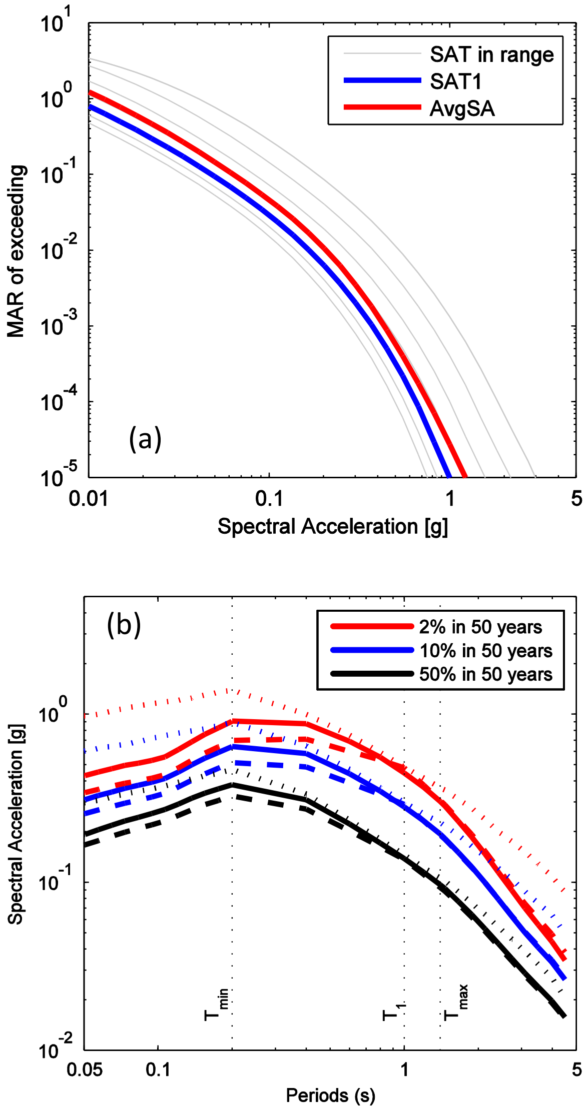

Figure 5.1(a) Site seismic hazard curves for *AvgSA*, for *SAT*1 at T_1=1.0s, and for the six intermediate periods considered in the T_{min} to T_{max} range, (b) Comparison between UHS, CMS(*SAT*1) and CMS(*AvgSA*) for the 2%, 10% and 50% in 50 years hazard levels. (Legend: Dotted lines: UHS, dashed lines: CMS(*SAT*1), Solid lines: CMS(*AvgSA*)).

5.4 CASE STUDY AND GROUND MOTION SELECTION

5.4.1 BUILDING EXAMPLE AND MODELING ASSUMPTIONS

To test our methodology, we developed two-dimensional centerline models using OpenSees [McKenna *et al.*, 2000] of four plan-symmetric reinforced-concrete moment-resisting frames with 4-, 7-, 12- and 20-stories. They are modern structures built to post-1980 seismic design provisions for high-seismicity regions (site class D). The behavior of the structural members was modeled using lumped-plasticity elements, with properties estimated from the empirical equations proposed by Panagiotakos and Fardis [2001]. These elements increase speed of computation and improve numerical convergence for large deformations. Geometric nonlinearities in the form of P-Δ effects were considered. The details of the building modeling can be found in Kazantzi and Vamvatsikos [2015]. The relevant periods of vibration of these four structures are shown in Table5.2.

Table5.2. Description of the conditioning IMs used for record selection and structural response estimation. The periods are expressed in seconds.

	*SAT*1	*SAT*2	*SATH*	*AvgSA*
	*T*1	*T*2	1.5·*T*1	Period range
4-story	1.82	0.57	2.73	0.57:0.2:2.77
7-story	1.60	0.52	2.40	0.52:0.2:2.52
12-story	2.10	0.73	3.15	0.73:0.2:3.13
20-story	2.85	0.92	4.28	0.92:0.2:4.32

5.4.2 IMS USED FOR RECORD SELECTION AND RESPONSE PREDICTION

To illustrate the procedure, we selected ground motion ensembles to match two different definitions of CS: CS(*SAT*) and CS(*AvgSA*). The CS(*SAT*) was computed for three single-period conditioning spectral accelerations: *SAT*1, *SAT*2, and *SATH*, where *T*1 and *T*2 are the periods at first and second mode of vibration of each building and *TH* =1.5·*T*1. The average spectral accelerations considered here for computing CS(*AvgSA*) is defined with period increments of 0.2s in the T_{min}=*T*2 and T_{max}=*TH* range (see Table 2). In all these CS, 13 IM levels corresponding to mean return periods (MRPs) of exceedance for the site ranging approximately from 10 to 10^6 years were considered for carrying out risk-based assessment. Both versions of the CS were derived using the GMPE of Boore and Atkinson [2008], which is the same used for performing the PSHA calculations.

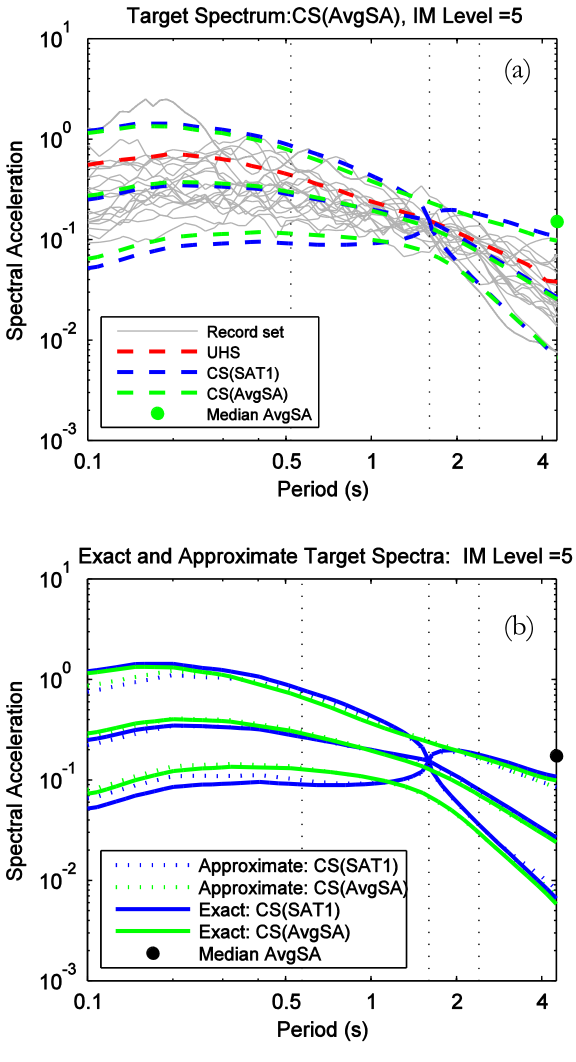

Figure 5.2. Conditional Spectrum based record selection for IM level 5 correspodning to 10% in 30 years for the 7- story building with first mode of vibration equal to 1.6s: (a) Target CS for different conditioning IMs and the 20 individual records selected for CS(*AvgSA*), (b) comparison between the exact and approximate CS target for CS(*SAT1*) and CS(*AvgSA*). (Note: the dots in the right side of each figure represent the median value of the conditioning *AvgSA*).

Figure 5.2(a) shows the CS target spectra for CS(*SAT*1) and CS(*AvgSA*) obtained using the procedure presented in the previous section. Figure 5.2(b) shows instead a comparison between the "exact" and "approximate" CS, conditioned on *AvgSA* and *SAT*1 [Lin et al., 2013b]. In the exact method all the causative scenarios are incorporated in the generation of the target CS, whereas the CS in the approximate method is based on only one scenario, usually the mean hazard-contributing scenario, as done here. These two CS may differ significantly in those cases when the hazard is not controlled by a single scenario. Here the difference between the approximate and exact CS versions is not large and mostly noticeable in their conditional mean (of the log) plus and minus one-standard deviation lines, especially at spectral ordinates for oscillator periods far removed from the conditioning one. Of course, the variability is higher in the exact method of CS. The mean conditional spectra, however, are very similar. All the record sets used in the response analysis of the buildings are based on the "exact" CS method.

5.4.3 SELECTION PROCEDURE OF GROUND MOTION RECORD ENSEMBLES

The suite of ground motions to match the three CS(*SAT*) were selected and processed according to the algorithm originally developed by Jayaram *et al.* [2011]. This algorithm was modified to select records that match the CS(*AvgSA*) computed according to Equations (5.1) to (5.7). In both cases the algorithm extracts and scales arbitrarily chosen horizontal components of ground motions from the PEER NGA West 1 database. Note that in this record selection exercise we did not distinguish records with and without pulse-like characteristics. The modified algorithm is available at Kohrangi [2015b].

In order to avoid potential bias in structural responses from overly-scaled records, we intended to limit scaling factors to a maximum value of four [Luco and Bazzurro, 2007a]. This goal was achieved for all the 13 *AvgSA* hazard levels and for the lower hazard levels of *SAT*1, *SAT*2 and *SATH*. In the extreme cases corresponding to very high *SAT*1, *SAT*2 and *SATH* levels scale factors up to 10 were necessary to attain a good CS(*SAT*) match. Therefore, and not surprisingly, records that are hazard consistent with CS(*AvgSA*) can be scaled, on average, less than records that are hazard consistent with CS(*SAT*). This outcome is general and can be considered as a positive feature of using *AvgSA* instead of single period spectral accelerations for CS-based record selection. For illustration purposes, Figure 5.2(a) introduced earlier shows also the response spectra of 20 ground motions selected and scaled to match the CS(*AvgSA*) corresponding to 10% in 30 years probability of exceedance (i.e., the IM level 5 in this study).

The consistency of the response spectra of all the selected ground motion ensembles with the four target CS is explored in Figure 5.3(a) and (b). The target CS conditional mean ($\mu_{\ln SAT|\ln IM*}$) and standard deviation ($\sigma_{\ln SAT|\ln IM*}$) are compared with those of the selected records for different conditioning IMs, called IM* in the notation. The agreement is excellent. The four CS shown in this figure refer, again, to the IM hazard level 5 but the agreement is equally good for all other IM levels.

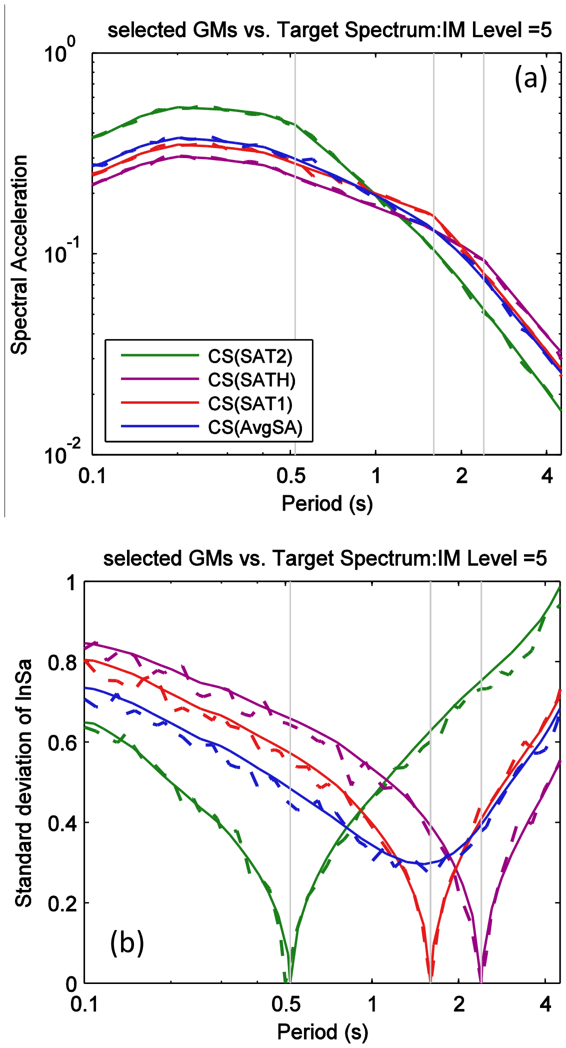

Figure 5.3. Comparison between the four target spectra and the corresponding empirically derived conditional spectra of the selected record ensembles (solid line: target, dotted line: selected records) based on CS(*SAT*2), CS(*SAT*1), CS(*SATH*) and CS(*AvgSA*). Panel a: mean (of the log), and (b) standard deviation (of the log) of the record-based spectra for the ensemble corresponding with IM Level 5.

Since the CS(*AvgSA*) provides, as expected, a compromise between the CS conditioned on *SAT*2, *SAT*1 and *SATH*, the records selected according to CS(*AvgSA*), as far as spectral content is concerned, are neither very aggressive nor very benign in any period range. This is another positive feature of using CS(*AvgSA*) for record selection. As mentioned in the introduction, when records are selected using CS(*SAT*), as usually done, the systematically different spectral content at periods away from the conditioning one generates very different intensity-based assessments depending on which conditioning period T^* is chosen. For example, records selected according to CS(*SAT*2) have, on average, spectral accelerations significantly lower than those of records selected based on *AvgSA* at periods shorter than *T*2 and, conversely, spectral accelerations significantly higher at periods longer than *T*2 (i.e., at periods close to *T*1 and *TH*). Thus, the records selected based on CS(*SAT*2) tend to yield lower values of displacement-sensitive EDPs, such as the peak IDR at the lower floors, and higher demands for acceleration- sensitive EDPs, such as PFA at the mid-height of the building. Of course, an opposite trend holds in the case of records selected according to CS(*SATH*). These discrepancies can be significantly curtailed by selecting records based on CS(*AvgSA*) for intensity-based assessments.

Another positive aspect of using CS(*AvgSA*) for record selection is its capability to provide records with moderate conditional variability at all spectral ordinates as opposed to no variability at the conditioning period and large variability at periods far from it, as is the case for CS(*SAT*). Loosely speaking, the "butterfly" look of the ensemble of the response spectra of records selected to match the CS at a given hazard level is greatly reduced if CS(*AvgSA*) is used.

This is intuitive to understand because the variability in the *AvgSA* for a given period range caused at a given site by a specific earthquake is lower than the variability of any spectral ordinate at any specific period included in the averaging operation (Figure 5.4). The red curve shows the value of $\sigma_{IM\,|\mathrm{rup}}$ of the GMPE at any *IM*=*SAT*1 for any specific period *T*1, while the blue curve is the value of $\sigma_{IM\,|\mathrm{rup}}$ of the GMPE for *AvgSA* (see Equations 3 and 4) computed for periods ranging from $0.2 \cdot T1$ to $1.5 \cdot T1$. The values shown were computed for the IM of an arbitrary horizontal component of a ground motion using the GMPE of Boore and Atkinson [2008]. Figure 5.4 shows clearly the significant gain in the predictability of *AvgSA* with respect to *SAT*1 regardless of the value of *T*1.

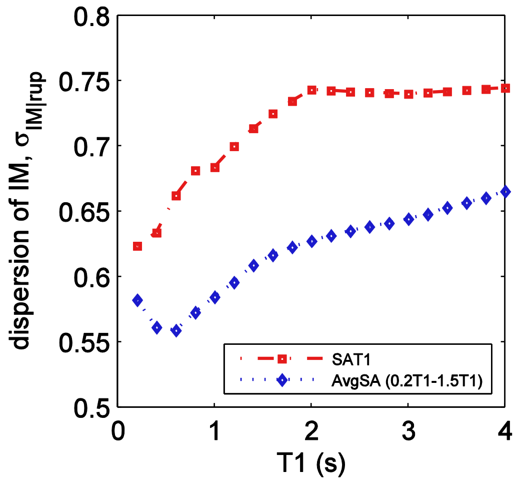

Figure 5.4. Comparison between the values of $\sigma_{IM\,|\mathrm{rup}}$ in the Boore and Atkinson [2008] GMPE for *IM=SAT*1 and *IM=AvgSA* defined for different oscillator periods T_1.

The lower the variability in the IM for a given earthquake rupture (i.e., the $s_{IM|\mathrm{rup}}$ in the GMPE), the lower the uncertainty in the estimate of the response, measured by an EDP for the same earthquake rupture [Kramer and Mitchell, 2006; Bradley, 2009]. This reduction in $\sigma_{\ln EDP|\mathrm{rup}}$ can be easily appreciated by considering the following equation [Shome *et al.*, 1998]:

$$\sigma_{\ln EDP|\mathrm{rup}} = \sqrt{\sigma^2_{\ln EDP|IM} + b^2 \cdot \sigma^2_{IM|\mathrm{rup}}} \;, \tag{5.8}$$

which was derived assuming that the relationship between EDP and *IM* is linear in log-log space, namely $EDP = a + b \times \ln IM + e_r$, in which *a* and *b* are the regression coefficients and ε_r is the regression residual. Cornell et al. [2002], showed that *b* is often equal to one; therefore, the total uncertainty is simply the square root sum of square of the $\sigma_{IM\,|\mathrm{rup}}$ and $s_{\ln EDP|IM}$.

A final positive aspect of selecting records based on CS(*AvgSA*) rather than CS(*SAT*) is that, as it will be clear in the following sections, *AvgSA* is also moderately efficient (as per the definition of efficiency in Luco and Cornell, 2007b) in predicting *at all stories* the different EDP types (e.g., IDR and PFA) that are used for loss estimation (see Kohrangi *et al.*, 2015f, for details). This means that when *AvgSA* is used as predictive IM, the

$\sigma_{\ln EDP|IM}$ is also low at all stories and, therefore, the loss estimates are more accurate than if period-specific spectral accelerations are used as EDP predictors. Of course, an even more efficient, but certainly more complicated, approach would be to use as predictors a vector of these spectral accelerations without averaging them in a single random variable, *AvgSA*. This vector approach was investigated in a different study [Kohrangi et al., 2015f] and is not discussed here.

5.4.4 HAZARD CONSISTENCY

The interface between the hazard and the structural response in the PBEE approach utilized in this study is limited to ground motion spectral quantities. Hence, for ensuring that the building response estimates computed via nonlinear dynamic analysis are representative of those that could be experienced in the future by the considered structure, it is important that the selected records used for response estimation are consistent with the hazard at the site [Lin *et al.*, 2013b]. More precisely, a set of records are said to be ”hazard consistent” for a given IM if the rates of exceedance of that IM are similar if not identical to those extracted from the hazard curve computed using PSHA at that site for that IM.

Figure 5.5 show that the ensembles of records selected based on CS(*SAT*1) and CS(*AvgSA*) are indeed consistent with the PSHA-based hazard curves for this site. This good consistency is due to the adoption of the “exact” approach to CS calculation and to the usage of a single GMPE for both hazard and CS calculation. The hazard consistency for *SAT*2*,* however, is somewhat poorer. It should be noted that, strictly speaking, the hazard consistency should also be checked (or, better, enforced) with respect to other characteristic of the earthquake-site specific combination, such as magnitude, source-to-site distance, Vs_{30}, etc. To do so one could use hazard disaggregation and site soil characteristics to inform the choice of records to be included in the ensembles that meet the CS specifications. This is not done here, however, because we assumed that response spectrum consistency with site hazard is adequate.

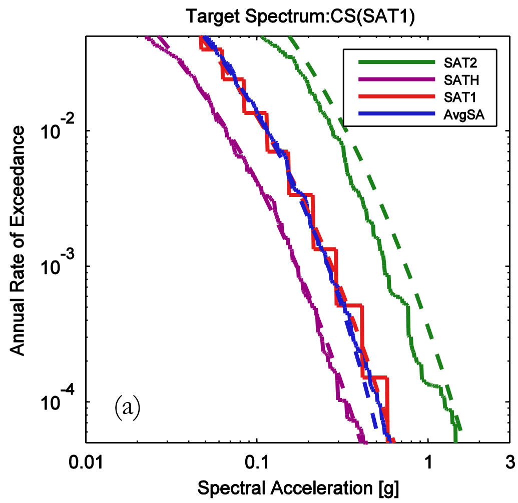

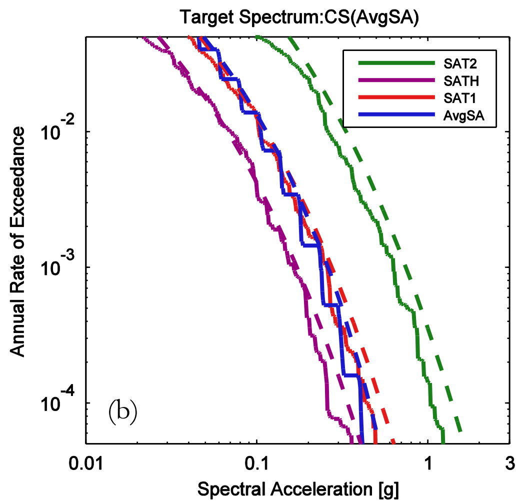

Figure 5.5. Hazard consistency with respect to spectral shape of the sets of records compatible with (a) CS(*SAT1*); and (b) CS(*AvgSA*). (Dashed line: hazard curve from PSHA, solid line: empirical hazard from selected record sets).

5.5 **STRUCTURAL ANALYSIS**

5.5.1 INTENSITY BASED ASSESSMENT

The ensembles of records selected based on the different conditional spectra discussed in the previous sections were used as input for nonlinear response history analysis of the 4-, 7-, 12- and 20-story RC frame buildings. For simplicity and space constraints, only results from single 7-story building structure are presented here. However, the response analyses that used sets of records selected according to the same procedure were repeated for the other buildings with similar findings [Kohrangi, 2015a-Appendix E].

Figure 5.6 summarizes for the overall 7-story building the intensity-based analysis results for each one of the 13 IM levels for which record selection was done. More specifically, Figure 5.6(a) and (b) show the median and logarithmic standard deviation of MIDR. It is worth noting that, even though hazard-consistent record selection using the exact CS approach (i.e. considering all contributing causal earthquake ruptures in the hazard of the conditioning IM) was applied, the responses conditional on different IMs with same MRP at the site are quite different. These findings are in line with those obtained in other studies as well [NIST, 2011; Lin *et al.*, 2013b; Bradley, 2012d]. Again, since MIDR is more sensitive to spectral content of the records at $T1$ than, say, at $T2$, when records based on CS($SAT1$) are used the median MIDR for a given MRP tends to be higher than when CS($SAT2$)-based records at the same MRP are used instead. The latter ensemble of records tend to have response spectrum values at $T1$ that are, on average, lower than the single conditioning $SAT1$ value of the former ensemble of records especially for long-MRP, high-IM levels. Hence, it follows naturally that the median of MIDR generated by records that are selected based on CS($SAT2$) at a given MRP is lower than the median of MIDR generated by records that are selected based on CS($SAT1$) at the same MRP. In this respect note that the median of MIDR for the CS($SAT1$) ensemble for highest IM level 13 is missing in the figure (i.e., this means collapse) while it is about 0.05 for the CS($SAT2$) ensemble.

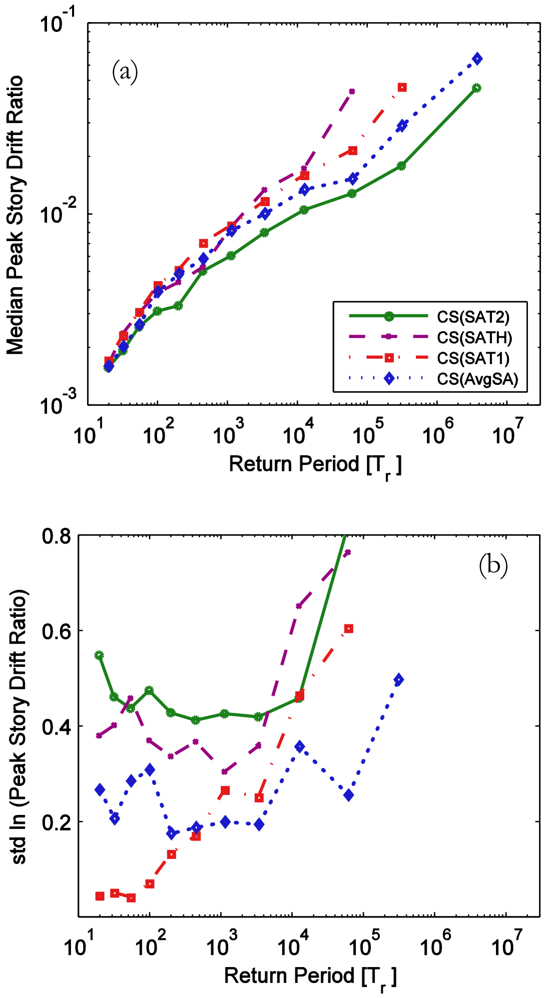

Figure 5.6. Structural analysis results for the 7-story building for 13 different amplitude levels of different IMs of same MRP at the site: (a) Median of the MIDR; (b) logarithmic standard deviation of the MIDR.

As Bradley [2013] mentioned, by conditioning the response on a single IM, only the causal sources that dominate the hazard for that IM are considered while those that dominate the hazard for other IMs are somewhat disregarded. This is true when the single IM is related to a specific oscillator period, such as *SAT*1, *SAT*2 and *SATH* here, but less so for IMs such as *AvgSA* whose reach is wider than a single period. In fact, the median estimates of MIDR given *AvgSA* tends to be bracketed by the medians of MIDR given *SAT*1 and *SAT*2 for all MRPs. Hence, the use of *AvgSa* instead of *SAT*1 could remove some of the conservativism in the estimate of the rate, $\lambda_{ij,h}$, of exceeding any different level *j* of EDP *i* for a given hazard level*, h.,* that was mentioned in the introduction. We will discuss this positive feature of *AvgSA*-based response estimates more in detail later when discussing the risk-based calculations.

As expected, Figure 5.6(b) shows that for all MRPs the dispersion of MIDR is lower for *SAT*1 and *SATH* than it is for *SAT*2, which is not a good predictor of this EDP. Furthermore, the dispersion of MIDR is, of course, much smaller at low hazard levels for *SAT*1 than it is for *SATH* because the structure responds almost linearly for low amplitude ground motions and the contributions of the first mode of vibration are high. The two estimates of the MIDR dispersion tends to become similar at high hazard levels when the fundamental oscillator periods lengthen from *T*1 to periods close to or larger than *TH* and, therefore, *SATH* predictive power increases. It is interesting to note that the dispersion of MIDR given *AvgSA* is in between the dispersion of MIDR given *SAT*1 and given *SATH* for the low hazard levels but lower than both for the high hazard levels. Again, we will revisit this issue later when discussing the findings of risk-based calculations.

Finally, note that here, unlike in the aforementioned studies, we do not always detect a negative correlation between the median and dispersion of an *EDP*|*IM* (i.e. the higher the median, the lower the dispersion and vice versa) when hazard consistent records are used. For instance, both the estimates of the median and of the dispersion of MIDR obtained for *AvgSA* are lower than those obtained for *SAT*1 for the high amplitude stripes corresponding to long MRPs. This could be explained by the characteristics of *AvgSA* that, by design, is sensitive to the spectral content of the records at periods both shorter and longer than *T*1.

As a foreshadow to risk-based calculations, where the ability of accurately assessing story-specific measures of response in addition to overall ones such as MIDR is of paramount importance, we shift our focus here to IDR and PFA. The median and logarithmic standard deviation values of the IDR at each floor for IM level 5 are displayed in Figure 5.7(a) and Figure 5.7(c) while Figure 5.7(b) and Figure 5.7(d) show the same for PFA.

When the records selected according to CS(*SAT*1) are used the median of IDR is maximized for this IM level (Panel a) at many floors but not all. For this building (and the other 3 analyzed but omitted here) the ensemble of CS(*SAT*2)-based records instead always maximize the median of PFA at all IM levels at least when compared with the medians computed from records selected using CS(*SAT*1) and CS(*SATH*). As mentioned in the introduction, Lin *et al.* [2013c] and Bradley [2013] for intensity-based assessment at a given hazard level involving one or more EDPs suggest performing multiple record selections based on different IMs and use, conservatively, the worst-case scenario for each EDP. In plain words, this translates into picking the IM that predicts the highest median value of the EDP at the hazard level of interest. For this building this approach could be implemented for PFA since the ensemble of records based on CS(*SAT*2) always predict higher median PFA values. However, given that neither *SAT*1 nor *SATH*, nor any other period-specific *SAT* for that matter, provide always the highest median values of IDR at all floors even for the same IM level (Panel b), this suggestion would be hard to implement in practice.

Even if *SAT*1 were to predict the highest values of IDR at all floors, it would perhaps be acceptable and even preferred for design purposes to pick always the IM that provides the highest EDP estimates for each EDP but certainly, as discussed earlier, this approach would not be appropriate for risk-assessment calculations. The highest values of all the EDPs as estimated using this worst-case scenario approach are not realizable, namely they cannot be simultaneously caused by the same set of records. For example, if *SAT*2 is far from *SAT*1, the very extreme hazard levels of *SAT*2 among the 13 considered here cause very high PFA values but very low IDR values. The opposite holds for CS(*SAT*1)-based records for high *SAT*1 values that bring the structure close to collapse (i.e., high IDR values) but cause relatively low levels of PFAs. The conservativism of picking the worst-case scenario for estimating all the EDPs at every IM level is obviously unacceptable if applied to risk-based calculations. CS(*AvgSA*)-based records, however, provide median values of *both* IDR and PFA which are moderately high *at all stories for all* IM *levels*. Therefore, the results shown here, may suggest an alternative solution to the problem of selecting a single IM that provides joint estimates for all EDPs that are not conservative. The medians of IDR and PFA based on CS(*AvgSA*)-based records for all hazard levels are not the maximum observable but they are inherently consistent since they have been caused by the same set response analyses that used the same set of ground motion records as input.

In addition, Figure 5.7(c) and (d) show that CS(*AvgSA*)-based records also provide, again *for both* MIDR and PFA along the entire height of the building, values of dispersion that are almost as low as, and sometimes lower than, the values provided by the records based on CS(*SAT*1) for IDR and on CS(*SAT*2) for PFA. This relatively low variability for all 13 hazard levels (all omitted here besides IM level 5) and for all stories, enables the prediction of IDR and PFA at all stories for any given hazard level more efficiently and more practically than the worst-case scenario approach discussed above. This robustness is clearly not shared by CS(*SAT*)-based records regardless of the specific oscillator period utilized. In this case, ensemble of records based on *SAT*1, *SAT*2 and *SATH* may yield low dispersion in the IDR and PFA at some IM levels and high at other IM levels, or high at some floors and low at other floors for the same IM level. Based on these premises, the use of CS(*AvgSA*) to select ground motion records ensemble for risk-assessment purposes involving multiple EDPs and multiple hazard levels seems a plausible and, arguably superior, alternative, which is investigated in the next section.

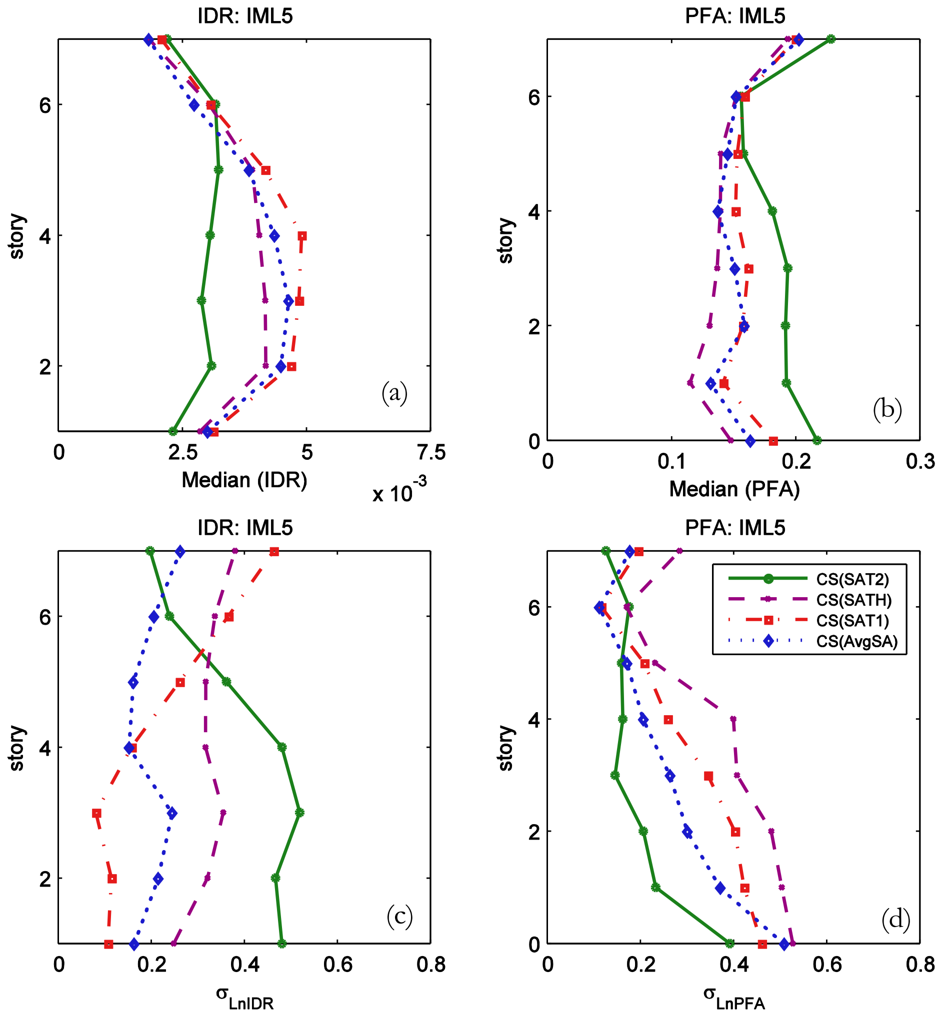

Figure 5.7. The median and logarithmic standard deviation profile along the height for the 7-story building based on four record selection approaches: CS(*SAT1*), CS(*SAT2*), CS(*SATH*), and CS(*AvgSA*): (a) Median IDR, (b) Median PFA, (c) IDR dispersion, and (d) PFA dispersion computed for the IM level 5.

5.5.2 RISK-BASED ASSESSMENT

The response hazard curves for IDR and PFA at the 5-th floor of the 7-story building computed using different CS record selections are shown in Figure 5.8(a) and (b), respectively. It is apparent that the response hazard curves are not too similar, especially for PFA, as one may have expected. Although theoretically the choice of the conditioning variable would not matter if we had an infinite database of ground motion records appropriate for the site under consideration, in practice we do not and, therefore, it does matter as discussed in Bradley [2012d]. In that study, it was shown that in a practical context, if hazard consistent record selection is used (i.e., based on CS or GCIM), the estimate of the response hazard curve is prone to inaccuracies mainly because of the (i) poor interpolation of the response distribution (i.e. $EDP|IM$) and (ii) limited number of ground motion records used to obtain the response distribution.

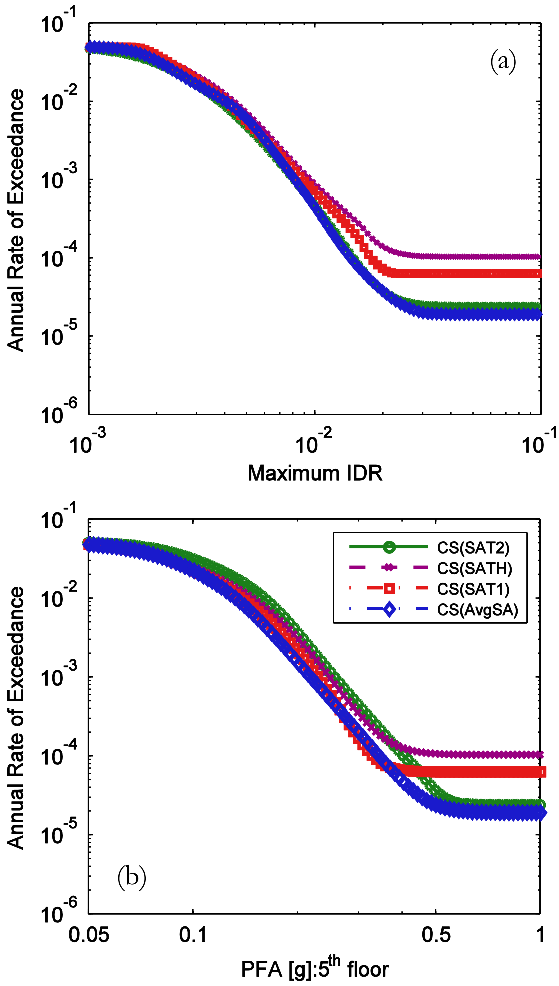

Figure 5.8. Response hazard curves for the 7-story building. Comparison between different record selection approaches: (a) Maximum inter story drift ratio along the height (MIDR); (b) Peak Floor Acceleration at the 5th floor.

Hence, why should we use the comparatively more complicated CS(*AvgSA*) instead of the simpler option of CS conditioned at a single period, such as *SAT*1? We find several reasons to favor a CS(*AvgSA*)-based approach:

- *AvgSA* has a lower dispersion in the GMPE (i.e., lower $\sigma_{IM\,|\mathrm{rup}}$, which implies higher predictability) compared with, that of any spectral acceleration, as shown in Figure 5.4, for *SAT*1. This is an advantage in reducing the total uncertainty of the PBEE procedure, as seen by inspecting Equation 5.8. Note that we observed here, in agreement with Bradley *et al.* [2009b], that this dispersion is generally the dominant one in assessing the total dispersion of the EDP.
- *AvgSA* is an IM with an efficient prediction power, namely low $s_{\ln EDP|IM}$, for very different EDPs such as IDR and PFA that are instrumental in risk assessment and loss estimation. This does not occur for spectral accelerations at any single oscillator period.
- The dispersion $s_{\ln EDP|IM}$ is also more constant along the height of the building at different IM levels than for other IMs (such as *SAT*1, for example). This means that the level of accuracy in estimating IDR and PFA *at each story* is comparable. When using *SAT*1, for example, the accuracy is usually much higher at the lower stories than it is at the higher stories.
- Given that $\sigma_{IM\,|\mathrm{rup}}$ and, on average, $s_{\ln EDP|IM}$ tend to be lower when *AvgSA* is used than the corresponding values when other spectral accelerations are used, it is reasonable to expect that the total uncertainty in the EDP estimate (see Equation 5.8) and, in turn, in the loss estimates, which are often the main objective of risk assessment studies, are more accurate. Figure 5.9 compares for the IM level 5, as an example, the total dispersion of IDR (Panel a) and of PFA (Panel b) along the height of the 7-story building computed using different record selection approaches. The advantage of using the CS(*AvgSA*) approach is clear. Similar results can be found for other IM levels.

- The estimate of losses caused by earthquakes at any floor of a building are due to damage to both deformation-sensitive components, whose extent is well predicted by IDR, and acceleration-sensitive components, whose extent is instead well predicted by PFA. Only an accurate prediction of both can ensure an accurate prediction of the total losses. *AvgSA* is a relatively good predictor of both EDPs, unlike any other single spectral accelerations considered here. Therefore, using records based on CS(*AvgSA*) can be efficiently used to predict losses. Other proposals found in the literature suggested using multiple sets of analyses for assessing each EDP, with an evident waste of resources.
- Again with focus on the loss estimation, as discussed in the text using a set of analyses using, say, CS(*SATH*)-based records for estimating IDR and, from it damage to drift-sensitive components and a separate set of analyses using CS(*SAT*2)-based records for estimating PFA may lead to biased loss estimates. High IDR values and high PFA values do not occur for the same record. CS(*SATH*)-based records tend to emphasize IDR estimates and, therefore, IDR-related damage and losses. On the other hand, CS(*SAT2*)-based records tend to emphasize PFA-related damage and losses. Summing the former losses with the latter for each IM level is likely to lead to overestimating the total losses. Record selected based on CS(*AvgSA*) do not have this negative feature provided that the spectral ordinates averaged are not skewed towards either long periods, such as *TH*, or shorter ones, such as *T*2.

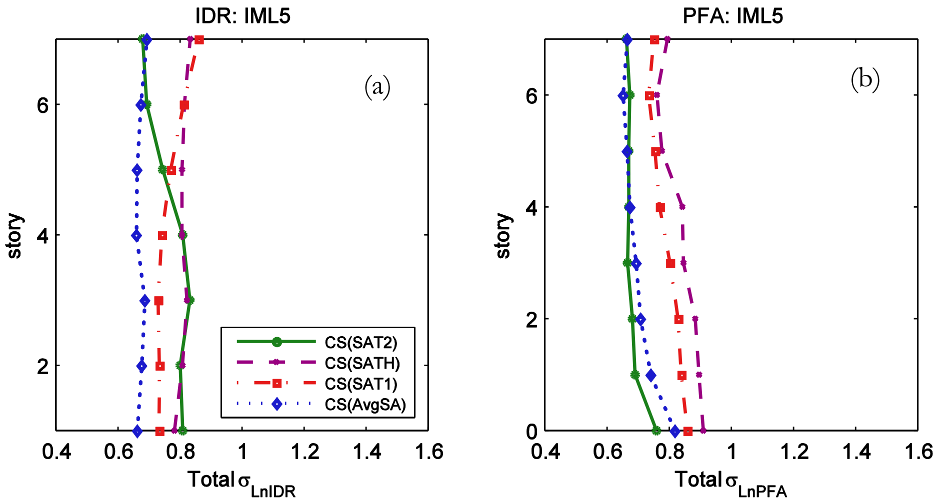

Figure 5.9. Comparison between the total logarithmic standard deviation of the response based on different record selection approaches: (a) PFA; (b) MIDR dispersion profiles for IM level#5.

- When using a CS(*AvgSA*) approach to record selection, the hazard consistency at high IM levels (i.e., rarer, high-amplitude spectral ordinates) can be achieved with lower scale factors than when using a CS(*AvgSA*) or other single-period CS methods. Scaling records to very high IM levels is necessary when assessing the collapse capacity of modern structures given the scarcity of records that naturally have such high spectral ordinates. Since over-scaling records may cause biased responses, limiting the scale factors while maintaining the hazard consistency is certainly advantageous. Scale factors and the spectral mismatch with CS(*SAT*1) of records that were observed for high IM levels are documented in Kohrangi [2015a]-Appendix E.
- The CS(*AvgSA*)-based record selection combines different causal earthquakes from all possible scenarios contributing to the site hazard for different spectral ordinates of interest into the target spectrum. It could be argued that using *AvgSA* more dominant events for the site are considered in the record selection compared to the causal events controlling the *SAT* hazard only.

5.6 **CONCLUSIONS**

In this study we explored the use of an alternative approach to probabilistic seismic demand analysis (PSDA) that uses ground motion records selected from a conditional spectrum based on the average spectral acceleration, *AvgSA*, in the period range that matters for the response of the considered building. *AvgSA* has already been shown in previous studies to be an efficient and sufficient IM for building response prediction but *AvgSA* has not been used so far both for informing hazard analysis and also for selecting ground motion records to be used as input to structural response assessment. Here *AvgSA* is utilized in the implementation of an extension of the traditional conditional spectrum, called here CS(*AvgSA*), to explicitly hinge on the average of multiple spectral accelerations and also in the probabilistic hazard calculations. The entire chain of probabilistic seismic demand analysis (PSDA), which is the first step to loss estimation, is internally fully consistent.

The proposed methodology was tested for four 4-, 7-, 12- and 20-story RC buildings located in a highly seismic site in south of Marmara Sea in Turkey. The 2D structural models of such buildings were subject to both *Intensity* and *risk based assessment* calculations for using ground motions selected according to CS(*AvgSA*) and CS(*SAT*) at multiple periods ranging from $0.2 \cdot T1$ to $1.5 \cdot T_1$, where T_1 was the fundamental frequency of the linear elastic building *AvgSA* is an intensity measure that has many qualities that range from a higher predictability than the single period spectral accelerations and overall a superior prediction power for both EDPs that control the building seismic performance, namely the peak in time interstory drift (IDR) and the peak floor acceleration (PFA) at each story. This holds for different IM levels, both weak and intense.

The efficiency of *AvgSA for both IDR and PFA* is essential in risk-based assessment for which the building response distribution at all IM levels is necessary. In this respect, it is advantageous to work with a single conditioning IM that performs moderately well for different EDPs at all stories and at all IM levels rather than identifying the very best IM that is only efficient for estimating a single EDP and perhaps not even at all stories of a building (e.g., *SAT*1 is not a good predictor for IDR at high stories of a building) and not for all IM levels (e.g., *SATH* is very good for estimating IDR at high ground motion intensity levels but poor at weak ones). Using multiple IM predictors forces the analyst to repeat response analyses for multiple sets of records selected according to different IMs, with an evident waste of resources. It is also argued here that such an approach would not only be wasteful and impractical but also potentially conservative when employed for risk-based calculations. Finally, the use of CS(*AvgSA*) showed more flexibility during record scaling to match the CS amplitude levels than the use of CS conditioned on single period spectral accelerations. A good hazard consistency to CS(*AvgSA*) for the severe hazard levels necessary to test the ultimate capacity of these buildings was ensured by limiting the scale factors to four while scale factors up to 10 were necessary when using the CS(*SAT*1). The potential for overscaling and, therefore, of using records with unrealistic characteristics that may cause biased EDP estimates is greatly reduced when CS(*AvgSA*)-based records are utilized.

6. SITE DEPENDENCE AND RECORD SELECTION SCHEMES FOR BUILDING FRAGILITY AND REGIONAL LOSS ASSESSMENT

6.1 **INTRODUCTION**

Vulnerability functions are commonly obtained based on: 1) empirical methods, 2) Analytical methods, 3) engineering judgment; and 4) hybrid methods. In the first method, the data related to the structural damages occurred in a site after an earthquake are collected and used for generation of the vulnerability functions [Braga, 1982; Di Pasquale *et al.*, 2005; Dolce *et al.*, 2003; Giovinazzi and Lagomarsino, 2004; Orsini *et al.*, 1999; Rossetto and Elnashai, 2003; Rota *et al.*, 2006; Sabetta *et al.*, 1998; Spence *et al.*, 1992; e.g. Whitman *et al.*, 1973]. This method, if enough data is available, is perhaps the most reliable of all. When enough empirical data is not accessible, numerical analyses (analytical approach) could be used. This approach is based on the structural modeling and simulation [Dumova-Jovanoska, 2004; HAZUS: FEMA, 1999; 2001, 2003; Giovinazzi *et al.*, 2005; Masi, 2003; Park and Ang, 1985; Rossetto and Elnashai, 2005; Whitman *et al.*, 1997; Silva *et al.*, 2014a; Silva *et al.*, 2014b]. The next method is collecting data based on the opinion of a group of engineers regarding the damage of different types of structures and relying on their experience such as ATC-13 ATC, 1985. In the hybrid method, a combination of all other three methods is used [Barbat *et al.*, 1996;Bommer and Crowly, 2006; e.g. Kappos *et al.*, 1995; Kappos *et al.*, 1998].

When the analytical methods are used, the structural models of different building types as SDOF or MDOF should be generated and different analysis methods such as Capacity-spectrum based method using pushover analysis [Calvi and Pinho, 2004; e.g. HAZUS, 2003; Sousa *et al.*, 2004], displacement-based methods (e.g. Pinho *et al.*, 2002; Restrepo-Vélez and Magenes, 2004) or Nonlinear Dynamic Analysis, NDA, (Haselton and Baker, 2011) depending on the desired level of preciseness of the methodology could be applied for the assessment. When nonlinear dynamic analysis (or even nonlinear static analysis) is performed for the vulnerability assessment, one challenge is the record selection. Unlike previous methods, in analytical approach, the analyst has control on the collected data by choosing the IM and the IM levels at which the analysis is needed to be performed. The structural response is, generally, dependent on the structural characteristics, the site conditions and location of the building. For instance, the same reinforced concrete buildings with the same characteristics and design would have different vulnerability functions at two different sites within the same country at two different regions. The site seismicity, the closest fault rupture distance to the building, the soil type, etc. can alter the building response and consequently the predicted damages. This suggests that, the record selection which links the seismic hazard of the site to the building seismic response should be representative of the characteristics of that specific site (site-specific). In addition, in a portfolio analysis, different classes of buildings (e.g. steel, Reinforced Concrete, Masonry) with different properties (e.g. low-rise, mid-rise and high-rise) should be analyzed. The record selection, therefore, should be also building-specific. In recent years several record selection approaches for building- and site- specific record selection such as Conditional Mean Spectrum (CMS) [Baker, 2011], Conditional Spectrum (CS) [Jayaram *et al.*, 2011] and Generalized Conditional Intensity Measure (GCIM) approach [Bradley, 2010a] are proposed.

When the vulnerability of a portfolio at multiple sites with different seismic characteristics is of interest, it is common that one set of records regardless of its consistency with the hazard of the site is used and Incremental Dynamic Analysis [Vamvatsikos and Cornell, 2002] or some other form of stripe or cloud analysis [Jalayer, 2003] is performed. This will result in identical damage functions for the buildings located in different sites. Ideally, however, one should perform multiple record selections for each site and building, separately, to obtain appropriate damage functions specific to the site and the building. Although this method is the most precise approach for such problems, it is cumbersome and might not seem appealing in practice.

To address this, Haselton et al. [2011] noticing the significance of the spectral shape in site-specific collapse assessment of building structures in a portfolio, proposed a simplified method for adjustment of epsilon [Baker and Cornell, 2006] accounting for spectral shape in order to be able to use a single set of records for collapse assessment of a class of buildings (by avoiding a careful record selection). Kazantzi and Vamvatsikos [2015a] proposed using averaged spectral acceleration [Bianchini *et al.*, 2010; Cordova *et al.*, 2000] for a range of periods (*AvgSA*) as Intensity Measure (IM) for a class of buildings in vulnerability studies. It was concluded in that study that even without a careful record selection, *AvgSA* is a good structural response predictor for a group of buildings compared with spectral acceleration at the first mode of vibration of the building, $Sa(T1)$, while it has also a higher sufficiency. Eads *et al.* [2015] using *AvgSA* for collapse assessment of a group of 700 buildings with different heights and types, showed that, in general, this IM, if an appropriate period range is selected, can be an alternative sufficient and efficient IM for building collapse risk assessment. Kohrangi *et al.*, [2015d] proposed a method based on the extension of the conditional spectrum based record selection approach conditioned on spectral acceleration at single period, CS(*SAT*), [Jayaram *et al.*, 2011], by changing the conditioning IM from spectral acceleration at a single period to the *AvgSA*, CS(*AvgSA*). This record selection scheme provides a suite of records that matches the mean and variation of the spectrum, maintaining the hazard consistency at the site.

An alternative record selection for portfolio seismic assessment is proposed in this study by implementing the CS(*SAT*) and CS(*AvgSA*). The method incorporates “multiple-site” seismic effects in record selection based on conditional spectrum method. It stands on the idea of "exact" conditional spectrum method when multiple causal earthquakes and multiple Ground Motion Prediction Equations (GMPEs) are incorporated in CS [Lin et al., 2013a]. As a result, a single set of records that are "hazard consistent" with all the sites is selected. This way, even though the same as the former method, identical damage functions for similar buildings located at different sites is obtained, we can argue that it is a more precise record set (closer to "true" damage function) for each site and controls the uncertainty in a systematic way. Such method avoids the post-processing adjustments proposed by Haselton *et al.* [2011] and also uses an IM that was shown to have a high sufficiency and efficiency. In addition, given the higher flexibility of *AvgSA* for amplitude-scaling [2015d], especially to obtain high amplitude ground motions (which is essential for collapse prediction of modern buildings) it is a better IM choice in order to use a relatively small scale factor while maintaining hazard consistency.

6.2 **PROBLEM DEFINITION**

Perhaps the most accurate and robust way of generation of building fragility functions at multiple sites for which the hazard seismicity is significantly different is to derive them building- and site-dependent and use the same specific fragilities for each site and building separately in the cost and loss estimations. This approach might not be appealing in practice because, firstly; deriving building specific fragility functions for each site means performing site-specific record selection for multiple IM levels and nonlinear dynamic analysis multiple times corresponding to each building, each site and each IM level. Secondly, when using the fragilities in the loss estimation procedure, it is an easier task to consider one fragility curve for a class of buildings everywhere within the region to avoid heavy book keepings. Therefore, an effort to define single fragility curve for multiple sites, on one hand, and further avoid deriving multiple fragility functions for multiple-sites is of interest. Two methodologies are introduced here to achieve this objective:

i) *incorporating multiple fragility functions* related to multiple-sites into a single function;
ii) *incorporating multiple sites in record selection* to perform record selection and nonlinear dynamic analysis only once.

In the following, both methodologies are explained.

6.2.1 FRAGILITY FUNCTION DEFINITION

There are different ways in deriving the fragility functions to be used in regional loss estimation. In this study, we are focused on the analytical approach. There are a number of ways to estimate parameter values for a fragility function which are consistent with the observed data, depending on the procedure used to obtain structural analysis data (Baker, 2015). The fragility functions are commonly defined as lognormal cumulative distribution functions, Φ (·), by means of the logarithmic mean (θ) and logarithmic standard deviation

(β) of the IM*s* causing exceedance of a specific limit state (LS). Such function is shown in Equation (6.1):

$$P(\mathrm{LS} \mid IM = x) = \Phi\left(\frac{\ln(x/\theta)}{\beta}\right) \tag{6.1}$$

Where: $\mathrm{P(LS} \mid IM = x)$ is the probability of exceedance of a certain limit state (LS) given the *IM* being equal with x. This fragility function could be called a building general fragility function and is meant to relate the overall damage state of a building with a ground motion IM. This fragility function is different than the one defined for building components which is used for detailed building-specific loss estimation. Two main approaches for estimation of fragility parameters ($\hat{\theta}, \hat{\beta}$) are the method of moments and the method of Maximum likelihood. In this study, we use method of moments for IDA and the method of maximum likelihood for the MSA. Unlike IDA, when MSA is used, the analysis need not be performed up to IM amplitudes where all ground motions exceed the predefined LS (e.g. collapse) such as the data points shown in Figure 6.6 (c) and (d). In this case, using the method of moments is not applicable [Baker, 2015].

6.3 METHODOLOGY TO INCORPORATE MULTIPLE FRAGILITIES OBTAINED FROM MULTIPLE SITES

With the assumption of log normal distribution of the fragilities, when the parameters of multiple fragility functions, using one of the methods, is estimated, multiple fragility functions could be incorporated into a single function using the *law of total variance*. The logarithmic mean and standard deviation of such fragility function is obtained based on the following expressions:

$$\hat{\theta}_{mean-frg} = \exp\left[\sum_{s=1}^{n} P_s \cdot \ln(\hat{\theta}_{IM_s})\right] \tag{6.2}$$

$$\hat{\beta}_{mean-frg} = \sqrt{\sum_{s=1}^{n} P_s \cdot \left[\hat{\beta}^2_{\ln IM_s} + \left(\ln\left[\frac{\hat{\theta}_{mean-frg}}{\hat{\theta}_{IM_s}}\right]\right)^2\right]} \tag{6.3}$$

In which: $\hat{\theta}_{mean-frg}$ and $\hat{\beta}_{mean-frg}$, are the median and logarithmic standard deviation of the IM, estimated parameters of the incorporated fragility, respectively. P_s, is the weight considered for site s, which is dependent on the significance of each site or could be defined in proportion with the number of buildings in each site, for instance. $\hat{\theta}_{IMs}$ and $\hat{\beta}_{IMs}$ are the median and logarithmic standard deviation of the fragility function obtained for site s. Here we used this method as a bench mark for examining the accuracy of the methodology explained in the following section.

6.4 METHODOLOGY TO INCORPORATE MULTIPLE SITES IN CS RECORD SELECTION

6.4.1 EXPLANATION OF ORIGINAL METHODOLOGY

A computationally efficient algorithm was proposed by Jayaram et al. [2011] to compute the conditional CS target which considers both the mean and variance of the spectral accelerations at different spectral ordinates. The procedure for a single scenario is summarized as follows. The conditional mean spectral ordinates at periods T_1 to T_n (i.e. vector of $\{\ln SaT_1,...,\ln SaT_n\}$) conditioned on IM* is defined as:

$$\mu = \begin{bmatrix} \mu_{\ln Sa(T_1)} + \rho_{\ln Sa(T_1),\ln IM^*} \cdot \varepsilon(IM^*) \cdot \sigma_{\ln Sa(T_1)} \\ \mu_{\ln Sa(T_2)} + \rho_{\ln Sa(T_2),\ln IM^*} \cdot \varepsilon(IM^*) \cdot \sigma_{\ln Sa(T_2)} \\ \vdots \\ \mu_{\ln Sa(T_n)} + \rho_{\ln Sa(T_n),\ln IM^*} \cdot \varepsilon(IM^*) \cdot \sigma_{\ln Sa(T_n)} \end{bmatrix}, \tag{6.4}$$

In which: $\mu_{\ln Sa(T_i)}$ and $\sigma_{\ln Sa(T_i)}$ are the logarithmic mean and standard deviation of the spectral acceleration at period T_i, obtained from GMPE for a given scenario (e.g. magnitude and closet-rupture-to-site distance and fault type). $\rho_{\ln Sa(T_1),\ln IM^*}$ is the correlation coefficient between spectral accelerations at periods T_i with IM*. $\varepsilon(\mathrm{IM}^*)$ is the number of standard deviations by which a given $\ln IM^*$ of a recorded ground motion differs from the mean, predicted by a GMPE. In general, epsilon could be defined according to Equation (6.5):

$$\varepsilon(IM) = \frac{\ln IM - \mu_{\ln IM}}{\sigma_{\ln IM}}, \tag{6.5}$$

In which: $\ln IM$ is the ground motion's natural value of IM. The covariance matrix of the spectral accelerations at multiple ordinates conditioned on IM* is therefore defined as:

$$\Sigma = \Sigma_0 - \frac{1}{\sigma^2_{\ln IM^*}} \cdot \Sigma \cdot \Sigma_1', \tag{6.6}$$

In Equation (6.6), Σ_1 is defined as follows:

$$\Sigma_1 = \begin{bmatrix} \rho_{\ln Sa(T_1),\ln IM*} \cdot \sigma_{\ln Sa(T_1)} \cdot \sigma_{\ln IM*} \\ \dots \\ \rho_{\ln Sa(T_n),\ln IM*} \cdot \sigma_{\ln Sa(T_n)} \cdot \sigma_{\ln IM*} \end{bmatrix}, \tag{6.7}$$

Where Σ_0 denotes the (unconditional) covariance matrix of the vector $\{\ln Sa(T_1),\dots,\ln Sa(T_n)\}$ and can be computed by Equation (6.8). The *i*-th element of the diagonal of matrix Σ_0 is equal with $\sigma^2_{\ln Sa(T_i)}$:

$$\Sigma_0 = \begin{bmatrix} \sigma^2_{\ln Sa(T_1)} & \dots & \rho_{\ln Sa(T_1),\ln Sa(T_2)} \cdot \sigma^2_{\ln Sa(T_1)} \cdot \sigma^2_{\ln Sa(T_n)} \\ \vdots & \ddots & \vdots \\ \rho\ (T_n, T_1) \cdot \sigma_{\ln Sa(T_n)} \cdot \sigma_{\ln Sa(T_1)} & \dots & \sigma^2_{\ln Sa(T_n)} \end{bmatrix}, \tag{6.8}$$

The diagonal element of Σ denoted by $\Sigma_{i,i}$ can be expressed as Equation (6.9):

$$\Sigma_{i,i} = \sigma^2_{\ln Sa(T_i)} - \frac{1}{\sigma^2_{\ln IM*}} \cdot \rho^2_{\ln Sa(T_i),\ln IM*} \cdot \sigma^2_{\ln Sa(T_i)} \cdot \sigma^2_{\ln IM*}, \tag{6.9}$$

The standard deviation of $Sa(T_i)$ conditioned on IM^* is therefore defined by Equation (6.10):

$$\sigma_{\ln Sa(T_i)|\ln IM*} = \ln Sa(T_i) \cdot \sqrt{1 - \rho^2_{\ln Sa(T_i)|\ln IM*}}, \tag{6.10}$$

6.4.2 INCORPORATION MULTIPLE CAUSAL EARTHQUAKE, GMPEs AND SITES

A formulation by Lin *et al.* [2013a] was proposed for computation of conditional spectrum incorporating multiple causal earthquakes and GMPEs at a single site based on the *law of total variance*. This method is adopted here and extended to incorporate the hazard and disaggregation for multiple sites. Such CS target could be used for selection of single set of records for vulnerability analysis of a class of buildings located in different sites. We can consider the "exact" solution for multiple causal earthquakes, GMPEs and sites weighting all the scenarios (numbered by j) and GMPEs (numbered by k), and sites (numbered by s) using Equation(6.11) and Equation(6.12):

$$\mu_{\ln Sa(T_i)|\ln IM*} = \sum_s \sum_j \sum_k p_{s,j,k} \cdot \mu_{\ln Sa,s,j,k(T_i)|\ln IM*}, \tag{6.11}$$

$$\sigma_{\ln Sa(T_i)|\ln Sa(T*)} = \sqrt{\sum_s \sum_j \sum_k p_{s,j,k} \cdot \left[\sigma^2_{\ln Sa,s,j,k(T_i)|\ln IM*} + \left(\mu_{\ln Sa,s,j,k(T_i)|\ln Sa(T*)} - \mu_{\ln Sa(T_i)|\ln IM*} \right)^2 \right]} \tag{6.12}$$

Where: $\sigma_{\ln Sa(T_i)|\ln IM*}$ is the *i*-th element of the co-variance matrix. $p_{s,j,k}$ is the proportion of *j*-th scenario, *k*-th GMPE and *s*-th site on the logarithmic mean value of the conditional spectral accelerations.

In order to show the methodology explained above in incorporation of multiple sites in CS record selection, an illustrative example is shown as follows. We have assumed that the mean disaggregation results for an IM level equal to 0.6g for six sites are given as shown in Table 6.1. In this example, we have considered an exaggerated difference between the most probable points in the distribution of disaggregation results of the sites. Such disaggregation scenarios ($\tilde{M}$ and $\tilde{R}$) are used for CS computation of each site. It should be noted that, we have neglected the effect of multiple causal events for simplicity and the mean scenario has been assumed to be sufficient for the CS target computations.

Table 6.1. The mean disaggregation results for six hypothetic sites

Site #	$\tilde{R}$ (km)	$\tilde{M}$
S1	10	6
S2	10	7
S3	30	6
S4	30	7
S5	50	6
S6	50	7

In Figure 6.1, the target CS, conditioned on spectral accelerations at different periods of 0.5, 1.0, 2.0 and 3.0s and for different sites of Table 6.1 as well as the most contributing scenarios based on the methodology explained above, are compared. As can be seen, the target spectra for different sites are quite sparse. The black lines are CS when multiple sites are incorporated.

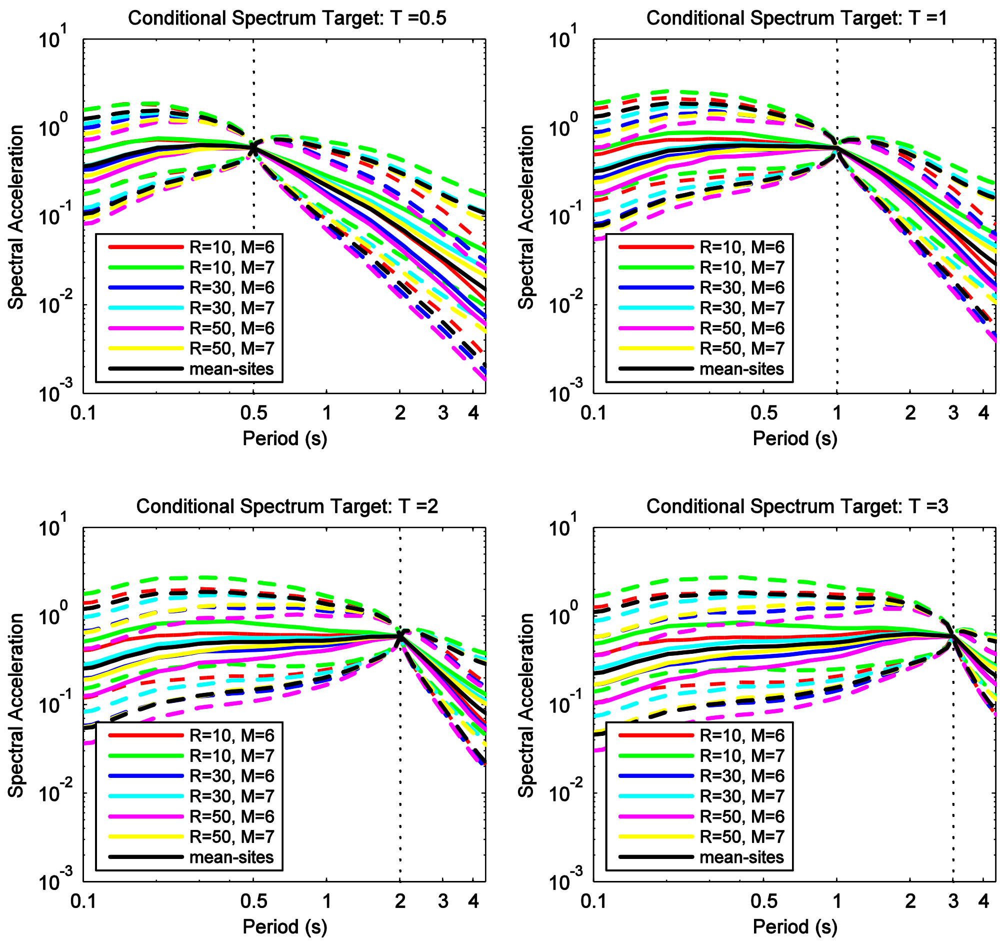

Figure 6.1. Conditional Spectrum target conditioned on single period spectral acceleration at six hypothetic sites with different mean dominating scenarios (The black line is the CS target which incorporates all the sites).

The CS(*AvgSA*), in which *AvgSA* is defined in a period range of 0.3:0.2:3.1s is also adopted as the record selection target spectrum. The target CS(*AvgSA)* computed for all the scenarios corresponding to different sites are shown in Figure 6.2. The black line in the figure shows the CS, incorporating different sites. A visual comparison between Figure 6.1 and Figure 6.2, suggests that the scatter in the target spectrum when using *AvgSA* as conditioning IM, at least at the period range of interest, is lower. In addition, this IM is well applicable to the buildings with different fundamental periods, as *AvgSA* is defined in a range of periods rather than at a single period.

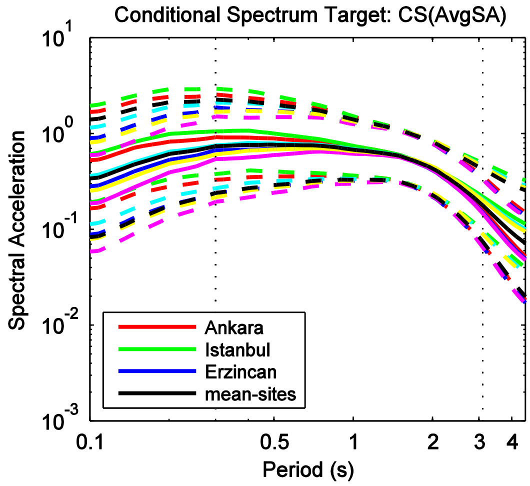

Figure 6.2. Conditional Spectrum target conditioned on AvgSA at period range of 0.3:0.2:3.1s for six hypothetic sites with different scenarios (The black dashed-line is the target CS which incorporates all the sites and the single dot in right hand side of figure is the value of the conditioning IM).

6.5 CASE STUDY BUILDING EXAMPLE, SITES AND HAZARD COMPUTATIONS

A plan-symmetric reinforced-concrete moment-resisting frame with 4-stories was selected in this study. It refers to modern structures built to post-1980 seismic design provisions for high-seismicity regions (site class D). A 2-D centerline idealization of such building was modeled using OpenSees [McKenna *et al.* 2000]. The behavior of the structural members was depicted by lumped-plasticity elements, with properties estimated from the empirical equations proposed by Panagiotakos and Fardis [2001]. Lumped-plasticity elements were used to increase speed of computation and to improve numerical convergence for large deformations. Geometric nonlinearities in the form of P-Δ effects were considered. For more details of the building modeling refer to Kazantzi and Vamvatsikos [2015a]. The first and second mode of the structure are 1.6s and 0.52s.

For this study we assumed that the vulnerability functions are meant to be derived for three different cities of Ankara, Istanbul and Erzincan in Turkey. The precise location of these three points are shown in Table 6.2 and the location of these points on the map as well as the faults (red lines in Figure 6.3b) can be seen in Figure 6.3. The OpenQuake [Monelli *et al.*, 2012], open-source software for seismic hazard and risk assessment, developed by the Global Earthquake Model (GEM) foundation, was used to perform the seismic hazard computations. These computations are based on the SHARE Project [Giardini *et al.*, 2013]. We adopted the GMPE proposed by Boore and Atkinson [2008] for our computations. The hazard curves corresponding with the spectral acceleration at T=1.6s and $AvgSA$(0.3:0.2:3.1s) for three sites are shown in Figure 6.4.

Table 6.2. Location of the three selected sites

Location	latitude	longitude
Ankara	32.76	39.89
Istanbul	28.96	41.02
Erzincan	39.49	39.74

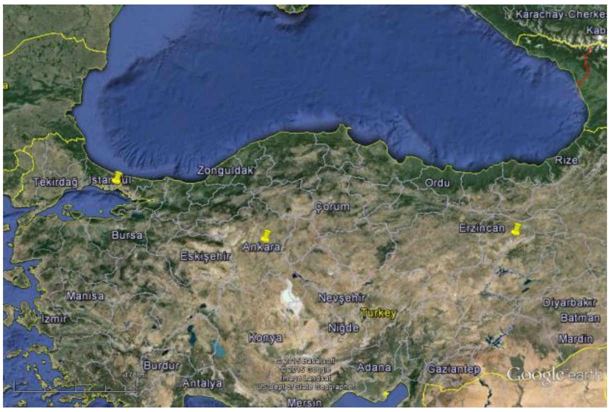

Figure 6.3. Location of the three sites on the map shown by yellow pin points

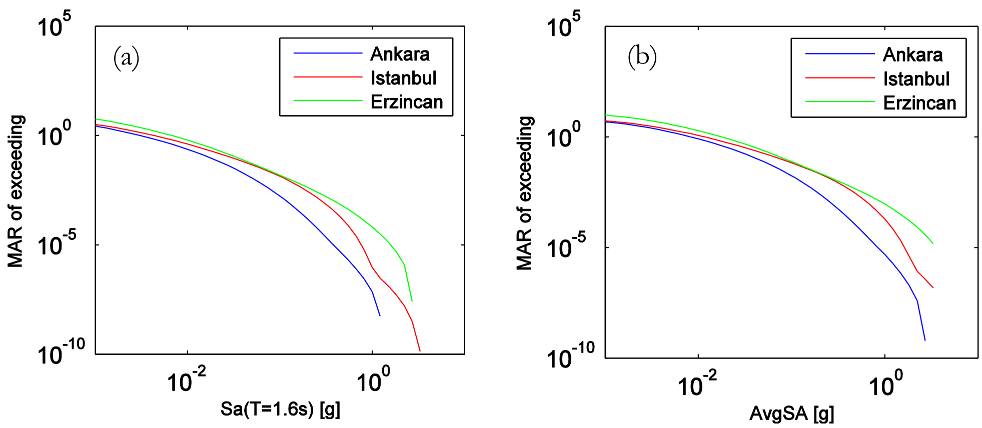

Figure 6.4. Hazard curves for three sites of Ankara, Istanbul and Erzincan for *SA*(1.6s) and AvgSA(0.3:0.2:3.1s).

6.6 **GROUND MOTION DATABASE**

In order to show how the building response and the fragility curves of the same building model would alter at different locations within a country or region when careful record selections with hazard consistency are performed, we generated nonlinear dynamic analysis for the 7-story RC building considering different record sets based on IDA [Vamvatsikos and Cornell, 2002] and Multiple Stripe Analysis, MSA [Jalayer, 2003]. In IDA a suite of ground motions is repeatedly scaled to find the IM level at which each ground motion causes collapse. MSA is performed at a specified set of IM levels, each of which has a unique ground motion set.

For this study, the IDA records include the 22 pair of motions that comprise the FEMA P695 (ATC-63) far-field ground motion set. MSA, on the other hand, was performed using the two target spectra of CS(*SAT*1) and CS(*AvgSA*) for three selected sites and the CS record sets incorporating the hazard of all three sites. Suites of records from NGA-west1 ground motion database were selected and scaled to collectively match the entire distribution of the CS. To do so, we used the original algorithm developed for CS(*SAT*) [Jayaram *et al.*, 2011] and its extended version for CS(*AvgSA*) [Kohrangi *et al.*, 2015d]. For CS record sets, 10 IM levels with fixed values were adopted to cover all ranges of the building response from linear to nonlinear and collapse. The target spectra were defined based on the mode (i.e. the most probable scenarios) of the disaggregation results obtained from the hazard analysis. These results in terms of magnitude and distance for *Sa*(1.6s) and for *AvgSA*(0.3:0.2:3.1), for different sites are listed in Table 6.3. Note that these fixed IM levels, although used for both IMs, are not directly comparable, as they tend to correspond to higher hazard levels (longer return periods) for *AvgSA* compared to *Sa*(1.6s). At each IM level, 44 records were selected to match the CS target mean and variance. Although changing the conditioning IM in IDA could be simply done by mapping the new IM on the available results of the IDA once performed; in MSA, the choice of the IM in record selection is critical since the same IM should be used also for the structural response estimation.

Table 6.3. Mode of Disaggregation results for three different sites of Ankara, Istanbul and Erzincan

		Sa(1.6s)						*AvgSA*(0.3:0.2:3.1s)					
		Ankara		Istanbul		Erzincan		Ankara		Istanbul		Erzincan	
IM level	*IM* Value [g]	$\tilde{M}$	$\tilde{R}$	$\tilde{M}$	$\tilde{R}$	$\tilde{M}$	$\tilde{R}$	$\tilde{M}$	$\tilde{R}$	$\tilde{M}$	$\tilde{R}$	$\tilde{M}$	$\tilde{R}$
1	0.01	6.25	107.5	5.75	17.5	5.75	7.5	6.25	107.5	5.75	17.5	5.75	7.5
2	0.05	6.75	107.5	6.75	17.5	6.25	2.5	6.75	107.5	6.75	17.5	6.25	2.5
3	0.08	6.75	107.5	6.75	17.5	6.75	2.5	6.75	107.5	6.75	17.5	6.75	2.5
4	0.15	7.25	107.5	6.75	17.5	7.25	2.5	6.25	2.5	7.25	17.5	7.25	2.5
5	0.25	6.25	2.5	7.25	17.5	7.25	2.5	6.25	2.5	7.25	17.5	7.25	2.5
6	0.35	6.25	2.5	7.25	17.5	7.25	2.5	6.25	2.5	7.25	17.5	7.75	2.5
7	0.50	6.25	2.5	7.25	17.5	7.75	2.5	6.25	2.5	7.25	17.5	7.75	2.5
8	0.65	6.25	2.5	7.25	17.5	7.75	2.5	6.25	2.5	7.75	17.5	7.75	2.5
9	0.80	6.25	2.5	7.25	17.5	7.75	2.5	6.25	2.5	7.75	2.5	7.75	2.5
10	0.95	6.25	2.5	7.75	2.5	7.75	2.5	7.25	7.5	7.75	2.5	7.75	2.5

In Figure 6.5(a) and (b), spectral acceleration of the CS(*SAT*) and CS(*AvgSA*), the 44 individual selected record sets in grey and the target spectra for each site and the mean of the three sites corresponding with IM level 5 (see Table 6.3) are shown. In Figure 6.5(c) and (d), the 44 records used for IDA analysis are scaled to *Sa*(T_1) and *AvgSA* corresponding with the IM level 5 for comparison reasons.

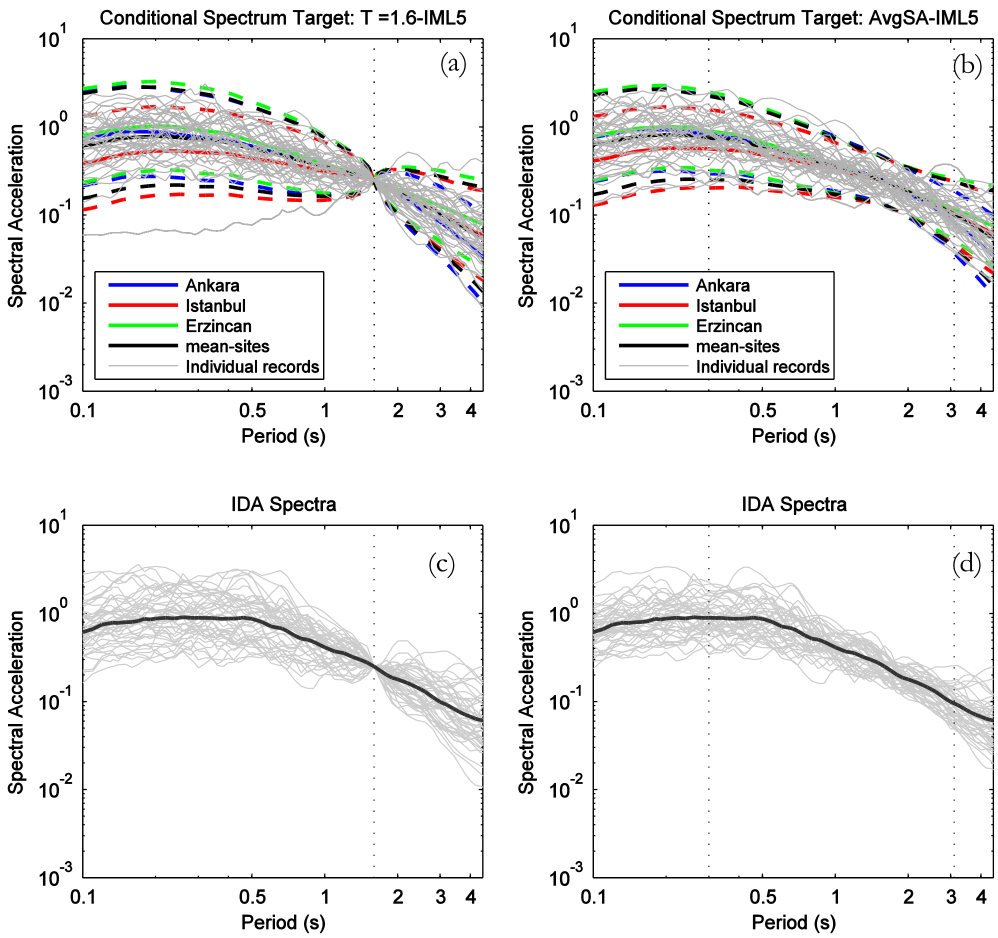

Figure 6.5. Record selection for three sites. Conditional spectra-based: a) CS(*SAT*), b) CS(*AvgSA*); and FEMA P-695 far field IDA record set scaled for: c) Sa(T_1) and d) AvgSA corresponding with the IM level #5 in Table 6.3.

6.7 ANALYSIS RESULTS

6.7.1 GENERAL RESPONSE OF THE BUILDING UNDER DIFFERENT RECORD SELECTION SCHEMES

The nonlinear dynamic analysis based on the IDA and MSA for the selected site of Ankara are shown in Figure 6.6. In Figure 6.6(a) and (b) the IDA curves corresponding with the maximum of MIDR along the height based on the conditioning IMs of *SAT*1 and *AvgSA* are illustrated, respectively. This Engineering Demand Parameter (EDP) is commonly used for collapse estimation. As can be seen, the dispersion in IDA, when *AvgSA* is used as the conditioning IM is lower than *SAT*1. This suggests the higher efficiency of *AvgSA* compared with *SAT*1. This observation is in lines with the similar findings in previous studies [e.g. Cordova *et al.*, 2000; Bianchini *et al.*, 2010, Eads *et al.*, 2015]. In Figure 6.6(c) and (d), the MIDR response versus IM, based on MSA and the conditioning IMs of *SAT*1 and *AvgSA* are depicted, respectively. Each stripe consists of 44 data points related to the MIDR response obtained from one nonlinear dynamic analysis. As was previously observed in Kohrangi *et al.* [2015d], the results obtained based on the record set of CS(*AvgSA*) tend to maintain a uniform dispersion at different IM levels, whereas the counterpart CS(*SAT*1), produces less dispersed results for MIDR in the lower IM levels and more dispersed results at higher IM levels with higher nonlinearity. Nonetheless, it is preferable for an IM to perform well in different IM levels and different locations within the building and with respect to different EDP types (i.e. acceleration- or displacement-sensitive).

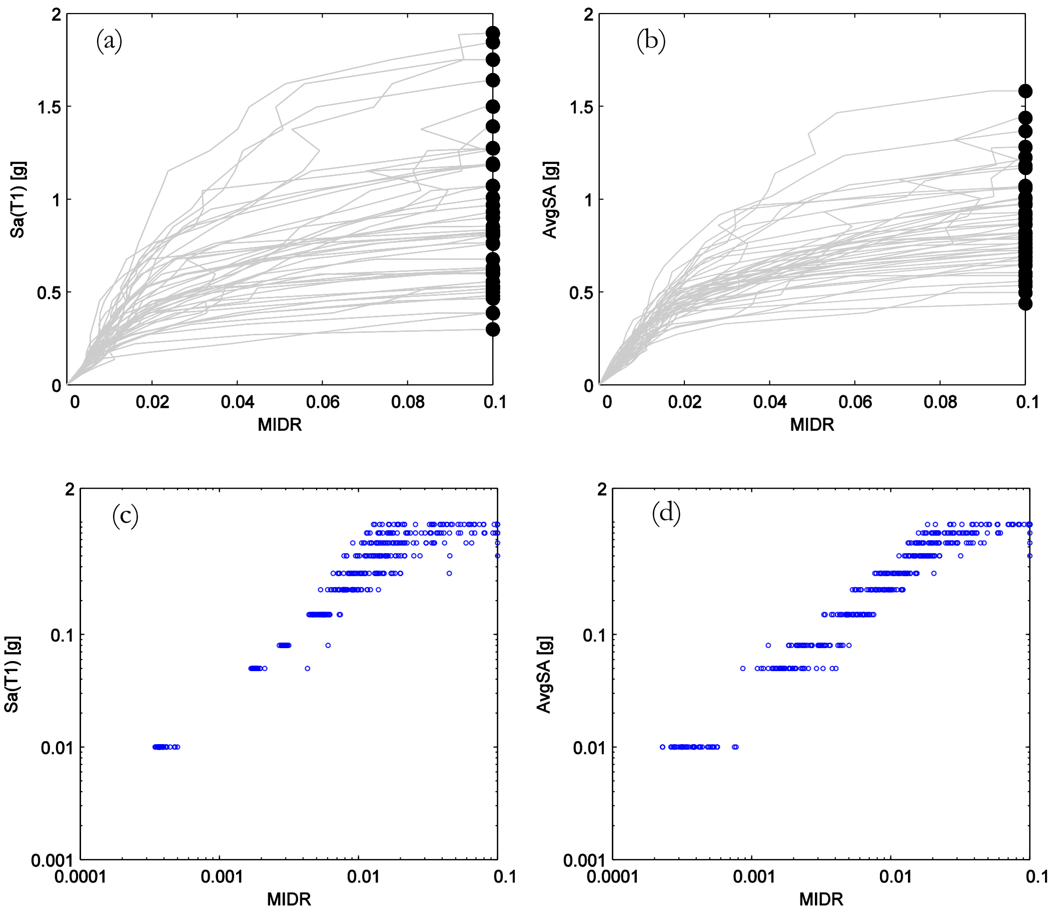

Figure 6.6. Nonlinear dynamic analysis results based on: a) IDA, IM= Sa(T1), b) IDA and IM=AvgSA, c) CS(SAT1) for Ankara; and d) CS(AvgSA) for Ankara.

The building response profile along the building height in terms of MIDR and maximum PFA obtained from different record selections at different sites are shown in Figure 6.7. In Figure 6.7(a) and (b), the response profile conditioned on *SAT*1 and in Figure 6.7(c) and (d) the ones conditioned on *AvgSA* are shown. Firstly, the results show a high difference in the building response related to multiple sites. For instance, for the same level of IM value, the building response in Erzincan is higher than other sites. This results confirms the initial goal of this study which is based on the idea that the building response at multiple sites is not unique and it is, in fact, site-dependent. IDA, on the other hand, by nature provides unique results regardless of the different site seismicity. In the case tested here, IDA highly overestimates the PFA especially for the case of CS(*SAT*1), however for MIDR, it is in lines with other record sets. Similar with what observed in the MIDR for single site, for which *AvgSA* produces lower dispersion in the building response, we can see here that the results obtained for multiple-sites when conditioned on *AvgSA* are less scatter compared with *SAT*1. This might address the higher sufficiency of *AvgSA* observed also by Eads *et al.* [2015] and Kazantzi and Vamvatsikos [2015], in which the conditional building response when conditioned on *AvgSA* is less dependent on other ground motion properties of the site (such as magnitude or distance). Even though, here we are not explicitly examine the dependency of the building response to other site-specific properties, the lesser scatter in the response for multiple-sites in application of *AvgSA* implicitly shows its higher sufficiency.

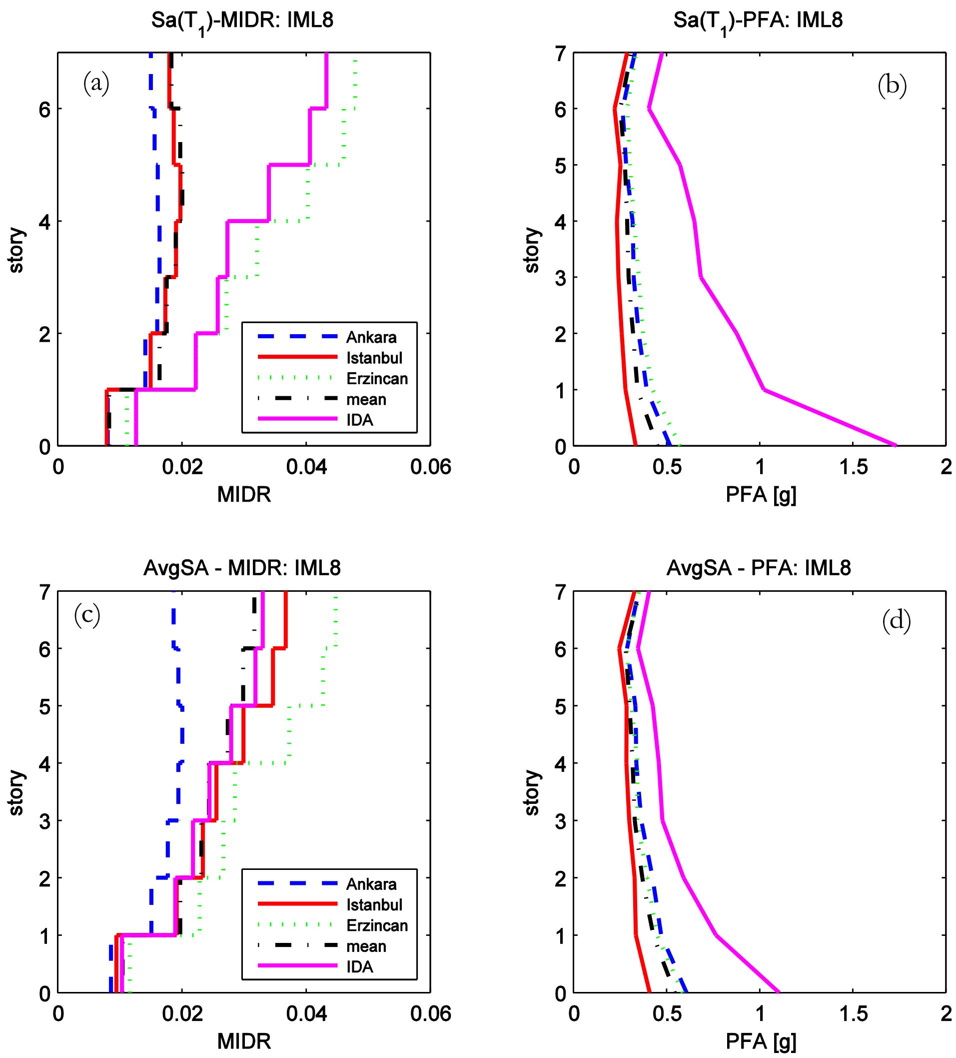

Figure 6.7. Building response profile of the 7-story for MIDR and PFA at IM level 8 based on different record selections and at different sites and two different conditioning IMs: a) EDP=MIDR, *IM=SAT1*; b) EDP=PFA, *IM=SAT1*; c) EDP=MIDR, *IM=AvgSA*; d) EDP=PFA, *IM=AvgSA*.

6.8 ANALYTICAL FRAGILITY FUNCTIONS

Several damage criteria have been proposed in literature [see Akkar *et al.*, 2005, for instance], to allocate buildings to a damage state. These may include the maximum roof displacement, inter story drift ratio, steel or concrete strain level, maximum base shear, and so on. In this study we considered maximum inter story drift ratio along the building height, MIDR, as a

global damage measure for the structure. In addition, we considered PFA at the third floor of the building as a more local damage measure which could be used for a more detailed loss estimation. PFA is mainly used for measuring the damages induced to building non-structural components rather than a global damage measure. Since the methodology explained in this study could be also used for a detailed component based loss estimation, for completion, we examined also PFA in a single floor of the building.
The results of fragility analyses in terms of MIDR and PFA, implementing different methodologies explained in previous sections are presented in this section. Three different limit states corresponding with the slight, moderate and severe damages were selected for each EDP type. For MIDR, the probability of exceeding 0.012, 0.02 and 0.04 were considered, whereas for PFA the Limit state thresholds were defined for the PFA values exceeding 0.5, 0.60 and 0.65g. The results of these fragility curves for MIDR and PFA are shown in Figure 6.8 and Figure 6.9, respectively. In these figures, the site-specific fragility curves for Ankara, Istanbul and Erzincan as well as the ones obtained from IDA are depicted. In addition, the fragility curves obtained using the two methodologies in this paper, by incorporation of multiple sites in record selection (i.e. mean-sites) or incorporation of the multiple fragility curves (i.e. mean-frg) are shown. In Table 6.4, the parameters of the fragility functions are summarized.

The followings could be observed from these figures:

1- As was expected based on the results presented in the building analysis section, the building fragility functions are also site-dependent. The difference in the curves for different sites suggests that, the common approach in application of *one* fragility function regardless of the seismic hazard of the region can bring large uncertainties into loss estimation procedure.
2- The IDA record set used here, in almost all of the cases, underestimates the building capacity. This might not be a general conclusion for every IDA record set, since a different set of IDA records might produce totally different fragility curves, perhaps even for some cases overestimating the building capacity. For instance, it seems that the IDA record set used here is well representative of the seismicity of the site of *Erzincan* in terms of MIDR, whereas it is too far from the results obtained for *Ankara*. However, what we can conclude from these results is that, using random record sets without consideration of spectral shape and hazard consistency when performing IDA, can generate erroneous results which is far from the "true" result and will produce wrong fragility and consequently less certain risk analysis results. One way out for this problem, observed when using IDA, is the methodology introduced by Haselton *et al.* [2011]. In this approach (adopted also in FEMA P695 by definition of spectral shape factor, SSF), the median parameter only (and not dispersion) of the fragility function obtained from IDA is adjusted based on the ratio between the mean of the epsilons of the records in the record set versus the expected mean epsilon in the site (from hazard disaggregation) corresponding to a relevant hazard return period. In this method which is calibrated in that study for collapse limit state of a group of buildings only, it is not

obvious whether it could produce an accurate result for any of the three sites tested here.

3- The results obtained using *AvgSA* seem to bring the fragility curves of different sites closer together when compared with those obtained from *SAT*1. This suggests that, perhaps, even if the user decides to use a single fragility function for multiple-sites without performing careful record selection and multiple times for each site, using *AvgSA* could be an acceptable solution while using IDA. This feature of *AvgSA* could be explained with reference to its rather higher efficiency and sufficiency in building response prediction compared with *SAT*1. Kohrangi *et al.* [2015d] showed that *AvgSA* can provide an efficient response estimation for buildings at different heights and at different IM levels. This efficiency was observed to be uniform at different IM levels, whereas *SAT*1 has lower efficiency especially for prediction of maximum MIDR for higher IM levels.

4- The two methodologies of mean-site and mean-frg used here provide very close results. Here, we have used the mean-frg method as a bench mark to compare its applicability with the mean-site method. These two methods both provide moderate results which sits in between the fragility functions obtained for all three sites. This means that one can use any of these two fragilities for risk assessment procedure as a fair average fragility, representing the response of such building class among all sites. The results shown here, however, suggest that to avoid performing CS record selection and NDA multiple times for each site (i.e. mean-frg method), one can use the mean-site method to perform the record selection and NDA analysis only once and obtain the same results.

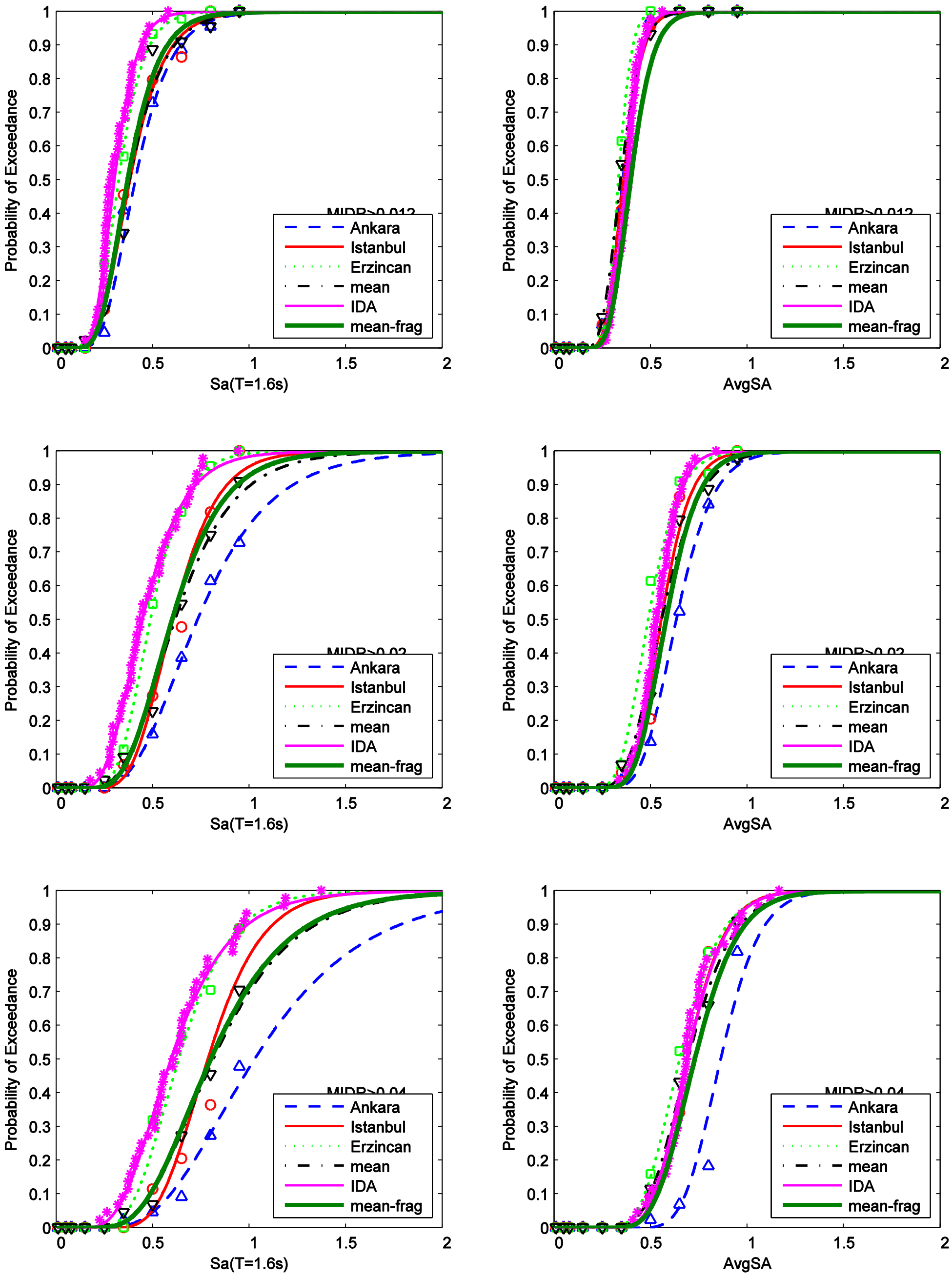

Figure 6.8. MIDR fragility curves obtained analytically for the 7-story building based on different IMs of *Sa*(*T*1) and AvgSA and record sets selected for different sites. (First row: MIDR>0.012, second row: MIDR>0.02 and third row: MIDR>0.04).

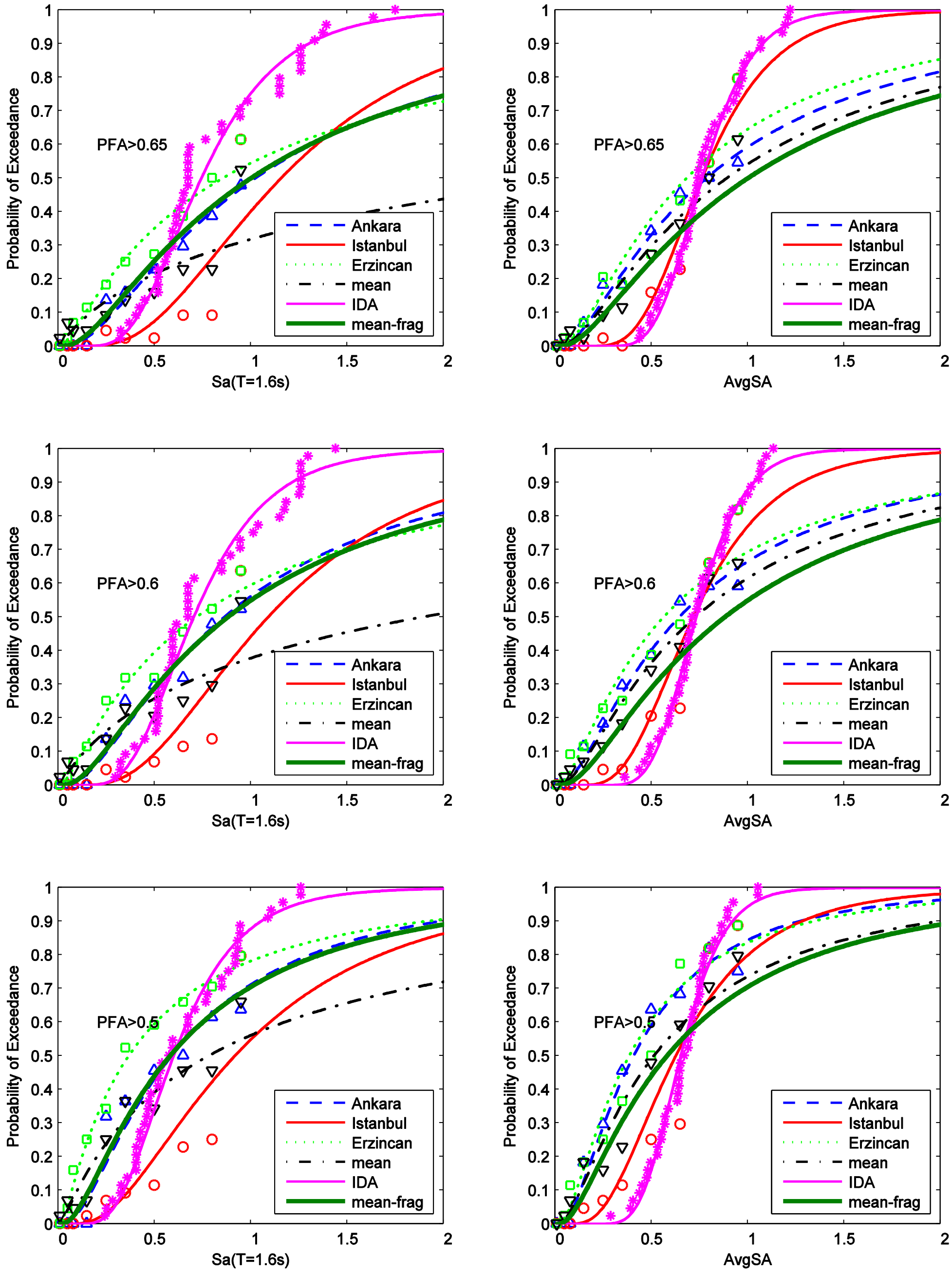

Figure 6.9. PFA at the 3-rd floor fragility curves obtained analytically for the 7-story building based on different IMs of *Sa*(*T*1) and *AvgSA* and record sets selected for different sites.

Table 6.4. Fragility function parameters obtained for the 7- story building based on different record selection schemes and at different sites.

	IML	MIDR				PFA- 3rd floor			
		*SAT*1		*AvgSA*		*SAT*1		*AvgSA*	
		$\hat{\theta}$	$\hat{\beta}$	$\hat{\theta}$	$\hat{\beta}$	$\hat{\theta}$	$\hat{\beta}$	$\hat{\theta}$	$\hat{\beta}$
Ankara	1	0.41	0.35	0.35	0.2	0.59	0.95	0.41	0.89
	2	0.73	0.4	0.63	0.24	0.86	0.96	0.64	1.03
	3	1.03	0.43	0.86	0.19	1.02	0.99	0.78	1.04
Istanbul	1	0.38	0.36	0.36	0.21	0.92	0.71	0.63	0.56
	2	0.6	0.3	0.55	0.22	1.09	0.59	0.72	0.45
	3	0.78	0.28	0.69	0.22	1.16	0.58	0.76	0.38
Erzincan	1	0.32	0.32	0.49	0.25	0.37	1.29	0.38	0.98
	2	0.49	0.29	0.55	0.22	0.72	1.37	0.56	1.14
	3	0.63	0.33	0.65	0.25	0.85	1.40	0.68	1.02
Mean-sites	1	0.38	0.38	0.34	0.24	0.78	1.62	0.51	1.06
	2	0.61	0.39	0.55	0.27	1.89	2.05	0.73	1.08
	3	0.81	0.39	0.65	0.25	2.82	2.20	0.89	1.09
IDA	1	0.31	0.29	0.37	0.17	0.60	0.44	0.65	0.27
	2	0.45	0.36	0.54	0.18	0.70	0.43	0.73	0.26
	3	0.60	0.40	0.70	0.23	0.74	0.44	0.76	0.27
Mean-frg	1	0.37	0.34	0.40	0.22	0.58	1.01	0.46	0.83
	2	0.60	0.33	0.58	0.23	0.88	1.02	0.64	0.92
	3	0.80	0.35	0.73	0.22	1.00	1.05	0.74	0.87

6.9 DISCUSSION

- The results presented in this study show that the fragility curves for risk based assessment are site-dependent and using one fragility curve for multiple sites without appropriate considerations in the site-to-site variability is not recommended when the seismicity of these regions is significantly different. The following solutions in the order of preciseness (not in terms of required time and effort to perform the method) could be recommended as follows:
  iii) Performing site-specific hazard consistent record selection and deriving multiple building fragility curves for each site and for each building to be used in risk assessment analysis.
  iv) Performing site-specific hazard consistent record selection for each site and incorporating multiple derived fragility curves into a single fragility curve to be used for all sites in risk assessment analysis.
  v) Performing one site-specific hazard consistent record selection, incorporating the seismicity of all sites together as well as performing NDA to derive single fragility curve to be used for risk assessment analysis of all sites.
  vi) Performing IDA and deriving single fragility curve to be used in risk assessment of all sites.
- It should be noted that, in all of the methods mentioned above, it was observed here that by using *AvgSA* as IM, instead of spectral acceleration at a single period, the scatter in the fragility curves of multiple sites will be reduced. In addition, although not tested here, the AvgSA, intuitively, has the potentials to be used as a building-independent IM as well. For instance, for the period range of *AvgSA* defined in this study (i.e. 0.3:0.2:3.1s), perhaps all buildings with a first modal period of vibration within 1.0 to 2.0s could be analyzed with rather high efficiency, whereas *SAT*1 is less flexible, in this regard.
- Even though, building-specific fragility curves should be obtained for different building types with different heights and dynamic properties, we suggest here that using *AvgSA* will help to have a consistent unique IM for a wide range of buildings, avoiding the needs to have too specific fragility curves using multiple IMs.
- It should be emphasized that there are many IMs introduced in literature that might have the same features as *AvgSA*, however, since hazard computations for *AvgSA* could be simply extended from the available GMPEs and PSHA codes, it might be more appealing compared with other IM proposals for practical purposes.
- In both the methodologies introduced in this paper (mean-site and mean-frg), there is a possibility to provide different weights (P_s) when incorporating the sites into a single record set or fragility function. For instance, for the case study presented here, even though the seismicity of Erzincan is higher than Istanbul or Ankara, there are more buildings in the two latter cities; in addition, these two cities are more populated than Erzincan, therefore, one can select to give more weight to Ankara and Istanbul to

provide a compromise in the fragility curves as these two cities are proportionally more prone to seismic losses or costs.

- The two methodologies described here in this study are tested only for an illustrative example of one 7-story reinforced concrete building and three sites with different seismicity. Our main focus here has been introduction of the methodology and illustration of its simple application. We believe that, even though it is worth testing this procedure for other building types and with different number of stories, to validate the methodology for general use, the mathematical concept of incorporation of multiple fragilities (mean-frg) and multiple-site record selection (mean-sites) is robust and could be applied in practice for building loss estimation.

6.10 **CONCLUSIONS**

The main focus of this study was to investigate whether or not building global fragility functions used in loss estimation procedures are independent of the site where the building is located. The current state of practice is application of identical fragility functions for similar building archetypes located in multiple-sites assuming that there is no effect of the site seismicity in building response. With this goal in mind, the building fragility functions for a reinforced concrete building example was derived using nonlinear dynamic analysis for three different sites with different seismicity. Careful hazard consistent record selection scheme based on conditional spectrum method as well as incremental dynamic analysis for comparison reasons were adopted. The results in this study, in contrary with the assumption described above, show that the building fragility functions at multiple sites are not identical. Such difference in the fragilities among sites, if not taken care of in practice, might cause significant errors in regional building loss assessments. This observation suggested further investigations for finding eventual solutions for this complexity.

In order to address this problem, two methodologies are proposed here. The first approach incorporates multiple fragilities obtained for each site into one fragility to be used for all the sites. The second approach incorporates multiple-sites using conditional spectrum based record selection considering the variability in the target spectrum of each site. The results here show that, these two methods provide fragility curves which are applicable to all the sites. In addition, the fragilities obtained from both methods are quite similar. This similarity is somehow a verification for the proposed record selection scheme incorporating multiple sites.

Finally, two different IMs of spectral acceleration at the first building mode of vibration, $Sa(T1)$, and averaged in a period range, *AvgSA*, were examined here. The results show that when *AvgSA* is used, the scatter in the response among different sites is diminished compared with $Sa(T1)$. In addition, conditional spectrum based record selection conditioned on *AvgSA*, CS(*AvgSA*), seems to be a better solution for portfolio seismic risk assessment, since, firstly, *AvgSA* is an efficient building response predictor. Secondly, given its definition being valid in a period range it can be used for a class of buildings with different periods within the defined period range.

7. SUMMARY, CONCLUSIONS AND FUTURE WORK

7.1 **USEFUL REMARKS**

The main focus of this study has been investigating alternative novel solutions for increasing the accuracy in building specific- and portfolio- seismic risk assessment in terms of building response prediction and loss estimation. We applied probabilistic seismic demand analysis (PSDA) and loss assessment in various forms to gauge the precision of each approach. Typically, the seismic demand or losses due to seismic actions in a region are estimated by connecting the hazard of the site to the structural response. This connection, in a practical state-of-the art, is mainly achieved using a ground motion Intensity Measure (IM), commonly adopted as the spectral acceleration at the first mode of vibration of the building, SAT1. In other words the building response is estimated conditioned on an IM of the ground motion. Nonlinear dynamic analysis carried out on a 2D model of the structure is then used to measure its response, whose severity is gauged in terms of one or more Engineering Demand Parameters (EDPs). A set of ground motion records, therefore, is needed as a tool to connect this EDP-IM interface. The engineer performing such seismic risk assessment faces two challenging choices. Firstly, among all the available proposed IMs in literature, "which one would serve better for response prediction?" Such IM should be a fair reflection of the seismic hazard of the site, on one hand, and it should be efficient (i.e. low response dispersion given IM) and sufficient (i.e. the demand is independent of other ground motion properties when conditioned on the selected IM) for building response prediction, on the other hand. Secondly, due to the tendency to use limited number of records to reduce the required analysis time, "which records should be used to best represent the seismicity of the site while being limited to as few records as possible?" This latter is named as hazard consistent record selection. In addition, to what extent and for what type of structures, 2D models could be used without losing the required preciseness in the procedure? This study deals with these two topics for seismic assessment and loss estimation with reference to 2D and 3D structural models.

In recent years various IMs have been proposed in literature to better predict the building response. Among these IMs, some of which are highly complicated, the vector IMs consisting of spectral accelerations at multiple spectral ordinates and scalar IM of spectral acceleration averaged in a period range, *AvgSA*, have shown to be promising IMs for building response prediction. Computing the seismic risk of realistic buildings for both loss estimation and collapse assessment requires monitoring building response measures that may include story-specific measures, such as peak inter story drifts and floor response spectra at all stories, and global measures, such as maximum peak inter story drift along the height of the building and residual, post-earthquake lateral displacement. A confident assessment of these response measures requires sophisticated structural and non-structural modelling that is better served by using 3D computer models of the building. Predicting the response of such models in both the main horizontal axis and, in some cases, vertical direction (e.g., for assessing the damage to suspended ceilings) is facilitated by the use of more than one IM of the ground motion in one or more directions and at one or more oscillator periods. C*hapters* 2 to 4 of this dissertation, investigate the implementation of such IMs, in various scalar and vector forms, for response and loss estimation of three RC buildings modelled as 3D structures in a full probabilistic performance based earthquake engineering (PBEE) framework.

Performing vector-valued PSHA for complex IMs that are derived from common ones (e.g., spectral accelerations at different periods) is not trivial and requires modifying the existing ground motion prediction models and computing the variance-covariance matrix of such IMs. *Chapter* 2 focuses on defining and computing the joint hazard of the IMs that are used as predictors of building response. Different aspects of such IMs are considered for the most common and practical IMs appearing in the literature namely spectral accelerations, ratios of spectral accelerations and averages of spectral accelerations over different periods and orientations, which are used as predictors of building response both in scalar form and in vector form. More precisely, the scalar IMs considered here are spectral accelerations at first mode period of the structure in each orthogonal main direction of the building, or at the average of the first modal periods in the two orthogonal directions. Another scalar IM used is the average spectral acceleration at multiple periods of oscillation that are important for the structures considered. It is emphasized, however, that the methodology described for performing vector-valued PSHA goes beyond the boundaries of these specific applications that use only spectral accelerations. Other less conventional IMs (e.g. *PGV, PGD*, Arias Intensity, duration, and Cumulative Absolute Velocity), can be used following the same approach provided that ground motion prediction models and correlation coefficients for those IMs are available.

For the applications produced in this study, the conventional scalar PSHA for scalar IMs and the vector-valued PSHA were performed using the software OpenQuake. The vector-valued PSHA were carried out using a methodology that was called the *"*Indirect*"* approach since it does not implement the numerical integration of the joint distribution of all the correlated IMs considered, as the "direct" approach does. The "indirect" approach uses the marginal hazard curve for each IM, the disaggregation results from those IMs, and the correlation coefficients for each pair of IMs to obtain the joint hazard. Hence, this method could be considered as a post processor of any available scalar PSHA code. This "indirect" method is arguably superior to the "direct" integration approach in many aspects as explained in the body of *Chapter* 2. However, when applying the "indirect" approach to vector PSHA, care should be exercised in the selection of the bin sizes that discretize the mutli-dimensional domain of the IMs. The bin sizes should be rather small especially in the part of the domain where the highest concentration of probability is located.

These scalar and vector IMs were used for response prediction of 3D models of RC infilled buildings in *Chapter* 3. The ground motion IM used as input to the response of these buildings is kept fully consistent with the hazard, which has been probabilistically computed for the same IM, be it simple or complex, scalar or vector, using appropriate Ground Motion Prediction Equations. Three 3D building examples of 3-, 5- and 8-story RC infilled frames typical of old Mediterranean construction were considered as test cases for testing this methodology. An ideal IM for 3D structures should be efficient in response prediction at any story within the building at both linear and nonlinear states of the structure. For a linear SDOF system or for a linear first mode dominated building, *SAT*1 is an appropriate IM. However, as the structure becomes nonlinear, the spectral acceleration at longer periods is needed. For MDOF systems, such as the ones tested herein, the effect of higher modes and spectral shape on the response becomes important. In addition, for a 3D structural model, with coupled response in two orthogonal directions, this IM should contain separated information about the excitations in both directions. Moreover, such an ideal IM should have fairly balanced predictive potential for different structural response types such as inter story drift ratio (IDR) and peak floor acceleration (PFA) and work well all along the height of the building. As a scalar IM, average spectral acceleration is shown to be an appropriate IM for response prediction of both PFA and IDR. However, we observed here that its efficiency decreases for 3D asymmetric buildings or buildings with well separated periods in two main orthogonal directions. Hence, a superior approach is offered that considers the average spectral acceleration of two orthogonal directions in a two-component vector IM. Such an IM, at least for the examples considered here, can enhance all of the advantages mentioned earlier for 3D buildings in terms of PFA and IDR. The use of a vector IM, however, comes at a price since vector hazard estimation needs to be performed rather than the routine scalar PSHA for carrying out long-term response hazard or loss calculations. This vector IM route is more accessible if one uses the indirect method to vector hazard analysis, discussed in *Chapter* 2, rather than its original formulation.

Chapter 4 focuses on the extension of the current state-of-the-art PBEE procedure for building-specific loss estimation beyond the use of simple ground motion IMs as predictor of EDPs and, in turn, of damage states and loss of realistic 3D structural models. The investigated set of IMs generated in *Chapter* 2 and used for response prediction in *Chapter* 3 was adopted for building-specific loss estimation. The PEER Center style loss estimation approach allows detailed component-based loss analysis considering the vector of building EDPs locally at all stories rather than using only one global response parameter (e.g., the maximum inter story drift ratio). The use of vector IMs, because of the correlation of the different EDPs with multiple spectral ordinates, increases the response estimation power, therefore, leading to less uncertain loss estimates. In addition, since the building response at each of the two orthogonal directions of the 3D building models is correlated to the ground motion excitation in the same direction, there is higher accuracy in the response prediction. For the building components that are sensitive to more than one response type and/or direction of excitation, component fragility surfaces could be adopted and parameterized on more than one EDP. The results here showed that even in such cases using vector IMs, given the lower dispersion in the collapse and response prediction, lead to less dispersed loss estimates. A procedure for considering the effect of the infill walls in-plane and out-of-plane interaction based on a function of the infill demand was also implemented. However, for the three tested building examples and compared with the total building repair cost, insignificant changes were observed in the total loss values and the Expected Annual Loss. Based on the methodology introduced in this study, this approach could be adopted for other types of building components (e.g., suspended ceilings) that are sensitive to more than one EDP. It is then emphasized that all the utilized IMs in this loss estimation exercise represent legitimate choices that are usable in practice. However, the results presented show that there is significant scatter in the estimates of the MAR of exceedance of losses. When vector IMs are used, at least of the kind utilized here, this scatter is considerably tightened.

The results of *Chapter* 2 to 4, which contains a full process of PBEE from hazard computations to demand and loss estimations, suggest that the use of vector IMs both in hazard assessment and response estimation might be considered cumbersome and less appealing in practice. However, using a vector IM, at the very least, can provide important insights on how far are MAR estimates obtained from simpler scalar choices from the 'true' but unknown response. Although only three buildings were studied and more research is still needed, it can be claimed that the loss assessment of 3D structures can benefit considerably from the explicit consideration of seismic intensity in the two orthogonal directions, preferably in a vector form or, at least, in a sophisticated scalar form, such as that based on spectral acceleration averaged over a building-specific period range used here. More specifically, based on the results of these analyses, the spectral acceleration at the first mode of vibration of the structure and PGA, provide loss estimates that can arguably be considered conservative when compared to those of the other sophisticated scalar and vector IMs tested here. This large difference may pose a question mark about the effectiveness of such simple scalar IMs in capturing well the story-specific engineering demand parameters needed for assessing losses in 3D structural models.

The other issue regarding the record selection was tackled as a separate topic in *Chapter* 5 and was extended in *Chapter* 6 to an application for building portfolio loss estimation at multiple sites. Good performance of average spectral acceleration in a period range, *AvgSA*, motivated more investigations on its application for record selection as well. In *Chapter* 5 we explored the use of an alternative approach to PSDA that uses ground motion records selected from a conditional spectrum (CS) -based on the *AvgSA*, in the period range that matters for the response of the considered building. *AvgSA* has already been shown in previous studies, as well as earlier chapters of this study, to be an efficient and sufficient IM for building response prediction but *AvgSA* has not been used so far both for informing hazard analysis and also for selecting ground motion records to be used as input to structural response assessment. In *Chapter* 5 *AvgSA* is utilized in the implementation of an extension of the traditional conditional spectrum, called here CS(*AvgSA*), to explicitly hinge on the average of multiple spectral accelerations and also in the probabilistic hazard calculations. The entire chain of PSDA, which is the first step to loss estimation, is made fully consistent here.

The proposed methodology was tested for four 4-, 7-, 12- and 20-story RC buildings located in a highly seismic site in south of Marmara Sea in Turkey. The 2D structural models of such buildings were subject to both *Intensity* and *risk based assessment* calculations for using ground motions selected according to CS(*AvgSA*) and CS(*SAT*) (namely the traditional conditional spectrum to a spectral acceleration at a given period *T*) at multiple periods ranging from T_2 to $SATH=1.5 \cdot T_1$, where T_1 and T_2 are the fundamental and second mode frequency of the linear elastic building. *AvgSA* is an IM that has many qualities that range from a higher predictability than the single period spectral accelerations and overall a superior prediction power for both EDPs that control the building seismic performance, namely the peak in time IDR and the PFA at each story. This holds for different IM levels, both weak and intense.

The efficiency of *AvgSA* for both IDR and PFA is essential in risk-based assessment for which the building response distribution at all IM levels is necessary. In this respect, it is advantageous to work with a single conditioning IM that performs moderately well for different EDPs at all stories and at all IM levels rather than identifying the very best IM that is only efficient for estimating a single EDP and perhaps not even at all stories of a building (e.g., *SAT*1 is not a good predictor for IDR at high stories of a building) and not for all IM levels (e.g., *SATH* is very good for estimating IDR at high ground motion intensity levels but poor at weak ones). Using multiple IM predictors forces the analyst to repeat response analyses for multiple sets of records selected according to different IMs, with an evident waste of resources. It is also argued here that such an approach would not only be wasteful and impractical but also potentially conservative when employed for risk-based calculations. Finally, the use of CS(*AvgSA*) showed more flexibility during record scaling to match the CS amplitude levels than the use of CS conditioned on single period spectral accelerations. A good hazard consistency to CS(*AvgSA*) for the severe hazard levels necessary to test the ultimate capacity of these buildings was ensured by limiting the scale factors to four while scale factors up to 10 were necessary when using the CS(*SAT*1). The potential for overscaling and, therefore, of using records with unrealistic characteristics that may cause biased EDP estimates is greatly reduced when CS(*AvgSA*)-based records are utilized.

The effectiveness of CS(*AvgSA*) recognized in *Chapter* 5 motivated its application as a tool in portfolio building loss estimation in *Chapter* 6. The main reason to generate such application started from the question, *are the global building fragility functions unique and site-independent?* The current state of practice in portfolio loss estimation is the application of identical fragility functions for similar building archetypes located in multiple-sites of the same region. This practice assumes that there is no effect of the site seismicity in building response. With this goal in mind, the building fragility functions for a RC building was derived using nonlinear dynamic analysis for three different sites with different levels of seismicity. Careful hazard consistent record selection scheme based on conditional spectrum method conditioned on both *STA*1 and *AvgSA* as well as incremental dynamic analysis for comparison reasons were adopted. The results presented in this *Chapter* 5, contrary to the assumption mentioned above, show that the building fragility functions at multiple sites are not identical. Such difference in the fragilities among sites, if not taken care of in practice, may cause significant errors in regional building loss assessments. This observation suggested further investigations for finding feasible yet practical solutions to this issue. In *Chapter* 6, therefore, two approaches are proposed to address this problem. The first approach incorporates multiple fragilities obtained for each site into one fragility to be used for all of the sites. The second approach incorporates multiple-sites into one set of records using conditional spectrum based record selection. This latter approach, inherently considers the variability in the target spectrum among different sites. The results here show that, these two methods provide fragility curves that are applicable to all the sites. In addition, the fragilities obtained from both methods are, not surprisingly, quite similar. This similarity is somehow a verification for the proposed record selection scheme incorporating multiple sites. Finally, between the two adopted different IMs of *SAT*1 *AvgSA*, the latter showed less scatter in the fragility curves obtained from different sites. In addition, the results for the single example tested here suggest that record selection conditioned on CS(*AvgSA*) may be a better solution for portfolio seismic risk assessment for multiple reasons. Firstly, *AvgSA* is an efficient building response predictor. Secondly, given its characteristics, it can be used for a class of buildings with different periods within the defined period range. This last comment, however, requires more investigations to be performed on different building types and various sites before being recommended in practice. Such comprehensive study is currently under development.

7.2 **Future work**

- The vector PSHA software generated in this study is used only for one site example using single GMPE. Although the methodology to incorporate multiple GMPEs in the indirect approach of VPSHA is explained in *Chapter* 2, it was not actually applied in this study. It is worth investigating such possibility in a real example of PSHA with a logic tree combining multiple GMPEs and to compare the resulting joint hazard with the direct approach in order to quantify the approximation induced in using the indirect method.
- The VPSHA software is used here for computation of joint hazard for spectral accelerations, spectral acceleration ratio and averaged spectral acceleration. The software is, however, generic and could be applied for other ground motion IMs such as duration, PGV, PGD, etc. As such, one interesting topic left to future research

would involve performing the joint hazard computations of vectors containing other IMs, if needed in practice.

- The approaches introduced in chapter 3 and 4 in application of different scalar and vector IMs for building-specific loss estimation was used only for three 3D RC building models. This approach could be used for other building types with different levels of irregularity in order to show the importance of application of vector IMs for such buildings. In addition, one useful application of vector IMs is in response prediction of tall buildings in which higher mode effects and the building elongated period play a significant role in the building response. Therefore, the use of a vector that consists of spectral accelerations at multiple spectral ordinates for such building may be advantageous.
- In the VPSHA study presented here, the effect of directivity in near fault sites was not considered. However, with the development of new generations of GMPEs in which PSHA could be performed with respect to the direction of the fault to the site, application of VPSHA for fault parallel and normal hazard could be useful, especially for risk assessment of buildings located close to active faults.
- In *Chapter* 4, a new approach for consideration of multiple EDPs in component based fragility functions (surfaces) applied for masonry infill walls was introduced. Such fragility surfaces are useful for building components that are sensitive to more than a single EDP. Therefore, firstly, a fresh look at the necessity of application of fragility surfaces for different such components could be investigated. In addition, further experimental studies should be planned in the near future with an eye on monitoring the influence of more than one IM on component vulnerability.
- The CS(*AvgSA*) record selection proposed in *Chapter* 5 was tested for spectral acceleration at one predefined period range of *AvgSA* which was assumed to be the most effective one based on preliminary investigations. However, undoubtedly using other ranges of periods may enhance the effectiveness of CS(*AvgSA*) in PBEE. In addition, CS(*AvgSA*) was used for 2D structural models and only RC frames for one definition (and perhaps the simplest) of *AvgSA*. More investigations should be performed on 3D structural models of other types of buildings and also to other variants of *AvgSA*.
- The portfolio loss estimation and the proposed approaches for consideration of multiple-sites introduced in *Chapter* 6 was meant to be a proof of concept. As such it was performed for a single building example and three sites. This example should be extended to multiple-buildings located at different sites before being proposed as a reliable approach.

Appendix A: VECTOR PROBABILISTIC SIESMIC HAZARD: BACK GROUND AND METHODOLOGY

In this Appendix a more detailed summary of the development of PSHA and VPSHA for direct and indirect approaches using integration notations is provided.

A.1 BACKGROUND ON PSHA

The main goal of performance based earthquake engineering (PBEE) is to assess or/and design the behavior of a structure within a given reliability level accounting for the seismic hazard of the site. The first topic that should be addressed in order to be able to predict the performance of a structure is the definition of the ground motion intensity level. Given the high uncertainty of the seismic hazard due to the uncertainty of the location (e.g. location of the epicenter, extension of fault rupture), size (magnitude) and resulting intensity of a future earthquake, Probabilistic Seismic Hazard Analysis (PSHA) was developed [Cornell, 1968; Kramer, 1996; 1995] as an analytical tool that can probabilistically characterize the seismic hazard of a region. The theoretical framework of PSHA was first developed with the objective of providing Mean Annual Rate (MAR) of *exceedance* of ground motion parameters, such as spectral acceleration, S_a.

PSHA integrates, according to the Total Probability Theorem (TPT), the contributions of all possible seismic sources and for each of them, all possible values of earthquake magnitude and source-to-site distance as:

$$\mathrm{MRE}_{Sa}(x) = \sum_{i=1}^{N} \nu_i \cdot \left\{ \iint \hat{\Phi}(x \mid m, r) \cdot \mathrm{f}_{M,R}(m, r)\, \mathrm{dmdr} \right\}_i \tag{A.1}$$

where:

- MRE(x) is the Mean Rate of the Exceedance of the ground motion parameter;
- N is the total number of faults;
- ν_i is the mean rate of occurrence of the earthquakes on fault *i* above a lower bound;
- $f_{M,R}(m,r)$ is the joint probability density function (pdf) of magnitude and distance, M, and source to site distance, R.
- The first term in the integrand, given the widely tested lognormality of the distribution of S_a, given $M=m$ and $R=r$, is the complementary standard Gaussian cumulative distribution function (cdf):

$$\hat{\Phi}(x \mid m,r) = 1 - \Phi_{Sa}\left(\frac{\ln x - m_{\ln Sa|m,r}}{\sigma_{\ln Sa|m,r}}\right) \tag{A.2}$$

Where Φ_{Sa} is the *standard Gaussian* cumulative distribution function (cdf) and $m_{\ln Sa|m,r}$ and $\sigma_{\ln Sa|m,r}$ are the conditional mean and standard deviation of (the natural logarithm of) S_a provided in any customary GMPE. GMPEs are typically developed by applying statistical regression analyses to data either recorded or derived from recordings. Different GMPEs for various *IM*s have been developed for different parts of the world.

$\mathrm{MRE}_{Sa}(.)$ is the hazard curve of S_a that makes the output of the conventional scalar PSHA. Bazzurro, 1998 defined the Mean Rate Density of Sa (MRD_{S_a}) by differentiation of Equation (A.1):

$$\mathrm{MRD}_{Sa}(x) = \sum_{i=1}^{N} \nu_i \cdot \left\{ \iint \hat{\Phi}(x \mid m,r) \cdot f_{M,R}(m,r)\,\mathrm{dmdr} \right\}_i \tag{A.3}$$

Where:

$$f_{Sa}(x \mid m,r) = \frac{1}{x \cdot \sigma_{\ln Sa|m,r}} \cdot \Phi_{Sa}\left(\frac{\ln x - m_{\ln Sa|m,r}}{\sigma_{\ln Sa|m,r}}\right) \tag{A.4}$$

where:

ϕ_{Sa}, is the standard Gaussian pdf. The mean rate of events at the site with Sa between a_1 and a_2 could then be calculated using the following equation:

$$\lambda_{a_1,a_2} = \int_{a_1}^{a_2} \mathrm{MRD}_{Sa}(x)dx \tag{A.5}$$

A.2 DIRECT APPROACH TO VPSHA BASED ON NUMERICAL INTEGRATION

The PSHA treatment in equation (A.3) uses the mean *rates* rather than the *probability* (equation A.2) of occurrence of events. For scalar PSHA using any of the two will lead to similar results and both of them are used in practice. For direct VPSHA, however, using probability rather than rates, can generate conceptual errors Bazzurro, and Cornell, 2002. The rates of the events in disjoint intervals can be added to obtain the joint rate for that interval but this manner cannot be used for probability values. Hence, the direct integration VPSHA is obtained in terms of rates rather than probability.

A vector of ground motion parameters consists of two or more IMs that could be spectral acceleration in two different periods or other ground motion parameters such as, duration of shaking, amplitude of velocity pulse, spectral displacement, inelastic spectral displacement, etc. Theoretically, VPSHA could be applied for a vector for all above-mentioned GM parameters; however, it is necessary to have a proper GMPE and the correlation matrix of all these parameters. The most common used parameter with available GMPE and correlation matrix is spectral acceleration which is used herein this context.

For a 2-Dimensional case of spectral accelerations, the mean rate density ($\mathrm{MRD}_{s_{a1},\, s_{a2}}$) at periods T_1 and T_2 is given by [Bazzurro, 1998]:

$$\mathrm{MRD}_{Sa}(x_1,x_2) = \sum_{i=1}^{N} v_i \cdot \left\{ \mathrm{f}_{Sa1,Sa2}(x_1,x_2 \mid m,r)\,\mathrm{f}_{M,R}(m,r)\,\mathrm{d}m\,\mathrm{d}r \right\}_i \tag{A.6}$$

The joint pdf of S_{a1}, S_{a2} conditional on M=m and R=r can be written in conditional form as follows:

$$\mathrm{f}_{Sa1,Sa2}(x_1,x_2 \mid m,r) = \mathrm{f}_{Sa1,Sa2}(x_1 \mid m,r) \cdot \mathrm{f}_{Sa2}\,|_{Sa1}\,(x_2 \mid x_1,m,r) \tag{A.7}$$

The first term in equation (A.7) is as given in scalar PSHA (equation A.4). The second term is the joint pdf of $S_{a1}=x_1$ conditional on $S_{a2}=x_2$ and $M=m$ and $R=r$. With the assumption that the joint distribution is jointly and marginally lognormal, we can write:

$$\mathrm{f}_{Sa}(x_2 \mid x_1,m,r) = \frac{1}{x_2 \cdot \sigma_{\ln Sa_2|x_1,m,r}} \cdot \Phi_{Sa}\left(\frac{\ln x_2 - \mathrm{m}_{\ln Sa_2|x_1,m,r}}{\sigma_{Sa_2|x_1,m,r}} \right) \tag{A.8}$$

The mean and standard deviation of the conditional distribution are:

$$m_{\ln Sa_2|x_1,m,r} = m_{\ln Sa_2|x_1,m,r} + \rho_{1,2} \cdot \frac{\sigma_{Sa_2|m,r}}{\sigma_{Sa_1|m,r}} \cdot \left(\ln x_1 - m_{\ln Sa_1|m,r}\right) \tag{A.9}$$

$$\sigma_{\ln Sa_2|x_1,m,r} = \sigma_{\ln Sa_2|x_1,m,r} \cdot \sqrt{1-\rho_{1,2}^2} \tag{A.10}$$

$m_{lnSa_2|m,r}$ and $\sigma_{lnSa_2|m,r}$ are obtained from GMPEs. $\rho_{1,2}$ is the coefficient of correlation being obtained from expressions presented in [Baker and Jayaram, 2008] . The two complementary cdf's of the marginal mean rates of S_{a1}, S_{a2} should coincide with the two corresponding conventional hazard curves from the scalar PSHA. The mean rate of events at the site with S_{a1} between $a_{1,1}$ and $a_{1,2}$ and S_{a2} between $a_{2,1}$ and $a_{2,2}$ is found by integrating equation (A.10):

$$\lambda_{Sa_1} \in [a_{1,1}, a_{1,2}]; \mathrm{Sa} \in [a_{2,1}, a_{2,2}] = \int_{a_{1,1}}^{a_{1,2}} \int_{a_{2,1}}^{a_{2,2}} MRD_{Sa_1,Sa_2}(x_1, x_2)\, \mathrm{d}x_1\, \mathrm{d}x_2 \tag{A.11}$$

The procedure above could be extended for more than two variables by replacing the full covariance matrix and use of multi-variate normal distribution theorem.

A.3 INDIRECT APPROACH TO VPSHA

The *indirect* approach explained in this section makes use of the procedure presented in [Bazzurro *et al.*, 2009, 2011] and extends them such that it may be used in conjunction with OpenQuake scalar PSHA results. The main novelty in the work presented herein is that the approach for VPSHA makes use of the OpenQuake probabilistic results, namely the seismic curve providing the mean annual rate of exceedance of a given spectral acceleration. This approach is based on the knowledge of the following three inputs:

- *Site-specific seismic hazard curves for all the ground motion IMs considered*
- *The variance-covariance matrix of all the ground motion IMs*
- *The disaggregation results from scalar PSHA*

The methodology here is first explained for a vector of two spectral accelerations and then it is extended to a vector of *n* variables.

A.4 INDIRECT APPROACH—TWO DIMENSIONAL

The *Mean Annual Rate* of S_{a1}, S_{a2} in neighborhood of x_1 and x_2 can be derived as follows:

$$\mathrm{MAR}_{Sa_1,Sa_2}[x_1,x_2]=\mathrm{P}_{Sa_2|Sa_1}[x_2\mid x_1].\mathrm{MAR}_{Sa_1}[x_1] \tag{A.12}$$

$MAR_{S_{a1}}[x_1]$ is the Mean Annual Rate of spectral acceleration (S_{a1}) *"equaling"* with value x_1 which is given by the scalar PSHA. The first term in equation A.12, could be computed as follows:

$$\begin{aligned}
\mathrm{P}_{Sa_2|Sa_1}[x_2\mid x_1] &= \int_{x_2-\Delta x_2/2}^{x_2-\Delta x_2/2} \mathrm{f}_{Sa_2|Sa_1}(x_2\mid x_1)\,\mathrm{d}x_2 \\
&= \int_{x_2-\Delta x_2/2}^{x_2-\Delta x_2/2}\left(\iint \mathrm{f}_{Sa_2|Sa_1,M,R}(x_2\mid x_1,m,r)\cdot \mathrm{f}_{M,R|Sa_1}(m,r\mid x_1)\,\mathrm{d}m\,\mathrm{d}r\right)\mathrm{d}x_2 \\
&= \iint \int_{x_2-\Delta x_2/2}^{x_2-\Delta x_2/2}\left(\iint \mathrm{f}_{Sa_2|Sa_1,M,R}(x_2\mid x_1,m,r)\,\mathrm{d}x_2\cdot \mathrm{f}_{M,R|Sa_1}(m,r\mid x_1)\,\mathrm{d}m\,\mathrm{d}r\right) \\
&= \iint \mathrm{P}_{Sa_2|Sa_1,M,R}[x_2\mid x_1,m,r]\cdot \mathrm{P}_{M,R|Sa_1}[m,r\mid x_1]\,\mathrm{d}m\,\mathrm{d}r
\end{aligned} \tag{A.13}$$

The first term is calculated as:

$$\begin{aligned}
&\mathrm{P}_{Sa_2|Sa_1}[x_2\mid x_1,m,r]= \\
&\mathrm{P}[Sa_2\geq x_2-\Delta x_2/2\mid x_1,m,r]-\mathrm{P}[Sa_2\geq x_2+\Delta x_2/2\mid x_1,m,r] \\
&=\left[1-\Phi\left(\frac{\ln\left(x_2-\Delta x_2/2\right)-m_{\ln Sa_2|x_1,m,r}}{\sigma_{\ln Sa_2|x_1,m,r}}\right)\right]- \\
&\left[1-\Phi\left(\frac{\ln\left(x_2+\Delta x_2/2\right)-m_{\ln Sa_2|x_1,m,r}}{\sigma_{\ln Sa_2|x_1,m,r}}\right)\right] \\
&=\Phi\left(\frac{\ln\left(x_2+\Delta x_2/2\right)-m_{\ln Sa_2|x_1,m,r}}{\sigma_{\ln Sa_2|x_1,m,r}}\right)- \\
&\Phi\left(\frac{\ln\left(x_2-\Delta x_2/2\right)-m_{\ln Sa_2|x_1,m,r}}{\sigma_{\ln Sa_2|x_1,m,r}}\right)
\end{aligned} \tag{A.14}$$

Where: Δx_2, is the bin interval considered for the numerical integration on x_2. $\Phi(.)$ corresponds to the standard normal CDF of the argument and $m_{lnSa_2|x_1,m,r}$ and $\sigma_{lnSa_2|x_1,m,r}$ correspond to the conditional mean and conditional standard deviation defining the conditional PDF of Sa_2 given Sa_1, m and r, similar to equations A.9, A.10.

The second term in equation (A.13) is the disaggregation of $S_{a1} = x_1$ for in the corresponding magnitude and distance. It should be noted that OpenQuake can provide the results (upon request), in the form of joint probability of $MAR_{S_{a1}}(S_{a1} \geq x_1, M, R)$. The disaggregation, therefore, for $S_{a1} = x_1$ given *M* and *R* can be calculated as follows:

$$\mathrm{P}_{M,\mathrm{R}|Sa_1[m,r|x_1]} = \frac{\mathrm{MAR}_{Sa_1}\left(Sa_1 \geq x_1 - \Delta x_1 / 2, M, \mathrm{R}\right) - \mathrm{MAR}_{Sa_1}\left(Sa_1 \geq x_1 + \Delta x_1 / 2, M, \mathrm{R}\right)}{\sum_M \sum_\mathrm{R}\left[\mathrm{MAR}_{Sa_1}\left(Sa_1 \geq x_1 - \Delta x_1 / 2, M, \mathrm{R}\right) - \mathrm{MAR}_{Sa_1}\left(Sa_1 \geq x_1 + \Delta x_1 / 2, M, \mathrm{R}\right)\right]} \quad \text{(A.15)}$$

A.5 INDIRECT APPROACH—N DIMENSIONAL VPSHA

The equations presented in the previous section (2-D) could be extended for a vector of with n parameters. For a vector of Ground Motion including *'n'* spectral accelerations at *n* different periods, the joint probability $\mathrm{MAR}_{S_{a1},\ldots,S_{an}}[x_1, \ldots, x_n]$ is calculated as follows:

$$\mathrm{MAR}_{Sa_1,\ldots,Sa_n}[x_1,\ldots,x_n] = \mathrm{P}_{Sa_n|Sa_{n-1},\ldots,Sa_1}[x_n \mid x_{n-1,\ldots,x_1}] \ldots \mathrm{MAR}_{Sa_1}[x_1] \quad \text{(A.16)}$$

The last term of equation (A.16), comes from scalar PSHA. In a similar manner showed in equation (A.13), other terms of equation (A.16) could be defined using the following expressions, here for brevity only the first term is presented:

$$\begin{aligned}&\mathrm{P}_{Sa_n|Sa_{n-1},\ldots,Sa_1}[x_n \mid x_{n-1,\ldots,x_1}] = \\ &\mathrm{P}_{Sa_n|Sa_{n-1},\ldots,Sa_1}[x_n \mid x_{n-1,\ldots,x_1}, m, r] \cdot \mathrm{P}_{M,\mathrm{R}|Sa_{n-1},\ldots,Sa_1}[m, r \mid x_{n-1,\ldots,x_1}]\end{aligned} \quad \text{(A.17)}$$

The first term of equation (A.17), could be determined as follows, under the assumption of joint log-normality between the spectral accelerations:

$$\begin{aligned}&\mathrm{P}_{Sa_n|Sa_{n-1},\ldots,Sa_1}[x_n \mid x_{n-1},\ldots,x_1,m,r] = \\ &= \Phi\left(\frac{\ln\left(x_n + \Delta x_n / 2\right) - m_{\ln Sa_n|x_{n-1},m,r}}{\sigma_{\ln Sa_n|x_{n-1}\ldots x_1,m,r}}\right) - \\ &\Phi\left(\frac{\ln\left(x_n - \Delta x_n / 2\right) - m_{\ln Sa_n|x_{n-1},m,r}}{\sigma_{\ln Sa_n|x_{n-1}\ldots x_1,m,r}}\right)\end{aligned} \quad \text{(A.18)}$$

where the conditional mean and conditional standard deviations can be computed assuming joint log-normality between the spectral accelerations and making use of the theorem of multivariate normal distributions.

$$m_{\ln Sa_n|x_{n-1}\ldots x_1,m,r} = m_{x_2} + \mathbf{\Sigma}_{21}\mathbf{\Sigma}_{11}^{-1}(\mathbf{x} - m_{x_1}) \tag{A.19}$$

$$\sigma_{\ln Sa_n|x_{n-1}\ldots x_1,m,r} = \mathbf{\Sigma}_{22} - \mathbf{\Sigma}_{21}\mathbf{\Sigma}_{11}^{-1}\mathbf{\Sigma}_{12} \tag{A.20}$$

where: **X** is a random vector of the natural logarithm of the spectral accelerations given ***M*** and ***R*** (obtained using a GMPE) that can be partitioned into: (*letters in bold show vectors*).

$$\begin{aligned}
&\mathbf{X} = \left\{\mathbf{X}_1^{\mathrm{T}};\mathbf{X}_2^{\mathrm{T}}\right\}^{T} \\
&\mathbf{X}_1 = \left\{(\ln Sa_1 \mid m,r),\ldots,(\ln Sa_{n-1} \mid m,r)\right\}^{\mathrm{T}}, \mathbf{X}_2 = \left\{\ln Sa_n \mid m,r\right\} \\
&m_{x_1} = \left\{m_{\ln sa_1|m,r},\ldots,m_{\ln sa_{n-1}|m,r}\right\}^{\mathrm{T}}, m_{x_2} = m_{\ln sa_n|m,r}
\end{aligned} \tag{A.21}$$

And ∑ is the varriance-covarriance matrix of the spectral accelerations:

$$\Sigma = \begin{bmatrix} \mathbf{\Sigma}_{11} & \mathbf{\Sigma}_{12} \\ \mathbf{\Sigma}_{21} & \mathbf{\Sigma}_{22} \end{bmatrix} \tag{A.22}$$

The second term of equation (A.17) corresponds to the *M-R* disaggregation for the joint hazard. The expression for the disaggregation of the joint hazard of the vector-***IM*** of size *n* is given by:

$$\mathrm{P}[M,\mathrm{R} \mid Sa_1 = x_1,\ldots,x_n] = \frac{An}{Bn} = \frac{\mathrm{P}[Sa_1 = x_1,\ldots,x_n,M,\mathrm{R}]}{\mathrm{P}[Sa_1 = x_1]} \tag{A.23}$$

In which:

$$\begin{aligned}
&An = \left(\prod_{i=1}^{n-1}\mathrm{P}\left[Sa_{n+1-i} = x_{q+1-i} \mid x_1,\ldots,x_{n-i},M,\mathrm{R}\right]\right).\mathrm{P}[\mathrm{M},\mathrm{R} \mid x_1] \\
&\mathrm{Bn} = \sum_{M}\sum_{R} An
\end{aligned} \tag{A.24}$$

Appendix B: COMPUTATION OF CORRELATION COEFFICIENTS

In this Appendix, the equations for computation of the correlation coefficients used in hazard and Conditional Spectra for different ground motion metrics are demonstrated.

The correlation coefficient between two parameters of X and Y could be obtained based on the following equation.

$$\rho_{X,Y} = \frac{C.o.V(\mathrm{X,Y})}{\sigma_X \cdot \sigma_Y} = \frac{E(\mathrm{X \cdot Y}) - \mathrm{E(X) \cdot E(Y)}}{\sigma_X \cdot \sigma_Y}, \tag{B.1}$$

By re-arranging Equation (B.1), we could also compute the E(X·Y) in terms of the correlation coefficient and standard deviation of X and Y, as is shown in Equation (B.2)

$$E(\mathrm{X \cdot Y}) = \rho_{X,Y} \cdot \sigma_X \cdot \sigma_Y + \mathrm{E(X) \cdot E(Y)} \tag{B.2}$$

These two equations are the base for all the calculations followed here.

B.1 CORRELATION COEFFICIENT BETWEEN SPECTRAL ACCELERATION RATIOS

$$X = \ln[\mathrm{Sa(T_1)}], \mathrm{E(X)} = \mu_X = \mu_{\mathrm{n[Sa(T_1)]}}, \sigma_X = \sigma_{\mathrm{ln[Sa(T_1)]}}, \tag{B.3}$$

$$\begin{aligned} &Y = \ln\left[\frac{\mathrm{Sa(T_3)}}{\mathrm{Sa(T_2)}}\right], \\ &\mathrm{E(Y)} = \mu_Y = \mu_{\ln[\mathrm{Sa(T_3)}]} - \mu_{\ln[\mathrm{Sa(T2)}]}, \\ &\sigma_Y = \sigma^2_{\ln[\mathrm{Sa(T_3)}]} + \sigma^2_{\ln[\mathrm{Sa(T2)}]} - 2 \cdot \rho_{\ln[\mathrm{Sa(T_3)}],\ln[\mathrm{Sa(T_2)}]} \cdot \sigma_{\ln[\mathrm{Sa(T_2)}]} \cdot \sigma_{\ln[\mathrm{Sa(T_3)}]} \end{aligned} \tag{B.4}$$

Using Equation (B.2), the following Equation which is the expected value of the product of X and Y, defined above.

$$
\begin{aligned}
&E(\mathrm{X}\cdot\mathrm{Y}) = \\
&\mathrm{E}\left(\ln\left[\mathrm{Sa}(\mathrm{T}_1)\right]\cdot\ln\left[\frac{\mathrm{Sa}(\mathrm{T}_3)}{\mathrm{Sa}(\mathrm{T}_2)}\right]\right) = \mathrm{E}\left(\ln\left[\mathrm{Sa}(\mathrm{T}_1)\right]\cdot\ln\left[\mathrm{Sa}(\mathrm{T}_3)\right] - \ln\left[\mathrm{Sa}(\mathrm{T}_1)\right]\cdot\ln\left[\mathrm{Sa}(\mathrm{T}_2)\right]\right) = \\
&\mathrm{E}\left(\ln\left[\mathrm{Sa}(\mathrm{T}_1)\right]\cdot\ln\left[\mathrm{Sa}(\mathrm{T}_3)\right]\right) - E\left(\ln\left[\mathrm{Sa}(\mathrm{T}_1)\right]\cdot\ln\left[\mathrm{Sa}(\mathrm{T}_2)\right]\right) = \\
&\rho_{\ln[\mathrm{Sa}(\mathrm{T}_1)],\ln[\mathrm{Sa}(\mathrm{T}_3)]}\cdot\sigma_{\ln[\mathrm{Sa}(\mathrm{T}_1)]}\cdot\sigma_{\ln[\mathrm{Sa}(\mathrm{T}_3)]} + \mu_{\ln[\mathrm{Sa}(\mathrm{T}_1)]}\cdot\mu_{\ln[\mathrm{Sa}(\mathrm{T}_3)]} - \\
&\left(\rho_{\ln[\mathrm{Sa}(\mathrm{T}_1)],\ln[\mathrm{Sa}(\mathrm{T}_2)]}\cdot\sigma_{\ln[\mathrm{Sa}(\mathrm{T}_1)]}\cdot\sigma_{\ln[\mathrm{Sa}(\mathrm{T}_2)]} + \mu_{\ln[\mathrm{Sa}(\mathrm{T}_1)]}\cdot\mu_{\ln[\mathrm{Sa}(\mathrm{T}_2)]}\right)
\end{aligned}
\qquad (B.5)
$$

By substituting equations (B.3), (B.4) and (B.5) in (B.2) and simplification we have:

$$
\rho_{\ln[\mathrm{Sa}(\mathrm{T}_1)],\ln\left[\frac{\mathrm{Sa}(\mathrm{T}_3)}{\mathrm{Sa}(\mathrm{T}_2)}\right]} = \frac{\rho_{\ln[\mathrm{Sa}(\mathrm{T}_1)],\ln[\mathrm{Sa}(\mathrm{T}_3)]}\cdot\sigma_{\ln[\mathrm{Sa}(\mathrm{T}_3)]} - \rho_{\ln[\mathrm{Sa}(\mathrm{T}_1)],\ln[\mathrm{Sa}(\mathrm{T}_2)]}\cdot\sigma_{\ln[\mathrm{Sa}(\mathrm{T}_2)]}}{\sqrt{\sigma^2_{\ln[\mathrm{Sa}(\mathrm{T}_3)]} + \sigma^2_{\ln[\mathrm{Sa}(\mathrm{T}2)]} - 2\cdot\rho_{\ln[\mathrm{Sa}(\mathrm{T}_3)],\ln[\mathrm{Sa}(\mathrm{T}_2)]}\cdot\sigma_{\ln[\mathrm{Sa}(\mathrm{T}_2)]}\cdot\sigma_{\ln[\mathrm{Sa}(\mathrm{T}_3)]}}} \qquad (B.6)
$$

B.2 CORRELATION COEFFICIENT BETWEEN SPECTRAL ACCELERATION RATIOS

$$
\begin{aligned}
&X = \ln\left[\frac{\mathrm{Sa}(\mathrm{T}_2)}{\mathrm{Sa}(\mathrm{T}_1)}\right], \\
&\mathrm{E}(X) = \mu_X = \mu_{\ln[\mathrm{Sa}(\mathrm{T}_2)]} - \mu_{\ln[\mathrm{Sa}(\mathrm{T}_1)]}, \\
&\sigma_X = \sigma^2_{\ln[\mathrm{Sa}(\mathrm{T}_1)]} + \sigma^2_{\ln[\mathrm{Sa}(\mathrm{T}2)]} - 2\cdot\rho_{\ln[\mathrm{Sa}(\mathrm{T}_1)],\ln[\mathrm{Sa}(\mathrm{T}_2)]}\cdot\sigma_{\ln[\mathrm{Sa}(\mathrm{T}_1)]}\cdot\sigma_{\ln[\mathrm{Sa}(\mathrm{T}_2)]}
\end{aligned}
\qquad (B.7)
$$

$$
\begin{aligned}
&Y = \ln\left[\frac{\mathrm{Sa}(\mathrm{T}_4)}{\mathrm{Sa}(\mathrm{T}_3)}\right], \\
&\mathrm{E}(\mathrm{Y}) = \mu_Y = \mu_{\ln[\mathrm{Sa}(\mathrm{T}_4)]} - \mu_{\ln[\mathrm{Sa}(\mathrm{T}_3)]}, \\
&\sigma_Y = \sigma^2_{\ln[\mathrm{Sa}(\mathrm{T}_3)]} + \sigma^2_{\ln[\mathrm{Sa}(\mathrm{T}_4)]} - 2\cdot\rho_{\ln[\mathrm{Sa}(\mathrm{T}_3)],\ln[\mathrm{Sa}(\mathrm{T}_4)]}\cdot\sigma_{\ln[\mathrm{Sa}(\mathrm{T}_3)]}\cdot\sigma_{\ln[\mathrm{Sa}(\mathrm{T}_4)]}
\end{aligned}
\qquad (B.8)
$$

$$
\begin{aligned}
&E(\mathrm{X}\cdot\mathrm{Y}) = \\
&\mathrm{E}\left(\ln\left[\frac{\mathrm{Sa}(\mathrm{T}_2)}{\mathrm{Sa}(\mathrm{T}_1)}\right]\cdot\ln\left[\frac{\mathrm{Sa}(\mathrm{T}_4)}{\mathrm{Sa}(\mathrm{T}_3)}\right]\right) = \\
&\mathrm{E}\left(\ln\left[\mathrm{Sa}(\mathrm{T}_2)\right]\cdot\ln\left[\mathrm{Sa}(\mathrm{T}_4)\right]\right) - E\left(\ln\left[\mathrm{Sa}(\mathrm{T}_2)\right]\cdot\ln\left[\mathrm{Sa}(\mathrm{T}_3)\right]\right) - \\
&\mathrm{E}\left(\ln\left[\mathrm{Sa}(\mathrm{T}_1)\right]\cdot\ln\left[\mathrm{Sa}(\mathrm{T}_4)\right]\right) + E\left(\ln\left[\mathrm{Sa}(\mathrm{T}_1)\right]\cdot\ln\left[\mathrm{Sa}(\mathrm{T}_3)\right]\right) = \\
&\rho_{\ln[\mathrm{Sa}(\mathrm{T}_2)],\ln[\mathrm{Sa}(\mathrm{T}_4)]}\cdot\sigma_{\ln[\mathrm{Sa}(\mathrm{T}_2)]}\cdot\sigma_{\ln[\mathrm{Sa}(\mathrm{T}_4)]} + \mu_{\ln[\mathrm{Sa}(\mathrm{T}_2)]}\cdot\mu_{\ln[\mathrm{Sa}(\mathrm{T}_4)]} - \\
&\left(\rho_{\ln[\mathrm{Sa}(\mathrm{T}_2)],\ln[\mathrm{Sa}(\mathrm{T}_3)]}\cdot\sigma_{\ln[\mathrm{Sa}(\mathrm{T}_2)]}\cdot\sigma_{\ln[\mathrm{Sa}(\mathrm{T}_3)]} + \mu_{\ln[\mathrm{Sa}(\mathrm{T}_2)]}\cdot\mu_{\ln[\mathrm{Sa}(\mathrm{T}_3)]}\right) - \\
&\left(\rho_{\ln[\mathrm{Sa}(\mathrm{T}_1)],\ln[\mathrm{Sa}(\mathrm{T}_4)]}\cdot\sigma_{\ln[\mathrm{Sa}(\mathrm{T}_1)]}\cdot\sigma_{\ln[\mathrm{Sa}(\mathrm{T}_4)]} + \mu_{\ln[\mathrm{Sa}(\mathrm{T}_1)]}\cdot\mu_{\ln[\mathrm{Sa}(\mathrm{T}_4)]}\right) + \\
&\left(\rho_{\ln[\mathrm{Sa}(\mathrm{T}_1)],\ln[\mathrm{Sa}(\mathrm{T}_3)]}\cdot\sigma_{\ln[\mathrm{Sa}(\mathrm{T}_1)]}\cdot\sigma_{\ln[\mathrm{Sa}(\mathrm{T}_3)]} + \mu_{\ln[\mathrm{Sa}(\mathrm{T}_1)]}\cdot\mu_{\ln[\mathrm{Sa}(\mathrm{T}_3)]}\right)
\end{aligned}
\tag{B.9)}
$$

By substituting equations (B.7), (B.8) and (B.9) in (B.1) and simplification we have:

$$
\rho_{2/1,4/3} = \frac{\rho_{1,3}\cdot\sigma_1\cdot\sigma_3 + \rho_{2,4}\cdot\sigma_2\cdot\sigma_4 - \rho_{1,4}\cdot\sigma_1\cdot\sigma_4 - \rho_{2,3}\cdot\sigma_2\cdot\sigma_3}{\sigma_{2/1}\cdot\sigma_{4/3}} \tag{B.10}
$$

in which $\rho_{i,j}$ is the correlation coefficient between $Sa(\mathrm{T}_i)$ and $Sa(\mathrm{T}_j)$, $\sigma_{i/j}$ is $\sigma_{\ln\left[Sa(\mathrm{T}_i)/Sa(\mathrm{T}_j)\right]}$, the dispersion of the spectral acceleration ratio.

B.3 CORRELATION COEFFICIENT BETWEEN *AVGSA* AND *AVGSA*

$$
\begin{aligned}
&X = \ln(AvgSA_X) = \ln\left(\left[\prod_{i=1}^{n} SA(\mathrm{T}_i)\right]^{1/n}\right) \\
&E(X) = \left(\frac{1}{n}\right)\cdot\sum_{i=1}^{n}\mu_{\ln(\mathrm{SA}(\mathrm{T}_i))} \\
&\mathrm{var}(X) = \left(\frac{1}{n}\right)^2\cdot\sum_{i=1}^{n}\sum_{j=1}^{n}\rho_{\ln SA(\mathrm{T}_i),\ln \mathrm{SA}(\mathrm{T}_j)}\cdot\sigma_{\ln SA(\mathrm{T}_i)}\cdot\sigma_{\ln SA(\mathrm{T}_j)}
\end{aligned}
\tag{B.11}
$$

$$Y = \ln(AvgSA_Y) = \ln\left(\left[\prod_{j=1}^{m} SA(\mathrm{T}_i)\right]^{1/\mathrm{m}}\right)$$

$$E(\mathrm{Y}) = \left(\frac{1}{n}\right)\cdot\sum_{j=1}^{m}\mu_{\ln(\mathrm{SA}(\mathrm{T}_j))}$$ B.12)

$$\mathrm{var}(Y) = \left(\frac{1}{m}\right)^2\cdot\sum_{i=1}^{n}\sum_{j=1}^{n}\rho_{\ln SA(\mathrm{T}_i),\ln\mathrm{SA}(\mathrm{T}_j)}\cdot\sigma_{\ln SA(\mathrm{T}_i)}\cdot\sigma_{\ln SA(\mathrm{T}_j)}$$

$$E(\mathrm{X}\cdot\mathrm{Y}) =$$

$$\mathrm{E}\left(\ln\left(\left[\prod_{i=1}^{n} SA(\mathrm{T}_i)\right]^{1/\mathrm{n}}\right)\cdot\ln\left(\left[\prod_{j=1}^{m} SA(\mathrm{T}_j)\right]^{1/\mathrm{m}}\right)\right) =$$ B.13)

$$\left(\frac{1}{m\cdot n}\right)\cdot E\left(\sum_{i=1}^{n}\sum_{j=1}^{m}\ln\left(SA(\mathrm{T}_i)\right)\cdot\ln\left(SA(\mathrm{T}_j)\right)\right) =$$

$$\left(\frac{1}{m\cdot n}\right)\cdot\sum_{i=1}^{n}\sum_{j=1}^{m}\left(\rho_{\ln\left(SA(\mathrm{T}_i)\right),\ln\left(SA(\mathrm{T}_j)\right)}\cdot\sigma_{\ln\left(SA(\mathrm{T}_i)\right)}\cdot\sigma_{\ln\left(SA(\mathrm{T}_j)\right)}+\mu_{\ln\left(SA(\mathrm{T}_i)\right)}\cdot\mu_{\ln\left(SA(\mathrm{T}_j)\right)}\right)$$

By substituting equations (B.11), (B.12) and (B.13) in (B.1) and simplification we have:

$$\rho_{\ln[AvgSA_X],\ln[AvgSA_Y]} = \frac{\sum_{i=1}^{n}\sum_{j=1}^{m}\left(\rho_{\ln\left(SA(\mathrm{T}_i)\right),\ln\left(SA(\mathrm{T}_j)\right)}\cdot\sigma_{\ln\left(SA(\mathrm{T}_i)\right)}\cdot\sigma_{\ln\left(SA(\mathrm{T}_j)\right)}\right)}{m\cdot n\cdot\sqrt{\mathrm{var}(\mathrm{X})\cdot\mathrm{var}(\mathrm{Y})}}$$ (B.14)

B.4 CORREKATION COEFFICIENT BETWEEN *AVGSA* AND *SA*

$$X = \ln\left(SA(\mathrm{T}^*)\right), E(X) = \mu_{\ln\left(SA(\mathrm{T}^*)\right)}, \sigma_X = \sigma_{\ln\left(SA(\mathrm{T}^*)\right)} \tag{B.15}$$

$$\begin{aligned} Y &= \ln(AvgSA_Y) = \ln\left(\left[\prod_{j=1}^{m} SA(\mathrm{T}_i)\right]^{1/\mathrm{m}}\right) \\ E(\mathrm{Y}) &= \left(\frac{1}{n}\right)\cdot\sum_{j=1}^{m}\mu_{\ln(\mathrm{SA}(\mathrm{T}_j))} \\ \mathrm{var}(Y) &= \left(\frac{1}{m}\right)^2\cdot\sum_{i=1}^{n}\sum_{j=1}^{n}\rho_{\ln SA(\mathrm{T}_i),\ln\mathrm{SA}(\mathrm{T}_j)}\cdot\sigma_{\ln SA(\mathrm{T}_i)}\cdot\sigma_{\ln SA(\mathrm{T}_j)} \end{aligned} \tag{B.16}$$

$$\begin{aligned} &E(\mathrm{X}\cdot\mathrm{Y}) = \\ &\mathrm{E}\left(\ln\left(SA(\mathrm{T}^*)\right)\cdot\ln\left(\left[\prod_{j=1}^{m} SA(\mathrm{T}_j)\right]^{1/\mathrm{m}}\right)\right) = \\ &\left(\frac{1}{m}\right)\cdot E\left(\ln\left(SA(\mathrm{T}^*)\right)\cdot\sum_{j=1}^{m}\ln\left(SA(\mathrm{T}_j)\right)\right) = \\ &\left(\frac{1}{m}\right)\cdot\sum_{j=1}^{m}\left(\rho_{\ln\left(SA(\mathrm{T}^*)\right),\ln\left(SA(\mathrm{T}_j)\right)}\cdot\sigma_{\ln\left(SA(\mathrm{T}^*)\right)}\cdot\sigma_{\ln\left(SA(\mathrm{T}_j)\right)}+\mu_{\ln\left(SA(\mathrm{T}^*)\right)}\cdot\mu_{\ln\left(SA(\mathrm{T}_j)\right)}\right) \end{aligned} \tag{B.17}$$

$$\rho_{\ln\left[SA(\mathrm{T}^*)\right],\ln\left[AvgSA_Y\right]} = \frac{\sum_{j=1}^{m}\left(\rho_{\ln\left(SA(\mathrm{T}^*)\right),\ln\left(SA(\mathrm{T}_j)\right)}\cdot\sigma_{\ln\left(SA(\mathrm{T}_j)\right)}\right)}{m\cdot\sqrt{\mathrm{var}(\mathrm{Y})}} \tag{B.18}$$

B.5 CORRELATION COEFFICIENT BETWEEN I_{NP} AND *SA*

$$X = \ln\left(SA(\mathrm{T}^*)\right), E(X) = \mu_{\ln\left(SA(\mathrm{T}^*)\right)}, \sigma_X = \sigma_{\ln\left(SA(\mathrm{T}^*)\right)} \tag{B.19}$$

$$
\begin{aligned}
&Y = \ln(I_{NP}) = \ln\left(SA(\mathrm{T}_1)\right) + \alpha \cdot \ln\left(\frac{AvgSA}{SA(\mathrm{T}_1)}\right) \\
&E(\mathrm{Y}) = \left(1-\alpha\right) \cdot \mu_{\ln\left[SA(\mathrm{T}_1)\right]} + \alpha \cdot \mu_{\ln\left[AvgSA\right]} \\
&\mathrm{var}(Y) = \alpha^2 \cdot \sigma^2_{\ln\left[AvgSA\right]} + \left(1-\alpha\right)^2 \cdot \sigma^2_{\ln\left[SA(\mathrm{T}_1)\right]} + \\
&2 \cdot \alpha \cdot (1-\alpha) \cdot \rho_{\ln\left[AvgSA\right],\ln\left[SA(\mathrm{T}_1)\right]} \cdot \sigma_{\ln\left[AvgSA\right]} \cdot \sigma_{\mathrm{n}\left[SA(\mathrm{T}_1)\right]}
\end{aligned}
\tag{B.20}
$$

$$
\begin{aligned}
&E(\mathrm{X} \cdot \mathrm{Y}) = \\
&\mathrm{E}\left(\ln\left(SA(\mathrm{T}^*)\right) \cdot \left(\left(1-\alpha\right) \cdot \mu_{\ln\left[SA(\mathrm{T}_1)\right]} + \alpha \cdot \mu_{\ln\left[AvgSA\right]}\right)\right) = \\
&E\left(\ln\left(SA(\mathrm{T}^*)\right) \cdot \ln\left(SA(\mathrm{T}_1)\right) + \alpha \cdot \ln\left(SA(\mathrm{T}^*)\right) \cdot \ln\left(AvgSA\right) - \alpha \cdot \ln\left(SA(\mathrm{T}^*)\right) \cdot \ln\left(SA(\mathrm{T}_1)\right)\right) = \\
&\rho_{\ln\left(SA(\mathrm{T}^*)\right),\ln\left(SA(\mathrm{T}_1)\right)} \cdot \sigma_{\ln\left(SA(\mathrm{T}^*)\right)} \cdot \sigma_{\ln\left(SA(\mathrm{T}_1)\right)} + \mu_{\ln\left(SA(\mathrm{T}^*)\right)} \cdot \mu_{\ln\left(SA(\mathrm{T}_1)\right)} + \\
&\alpha \cdot \rho_{\ln\left(SA(\mathrm{T}^*)\right),\ln\left(AvgSA\right)} \cdot \sigma_{\ln\left(SA(\mathrm{T}^*)\right)} \cdot \sigma_{\ln\left(AvgSA\right)} + \alpha \cdot \mu_{\ln\left(SA(\mathrm{T}^*)\right)} \cdot \mu_{\ln\left(AvgSA\right)} - \\
&\alpha \cdot \rho_{\ln\left(SA(\mathrm{T}^*)\right),\ln\left(SA(\mathrm{T}_1)\right)} \cdot \sigma_{\ln\left(SA(\mathrm{T}^*)\right)} \cdot \sigma_{\ln\left(SA(\mathrm{T}_1)\right)} - \alpha \cdot \mu_{\ln\left(SA(\mathrm{T}^*)\right)} \cdot \mu_{\ln\left(SA(\mathrm{T}_1)\right)}
\end{aligned}
\tag{B.21}
$$

$$
\rho_{\ln\left[SA(\mathrm{T}^*)\right],\ln\left[I_{NP}\right]} = \frac{S}{\sqrt{\mathrm{var}(\mathrm{X}) \cdot \mathrm{var}(\mathrm{Y})}}
\tag{B.22}
$$

In which S is obtained from the following equation:

$$
\begin{aligned}
&S = (1-\alpha) \cdot \rho_{\ln\left(SA(\mathrm{T}^*)\right),\ln\left(SA(\mathrm{T}_1)\right)} \cdot \sigma_{\ln\left(SA(\mathrm{T}^*)\right)} \cdot \sigma_{\ln\left(SA(\mathrm{T}_1)\right)} + \\
&\alpha \cdot \rho_{\ln\left(SA(\mathrm{T}^*)\right),\ln\left(AvgSA\right)} \cdot \sigma_{\ln\left(SA(\mathrm{T}^*)\right)} \cdot \sigma_{\ln\left(AvgSA\right)} + \\
&\alpha \cdot \mu_{\ln\left(SA(\mathrm{T}^*)\right)} \cdot \mu_{\ln\left(AvgSA\right)}
\end{aligned}
\tag{B.23}
$$

Appendix C: BUILDING DESCRIPTIONS AND MODELING FOR THE EXAMPLES USED IN CHAPTER 2 , 3 AND 4

C.1 BUILDING EXAMPLE AND MODELING DESCRIPTIONS

Case study buildings

1. ***3 story building (SPEAR):*** The building selected as a case study is the so-called “SPEAR building”, an irregular full-scale 3-storey RC frame structure built and tested within a European research project at JRC-Elsa in 2004. The building is representative of typical old constructions in Southern Europe designed without specific provisions for earthquake resistance. The plan configuration is non-symmetric in X and Y directions, with two bay frames spanning from 3.0 to 6.0 m and a story height of 3.0 m. Almost all columns have a square 0.25x0.25m^2 cross-section; the only one that differs, column C6 in Figure C.1, has a cross-section of 0.25x0.75m^2, which makes it much stiffer. Detailed information on the structure is available in Fardis [2002]. A plan of the building could be seen in Figure C.1.
2. ***5 story building:*** is real existing Turkish reinforced concrete 5 storey building. It experienced the 1999 Golcuk earthquake without any damage. The building is symmetric along the Y axis, and all the floors have the same height of 2.85m. The columns sections keep the same geometrical and reinforcement features along the height of the building. The beam sections are mainly 0.20x0.50m^2 except the two located in the center of the building that are 0.20x0.60m^2. The stirrups have 20cm spacing both for beams and columns. The slabs are 0.10m and 0.12m thick. For more details on the building’s characteristics see [Bal, *et al.,* 2008].

3. ***8 story building***: A real existing Turkish reinforced concrete 8 storey building. It is a plan-irregular structure since it is asymmetric along the X and Y axis). The first storey height is 5.00m and the other floors have the same height of 2.70m. There are also walls and elongated columns, as presented in), with the higher dimension always along the Y direction. For this reason, the structure will be more stiff and resistant along the Y direction. The columns sections and reinforcement keep the same geometrical features along the height of the building, except the column S52 that varies from 1.1x0.3m^2 (on the first floor) to 0.8x0.3m^2 (on the last floor). The height of this section is reduced in 0.1m at every two stories. The beam sections are mainly 0.20x0.50m^2 except the two located in the center of the building along the X direction that are 0.30x0.50m^2 and 0.25x0.50m^2 respectively. The slabs are 0.12m thick. For more details on the building's characteristics see [Bal *et al.,* 2008].

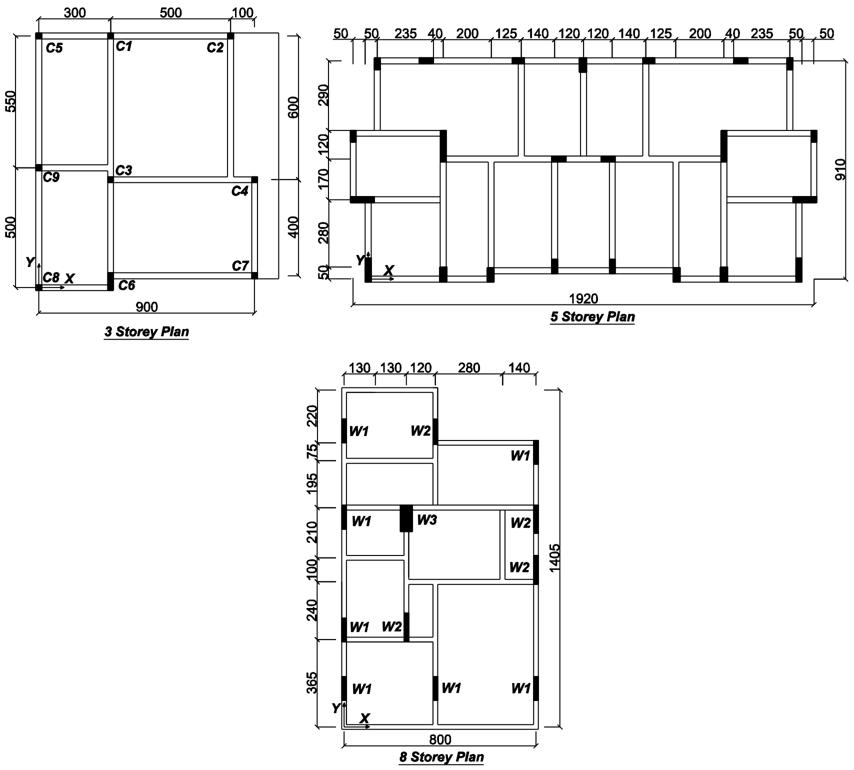

Figure C.1. Plan view of the three considered structures (dimensions in cm)

C.2 STRUCTURAL MODELING

3-D nonlinear models of the building structures were created in OpenSees [McKenna 2000]. In the building model, beams and columns are modeled using force-based nonlinear frame elements [Spacone *et al.*, 1996]. Each element has five Gauss–Lobatto integration points along the element length in order to match the plastic hinge length of the columns with the tributary length of the first integration point [Coleman *et al.*, 2001]. At each integration point, the section is discretized using a fiber model. Concrete behavior is described by material concrete01 Kent-Scott-Park concrete material object with degraded linear unloading/reloading stiffness according to the work of Karsan-Jirsa and no tensile strength while steel behavior is represented by material Steel02 Giuffré-Menegotto-Pinto model with Isotropic Strain Hardening. The cross-sectional response, based on the fiber discretization, is capable of capturing the stiffness degradation and strength deterioration due to concrete cracking, concrete crushing, and steel yielding as well as bar rupture based on the uniaxial material constitutive laws adopted. The fiber cross-section automatically accounts for the interaction between axial force and biaxial bending. Cross-section and element shear and torsional behaviors are assumed linear elastic, uncoupled, and aggregated to the nonlinear inelastic fiber cross-section behavior based on the cracked section shear and torsional stiffness [Miranda *et al.*, 2005]. Thus, the beam-column elements do not account for stiffness degradation and strength deterioration in the shear and torsional behavior of the beams and columns. All material and structural properties are taken at their best deterministic estimates.

Rheological effects, such as volumetric changes caused by creep, shrinkage and temperature have been disregarded in the models. The actual properties of the floor are considered by means of equivalent X-diagonal bracing system that represents the in-plan stiffness of the slab [Mpampatsikos, 2008].

The masonry infill panels were considered based on the model proposed by Kadysiewski and Mosalam [2009]. In this model, the IP strength of the infill panel is modeled by a diagonal strut, following the procedures of FEMA 356 (FEMA 2000). The OOP strength of the URM infill wall is determined based on arching action, the expected OOP capacity of the infill is therefore given using the expected compressive strength of the masonry and the slenderness parameter defined in FEMA356. Except for the consideration of the in-plane and out-of-plane interaction, another important feature of the element is its ability to remove the element representing infill panel that have collapsed during an on-going finite element simulation. The properties of the infill panels were adopted from [Bal *et al.,* 2008] for the Turkish buildings and from [Ali, 2009] for SPEAR.

Rayleigh damping was assumed based on the tangent stiffness matrix of the structure with a 2.5% damping ratio in the initial modes 1 and 3 of each building. Since the hysteretic energy dissipation is already explicitly accounted for at the material level, the damping ratio used is lower than the 5.0% value, commonly suggested for linear analyses. Geometric nonlinearities, namely second-order effects, are taken into account using P-Delta transformations. The floor masses used in the dynamic analyses include all dead loads and 30% of live load according to Eurocode 8. The distributed floor mass was discretized based on tributary areas into lumped masses (of equal values in the X, Y, and Z- directions) assigned to each beam-column joint. The mass of the infill panels are assigned to the central node in the strut in the out-of-plane direction only. The rotatory inertia of the floor diaphragms is automatically accounted for. The dynamic time-history analyses are performed after the model is loaded with the gravity loads during an initial nonlinear static analysis. The constant average acceleration Newmark method was used to integrate the equations of motion. The Newton–Raphson algorithm was used to find convergence of the dynamic equilibrium at each time step.

Appendix D: LITERATURE REVIEW AND MODEL VERIFICATION FOR MASONRY INFILL WALLS

D.1 INTRODUCTION

Since the first attempts to model the structural behavior of infilled frames, a number of analytical models have been developed. These models, based on their complexity and the amount of information they provide about the behaviour of the structure, can be classified as *macro* and *micro* models. Macro or simplified models tend to represent the overall behavior of the structural elements without considering all possible modes of failure. Micro models, on the other hand, describe the structural behaviour of a structural element with details trying to include all possible failure modes. A summary of all representative macro and micro elements for infilled frames is provided in Asteris, 2008. A brief review of the development of most used macro models in literature, which is the focus of this study, is presented in the following section. More detail information about the *macro/micro* elements can be found in Hak, 2010.

D.2 BRIEF REVIEW ON DEVELOPMENT OF MACRO MODELS FOR INFILL PANELS

The first conceptual studies about modelling of infill panels- started in mid 1950s- were based on the opinion that a diagonal strut with appropriate geometrical and mechanical properties could be a solution of the problem. The first suggestions were representing the effect of infill walls as equivalent to diagonal bracing Polyakov, 1960 which was extended later Holmes, 1961 infill by an equivalent pin-joined diagonal strut of the same material having the same thickness as the infill panel with a width equal to one third of the infill diagonal length.

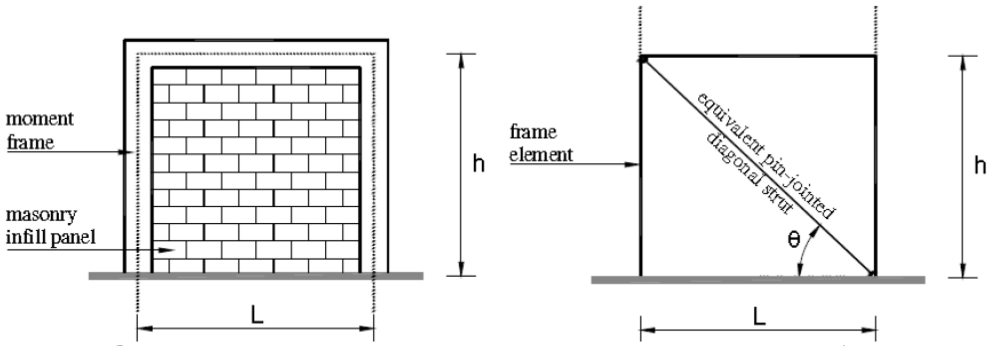

Figure D.1. Equivalent strut model for masonry infill panel in frame structures Asteris, 2008

Stafford Smith, 1966 related the width of the equivalent diagonal strut to the contact length between the frame and the infill by analogy to a beam on elastic foundation and defined a dimensionless relative stiffness parameter to determine the degree of frame infill interaction. Subsequently other developments for the properties of the strut was proposed by other researchers Mainstone, 1971.

Decanini, *et al.* 1993, based on the experimental results, developed a skeleton curve of the lateral force-displacement (V_m-d) relationship (horizontal) for the infilled panel. This envelope curve consists of four branches representing different physical states of the panel (Figure D.2). In this figure, the first branch (path OA) is used to model the linear elastic behavior of the infill in the beginning of the lateral load. The second branch (path AB) represents the post-cracking phase up to the development of the maximum strength (V_{mP}). The point B corresponds to the complete cracking stage of the infill panel. The descending third branch (path BC) describes the post-peak strength deterioration of the infill up to reach the residual strength and displacement, V_{mR} and d_R, respectively (horizontal line after C).

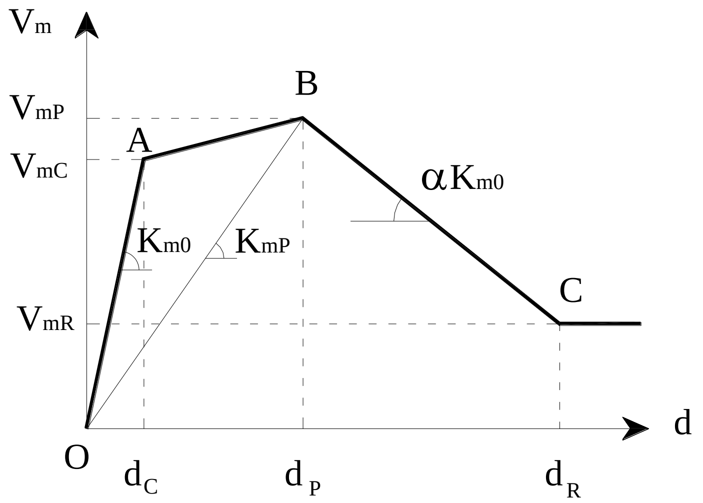

Figure D.2. In-plane lateral force-displacement envelope relationship of the proposed model

Madan, *et al.* 1997 referring to an elastic-perfectly plastic equivalent strut model with parameters expressed as a function of the dimensions of the infilled frame subassemblies, linked the mechanical properties of the component materials and additional empirical parameters depending on the frame-infill interaction Žarnic, 1990. A significant limitation of this type of model was found to be its ineffective account for the force transfer and slip along the frame-panel interface. Mosalam, 1996 established an improved model based on the application of empirically determined correction factors to successfully overcome these problems.

Shing, and Mehrabi 2002 pointed out, the use of strut models is not always adequate, if they account for only one of the possible failure modes. Therefore, limit analysis methods which can account for a variety of potential failure modes are referred to as a more promising approach. Such a model, integrated with a smooth hysteretic curve, has been introduced by Madan, *et al* 1997, and incorporated in a nonlinear structural analysis program *IDARC2D 4.0* for quasi-static cyclic and dynamic analysis of masonry infilled frames. The proposed analytical development assumes that the contribution of the masonry infill panel can be modeled by a system of two diagonal masonry compression struts. The stress-strain relationship for masonry in compression has been idealized by a polynomial function, while the lateral force-deformation relationship for the infill panel has been assumed to be a smooth curve bounded by a bilinear strength.

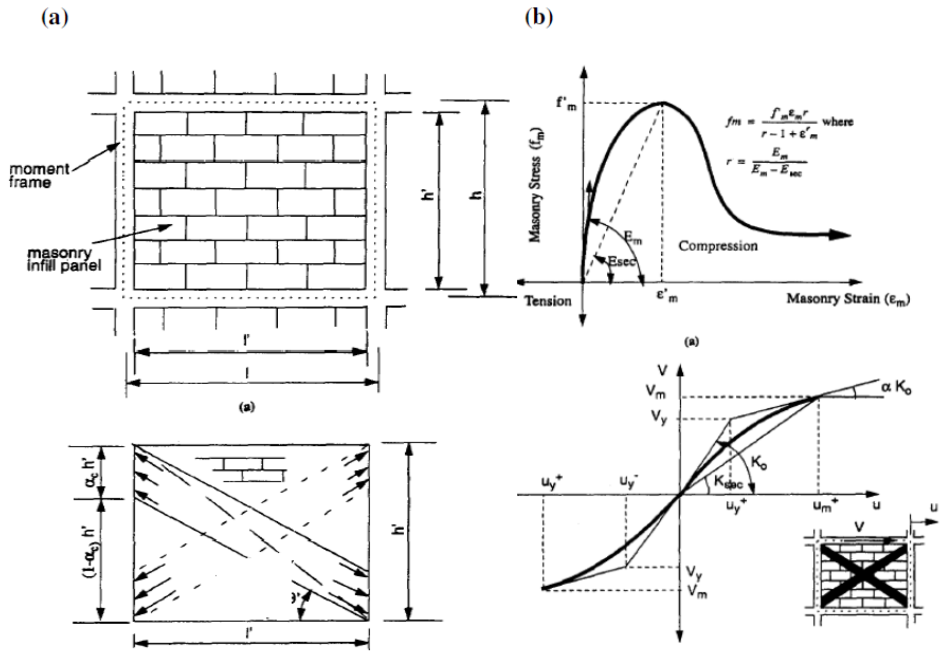

Figure D.3 (a) Equivalent strut model; (b) Constitutive models for masonry infills [Madan *et al.*, 1997]

Crisafulli, 1997b based on experimental test and numerical calibrations proposed an advanced nonlinear cyclic model showing significant advantages in its application and implementation, in particular, it accounts for the interaction between infill panel and its surrounding frame. In addition, different configurations of struts have been introduced for the principle modes of infill failure. The proposed hysteretic rule was originally used in the computer program RUAUMOKO Carr, 2007. Smyrou, 2006 has further adopted this model and worked on its implementation in the fibre-based finite element program SeismoStruct SeismoSoft, 2013. Although this model is fairly capable in capturing the in-plane behaviour and/or failure of the infill panel, the out-of-plane failure is introduced in a percentage of storey height which dictates the de-activation of the element, i.e. once the panel, not the frame, reaches a given out-of-plane drift, the panel no longer contributes to the structure's resistance nor stiffness, since it is assumed that it has failed by means of an out-of-plane failure mechanism. Reports of past earthquakes as well as research studies have shown that during a seismic event, unreinforced masonry infills experience loading simultaneously in both in-plane and out-of-plane directions; therefore, the out-of-plane capacity of the unreinforced masonry infills may be significantly affected by the already present in-plane shear cracks along the mortar joint, which could be crucial to the stability of the wall (Angel, 1994, Flanagan, 1999[Angel 1994, Flanagan 1999, Bashandy, 1995, Komaraneni, 2009).

Kadysiewski, and Mosalam 2009 proposed a new model that tends to solve this problem. This model, which consists of diagonal beam-column members utilizing fiber element cross sections, is suitable for use in a nonlinear time history analysis. The model considers both the in-plane (IP) and out-of-plane (OOP) response of the infill, as well as the interaction between IP and OOP capacities. The behavior is elastoplastic, and limit states may be defined by deformations or ductilities in the two directions.

In another recent study, proposals have been established by Puglisi, 2009a. Besides the concept of an equivalent strut, their model has been established based on the theory of plasticity. Instead of representing the infill with two independent elements, it introduces a new concept - the plastic concentrator, which links the two bars of the strut model, and allows for a transfer of effects between the bars in order to represent the infill panel more realistically as a unique element (Figure D.4). An extension of the model based on damage mechanics has been proposed subsequently Puglisi, 2009b to account for cracking and damage of the masonry infill panels.

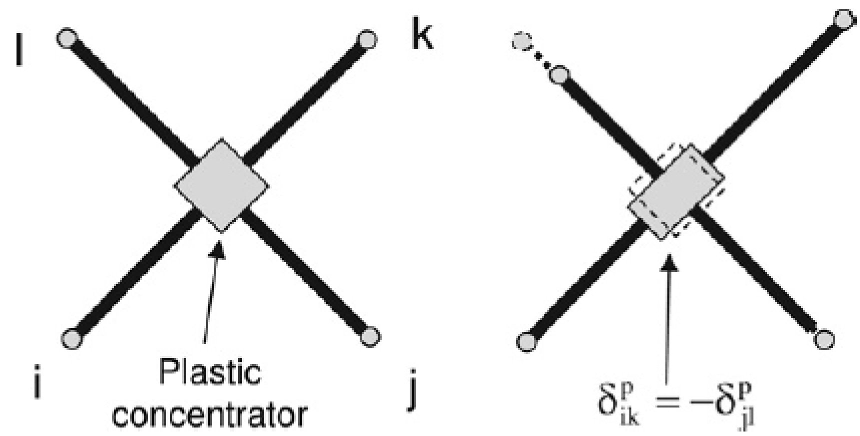

Figure D.4. Infill panel with plastic concentrator [Puglisi *et al.*, 2009]

In a similar study, Rodrigues, *et al.* 2008 and Rodrigues, *et al.* 2010 have proposed an improved numerical model for the simulation of the behavior of masonry infill walls subjected to earthquake loads and analyzed its ability to upgrade the equivalent bi-diagonal compression strut model, commonly used for the nonlinear behavior of infill masonry panels subjected to cyclic loads. In the proposed infill panel model, each masonry panel is structurally defined by four rigid support strut-elements and a central strut element, where the nonlinear hysteretic behavior, described by a multi-linear envelope curve, is concentrated (Figure D.5). The forces developed in the central element are purely of tensile or compressive nature, indicating that the masonry panel is assumed not to carry any vertical force. The calibration of the model has been based on two series of experimental tests: a single one story one bay frame tested at the LNEC Laboratory and a full-scale four-story and three bay frames tested at the ELSA laboratory.

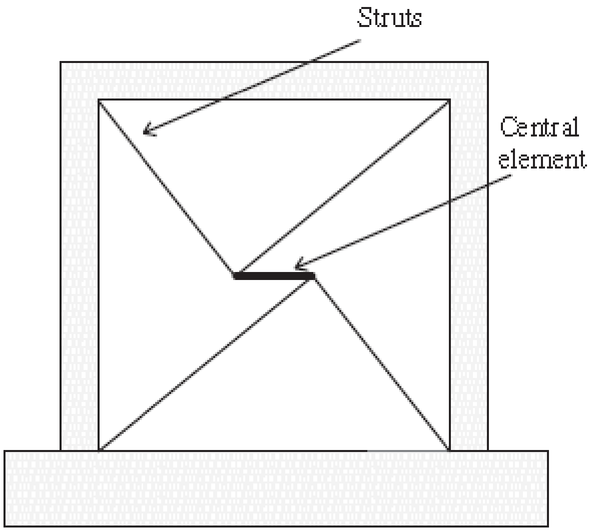

Figure D.5. Macro-model for the simulation of an infill masonry panel Rodrigues, et al 2008

D.3 DESCRIPTION OF THE MACRO-MODEL PROPOSED BY CRISAFULLI, 1997a

This model is implemented in SeismoStruct SeismoSoft, 2013 as a macro model featuring a double-strut approach developed by Crisafulli, 1997b. As illustrated in Figure D.6, the nonlinear element is defined by two components compressive/tension struts and shear springs. Each panel is represented by six struts; each diagonal direction features two parallel struts to carry axial loads across two opposite diagonal corners and a third one to carry the shear from the top to the bottom of the panel. This latter strut only acts across the diagonal that is on compression; hence its "activation" depends on the deformation of the element. Moreover, four internal nodes are employed to account for the actual points of contact between the frame and the infill panel (i.e. to account for the width and height of the columns and beams, respectively), whilst four dummy nodes are introduced with the objective of accounting for the contact length between the frame and the panel. Finally, it is important to refer that this element accounts for the out-of-plane failure drift regardless of its interaction with the in-plane failure of the panel given a drift limit for the out-of-plane failure of the panel by the user.

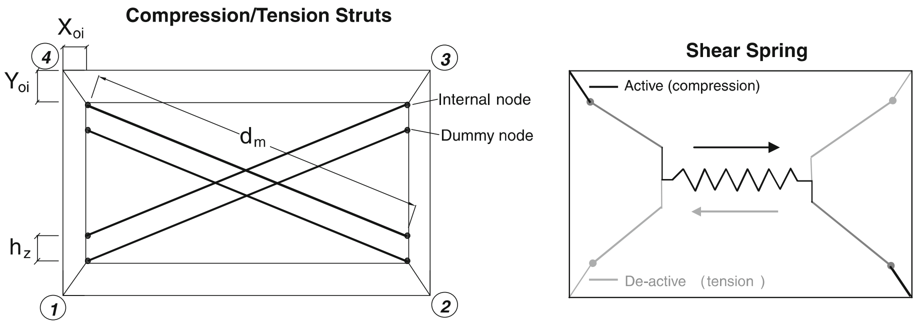

Figure D.6. Infill panel model Crisafulli, *et al.* 2007

D.4 DESCRIPTION OF MACRO-MODEL PROPOSE BY KADYSIESWSKI AND MOSALAM 2009

This model explicitly considers the in-plane (IP) and out-of-plane (OOP) behavior of the infill panel as well as their interaction. A sketch of this model is shown in Figure D.7. For each infill panel, representing a single bay in a single story, the model consists of one diagonal member which is composed of two beam-column elements, joined at the midpoint node. This node is given a lumped mass in the OOP direction. To this end, using the available features of the fiber elements all IP, OOP and the interaction of the three is modeled as follows.

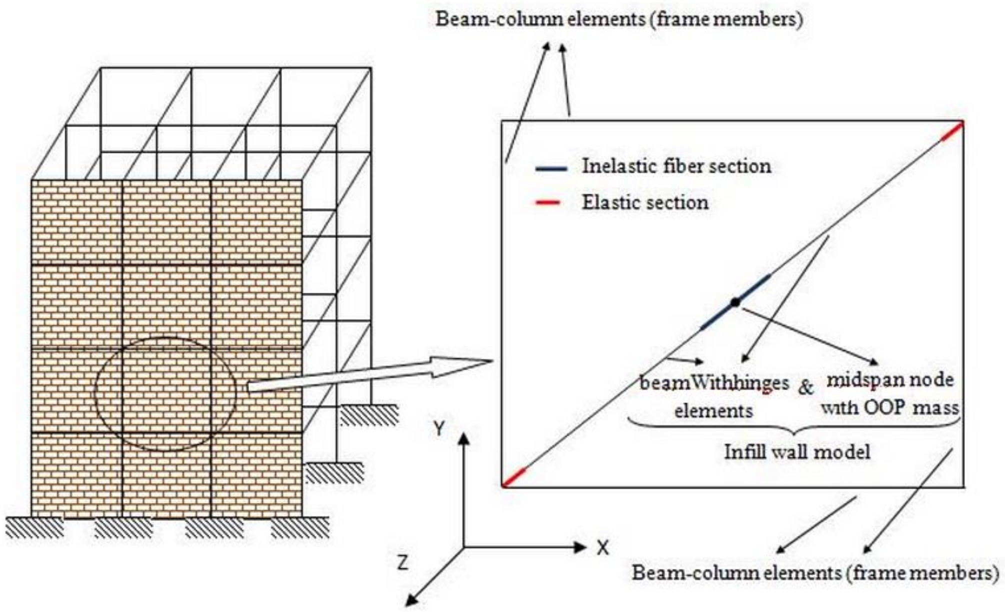

Figure D.7 Schematic view of the structural model

The IP strength of the infill panel is modeled by a diagonal strut, following the procedures of FEMA 356 (FEMA 2000). The strut is given a thickness and width accordingly based on the geometry and modulus of elasticity of the frame and infill panel. The axial strength of the equivalent strut of the infill panel for pure IP loading is determined by transforming the expected infill shear strength of the panel. Since the infill panel is modeled with only one diagonal strut, it has equal capacity for loading in either the positive or negative IP horizontal directions and the axial capacity of the member is identical in tension and compression. Accordingly, based on the element axial stiffness, strength and Collapse Prevention (CP) limit state described in FEMA356, the yield and collapse horizontal displacement limit states in plane of the panel are calculated. These Limit state displacements calculated in this way are not used in modeling approach, however, potential attainment of the limit state is determined by post-processing of the calculated displacements.

The OOP strength of the URM infill wall is determined based on arching action, the expected OOP capacity of the infill is therefore given using the expected compressive strength of the masonry and the slenderness parameter defined in FEMA356. As stated previously, the described infill wall element is comprised of two equal size diagonal beamWithhinges elements and a mid-span node with OOP mass. This mass at the mid-span node is calculated as 0.81M, where M is the total mass of the infill wall panel. This value is the first mode effective mass of the infill wall panel when it is defined as a beam spanning vertically with distributed mass and with simple supports at the ends. Knowing the concentrated mass and the frequency of the proposed model, the required equivalent OOP bending stiffness of the model beam-column member (with span equal to the infill wall diagonal) is determined. In a similar manner, the yield and CP displacement limit states in out-of-plane of the wall is calculated. The CP displacement is limited to the minimum of the 5% of the wall height and the wall thickness.

Kadysiewski, and Mosalam 2009 show that an interaction curve of the following form provides a good match to the FE model results:

$$\left(\frac{P_N}{P_{N0}}\right)^{3/2} + \left(\frac{P_H}{P_{H0}}\right)^{3/2} \leq \mathbf{1.0} \qquad \text{(D.1)}$$

where P_N is the OOP capacity in the presence of IP force, P_{N0} is the OOP capacity without IP force, P_H is the IP capacity in the presence of OOP force, and P_{H0} is the IP capacity without OOP force.

Finally, using the above IP and OOP strength and the interaction presented in equation (1), an inelastic fiber section by strategically locating a collection of nonlinear fiber elements is generated. The fibers are located along a line in the OOP direction (Z-direction in Figure D.7). As such, the beam-column element acts as a truss element and a flexural element in the IP and OOP directions, respectively.

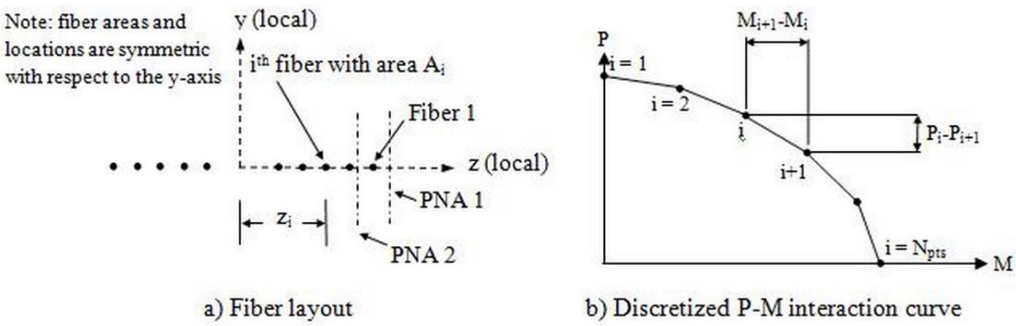

Figure D.8 Fiber layout and discretized P/M interaction curve

Except for the consideration of the in-plane and out-of-plane interaction, another important feature of the element is its ability to remove the element representing infill panel that have collapsed during an on-going finite element simulation. In other words, the model can simulate the progressive collapse of the masonry infill. The element follows the progressive collapse algorithm developed by Talaat, *et al.* 2008 and 2009. This algorithm is based on the dynamic equilibrium and resulting transient change in system kinematics. The progressive collapse algorithm was implemented in OpenSees module Mosalam, 2009, and it is called by the main analysis module after each converged load step to check each element for possible violation of its respective removal criteria.

D.5 COMPARISON OF NUMERRICAL ANALYSIS WITH EXPERIMENTAL RESULTS

Description of the experiment Calvi, and Bolognini 1999

The experimental program supported by numerous numerical analyses, performed with the objective to study the in-plane and out-of-plane behavior of newly designed reinforced concrete frames infilled with clay brick masonry infill walls, was used herein to verify and compare the two modeling approaches presented above. A full-scale one-floor, one-bay frame specimen with a height of 3.00 m and a span length of 4.50 m were considered with the objective to preserve the frame to infill stiffness ratio and obtain more reliable results (see Figure D.9). The main scope of this experimental test has been to investigate the in-plane and out-of-plane performance of RC frames with weakly reinforced masonry panels. However, in this study, only two cyclic tests related to the bare frame and frame with non-reinforcement masonry panels are examined.

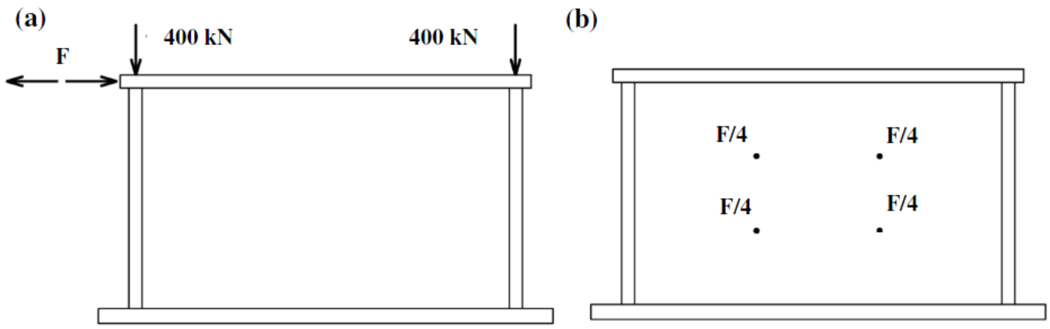

Figure D.9 Application of forces: (a) In-plane and (b) Out-of-plane Calvi, and Bolognini 1999

During the in-plane testing, specimens were subjected to three stages of static loading, defined by the drift target levels of 0.4%, 1.2% and 3.6 % (3.6% only for the bare frame). A second set of tests was executed to explore a more restricted drift range, with a sequence of drifts established at 0.2%, 0.3% and 0.4%. At each drift level three loading cycles were performed. Preliminary cycles at maximum 0.1 % drift were executed to evaluate the value of pre-cracking stiffness. In Figure D.10, the applied displacement history is depicted.

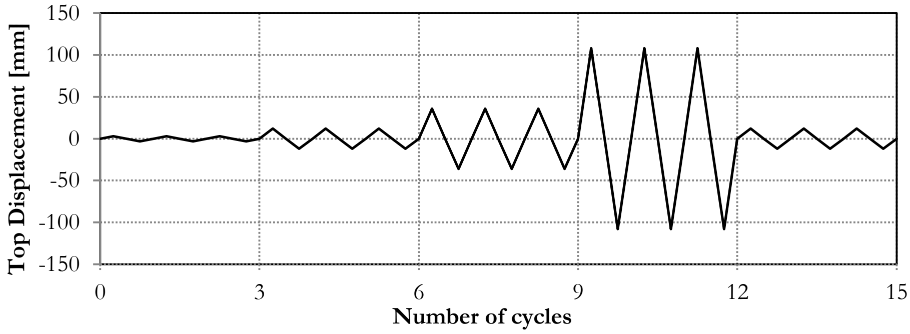

Figure D.10. Applied displacement history for the bare frame (for infilled frame only 9 cycles)

The out-of-plane tests were executed immediately after the in-plane loading cycles. In particular, the first set of specimens was subjected to a transversal load following an in-plane drift of 1.2 %, if allowed by the level of damage, while the second set of specimens was tested out-of plane after each in-plane drift up to 0.4 %.

All displacements were imposed applying hydraulic actuators, by means of a single horizontal force at the beam-column joint throughout the in-plane tests and through the application of four equally distributed transversal forces during the out-of plane tests. Initially, a compressive axial load of 400 kN was applied on every column (Figure D.9a).

Preliminary tests were performed for all material components creating the final specimen of interest. Clay brick units with dimensions of 245 x 115 x 245 mm, a void ratio of 60 % and an average weight of 34.8 kN were used for the construction of the panels. The infill panels were constructed with horizontal holes; therefore the values of the second and third lines of the table are more appropriately representing the real situation.

Based on the summary of the results obtained from tests on specimens with approximate size of $800 \times 800 \times 120$ mm, an average compression strength ($f_{m\ ave}$) of 1.1 MPa, average modulus of elasticity ($E_{m\ ave}$) of 1873 MPa, an average shear strength ($F_{v0,ave}$) of 0.09 MPa is suggested to be implemented for the numerical analysis.

The major in-plane and out-of-plane experiments were performed on a series of specimens, including a bare frame (T#1), three non-reinforced infilled frames (T#2, T#6, T#10), and seven infilled frames strengthened with different reinforcing techniques (horizontal reinforcing steel bars for T#3, T#7; Murfor trusses for T#4, T#8, T#11; reinforcing steel meshes for T#5, T#9). The force-displacement curves obtained during the in-plane tests of the bare frame and the non-reinforced infilled frame are displayed in Figure D.12. The crack patterns obtained during the tests on a non-reinforced specimen at different drift levels are displayed in Figure D.13.

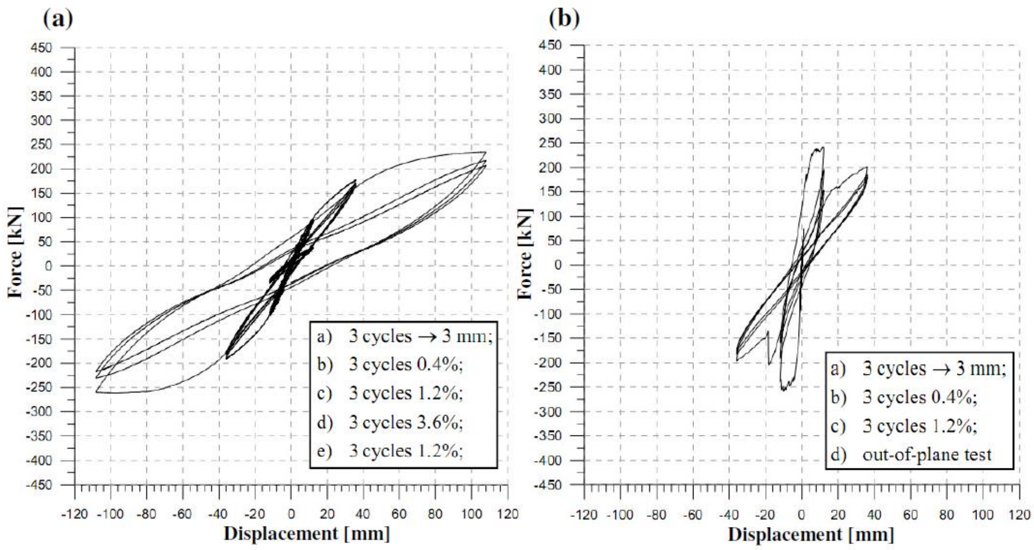

Figure D.11. In-plane force-displacement: (a) Bare (T#1) (b) Infilled frame (T#2) [Calvi & Bolognini, 1999]

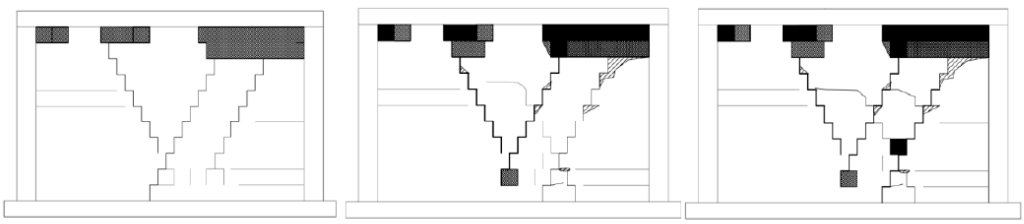

Figure D.12. Crack patterns (T#2): 0.4 % drift (left), 1.2 % drift (middle), Out-of-plane (right) [Calvi & Bolognini, 1999]

D.6 NUMERICAL RESULTS

The response of the bare and infilled frame is estimated using two different software. Beams and columns of the structure are modelled using flexibility-based nonlinear beam-column elements with fibre-section distributed. Concrete and steel behavior and the corresponding applied models using two different programs are illustrated in Table D.1. The material properties used in modelling are listed in Table D.2.

Table D.1. Material models used in the modeling based on Opensees and Seismostruct

Material	*Opensees*	*Seismostruct*
Concrete	***concrete01*:** Kent-Scott-Park concrete material object with degraded linear unloading/reloading stiffness according to the work of Karsan-Jirsa and no tensile strength	***con_ma* :** Mander *et al.* nonlinear concrete model with zero tensile strength
Steel bars	***Steel02:*** Giuffré-Menegotto-Pinto Model with Isotropic Strain Hardening	***Stl-mp:*** Menegotto-Pinto steel model

Table D.2. Geometric and Material Properties of the R/C Frame

Cover to flexural reinforcement	c	3.0 mm
Concrete compressive strength (unconfined)	$f_c^{'}$	35 MPa
Concrete strain at maximum strength (unconfined)	ε_c	0.002
Concrete crushing strength (unconfined)	f_{c20}	6 MPa
Concrete strain at crushing strength (unconfined)	ε_{cu}	0.003
Concrete strain at maximum strength (confined)	ε_{cc}	0.0035
Concrete crushing strength (confined)	f_{cc20}	7 MPa
Concrete strain at crushing strength (confined)	ε_{ccu}	0.035
Reinforcement yield strength	f_y	600 MPa
Young's modulus of reinforcement steel	E_s	210 GPa
Strain hardening ratio of reinforcement steel	b	0.01
Menegotto Pinto constitutive model parameters for reinforcement steel	R_0, R_1, R_2	23, 0.97, 0.05
	a_1, a_2, a_3, a_4	0.0, 1.0, 0.1, 1.0

In the first step, the hysteretic response of the bare frame is verified using Opensees and Seismostruct. As can be seen, both softwares provide a good agreement between the experimental and numerical results.

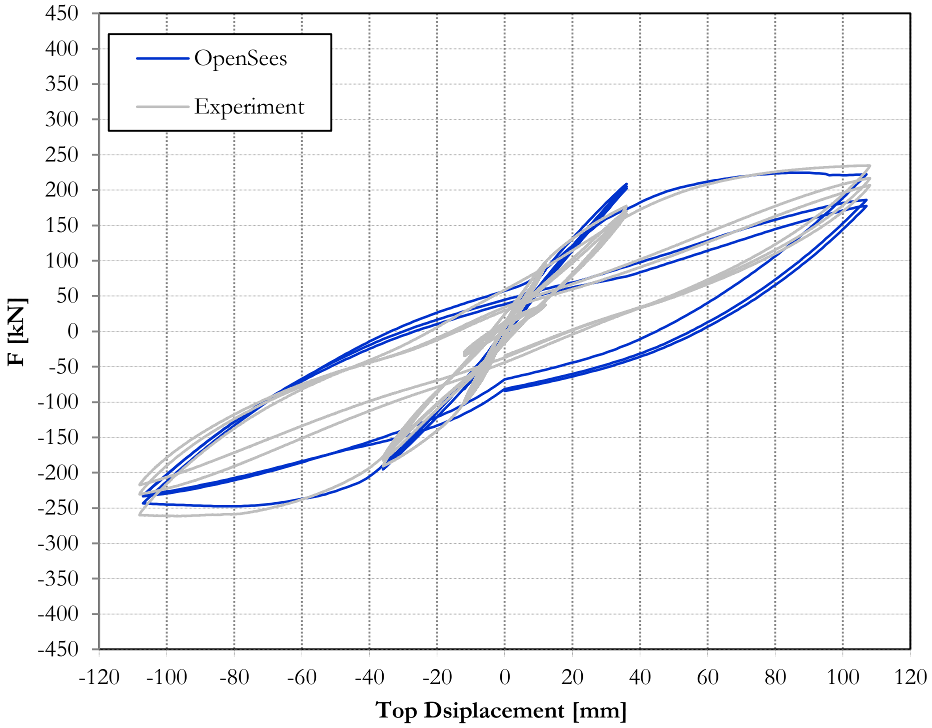

Figure D.13. Comparison of experimental and analytical force-displacement curve for the bare frame using OpenSees

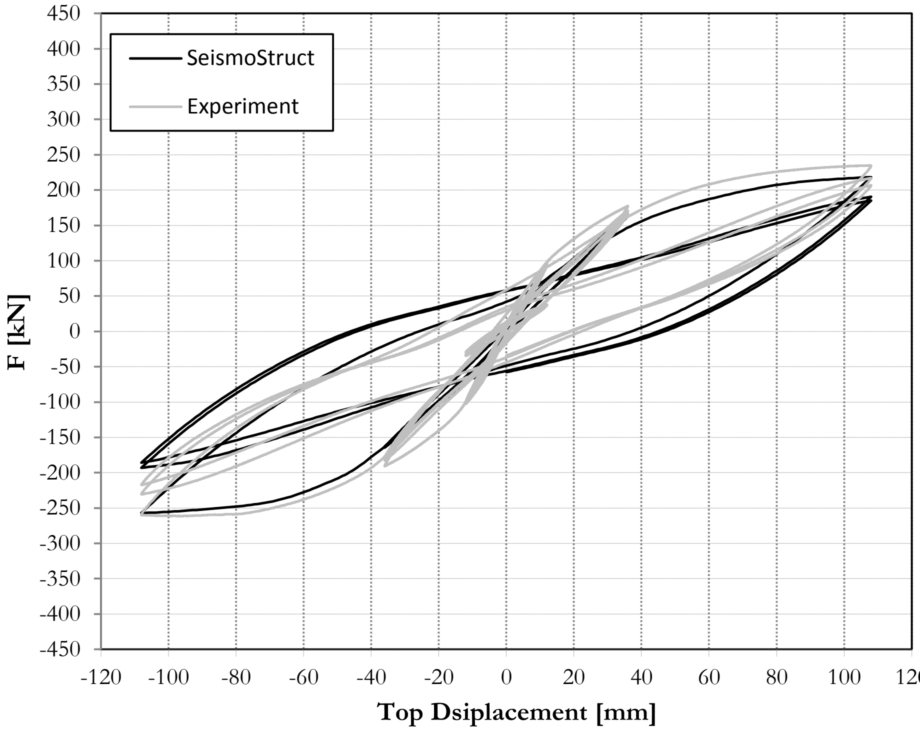

Figure D.14. Comparison of experimental and analytical force-displacement curve for the bare frame using Seismostruct

In a second step, the infill panel is added to the models based on the two considered modelling approaches. In Table D.3, the parameters assumed for modelling the hysteretic behaviour of the strut, the geometric properties of the panel using SeismoStruct (SS) based on the model of [Crisafulli 1997] are listed. In order to model the equivalent strut element and the definition of the fibre section in OpenSees (OS), based on the [Kadysiewski and Mosalam 2009] (K&M, 2009), a spread sheet has been generated. Table D.4 summarize the final equivalent section used in the model. In Figure D.15 and Figure D.16, the results of the hysteretic behaviour of the two applied models of [Crisafulli 1997] and K&M [2009] are compared with the experimental results.

Table D.3 Summary of applied parameters for the infill panel model (Seismostruct)

Strut curve Parameters (N, m)		
Initial Young moduls	E_m	1873
Compressive strength	f_m	1.1
Tensile strength	f_t	0.12
Strain at maximum stress	ε_m	0.0013
Ultimate strain	ε_u	0.0046
Closing strain	ε_{cl}	0.0003
Strut area reduction strain	e_1	0.0006
Residual strut area strain	e_2	0.002
Starting unloading stiffness factor	g_u	5
Strain reloading factor	a_r	0.2
Strain inflection factor	a_{ch}	0.7
Complete unloading strain factor	b_a	2
Stress inflection factor	b_{ch}	0.9
Zero stress stiffness factor	g_{pu}	1
Reloading stiffness factor	g_{pr}	1.1
Plastic unloading stiffness factor	e_{x1}	3
Repeated cycle strain factor	e_{x2}	1
Shear curve Parameters		
Shear strength		0.09
Friction		0.7
Max shear resistance		0.10
Reduction shear factor		1.5
Panel geometric properties		
Panel thickness		135
Out of plane failure drift (%)		0.5
Strut area 1 (before reduction)		22000
Strut area 2 , % of area 1 (after reduction)		20
Equivalent contact length h_z (% of vertical panel side)		0.08
Horizontal offset x_o (% of horizontal panel side)		3.33
Vertical offset y_o (% of vertical panel side)		4.17
Proportion of stiffness assigned to shear (%)		7.5

Table D.4. Equivalent strut section (fibre properties)

Fiber Number	Fiber area (m^2)	Fiber yield stress (N/m^2)	Fiber location (m)
1	0.057	101242.8	0.200
2	0.025	437430.1	0.104
3	0.017	950361.2	0.074
4	0.011	1965076.8	0.053
5	0.005	8389034.7	0.028
6	0.005	8389034.7	-0.028
7	0.011	1965076.8	-0.053
8	0.017	950361.2	-0.074
9	0.025	437430.1	-0.104
10	0.057	101242.8	-0.200

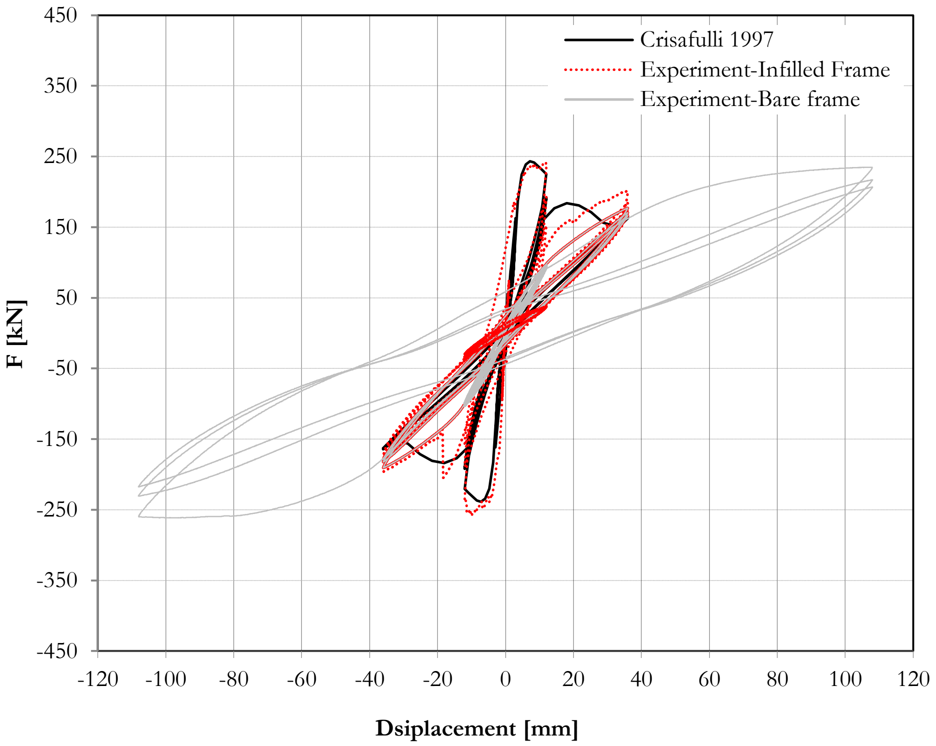

Figure D.15. Numerical modelling of the infilled frame using proposed model by [Crisafulli 2009]

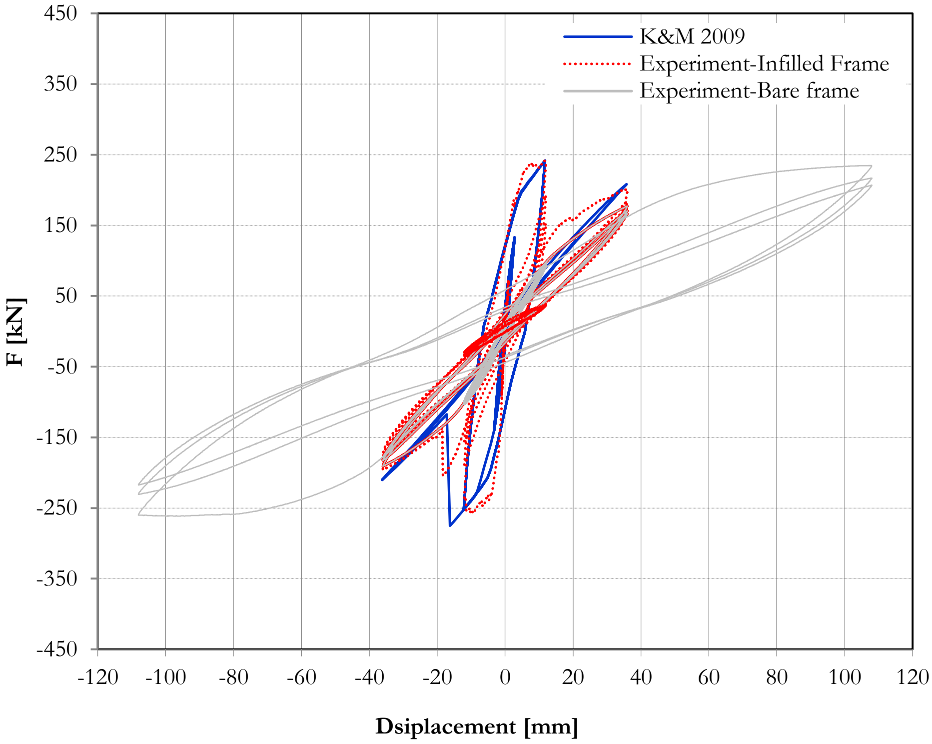

Figure D.16. Numerical modelling of the infilled frame using proposed model by [Kadysiewski and Mosalam 2009].

The following observations could be addressed from this investigation:

1- Both models seem to be fairly capable to estimate the infilled frame strength and the initial stiffness.
2- It should be noted that in order to capture a proper match for the initial stiffness from the K&M [2009] model, the equivalent strut area has been slightly modified in this study with respect to the suggestions of the K&M model. As such, the pragmatic proposals of [Holmes 1961] or [Paulay and Priestley 1992] of simply assuming a value of strut width (b_w) which is respectively equal to 1/3 or 1/4 of strut diagonal length (d_m) has been used.
3- The expected hysteretic behaviour observed from experiment is represented very well by SS. OS, on the other hand, given the bilinear nature of the model, although provides a good estimate of the hysteretic curve in the first cycles before the collapse limit state is reached, it fails to capture the whole hysteretic loop afterwards. This can be also explained as follows: in OS, since the strut is removed after the collapse criteria is reached, the residual strength of the infill panel is

ignored, whereas the residual drift of the panel is considered in SS during all the cycles.

4- The drop in the strength, after the infill reaches the collapse limit state, is very well estimated by both models.

The nonlinear response history of the bare and infilled frames into the Coyote Lake, 1979, earthquake recorded at the station of Gilroy Array #6 obtained from different modelling approaches is shown in Figure D.17. A damping ratio of 2.5% proportional to tangent stiffness has been considered in analysis. As can be seen, both models estimate the response very similar, especially the maximum drift ratio that is estimated is very well close. Figure D.18 the shows the OOP and IP displacement interaction curve and the criteria used for the removal of the element.

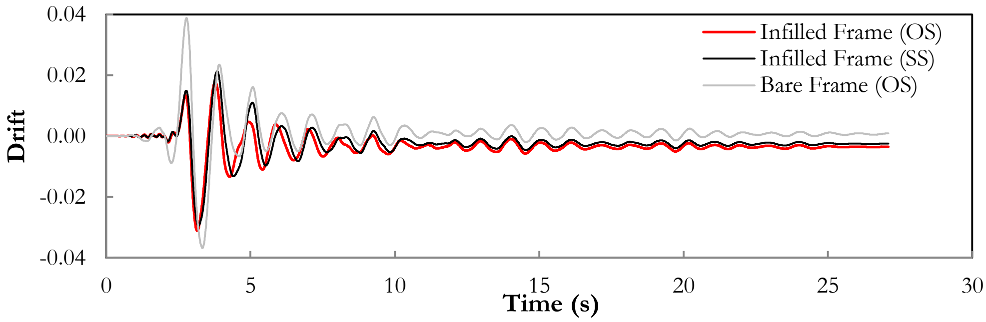

Figure D.17. Nonlinear response history of the infilled and bare frames using different modelling approaches

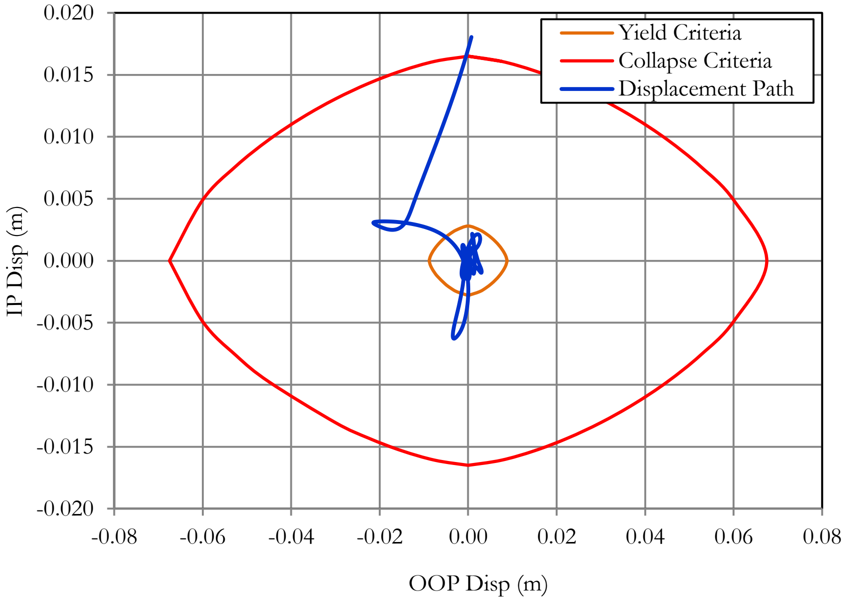

Figure D.18. OOP and IP displacement path of the infilled frame from the response history analysis (up to the collapse of the infill panel)

Appendix E: **Conditional Spectrum based record selection— Additional results**

E.1 DEFINITION OF CS(*INP*)

An alternative version of average spectral acceleration considered here is called I_{NP} [Bojórquez, and Iervolino, 2011] and is defined as:

$$I_{NP} = SAT1 \cdot N_P^{\alpha}\,, \tag{E.1}$$

In which N_P is the average spectral acceleration in the range T_1 to T_N, where T_N is a period longer than T_1, normalized by $Sa(T_1)$:

$$N_p = \frac{AvgSA(\mathrm{T}_1 \ldots \mathrm{T}_N)}{SAT1}\,, \tag{E.2}$$

The exponent α provides a weight to the importance of the spectral shape in the period range beyond T_1. Clearly $\alpha = 0$ yields N_p=$SAT1$ and $\alpha = 1$ yields N_p=$AvgSA$. By applying the natural logarithm to both sides of Equation E.1, we have:

$$\ln(I_{NP}) = \ln\left(SA(\mathrm{T}_1)\right) + \alpha \cdot \ln\left(\frac{AvgSA}{SA(\mathrm{T}_1)}\right), \tag{E.3}$$

the mean and variance of $\ln I_{NP}$ are then computed as:

$$\mu_{\ln INP} = (1-\alpha)\cdot \mu_{\ln[SA(\mathrm{T}_1)]} + \alpha \cdot \mu_{\ln[AvgSA]}\,, \tag{E.4}$$

$$\begin{aligned} \mathrm{var}(\ln INP) = \alpha^2 \cdot \sigma^2_{\ln[AvgSA]} + (1-\alpha)^2 \cdot \sigma^2_{\ln[SA(\mathrm{T}_1)]} + \\ 2\cdot\alpha\cdot(1-\alpha)\cdot \rho_{\ln[AvgSA],\ln[SA(\mathrm{T}_1)]} \cdot \sigma_{\ln[AvgSA]} \cdot \sigma_{\mathrm{n}[SA(\mathrm{T}_1)]} \end{aligned} \tag{E.5}$$

In these Equations $\mu_{\ln[AvgSA]}$ and $\sigma^2_{\ln[AvgSA]}$ are the logarithmic mean and variance of *AvgSA* from. $\rho_{\ln[AvgSA],\ln[SA(T_1)]}$ is the correlation coefficient between *AvgSA* and *SAT1*, which is derived from Equation E.6. In order to compute the CMS conditioned on I_{NP} (called here CMS(I_{NP})), the correlation coefficients of I_{NP} with spectral accelerations at different periods (*SA(T)*) are needed. These coefficients can be computed as follows:

$$\rho_{\ln[SA(\mathrm{T})],\ln[I_{NP}]} = \frac{S}{\sigma_{\ln[\mathrm{INP}]} \cdot \sigma_{\ln[SA(\mathrm{T})]}} \tag{E.6}$$

where S is given by

$$\begin{aligned} S &= (1-\alpha)\cdot \rho_{\ln(SA(\mathrm{T})),\ln(SA(\mathrm{T}_1))} \cdot \sigma_{\ln(SA(\mathrm{T}))} \cdot \sigma_{\ln(SA(\mathrm{T}_1))} + \\ &\alpha \cdot \rho_{\ln(SA(\mathrm{T})),\ln(AvgSA)} \cdot \sigma_{\ln(SA(\mathrm{T}))} \cdot \sigma_{\ln(AvgSA)} + \\ &\alpha \cdot \mu_{\ln(SA(\mathrm{T}^*))} \cdot \mu_{\ln(AvgSA)} \end{aligned} \tag{E.7}$$

In this Equation, $SAT1$ and $AvgSA$ are the ones used in the definition of I_{NP}.

E.2 INTRODUCTION

In this Appendix, the nonlinear dynamic analysis results based on different record selection approaches proposed in Chapter 5 are presented. The results include Maximum interstory drift ratio (MIDR) for different IM levels, IDR and PFA profiles along the building height, response hazard and collapse fragility curves for the 4-, 7-, 12- and 20- story buildings. The description of the selected IMs and the period ranges for the tested buildings are shown in Table E.1. In the end of this appendix, the hazard consistency verification for the selected record sets are shown.

Table E.1. Description of the conditioning IMs used for record selection and structural response estimation

	SAT1	SAT2	SATH	AvgSAT2	INP	
	T1	T2	1.5·T1	Period range	Period range	alfa
4- story	1.82	0.57	2.73	0.57:0.2:2.77	1.82:0.2:3.82	0.4
7- story	1.60	0.52	2.40	0.52:0.2:2.52	1.60:0.2:3.2	0.4
12- story	2.10	0.73	3.15	0.73:0.2:3.13	2.1:0.2:4.3	0.4
20- story	2.85	0.92	4.28	0.92:0.2:4.32	2.85:0.2:5.65	0.4

E.3 RESULTS OF THE 4-STORY BUILDING

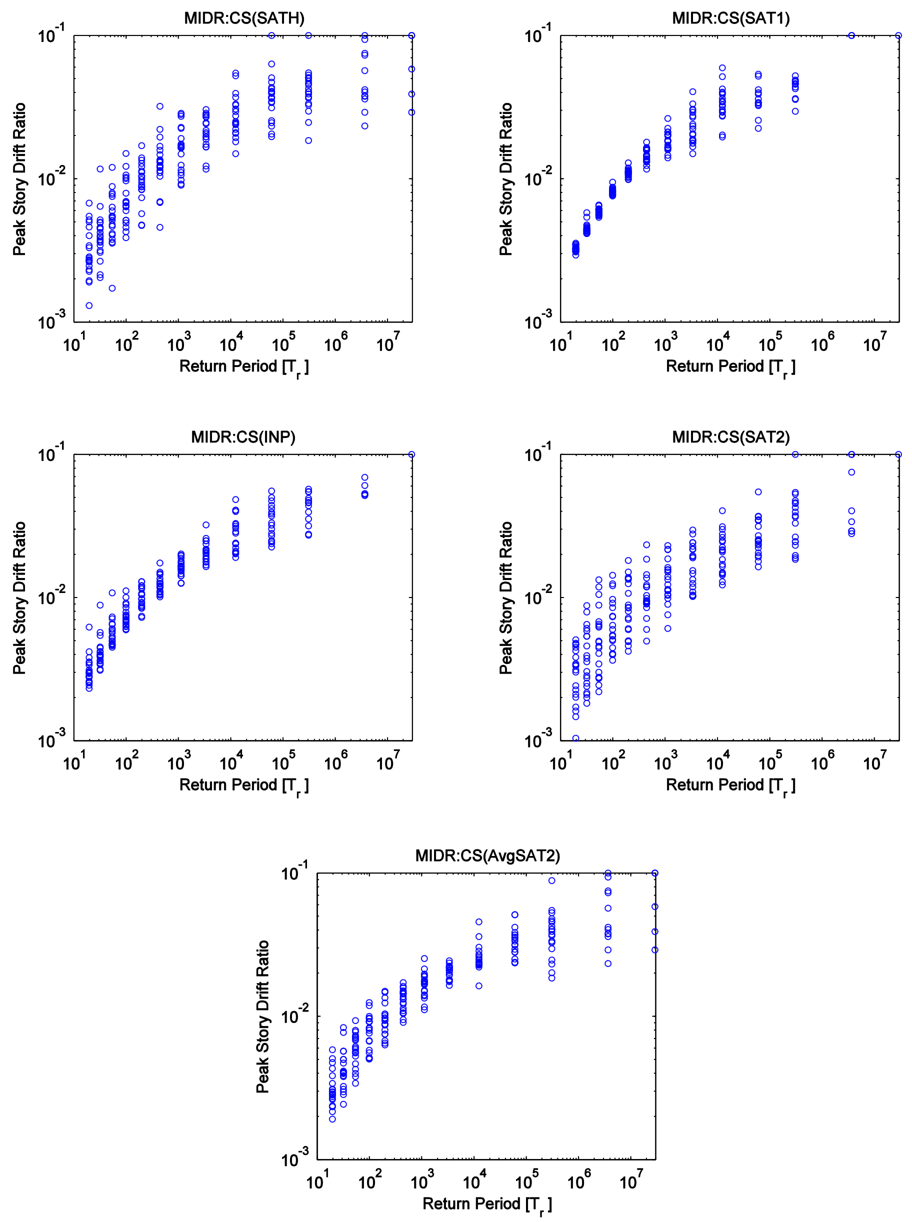

Figure E.1 Maximum Inter-story Drift Ratio (MIDR) along the height obtained from nonlinear dynamic analysis for the 4-story building based on different record selection approaches

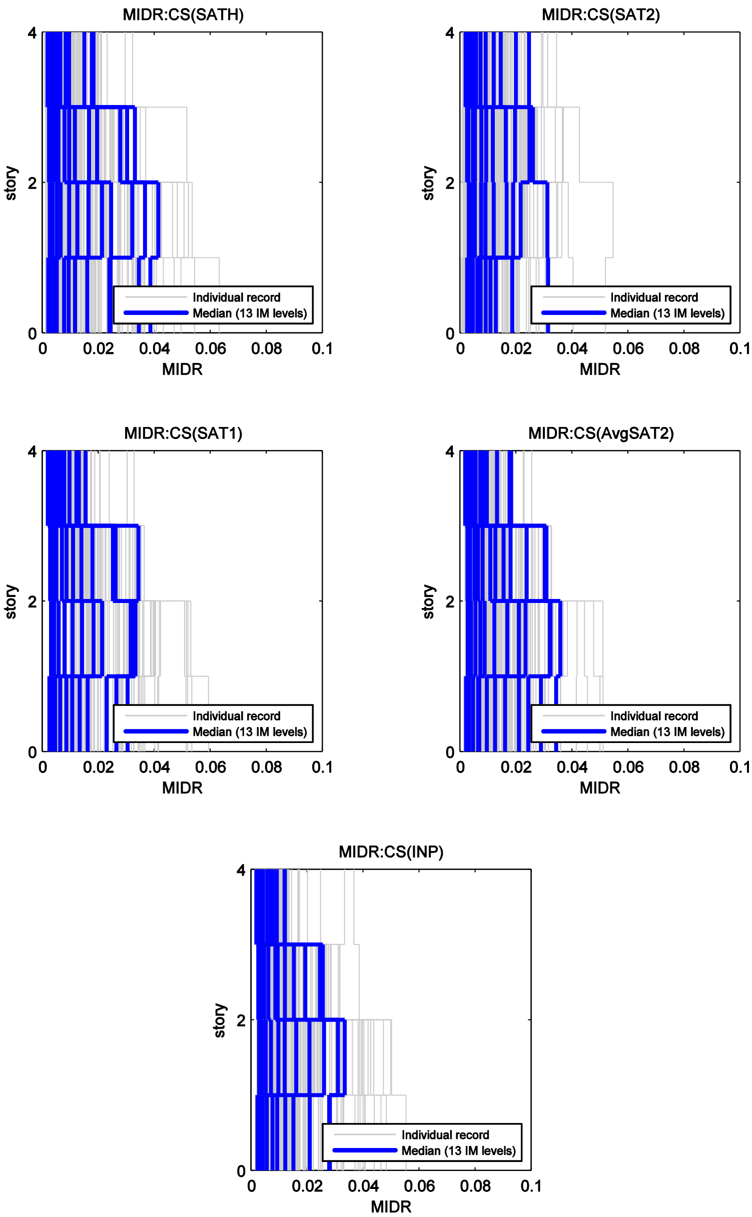

Figure E.2 Maximum Inter-story Drift Ratio (MIDR) profile obtained from nonlinear dynamic analysis for the 4-story building based on different record selection approaches

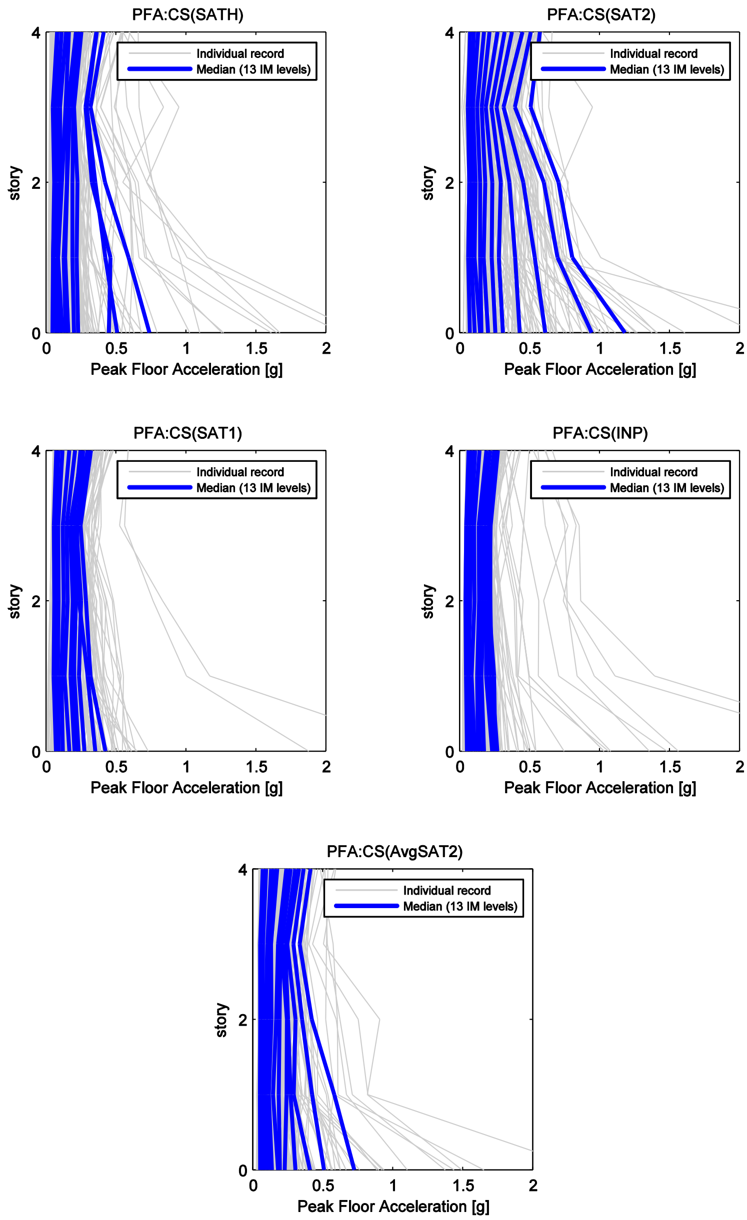

Figure E.3 Peak Floor Acceleration (PFA) profile obtained from nonlinear dynamic analysis for the 4-story building based on different record selection approaches

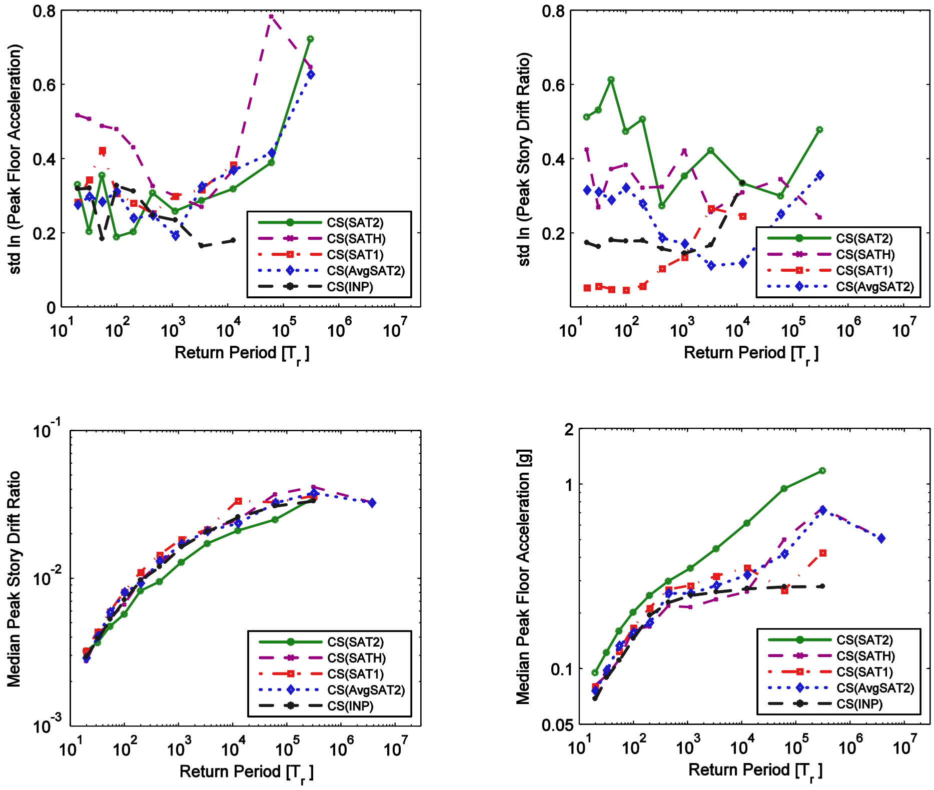

Figure E.4 Median and logarithmic standard deviation of Maximum Inter story Drift Ratio (MIDR) and Maximum Peak Floor Acceleration (MPFA) along the height obtained from nonlinear dynamic analysis for the 4-story building based on different record selection approaches

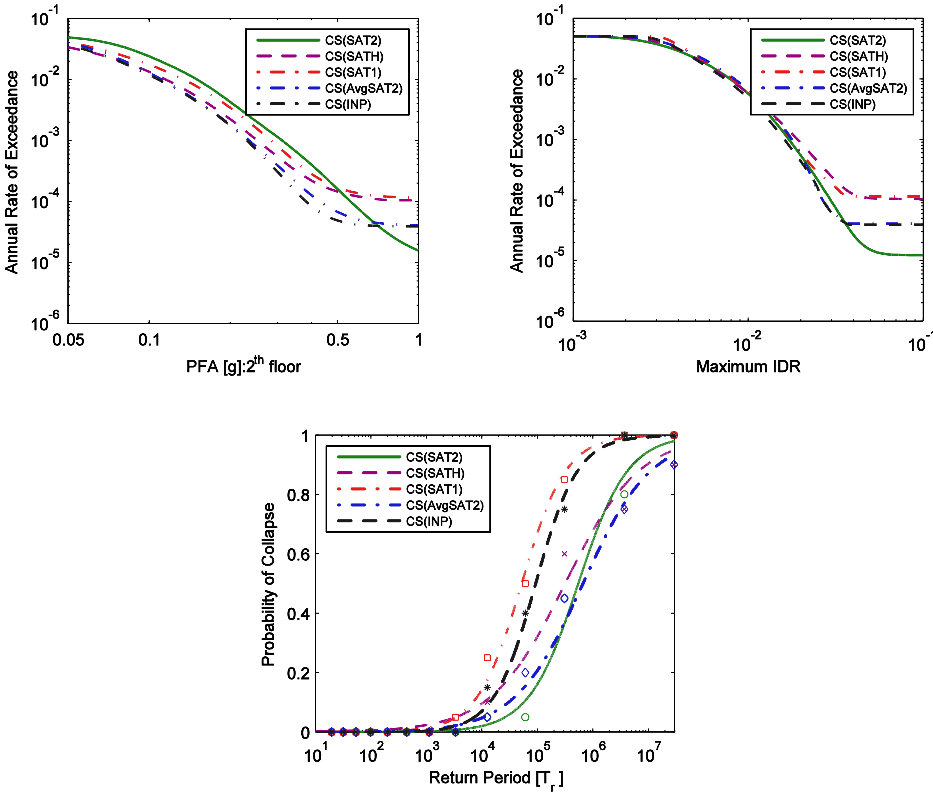

Figure E.5 Response hazard and collapse fragility curves obtained from nonlinear dynamic analysis for the 4-story based on different record selection approaches

E.4 RSULTS OF THE 7-STORY BUILDING

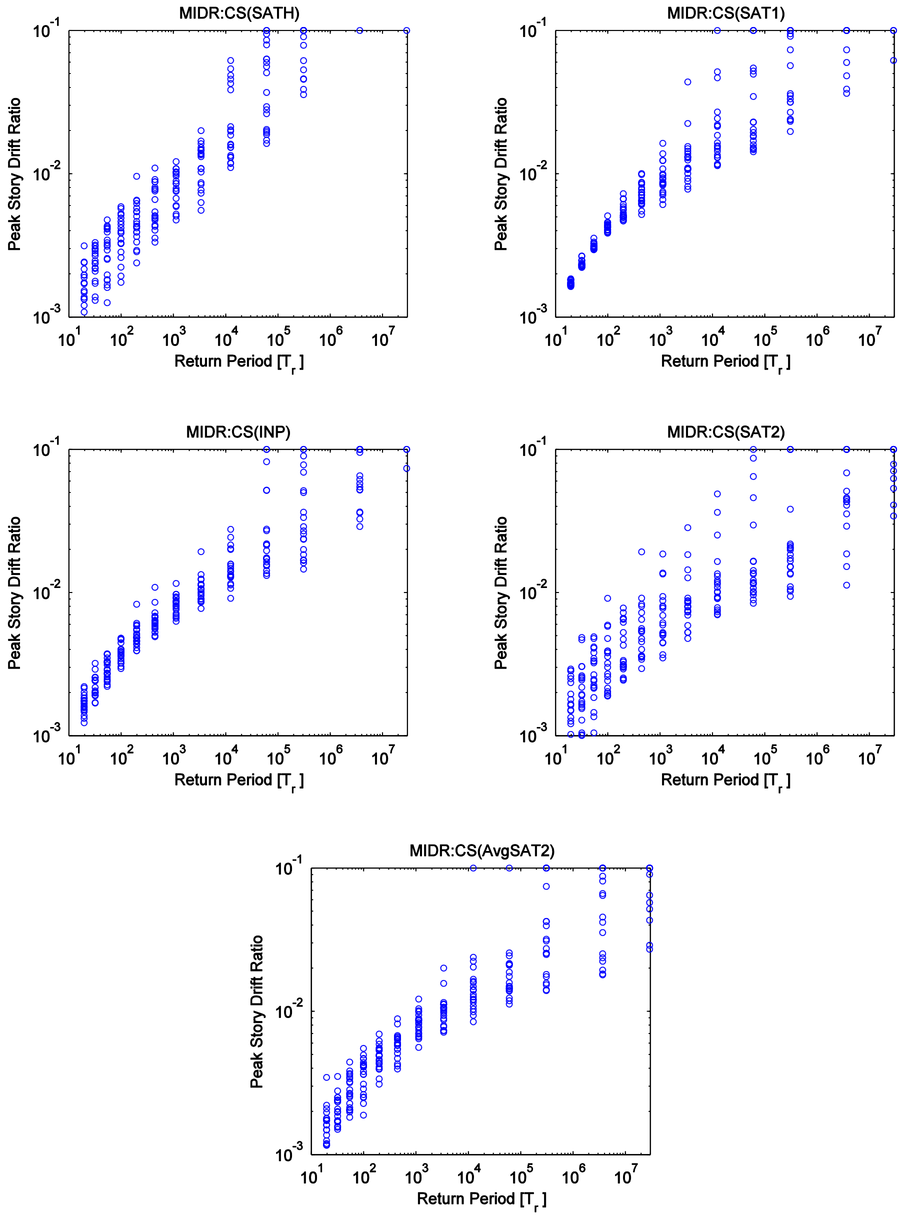

Figure E.6Maximum Inter-story Drift Ratio (MIDR) along the height obtained from nonlinear dynamic analysis for the 7-story building based on different record selection approaches

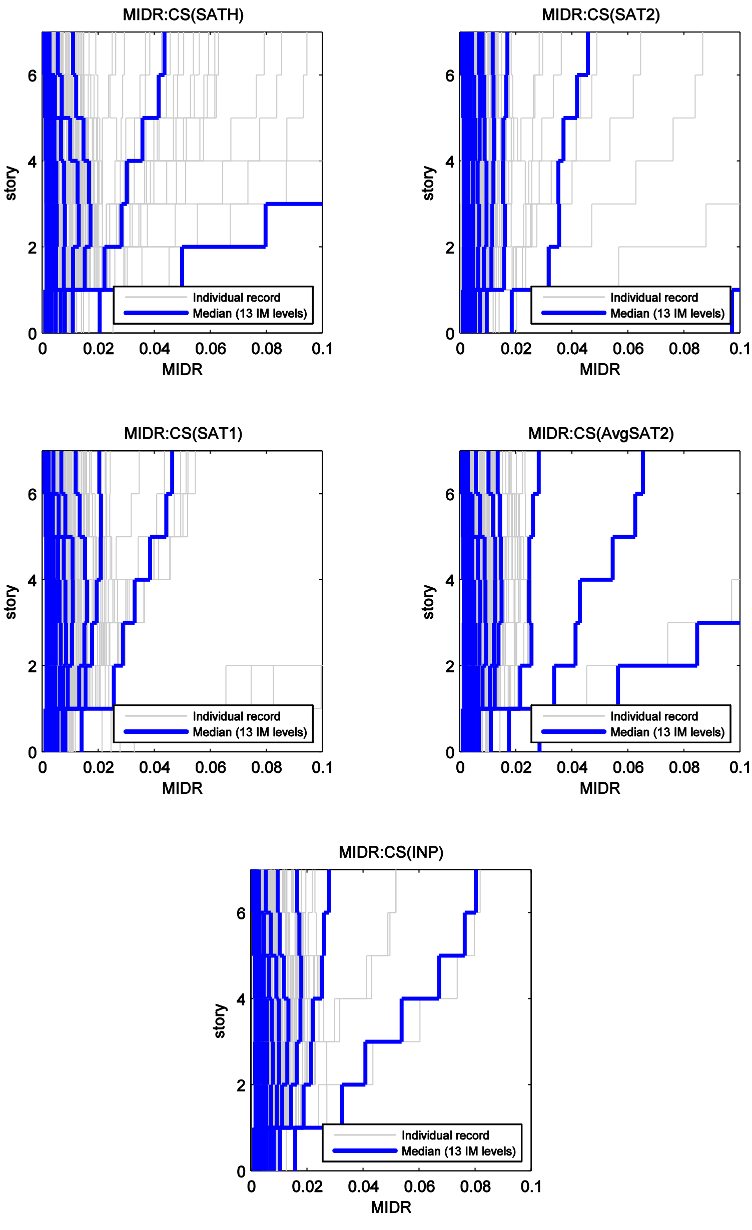

Figure E.7 Maximum Inter-story Drift Ratio (MIDR) profile obtained from nonlinear dynamic analysis for the 7-story building based on different record selection approaches

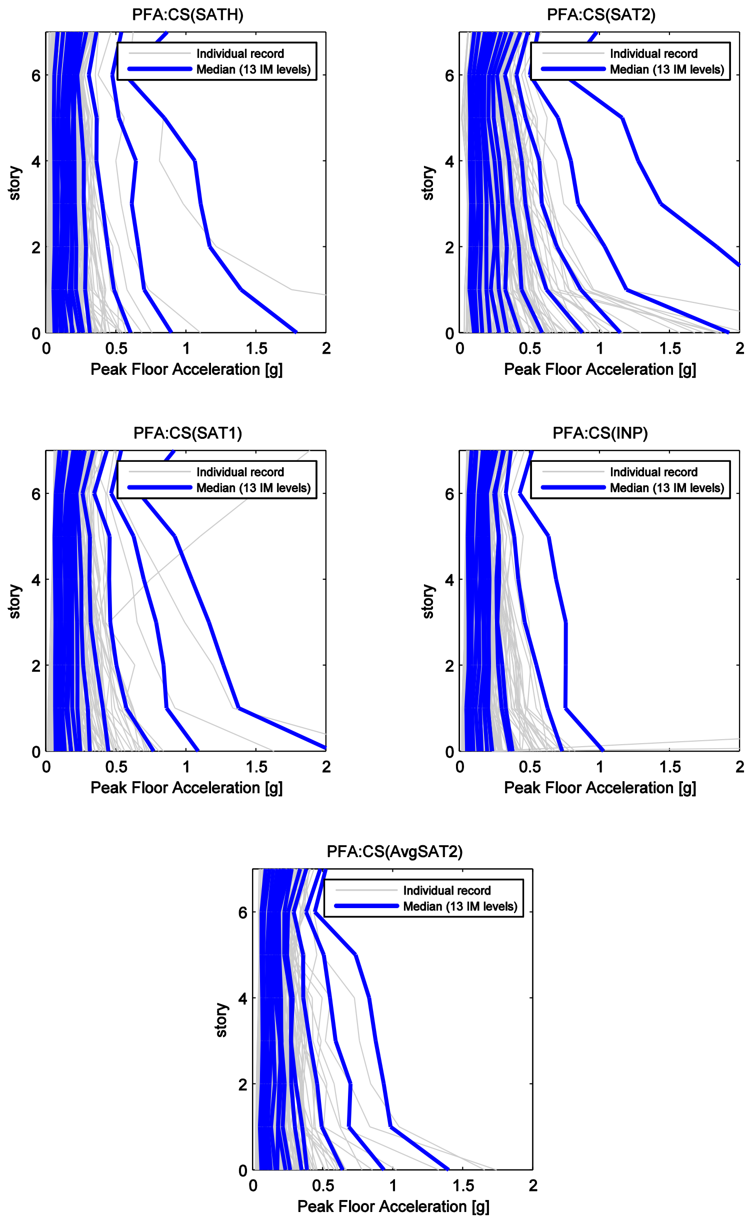

Figure E.8 Peak Floor Acceleration (PFA) profile obtained from nonlinear dynamic analysis for the 7-story building based on different record selection approaches

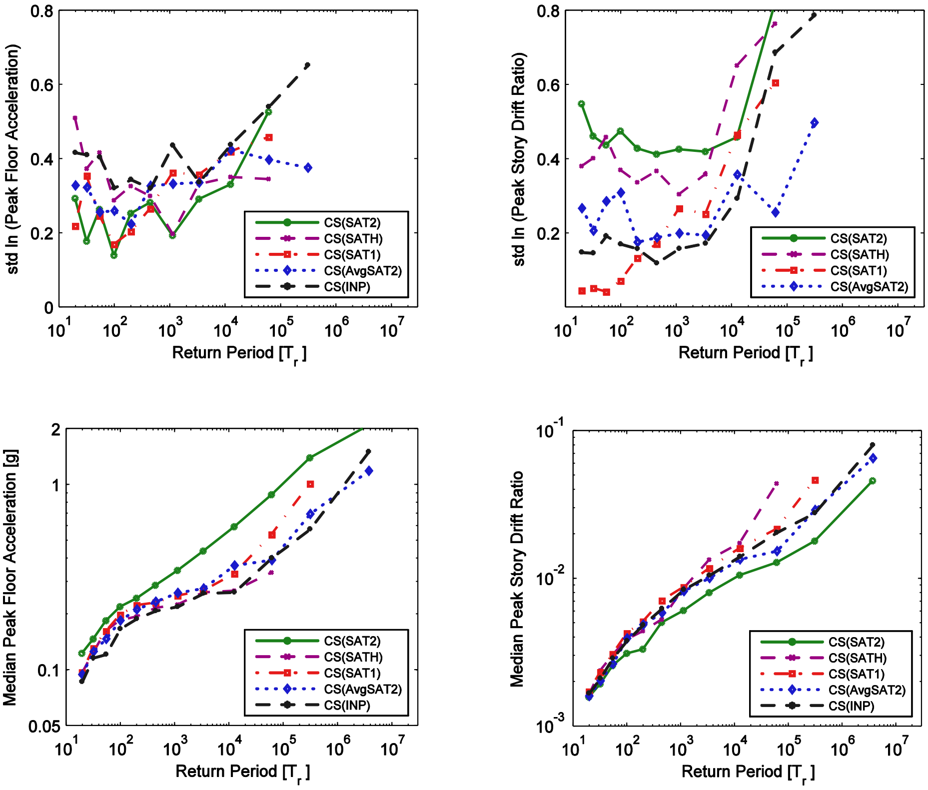

Figure E.9 Median and logarithmic standard deviation of Maximum Inter story Drift Ratio (MIDR) and Maximum Peak Floor Acceleration (MPFA) along the height obtained from nonlinear dynamic analysis for the 7-story building based on different record selection approaches

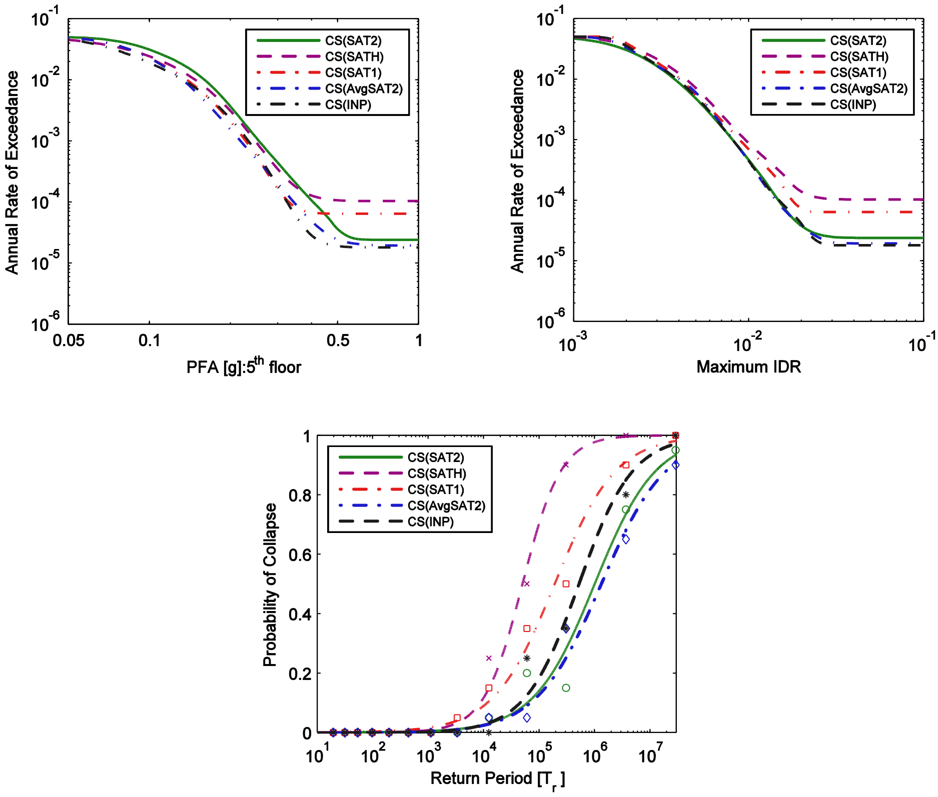

Figure E.10 Response hazard and collapse fragility curves obtained from nonlinear dynamic analysis for the 7-story based on different record selection approaches

E.5 RESULTS OF THE 12-STORY BUILDING

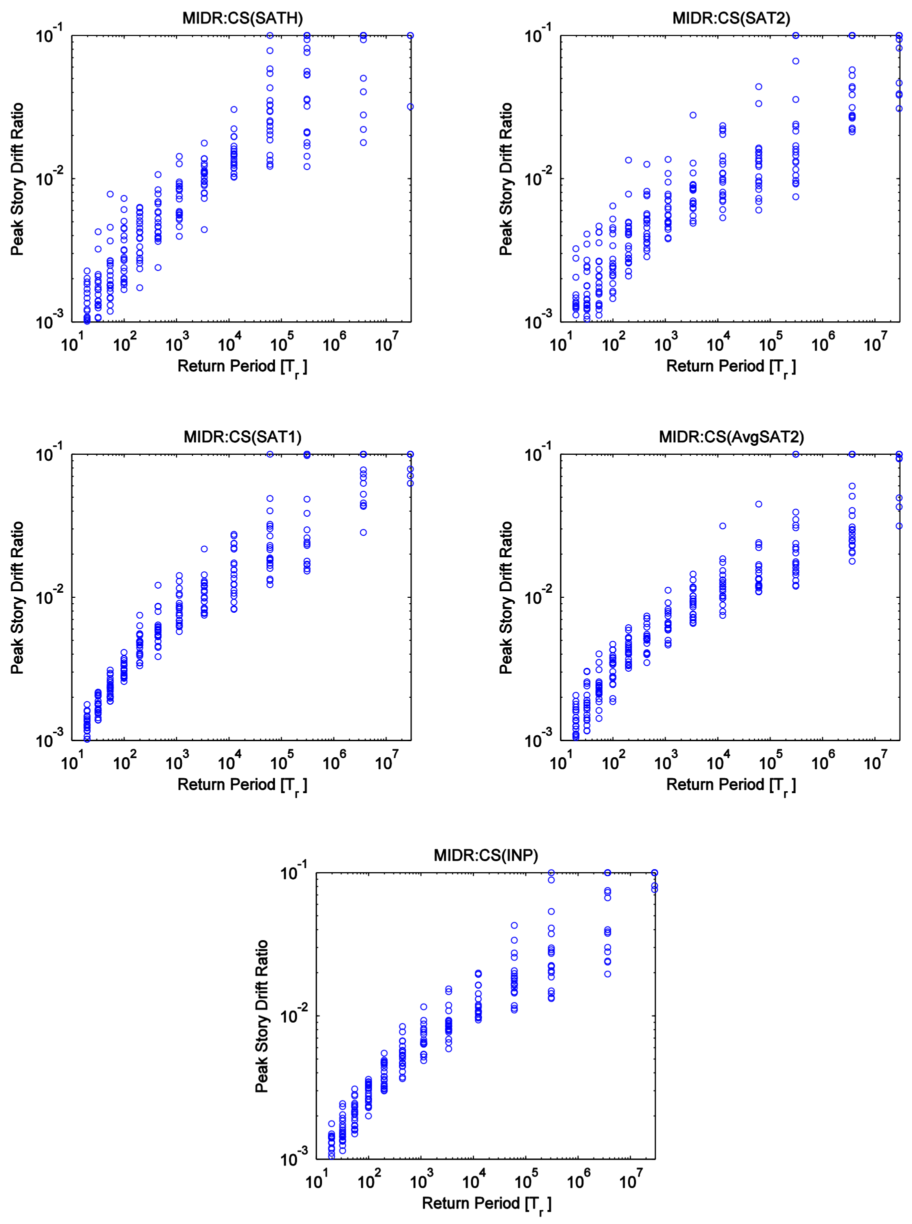

Figure E.11 Maximum Inter-story Drift Ratio (MIDR) along the height obtained from nonlinear dynamic analysis for the 12-story building based on different record selection approaches

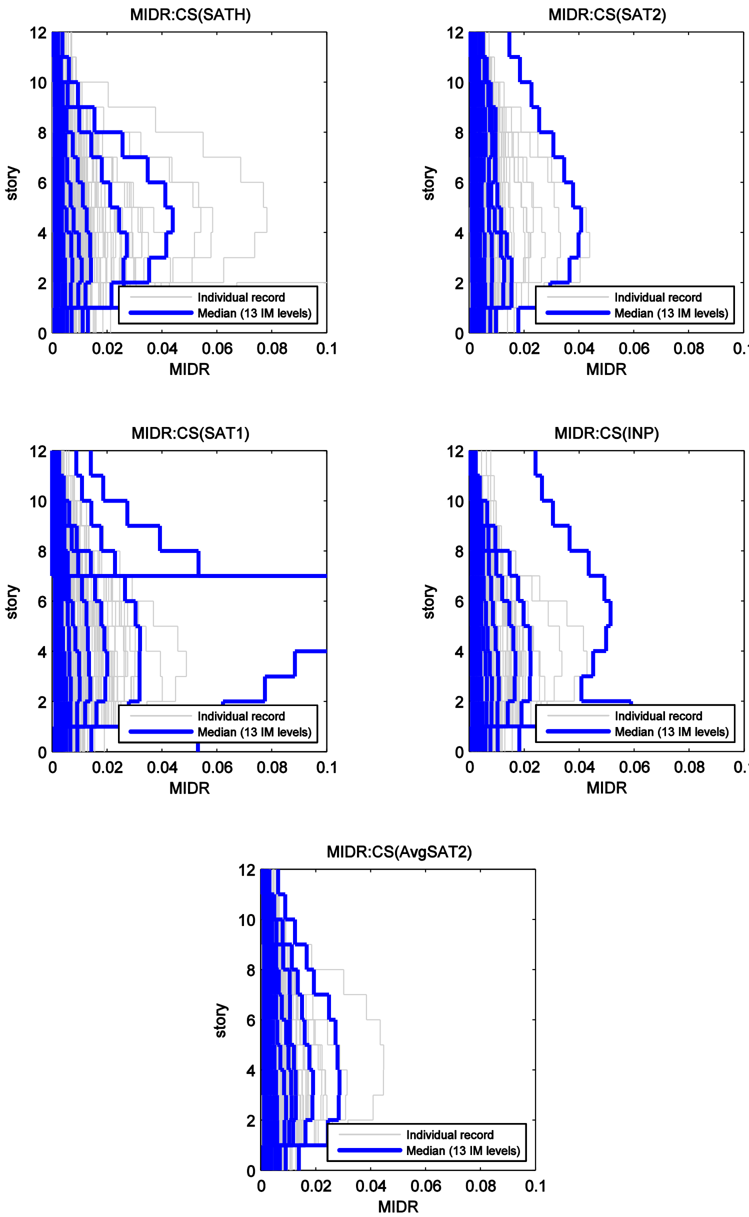

Figure E.12 Maximum Inter-story Drift Ratio (MIDR) profile obtained from nonlinear dynamic analysis for the 12-story building based on different record selection approaches

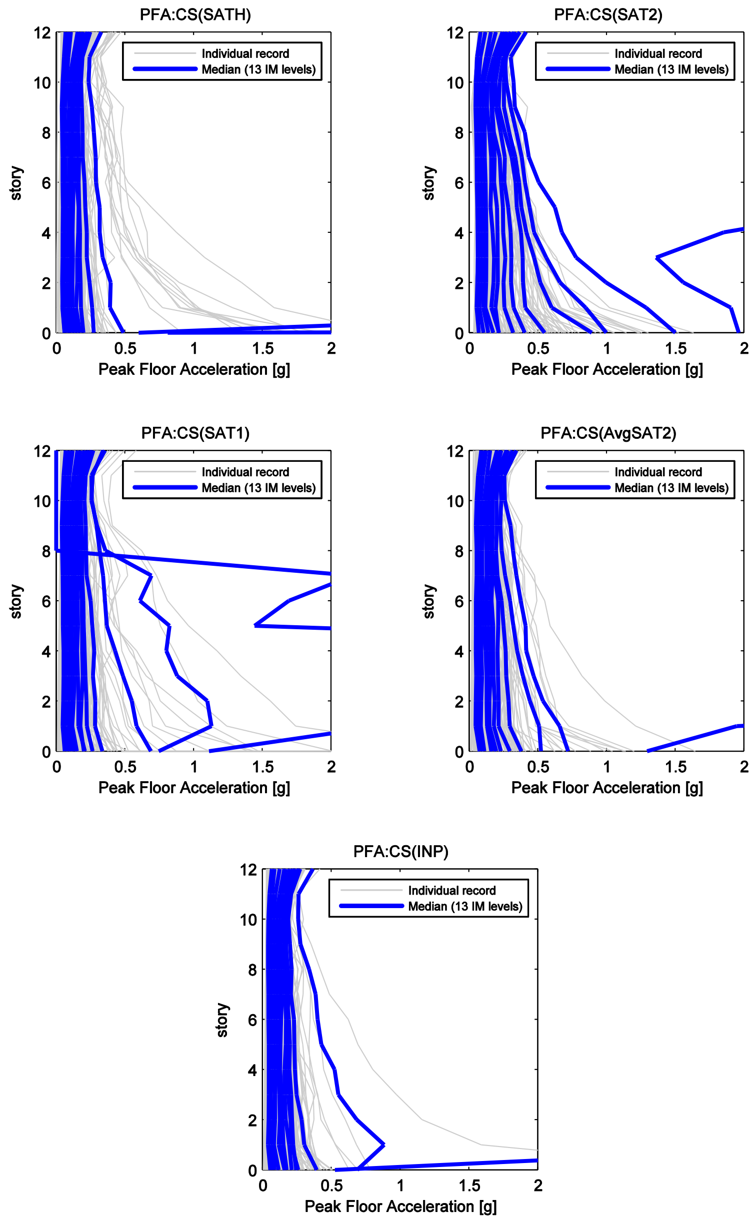

Figure E.13 Peak Floor Acceleration (PFA) profile obtained from nonlinear dynamic analysis for the 12-story building based on different record selection approaches

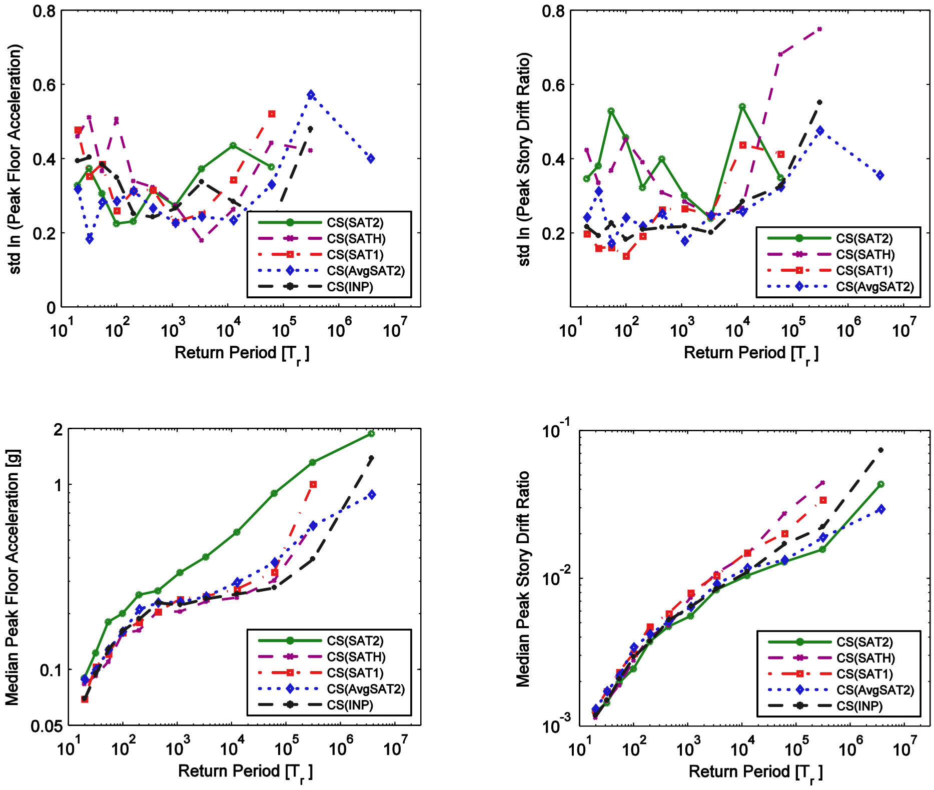

Figure E.14 Median and logarithmic standard deviation of Maximum Inter story Drift Ratio (MIDR) and Maximum Peak Floor Acceleration (MPFA) along the height obtained from nonlinear dynamic analysis for the 12-story building based on different record selection approaches

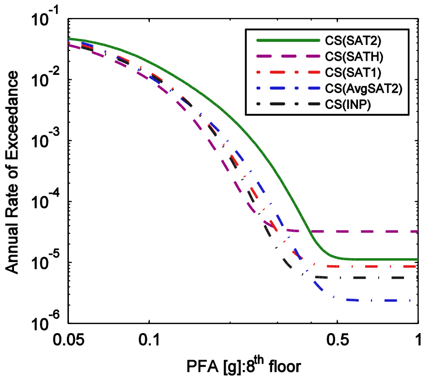

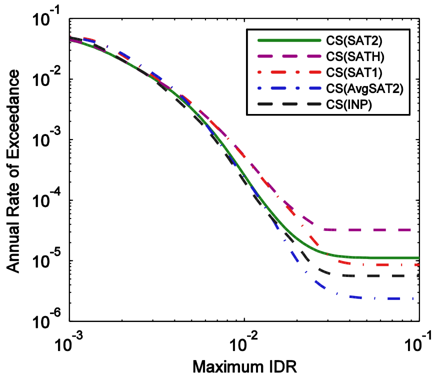

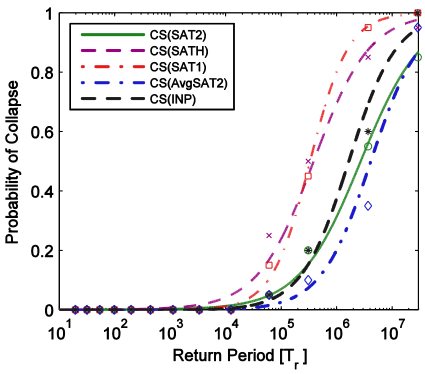

Figure E.15 Response hazard and collapse fragility curves obtained from nonlinear dynamic analysis for the 12-story based on different record selection approaches

E.6 RESULTS OBTAINED FOR THE 20-STORY BUILDING

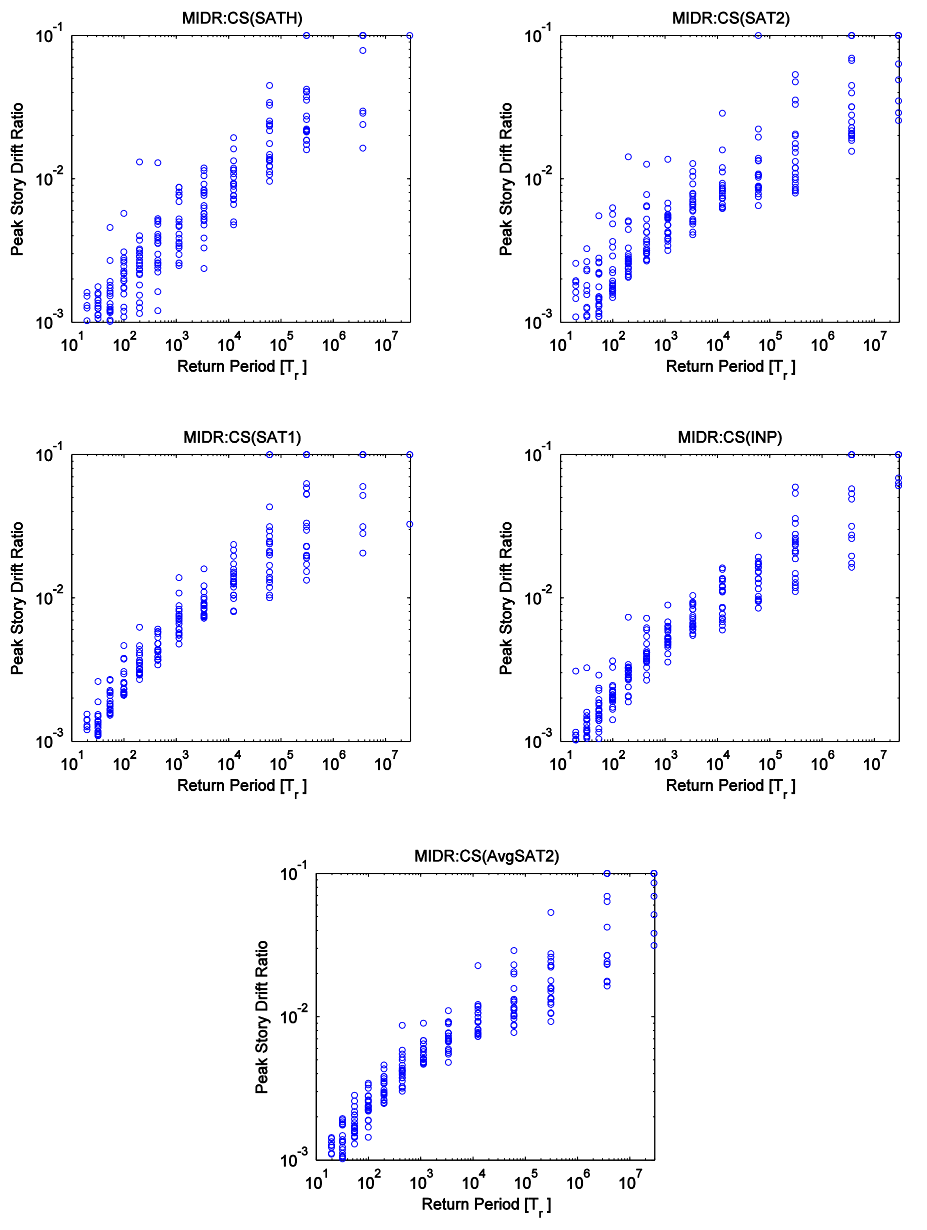

Figure E.16 Maximum Inter-story Drift Ratio (MIDR) along the height obtained from nonlinear dynamic analysis for the 20-story building based on different record selection approaches

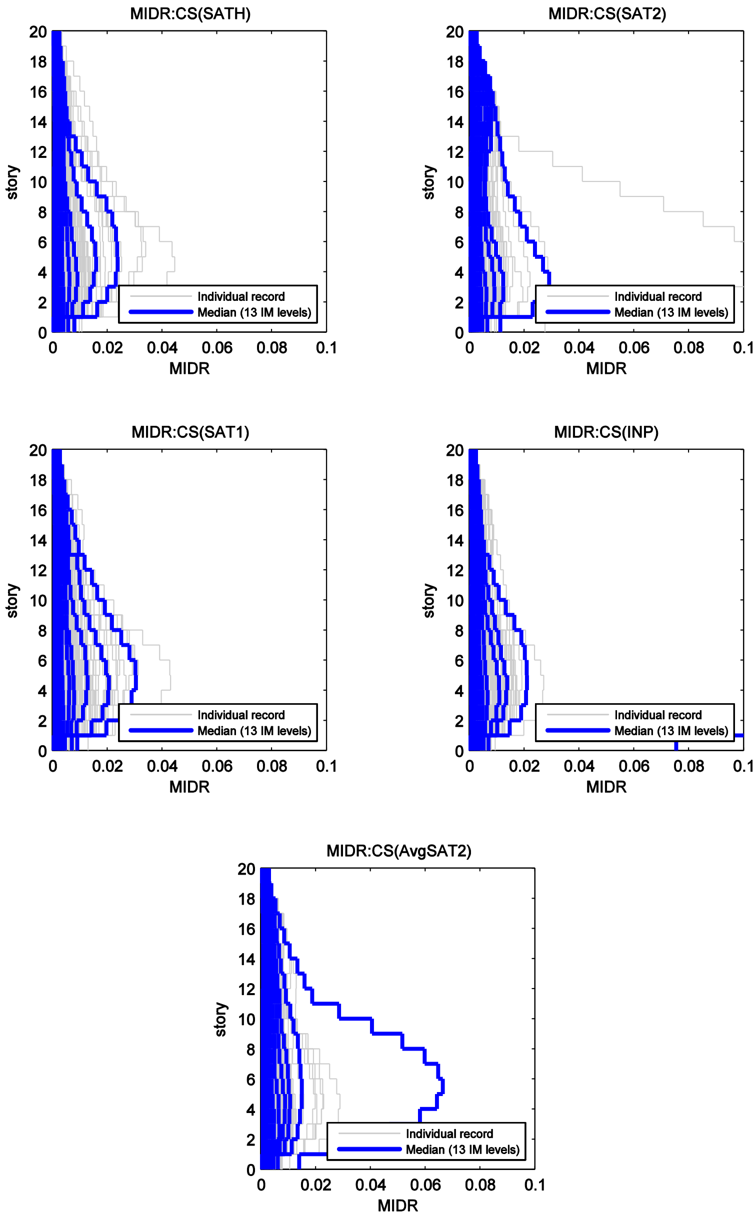

Figure E.17 Maximum Inter-story Drift Ratio (MIDR) profile obtained from nonlinear dynamic analysis for the 20-story building based on different record selection approaches

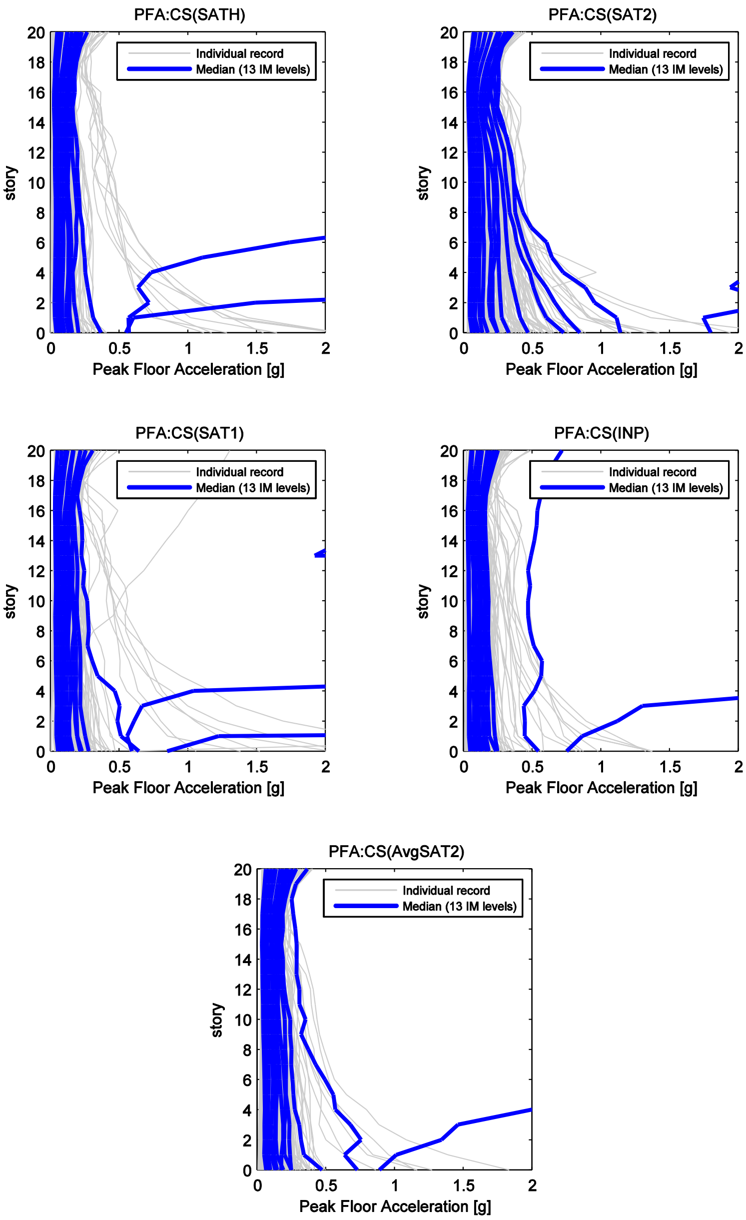

Figure E.18 Peak Floor Acceleration (PFA) profile obtained from nonlinear dynamic analysis for the 20-story building based on different record selection approaches

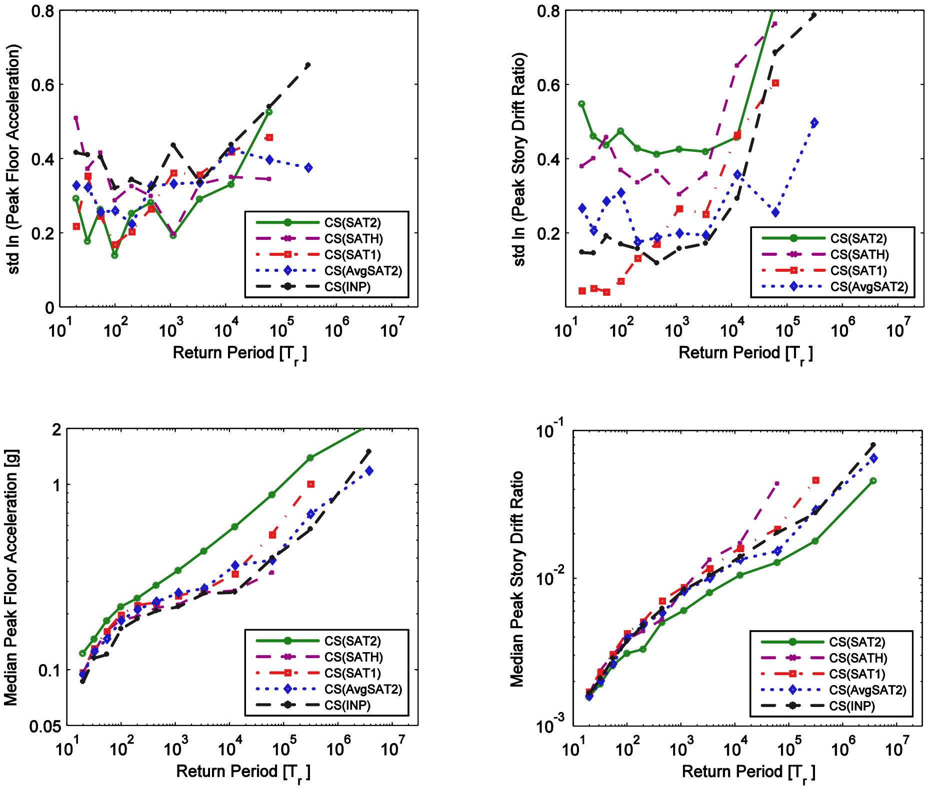

Figure E.19 Median and logarithmic standard deviation of Maximum Inter story Drift Ratio (MIDR) and Maximum Peak Floor Acceleration (MPFA) along the height obtained from nonlinear dynamic analysis for the 20-story building based on different record selection approaches

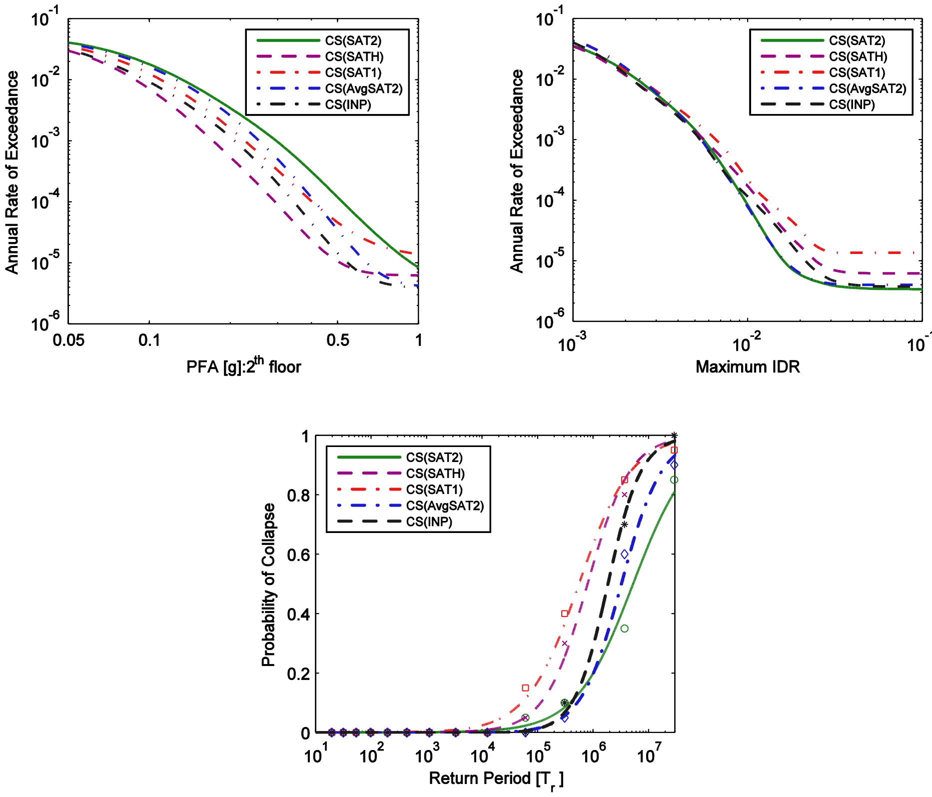

Figure E.20 Response hazard and collapse fragility curves obtained from nonlinear dynamic analysis for the 20-story based

E.7 HAZARD CONSISNTENCY VERIFICATION— 4-STORY

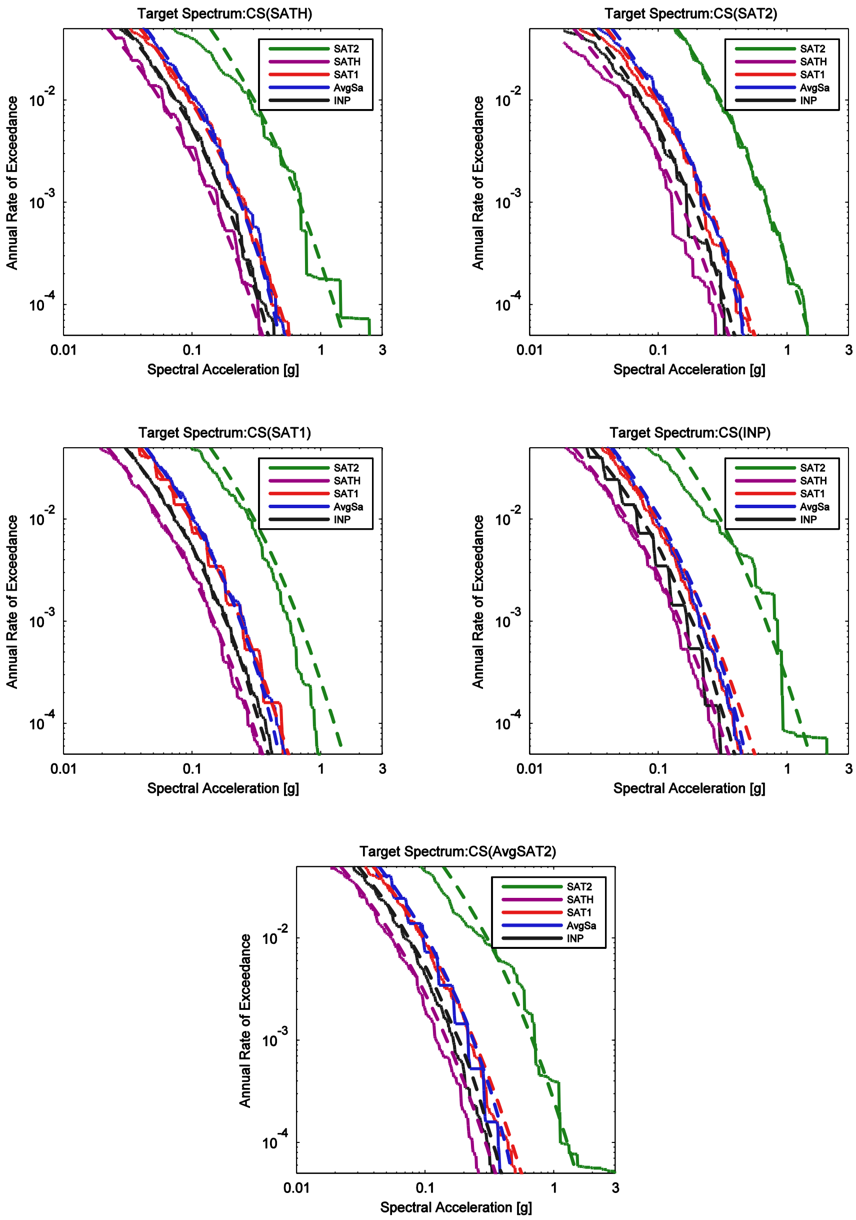

Figure E.21 Hazard consistency verification for conditional-spectrum based record sets selected for nonlinear dynamic analysis the 4- story building.

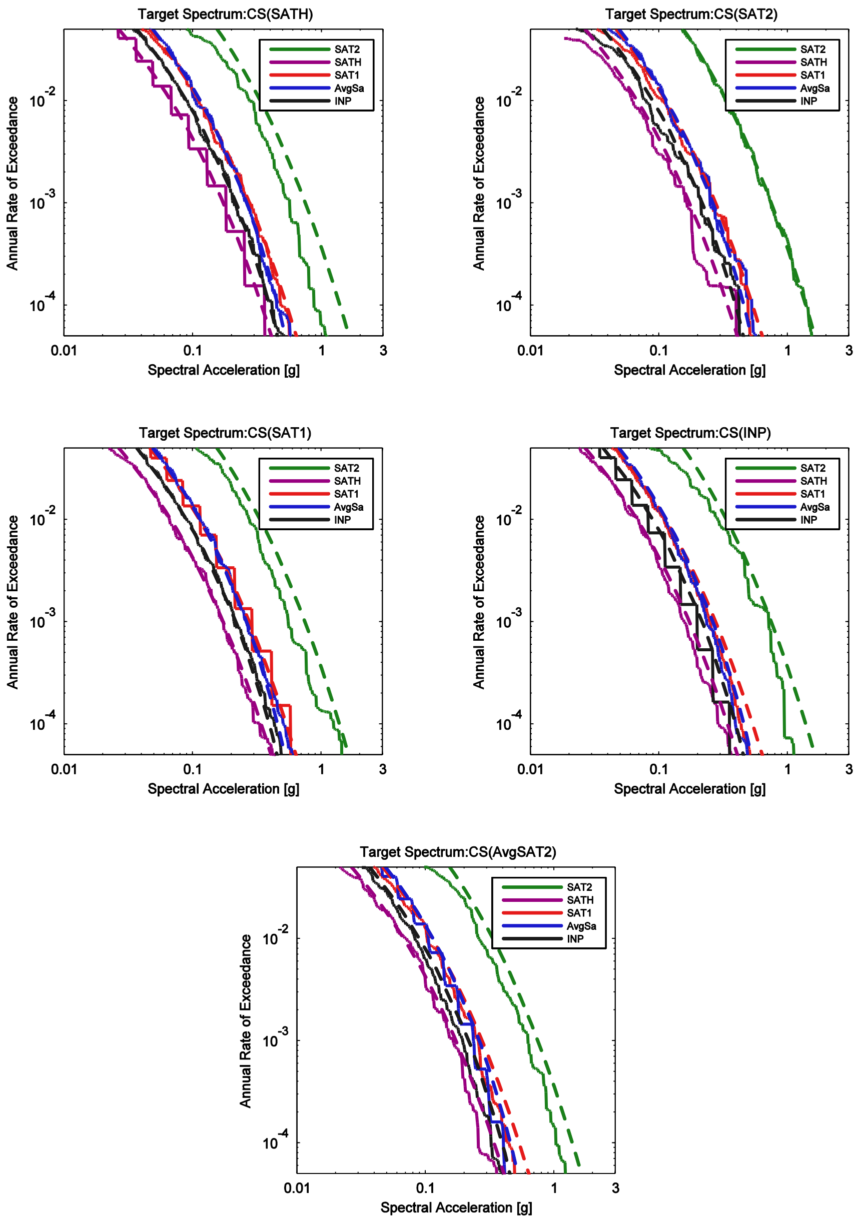

Figure E.22 Hazard consistency verification for conditional-spectrum based record sets selected for nonlinear dynamic analysis the 7- story building

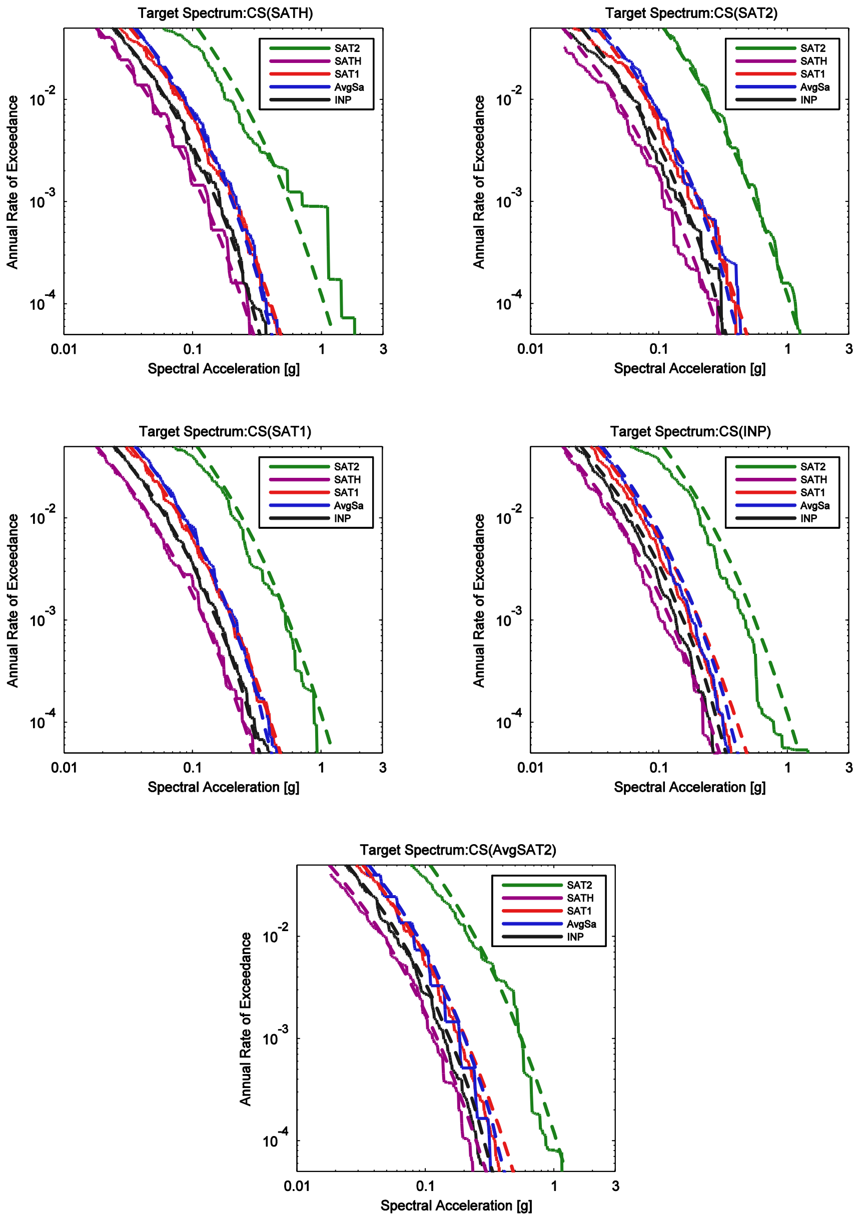

Figure E.23 Hazard consistency verification for conditional-spectrum based record sets selected for nonlinear dynamic analysis the 12- story building

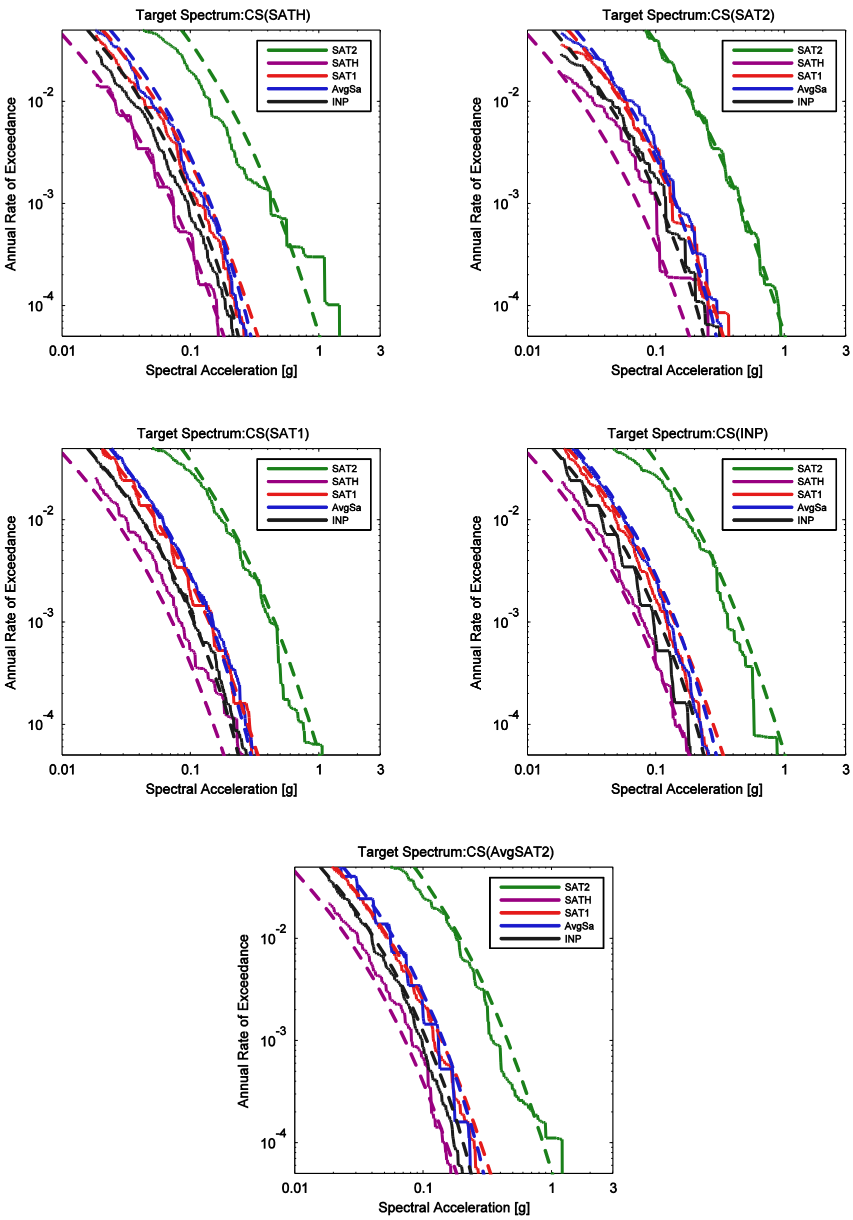

Figure E.24 Hazard consistency verification for conditional-spectrum based record sets selected for nonlinear dynamic analysis the 20- story building

E.8 HAZARD CONSISTENCY AND SCALE FACTOR

One of the features of the *AvgSA* in record selection as was discussed in chapter 5 is it its felexibity in scaling and hazard consistency. For selection of records with high return periods (rare event), when *SAT*1 is used, in order to provide a hazard consistent record set, the record selection is subjected to over-scaling of the ground motions (even more than 10) because there are not many natural rare records that are highly peaked in a single period. *AvgSA*, on the other hand, given that it is an average of the spectral accelerations in a period range, it is more likely to be present in the available records data bases and therefore, one can avoid over-scaling using CS(*AvgSA*). To illustrate this idea, an example is of record selection for 7- story building using SAT1 and *AvgSA* is performed. In this exercise the scale factor is limited to a maximum value of 2. A comparison between the target and the selected record set for the mean and standard deviation for IM level 12 is shown in Figure E.25. As can be seen for this IM level, CS(*AvgSA*) even with low scale factors (SF<2) is capable of providing a good match with the target; whereas, CS(*SAT*1) fails with this regard.

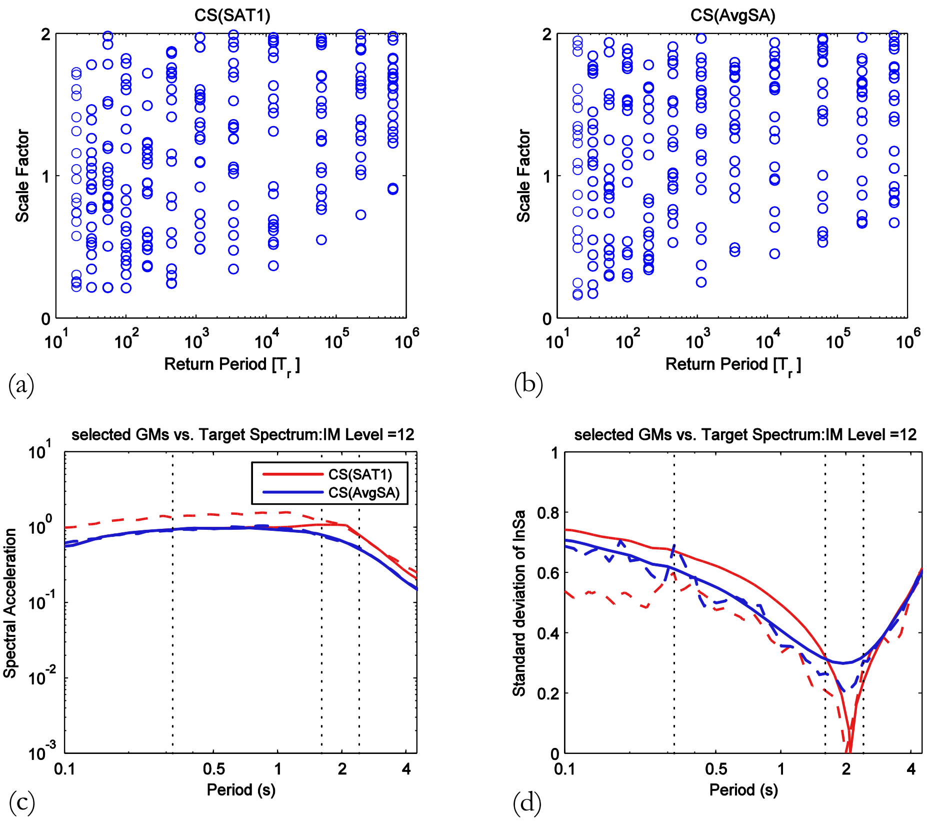

Figure E.25 Comparison between the scale factor and provided match when using CS(SAT1) and CS(AvgSA): a) Scale factors for CS(SAT1), b) Scale factors for CS(AvgSA), c) comparison of mean target spectrum and selected records, d) comparison of target and selected standard deviation of spectral acceleration.

Therefore, in all the records selected in this study, even though the scale factor was limited to be less than 4, in the case of CS($SAT1$), CS($SAT2$), CS($SATH$) for high return periods, this constrain was released (to less than 10) in order to have a good match between the selected records and target. The mean scale factors for each IM level and for all the IMs used here are shown in the Figure E.26. As can be seen in the last IM levels the scale factors related to single period *IMs* are increased to around 6 and 8.

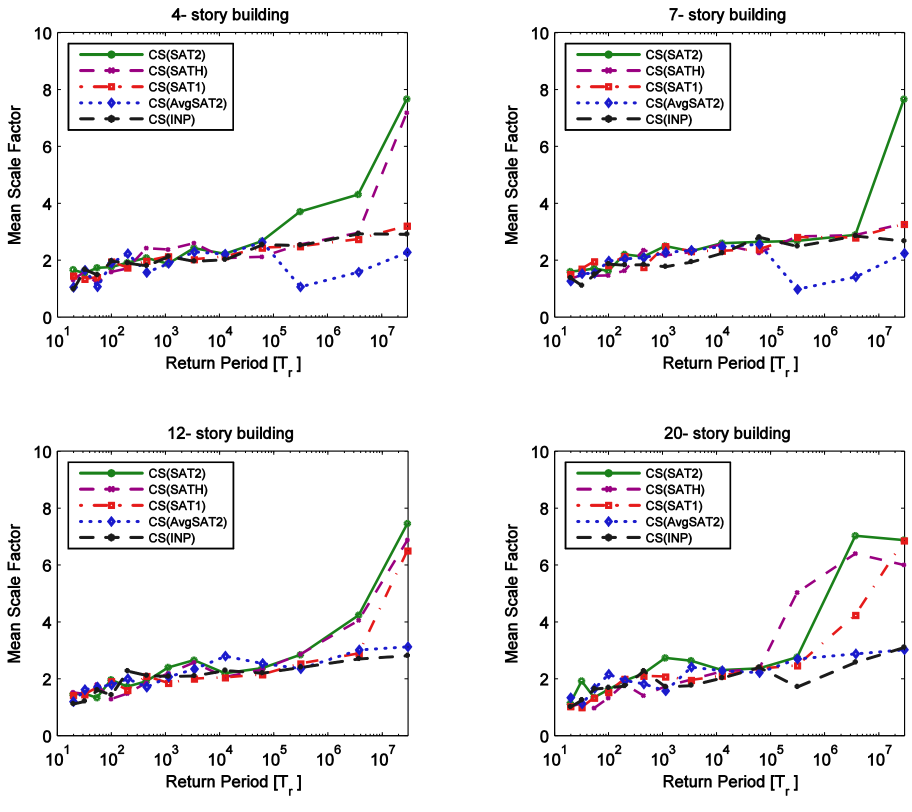

Figure E.26. Mean scale factors used in record selection for different IMs and for different buildings versus the IM return period

Appendix F: Building inventory components used for the loss estimation analysis in Chapter 4

Table F.1. Fragility functions & expected repair cost parameters for components of 3 story building

Comp.	Quant. per storey	Damage state	Fragility Function Parameters: Median IDR	Fragility Function Parameters: Median PFA [g]	Fragility Function Parameters: dispersion	Repair Cost: Median (€)	Repair Cost: dispersion	Reference
Beam-column (beam two sides)	6 X=3	DS1	0.0150		0.4	14750	0.28	FEMA P-58 B1041.061a
		DS2	0.0175		0.4	23300	0.23	
		DS3	0.0200		0.4	28300	0.22	
Beam-column (beam one side)	12 X=6	DS1	0.0150		0.4	14750	0.28	FEMA P-58 B1041.061a
		DS2	0.0175		0.4	23300	0.23	
		DS3	0.0200		0.4	28300	0.22	
Concrete stairs	1	DS1	0.0175		0.4	450	0.57	FEMA P-58 C2011.021a
		DS2	0.0225		0.4	2750	0.42	
		DS3	0.0322		0.4	18600	0.25	
Suspended Ceiling	6	DS1		0.9	0.4	250	0.39	FEMA P-58 C3032.001a
		DS2		1.5	0.4	1950	0.37	
		DS3		2.2	0.4	4400	0.15	
Hydraulic Elevator*	1	DS1		0.5	0.3	700	0.82	FEMA P-58 D1014.021
						3180	0.32	
						6060	0.44	
						1880	0.23	
Desktop electronics	5	DS1		0.4	0.4	700	0.3	FEMA P-58 E2022.023
Infill walls	8 per story 4: X	DS1	0.002	0.3	0.2	80(€/m²)	0.30	Obtained in this study
		DS2	0.008	0.4	0.3	200(€/m²)	0.20	
		DS3	0.011	0.6		300(€/m²)	0.15	

Table F.2. Fragility functions & expected repair cost parameters for components of 5- story building

Comp.	Quant. per storey	Damage state	Fragility Function Parameters			Repair Cost		Reference
			Median		dispersion	Median (€)	dispersion	
			IDR	PFA [g]				
Beam-column (beam two	17	DS1	0.015		0.4	14750	0.28	FEMA P-58
		DS2	0.017		0.4	23300	0.23	
	X=13	DS3	0.020		0.4	28300	0.22	B1041.061a
Beam-column (beam one side)	28	DS1	0.015		0.4	14750	0.28	FEMA P-58
		DS2	0.017		0.4	23300	0.23	
	X=10	DS3	0.020		0.4	28300	0.22	B1041.061a
Rectangular RC walls	23	DS1	0.005		0.36	6220	0.18	FEMA P-58
		DS2	0.010		0.30	14678	0.16	
	X=8	DS3	0.013		0.36	28498	0.15	B1044.001
Concrete stairs	1	DS1	0.017		0.4	450	0.57	FEMA P-58
		DS2	0.022		0.4	2750	0.42	
		DS3	0.032		0.4	18600	0.25	C2011.021a
Suspended Ceiling	8	DS1		0.9	0.4	250	0.39	FEMA P-58
		DS2		1.5	0.4	1950	0.37	
		DS3		2.2	0.4	4400	0.15	C3032.001a
Hydraulic Elevator*	1	DS1		0.5	0.3	700	0.82	FEMA P-58
						3180	0.32	D1014.021
						6060	0.44	
						1880	0.23	
Desktop electronics	20	DS1		0.4	0.4	700	0.3	FEMA P-58 E2022.023
Infill walls	19	DS1	0.002	0.3	0.2	80(€/m²)	0.30	Obtained in this study
		DS2	0.008	0.4	0.3	200(€/m²)	0.20	
	X=13	DS3	0.011	0.6		300(€/m²)	0.15	

Table F.3. Fragility functions & expected repair cost parameters for components of 8- story building

Comp.	Quant. per storey	Damage state	Fragility Function Parameters: Median IDR	Median PFA [g]	dispersion	Repair Cost: Median (€)	dispersion	Reference
Beam-column (beam two	11 X=2	DS1	0.0150		0.4	14750	0.28	FEMA P-58 B1041.061a
		DS2	0.0175		0.4	23300	0.23	
		DS3	0.0200		0.4	28300	0.22	
Beam-column (beam one side)	9 X=3	DS1	0.0150		0.4	14750	0.28	FEMA P-58 B1041.061a
		DS2	0.0175		0.4	23300	0.23	
		DS3	0.0200		0.4	28300	0.22	
Rectangular RC walls	12 X=12	DS1	0.0055		0.36	6220	0.18	FEMA P-58 B1044.001
		DS2	0.0109		0.30	14678	0.16	
		DS3	0.0130		0.36	28498	0.15	
Concrete stairs	1	DS1	0.0175		0.4	450	0.57	FEMA P-58 C2011.021a
		DS2	0.0225		0.4	2750	0.42	
		DS3	0.0322		0.4	18600	0.25	
Suspended Ceiling	4	DS1		0.9	0.4	250	0.39	FEMA P-58 C3032.001a
		DS2		1.5	0.4	1950	0.37	
		DS3		2.2	0.4	4400	0.15	
Hydraulic Elevator*	1	DS1		0.5	0.3	700	0.82	FEMA P-58 D1014.021
						3180	0.32	
						6060	0.44	
						1880	0.23	
Desktop electronics	15	DS1		0.4	0.4	700	0.3	FEMA P-58 E2022.023
Infill walls	10 X=4(0 at floor 1^{st}) Y=6	DS1	0.002	0.3	0.2	80(€/m^2)	0.30	Obtained in this study
		DS2	0.008	0.4	0.3	200(€/m^2)	0.20	
		DS3	0.011	0.6		300(€/m^2)	0.15	

REFERENCES

Akkar, S., Sucuoglu, H., and Yakut, A. [2005] "Displacement-based fragility functions for low- and mid-rise ordinary concrete buildings," *Earthquake Spectra*, Vol. 21, No. 4, pp. 901–927.

Akkar, S.M.A., Sandıkkaya, and B.Ö., A. [2014] "Compatible ground-motion prediction equations for damping scaling factors and vertical-to-horizontal spectral amplitude ratios for the broader European region," *Bulletin of Earthquake Engineering*, Vol. 12, No. 1, pp. 517-547.

Angel, R., Abrams, D., Shapiro, D., Uzarski, J., Webster, M. [1994] "Behaviour of reinforced concrete frames with masonry infills."

Aslani, H., and Miranda, E. [2005] "Probabilistic earthquake loss estimation and loss disaggregation in buildings," *Ph.D. thesis*, John A. Blume Earthquake Engineering Centre, Department of Civil and Environmental Engineering, Stanford University.

Asteris, P.G. [2008] "Finite element micro-modeling of infilled frames," *Electronic Journal of Structural Engineering*, Vol. 8, pp. 1-11.

ATC [1985] "Earthquake Damage Evaluation Data for California," Redwood City, California, U.S.A.

Azarbakht, A., Mousavi, M., Nourizadeh, M. and Shahri, M. [2014] "Dependence of correlations between spectral accelerations at multiple periods on magnitude and distance.," *Earthquake engineering and structural dynamics*, Vol. 43, pp. 1193–1204.

Baker J.W. and Cornell, C.A. [2005] "A Vector-Valued Ground Motion Intensity Measure Consisting of Spectral Acceleration and Epsilon," *Earthquake engineering and structural dynamics*, Vol. 34, No. 10, pp. 1193-1217.

Baker J.W. and Cornell, C.A. [2006] "Which Spectral Acceleration Are You Using? ," *Earthquake Spectra*, Vol. 22, No. 2, pp. 293–312.

Baker J.W. and Cornell, C.A. [2008a] "Vector-valued intensity measures for pulse-like near-fault ground motions," *Engineering Structures*, Vol. 30, No. 4, pp. 1048–1057.

Baker J.W. and Cornell, C.A. [2008b] "Vector-valued intensity measures incorporating spectral shape for prediction of structural response," *Journal of Earthquake Engineering*, Vol. 12, No. 4, pp. 534–554.

Baker, J.W. [2007] "Probabilistic structural response assessment using vector‐valued intensity measures," *Earthquake engineering and structural dynamics*, Vol. 36, No. 13, pp. 1861‐1883.

Baker, J.W. [2008a] "Introducing correlation among fragility functions for multiple components," *14th World Conference on Earthquake Engineering, Beijing, China*.

Baker, J.W. [2011] "The conditional mean spectrum: A tool for ground motion selection," *ASCE Journal of Structural Engineering*, Vol. 137, pp. 322–331.

Baker, J.W. [2015] "Efficient analytical fragility function fitting using dynamic structural analysis.," *Earthquake Spectra*, Vol. 31, No. 1, pp. 579-599.

Baker, J.W., and Cornell C.A. [2006] "Spectral shape, epsilon and record selection," *Earthquake engineering and structural dynamics*, Vol. 35, No. 9, pp. 1077–1095.

Baker, J.W., and Jayaram, N. [2008b] "Correlation of spectral acceleration values from NGA ground motion models," *Earthquake Spectra*, Vol. 24, pp. 299–317.

Bal, I., Crowley, H., Pinho, R and Gulay, G., [2007] "Structural characteristics of Turkish building stock in Northern Marmara Region for Loss Assessment Applications," IUSS Press.

Barbat, A.H., Yépez Moya, F. and Canas, J.A. [1996] "Damage Scenarios Simulation for Seismic Risk Assessment in Urban Zones," *Earthquake Spectra*, Vol. 12, No. 3, pp. 371-394.

Barrera, M.J. [2015] "Masonry Infill Wall Collapse Fragilities," *M.Sc. thesis*, UME School/ROSE Pragramme, IUSS Pavia.

Bashandy, T., R. Rubiano, R. Klinger [1995] "Evaluation and analytical verification of infilled frame test data," IL 61826-9005.

Bazzurro, P. [1998] "Probabilistic Seismic Demand Analysis," Department. of Civil and Environmental Engineering, Stanford University.

Bazzurro, P., and Cornell, C.A. [1999] "Disaggregation of Seismic Hazard," *Bulletin of Seismological Society of America*, Vol. 89, No. 2, pp. 501-529.

Bazzurro, P., and Cornell, C.A., [2001] "Vector-valued Probabilistic Seismic Hazard Analysis," *Seismological Research Letters*, Vol. 72, No. 2.

Bazzurro, P., Park, J, Tothong, P, [2010] "Vector-Valued Probabilistic Seismic Hazard Analysis of Correlated Ground Motion Parameters."

Bazzurro, P., Tothong, P., Park, J. [2009] "Efficient Approach to Vector-valued Probabilistic Seismic Hazard Analysis of Multiple Correlated Ground Motion Parameters," *10th International Conference on Structural Safety and Reliability (ICOSSAR09), Osaka, Japan*.

Bianchini, M., Diotallevi, P., and Baker, J. W. [2009] "Prediction of Inelastic Structural Response Using an Average of Spectral Accelerations," *10th International Conference on Structural Safety and Reliability (ICOSSAR09), Osaka, Japan*.

Bojórquez, E., Iervolino, I. [2011] "Spectral shape proxies and nonlinear structural response," *Soil Dynamics and Earthquake Engineering*, Vol. 31, No. 7, pp. 996–1008.

Bommer, J.J.a.C., H. [2006] "The Influence of Ground-Motion Variability in Earthquake Loss Modelling," *Bulletin of Earthquake Engineering and Design*, Vol. 4, No. 3, pp. 231-248.

Boore, D.M., and Atkinson, G. M [2008] "Ground-Motion Prediction Equations for the Average Horizontal Component of PGA, PGV, and 5%-Damped PSA at Spectral Periods between 0.01 s and 10.0 s," *Earthquake Spectra*, Vol. 24, No. 1, pp. 99-138.

Bradley, B.A. [2010a] "A generalized conditional intensity measure approach and holistic ground-motion selection," *Earthquake engineering and structural dynamics*, Vol. 39, No. 12, pp. 1321–1342.

Bradley, B.A. [2011a] "Correlation of significant duration with amplitude and cumulative intensity measures and its use in ground motion selection," *Journal of Earthquake Engineering*, Vol. 15, No. 6, pp. 809–832.

Bradley, B.A. [2011b] "Empirical correlation of PGA, spectral accelerations and spectrum intensities from active shallow crustal earthquakes," *Earthquake engineering and structural dynamics*, Vol. 40, No. 15, pp. 1707–1721.

Bradley, B.A. [2012a] "Empirical correlations between peak ground velocity and spectrum-based intensity measures," *Earthquake Spectra*, Vol. 28, No. 1, pp. 37-54.

Bradley, B.A. [2012b] "Empirical correlations between peak ground velocity and spectrum-based intensity measures.," *Earthquake Spectra*, Vol. 28, No. 1, pp. 17–35.

Bradley, B.A. [2012c] "Ground motion selection algorithm based on the generalized conditional intensity measure approach," *Soil Dynamics and Earthquake Engineering.*, Vol. 48, No. 0, pp. 48–61.

Bradley, B.A. [2012d] "The seismic demand hazard and importance of the conditioning intensity measure," *Earthquake engineering and structural dynamics*, Vol. 41, No. 11, pp. 1417–1437.

Bradley, B.A. [2013] "A comparison of intensity-based demand distributions and the seismic demand hazard for seismic performance assessment," *Earthquake engineering and structural dynamics*, Vol. 42, pp. 2235–2253.

Bradley, B.A., and Lee, D.S. [2010b] "Component correlations in structure-specific seismic loss estimation," *Earthquake engineering and structural dynamics*, Vol. 39, No. 3, pp. 237–258.

Bradley, B.A., Dhakal R.P., MacRae, G.A., and Cubrinovski, M. [2009a] "Prediction of spatially distributed seismic demands in specific structures: Ground motion and structural response," *Earthquake engineering and structural dynamics*, Vol. 39, pp. 501–520.

Bradley, B.A., Dhakal R.P., MacRae, G.A., and Cubrinovski, M. [2009b] "Prediction of spatially distributed seismic demands in specific structures: Structural response to loss estimation," *Earthquake engineering and structural dynamics*, Vol. 39, pp. 591–613.

Braga, F., Dolce, M. and Liberatore, D. [1982] "A Statistical Study on Damaged Buildings and an Ensuing Review of the MSK-76 Scale," *Proceedings of the Seventh European Conference on Earthquake Engineering*, Athens, Greece.

Calvi, G.M., Bolognini D. [1999] "Seismic response of R.C. frames infilled with weakly reinforced hollow masonry panels.," Università degli Studi di Pavia, Dipartimento di Meccanica Strutturale.

Calvi, G.M., Bolognini D. [2001] "Seismic response of R.C. frames infilled with weakly reinforced masonry panels," *Journal of Earthquake Engineering*, Vol. 5, No. 2, pp. 153 - 185.

Calvi, G.M.a.P., R. [2004] "LESSLOSS. A European Integrated Project on Risk Mitigation for Earthquakes and Landslides," European School for Advanced Studies in Reduction of Seismic Risk (ROSE School).

Carr, A.J. [2007] "Ruaumoko Manual, Volume 2: User manual for the 2-dimensional version RUAUMOKO2D.," Cristchurch, New Zealand.

Cordova, P.P., Deierlein, G.G., Mehanny, S.S., and Cornell, C.A. [2000] "Development of a two-parameter seismic intensity measure and probabilistic assessment procedure," *2nd US–Japan Workshop on Performance-based Earthquake Engineering Methodology for RC Building Structures, Sapporo, Hokkaido, 2000.*

Cornell, C., Jalayer, F., Hamburger, RO., Foutch DA [2002] "Probabilistic basis for 2000 SAC federal emergency management agency steel moment frame guidelines," *Journal of Structural Engineering*, Vol. 128, No. 4, pp. 526–533.

Cornell, C.A. [1968] "Engineering seismic risk analysis," *Bulletin of Seismological Society of America*, Vol. 58, pp. 1583-1606.

Cornell, C.A., and Krawinkler, H. [2000] "Progress and challenges in seismic performance assessment."

Crisafulli, F., Carr, A., Park, R. [1997a] "Analytical modeling of frame structures – a general review," *Bulletin of the NZ Society for Earthquake Engineering*, Vol. 33, No. 1, pp. 30-47.

Crisafulli, F.J. [1997b] "Seismic behaviour of reinforced concrete Sreuctures with masonry infills," *Ph.D. Thesis*, Department of Civil Engineering, University of Canterbury.

Di Pasquale, G., Orsini, G. and Romeo, R.W. [2005] "New Developments in Seismic Risk Assessment in Italy," *Bulletin of Earthquake Engineering,*, Vol. 3, No. 1, pp. 101-128.

Doherty, K., Griffith, M.C., Lam, N., and Wilson, J. [2002] "Displacement-based seismic analysis for out-of-plane bending of unreinforced masonry walls," *Earthquake engineering and structural dynamics*, Vol. 31, No. 4, pp. 833–850.

Dolce, M., Masi, A., Marino, M. and Vona, M. [2003] "Earthquake Damage Scenarios of the Building Stock of Potenza (Southern Italy) Including Site Effects," *Bulletin of Earthquake Engineering and Design*, Vol. 1, No. 1, pp. 115-140.

Dumova-Jovanoska, E. [2004] "Fragility Curves for RC Structures in Skopje Region," *Proceedings of the 13th World Conference on Earthquake Engineering*, Vancouver, Canada.

Eads, L., Miranda, E. and Lignos, D.G. [2015] "Average spectral acceleration as an intensity measure for collapse risk assessment " *Earthquake Engineering & Structural Dynamics*.

Faggella, M., Barbosa, A.R., Conte, J.P., Spacone, E., and Restrepo, J.I. [2013] "Probabilistic seismic response analysis of a 3-D reinforced concrete building," *Structural Safety*, Vol. 44, pp. 11–27.

Fajfar, P., Vidic, T., and Fishinger [1990] "A measure of earthquake motion capacity to damage medium-period structures," *Soil Dynamics and Earthquake Engineering*, Vol. 9, No. 5, pp. 236-242.

Fardis, M.N. [2002] "Design of an irregular building for the SPEAR project—description of the 3-storey structure," Structures Laboratory, Greece.

FEMA-2000, F.E.M.A. "Prestandard and Commentary for the Seismic Rehabilitation of Buildings," FEMA 356.

FEMA [1999] "HAZUS99 Technical Manual," Washington, DC, U.S.A.

FEMA [2001] "HAZUS99 Estimated Annualized Earthquake Loss for the United States," Washington, DC, U.S.A.

FEMA [2003] "HAZUS-MH Technical Manual," Washington, DC, U.S.A.

FEMA [2012] "Seismic Performance Assessment of Buildings, FEMA P-58-1," *Applied Technology Council for the Federal Emergency Management Agency*.

Flanagan, R.D., Bennett, R. M. [1999] "In-plane behaviour of structural clay tile infilled frames". Journal of Structural Engineering," *Journal of Structural Engineering*, Vol. 125, No. 6, pp. 590 - 599.

Genz, A., and Bertz, F., [1999] "Numerical computation of Multivariate t probabilities with application to power calculation of Multiple Contrasts," *J. Statist. Comput. Simul*, Vol. 63, pp. 361-378.

Genz, A., and Bertz, F., [2002] "Comparison of methods for computation of multivariate t probabilities," *J. Comp. Graph. Stat*, Vol. 11, No. 4, pp. 950-971.

Giardini, D., et al. [2013] "Seismic Hazard Harmonization in Europe (SHARE)," *Online data resource, Swiss Seismological Service*, pp. ETH Zurich, Zurich, Switzerland, [Available at: http://www.efehr.org:8080/jetspeed/].

Giovinazzi, S. [2005] "The Vulnerability Assessment and the Damage Scenario in Seismic Risk Analysis," Technical University Carolo-Wilhelmina at Braunschweig, Braunschweig, Germany and University of Florence, Florence, Italy.

Goda, K., Hong H.P. [2008] "Spatial correlation of peak ground motions and response spectra," *Bulletin of the Seismological Society of America*, Vol. 98, No. 1, pp. 354-365.

Goulet, C.A., Haselton, C.B., Mitrani-Reiser, J., Beck, J.L., Deierlein, G.G., Porter, K., and Stewart, J.P. [2007] "Evaluation of the seismic performance of a code-conforming reinforced-concrete frame building—from seismic hazard to collapse safety and economic losses," *Earthquake engineering and structural dynamics*, Vol. 36, No. 13, pp. 1973–1997.

Gülerce, Z., and Abrahamson, N.A. [2010] "Vector-valued Probabilistic Seismic Hazard Assessment for the Effects of Vertical Ground Motions on the Seismic Response of Highway Bridges," *Earthquake Spectra EERI*.

Hak, S. [2010] "Seismic behaviour of clay masonry infills in framed structures," Istituto Universitario di Studi Superiori di Pavia Università degli Studi di Pavia.

Haselton, C., Baker, J., Liel, A., and Deierlein, G. [2011] "Accounting for ground-motion spectral shape characteristics in structural collapse assessment through an adjustment for epsilon," *Journal of Structural Engineering*, Vol. 137, No. Earthquake Ground Motion Selection and Modification for Nonlinear Dynamic Analysis of Structures, pp. 332–344.

Holmes, M. [1961] "Steel frames with brckwork and concrete filling," *Proceedings of the Institute of Civil Engineers*.

Inoue, T. [1990] "Seismic Hazard Analysis of Multi-Degree-of-Freedom Structures," Stanford University, Stanford,.

Jalayer, F. [2003] "Direct Probabilistic Seismic Analysis: Implementing Non-linear Dynamic Assessment," Department of Civil and Environmental Engineering, Stanford University, Stanford, CA.

Jalayer, F., and Cornell, C.A. [2004] *A technical framework for probability-based demand and capacity factor design (DCFD) seismic formats*, University of California, Berkeley, PEER Report 2003/08, Pacific Earthquake Engineering Research Center.

Jalayer, F., and Cornell, C.A. [2009] "Alternative nonlinear demand estimation methods for probability-based seismic assessments," *Earthquake engineering and structural dynamics*, Vol. 38, No. 8, pp. 951–972.

Jayaram, N., and Baker, J. W., [2008] "Statistical tests of the joint distribution of spectral acceleration values," *Bulletin of the Seismological Society of America*, Vol. 28, pp. 2231–2243.

Jayaram, N., Lin, T., Baker, J.W. [2011] "A Computationally Efficient Ground-Motion Selection Algorithm for Matching a Target Response Spectrum Mean and Variance.," *Earthquake Spectra*, Vol. 27, No. 3, pp. 797–815.

Jayaram, N., Shome, N., Rahnama, M. [2012] "Development of earthquake vunerability functions for tall buildings," *Earthquake Engineering & Structural Dynamics*, Vol. 41, pp. 1495–1514.

Kadysiewski, S., and Mosalam, K.M. [2009a] *Modeling of Unreinforced Masonry Infill Walls Considering In-plane and Out-of-Plane Interaction*, University of California, Berkeley, PEER Report 2008/102, Pacific Earthquake Engineering Research Center.

Kadysiewski, S.a.M., K.M. [2009b] "Modeling of Unreinforced Masonry Infill Walls Considering In-plane and Out-of-Plane Interaction," Pacific Earthquake Engineering Research Center.

Kappos, A.J., Pitilakis, K. and Stylianidis, K.C. [1995] "Cost-Benefit Analysis for the Seismic Rehabilitation of Buildings in Thessaloniki, Based on a Hybrid Method of Vulnerability Assessment," *Proceedings of the Fifth International Conference on Seismic Zonation*, Nice, France.

Kappos, A.J., Stylianidis, K.C. and Pitilakis, K. [1998] "Development of Seismic Risk Scenarios Based on a Hybrid Method of Vulnerability Assessment," *Natural Hazards*, Vol. 17, No. 2, pp. 177-192.

Kazantzi, A.K., and Vamvatsikos, D. [2015a] "Intensity measure selection for vulnerability studies of building classes," *Earthquake engineering and structural dynamics*, pp. DOI: 10.1002/eqe.2603.

Kazantzi, A.K., and Vamvatsikos, D. [2015b] "Intensity measure selection for vulnerability studies of building classes," *Earthquake Engineering and Structural Dynamics*.

Kennedy, R.P., and Ravindra, M.K. [1984] "Seismic fragilities for nuclear power plant risk studies," *Engineering and Design*, Vol. 79, No. 1, pp. 47–68.

Kohrangi, M. [2015a] "Beyond scalar Intensity Measures in seismic risk assessment," *PhD Thesis*, UME School/ROSE Programme, IUSS-Pavia.

Kohrangi, M. [2015b] "CS(AvgSA) software,
https://drive.google.com/open?id=0B6og4ZbhkXLSVnlad19udXdWaTA."

Kohrangi, M. [2015c] "Vector PSHA software,
https://drive.google.com/file/d/0B1VUIW9KJ1exaFMwcHRUdk9xTkk/view?usp=sharing."

Kohrangi, M., Bazzurro, P., and Vamvatsikos, D. [2015d] "Conditional Spectrum-based ground motion selectuon using average spectral acceleration," *Earthquake engineering and structural dynamics*, Vol. (Under review).

Kohrangi, M., Bazzurro, P., and Vamvatsikos, D. [2015e] "Vector and Scalar IMs in Structural Response Estimation: Part I–Hazard Analysis," *Earthquake Spectra (Under review)*.

Kohrangi, M., Bazzurro, P., and Vamvatsikos, D. [2015f] "Vector and Scalar IMs in Structural Response Estimation: Part II–Building Demand Assessment," *Earthquake Spectra. (Under review)*.

Komaraneni, S. [2009] "Out of plane seismic behavior of brick masonry infilled panels with prior in plane damage," Dept. of Civil Engineering, Indian Institute of Technology, Kanpur.

Kramer, S.L. [1996] *Geotechnical Earthquake Engineering*, Prentice-Hall.

Kramer., S.a.M., RA., [2006] "Ground motion intensity measures for liquefaction hazard evaluation," *Earthquake Spectra*, Vol. 22, No. 2, pp. 413–438.

Krawinkler, H. [2005] *Van Nuys hotel building testbed report: exercising seismic performance assessment*, University of California, Berkeley, PEER Report 2005/11, Pacific Earthquake Engineering Research Centre.

Kutner, M.H., Nachtsheim, C. J., Neter, J., [2004] *Applied linear regression models*, McGraw-Hill.

Kutner, M.H., Nachtsheim, C.J., and Neter, J. [2005] *Applied linear regression models (5-th edition)*, McGraw-Hill/Irwin: New York.

Kwong, N.S., Chopra, A., K. and McGuire R., K., [2015] "A framework for the evaluation of ground motion selection and modification procedures," *Earthquake Engineering & Structural Dynamics*, Vol. 44, No. 5, pp. 795–815.

Liel, A.B., Haselton, C.B., Deierlein, G.G., and Baker, J.W. [2009] "Incorporating modeling uncertainties in the assessment of seismic collapse risk of buildings," *Structural Safety*, Vol. 31, No. 2, pp. 197–211.

Lin, T., Harmsen SC, Baker JW, Luco N., [2013a] "Conditional spectrum computation incorporating multiple causal earthquakes and ground motion prediction models," *BSSA*, Vol. 103, No. 2A, pp. 1103–1116.

Lin, T., Haselton, C.B. and Baker J.W. [2013b] "Conditional spectrum-based ground motion selection. Part I: Hazard consistency for risk-based assessments," *Earthquake engineering and structural dynamics*, Vol. 42, No. 12, pp. 1847-1865.

Lin, T., Haselton, C.B. and Baker J.W. [2013c] "Conditional spectrum-based ground motion selection. Part II: Intensity-based assessments and evaluation of alternative target spectra," *Earthquake engineering and structural dynamics*, Vol. 42, pp. 1867–1884.

Lucchini, A., Mollaioli, F., and Monti, G. [2011] "Intensity measures for response prediction of a torsional building subjected to bi-directional earthquake ground motion," *Bulletin of Earthquake Engineering*, Vol. 9, No. 5, pp. 1499–1518.

Luco, N. [2002] "Probabilistic seismic demand analysis, SMRF connection fractures, and near-source effects," *Ph.D. thesis*, Dept. of Civil and Env. Engineering, Stanford University, California.

Luco, N., and Bazzurro, P. [2007a] "Does amplitude scaling of ground motion records result in biased nonlinear structural drift responses?," *Earthquake engineering and structural dynamics*, Vol. 36, No. 13, pp. 1813-1836.

Luco, N., and Cornell, C.A. [2007b] "Structure-Specific Scalar Intensity Measures for Near-Source and Ordinary Earthquake Ground Motions," *Earthquake Spectra*, Vol. 23, No. 2, pp. 357–392.

Madan, A., Reinhorn, A. M., Mander, J. B., Valles, R. E. [1997] "Modelling of masonry infill panels for structural analysis," *Journal of Structural Engineering*, No. 123, pp. 1295-1302.

Mainstone, R.J. [1971] "On the stiffnesses and strengths of infilled frames."

Masi, A. [2003] "Seismic Vulnerability Assessment of Gravity Load Designed R/C Frames," *Bulletin of Earthquake Engineering and Design*, Vol. 1, No. 3, pp. 371-395.

McGuire, R.K. [1995] "Probabilistic seismic hazard analysis and design earthquakes: closing the loop.," *Bulletin of the Seismological Society of America*, Vol. 85, No. 5, pp. 1275-1284.

McKenna F, F.G., Jeremic B, Scott M., [2000] "Open system for earthquake engineering simulation."

Mehanny, S.S.F. [2009] "A broad-range power-law form scalar-based seismic intensity measure," Vol. 31, No. 7, pp. 1354–1368.

Mitrani-Reiser, J. [2007] "An ounce of prediction: probabilistic loss estimation for performance-based earthquake engineering," *Ph.D. thesis*, California Institute of Technology, Pasadena, California.

Modica, A., and Stafford, P.J. [2014] "Vector fragility surfaces for reinforced concrete frames in Europe," *Bulletin of Earthquake Engineering,*, Vol. 12, pp. 1725–1753.

Monelli, D., Pagani, M., Weatherill, G., Silva, V., and Crowley, H. [2012] "The hazard component of OpenQuake: The calculation engine of the Global Earthquake Model," *15th World Conference on Earthquake Engineering, Lisbon, Portugal.*

Morandi, P., Hak, S., and Magenes, G. [2015] "Simplified Out-of-plane Resistance Verification for Slender Clay Masonry Infills in RC Frames," Dipartimento di Ingegneria Civile ed Architettura.

Mosalam, K.M. [1996] "Modeling of the nonlinear seismic behaviour of gravity load designed infilled frames," Los Angeles, California, USA

Mosalam, K.M., Park, S., Günay, M.S. [2009] "Evaluation of an Element Removal Algorithm for Reinforced Concrete Structures Using Shake Table Experiments," *Proceedings of the 2nd International Conference on Computational Methods in structural Dynamics and Earthquake Engineering (COMPDYN 2009)*, Island of Rhodes, Greece.

NIST [2011] "Seleceting and scaling earthquake ground motions for performing response-history analyses."

Orsini, G. [1999] "A Model for Buildings' Vulnerability Assessment Using the Parameterless Scale of Seismic Intensity (PSI)," *Earthquake Spectra*, Vol. 15, No. 3, pp. 463-483.

Panagiotakos, T., Fardis MN. [2001] "Deformations of reinforced concrete members at yielding and ultimate," *ACI Structural Journal* Vol. 98, No. 2, pp. 135–148.

Park, Y.J.a.A., A.H.S. [1985] "Mechanistic Seismic Damage Model for Reinforced Concrete," *Journal of Structural Engineering*, Vol. 111, No. 4, pp. 722-739.

Pinho, R., Bommer, J.J. and Glaister, S. [2002] "A Simplified Approach to Displacement-Based Earthquake Loss Estimation Analysis," *Proceedings of the 12th European Conference on Earthquake Engineering*, London, U.K.

Polyakov, S.V. [1960] "On the interaction between masonry filler walls and enclosing frame when loading in the plane of the wall," Earthquake Engineering Research Institute

Porter, K.A., Beck, J.L., and Shaikhutdinov, R. [2002] "Sensitivity of Building Loss Estimates to Major Uncertain Variables," *Earthquake Spectra*, Vol. 18, No. 4, pp. 719–743.

Porter, K.A., Kennedy R.P., and Bachman R.E. [2007] "Creating fragility functions for performance-based earthquake engineering," *Earthquake Spectra*, Vol. 23, No. 2, pp. 471–489.

Porter, K.A., Kiremidjian, A.S., and LeGrue, J.S. [2001] "Assembly-Based Vulnerability of Buildings and its Use in Performance Evaluation," *Earthquake Spectra*, Vol. 17, No. 2, pp. 290–312.

Puglisi, M., Uzcategui, M., Flórez-López, J. [2009a] "Modeling of masonry of infilled frames, Part I: The plastic concentrator," *Engineering Structures*, Vol. 31, pp. 113-118.

Puglisi, M., Uzcategui, M., Flórez-López, J. [2009b] "Modeling of masonry of infilled frames, Part II: Cracking and damage," *Engineering Structures*, Vol. 31, pp. 119-124.

Rajeev, P., Franchin. P. and Pinto. P.E., [2008] "Increased Accuracy of Vector-IM-Based Seismic Risk Assessment? ," *Journal of Earthquake Engineering*, Vol. 12, No. 1, pp. 111-124.

Ramirez, C.M., and Miranda, E. [2009] "Building specific loss estimation methods and tools for simplified performance-based earthquake engineering," *Ph.D. thesis*, John A. Blume Earthquake Engineering Centre, Department of Civil and Environmental Engineering, Stanford University.

Restrepo-Vélez, L.F.a.M., G. [2004] "Simplified Procedure for the Seismic Risk Assessment of Unreinforced Masonry Buildings," *Proceedings of the 13th World Conference on Earthquake Engineering*, Vancouver, Canada.

Rodrigues, H., Varum, H., Costa, A. [2008] "A nonlinear masonry infill macro-model to represent the global behaviour of buildings under cyclic loading," *International Journal of Mechanics and Materials in Design*, Vol. 4, pp. 123 - 135.

Rodrigues, H., Varum, H., Costa, A. [2010] "Simplified macro-model for infill masonry panels," *Journal of Earthquake Engineering*, Vol. 14, No. 3, pp. 390 - 416.

Rossetto, T.a.E., A. [2003] "Derivation of Vulnerability Functions for European-Type RC Structures Based on Observational Data," *Engineering Structures*, Vol. 25, No. 10, pp. 1241-1263.

Rossetto, T.a.E., A. [2005] "A New Analytical Procedure for the Derivation of Displacement-Based Vulnerability Curves for Populations of RC Structures," *Engineering Structures*, Vol. 7, No. 3, pp. 397-409.

Ryu, K.P., Reinhorn, A.M. and Filiatrault, A [2012] "Full Scale Dynamic Testing of Large Area Suspended Ceiling System," *15th World Conference on Earthquake Engineering, Lisbon, Portugal.*

Sassun, K., Sullivan, T.J., Morandi, P., Cardone, D. [2016] "Characterising the in-plane seismic performance of infill masonry," *Bulletin of the New Zealand Society for Earthquake Engineering (under review).*

SeismoSoft, S. [2013] "A computer program for static and dynamic nonlinear analysis of framed structures."

Shahi, S. [2013] “A probabilistic framework to include the effects of near-fault directivity in seismic hazard assessment,” Stanford University, Stanford, CA.

Shing, P.B., Mehrabi, A. B. [2002] “Behaviour and analysis of masonry-infilled frames,” *Progress in Structural Engineering and Materials*, No. 4, pp. 320-331.

Shome, N., Cornell, C.A. [1999] “Probabilistic seismic demand analysis of nonlinear structures,” *Report No. RMS-35.*, John A. Blume Earthquake Engineering Centre, Department of Civil and Environmental Engineering Stanford University.

Shome, N., Cornell, CA., Bazzurro, P., Carballo, JE., [1998] “Earthquakes, records, and nonlinear responses. ,” *Earthquake Spectra*, Vol. 14, No. 3, pp. 469-500.

Silva, V., Crowley, H., Varum, H., Pinho, R. and Sousa, R. [2014a] “Evaluation of analytical methodologies used to derive vulnerability functions.,” *Earthquake Engng. Struct. Dyn.*, Vol. 43, pp. 181–204.

Silva, V., Crowley, H., Varum, H., Pinho, R. and Sousa, R. [2014b] “Investigation of the characteristics of Portuguese regular moment-frame RC buildings and development of a vulnerability model,” *Bull Earthquake Eng.*

Smyrou, E. [2006] “Implementation and verification of a masonry panel model for nonlinear dynamic analysis of infilled frames,” European School for Advanced Studies in Reduction of Seismic Risk (ROSE School), University of Pavia, Italy.

Soroushian, S., Zaghi, A., Maragakis, M., Echevarria, A., Tian, Y., and Filiatrault, A. [2015] “Analytical Seismic Fragility Analyses of Fire Sprinkler Piping Systems with Threaded Joints,” *Earthquake Spectra*, Vol. 31, No. 2, pp. 1125–1155.

Sousa, M.L., Campos Costa, A., Carvalho, A. and Coelho, E. [2004] “An Automatic Seismic Scenario Loss Methodology Integrated on a Geographic Information System,” *Proceedings of the 13th World Conference on Earthquake Engineering*, Vancouver, Canada.

Stafford Smith, B. [1966] “Behaviour of square infilled frames,” *Journal of the Structural Division*, Vol. 92, pp. 381 - 403.

Talaat, M.a.M., K.M. [2008] “Computational Modeling of Progressive Collapse in Reinforced Concrete Frame Structures,” Pacific Earthquake Engineering Research Center, .

Talaat, M.a.M., K.M. [2009] “Modeling Progressive Collapse in Reinforced Concrete Buildings Using Direct Element Removal,” *Earthquake engineering and structural dynamics*, Vol. 38, No. 5, pp. 609-634.

Tothong, P., and Luco, N., [2007] “ Probabilistic Seismic Demand Analysis Using Advanced Ground Motion Intensity Measures,” *Earthquake Engineering & Structural Dynamics*, Vol. 36, pp. 1837-1860.

Vamvatsikos, D., and Cornell C.A. [2002] “Incremental dynamic analysis.,” *Earthquake Engng. Struct. Dyn.*, Vol. 31, No. 3, pp. 491–514.

Vamvatsikos, D., Cornell, CA. [2005] “Developing efficient scalar and vector intensity measures for IDA capacity estimation by incorporating elastic spectral shape information,” *Earthquake Engineering & Structural Dynamics*, Vol. 34, pp. 1573–1600.

Whitman, R.V., Anagnos, T., Kircher, C.A., Lagorio, H.J., Lawson, R.S. and Schneider, P. [1997] “Development of a National Earthquake Loss Estimation Methodology,” *Earthquake Spectra*, Vol. 13, No. 4, pp. 643-661.

Whitman, R.V., Reed, J.W. and Hong, S.T. [1973] “Earthquake Damage Probability Matrices,” *Proceedings of the Fifth World Conference on Earthquake Engineering*, Rome, Italy.

Yang, T.Y., Moehle, J., Stojadinovic, B., and Der Kiureghian, A. [2006] “An application of PEER performance-based earthquake engineering methodology,” *8th U.S. National Conference on Earthquake Engineering, San Francisco, California.*

Yang, T.Y., Moehle, J., Stojadinovic, B., and Der Kiureghian, A. [2009] "Seismic performance evaluation of facilities: methodology and implementation," *Journal of Structural Engineering*, Vol. 135, No. 10, pp. 1146–1154.

Zareian, F., and Krawinkler, H. [2007] "Assessment of probability of collapse and design for collapse safety," *Earthquake engineering and structural dynamics*, Vol. 36, No. 13, pp. 1901–1914.